COLLEGE OF AGRICULTURE, ENGINEERING AND SCIENCE

DESIGN OF A NOVEL FLOATING OFFSHORE WIND TURBINE

Kumaresan Cunden

208501304

Thesis submitted in fulfilment of the requirements of the award of the degree of Doctor of Philosophy in Mechanical Engineering

Supervisor

Prof. Freddie L. Inambao

8 August 2023

SUPERVISORS DECLARATION

"As the candidate's academic supervisor, I agree to the Submission of this Thesis."

Prof. Freddie L. Inambao

Name of Supervisor Signature

DECLARATION 1 - PLAGIARISM

I, Kumaresan Cunden, declare that.

1. The research reported in this thesis, except where otherwise indicated, is my original research.

2. This thesis has not been submitted for any degree or examination at any other university.

3. This thesis does not contain other persons' data, pictures, graphs, or other information, unless specially acknowledged as being sourced from other persons.

4. This thesis does not contain other persons' writing, unless specially acknowledged as being sourced from other researchers. Where other written sources have been quoted, then:

a. Their words have been re-written, but the general information attributed to them has been referenced.

b. Where their exact words have been used, then their writing has been placed in italics and inside quotation marks and referenced.

5. This thesis does not contain text, graphics of tables copied and pasted from the internet, unless specially acknowledged, and the source being detailed in the thesis and in the reference's sections.

Signed: . . .  ……Date …08/08/2023

Student No: 208501304

DECLARATION 2 - PUBLICATIONS

The following articles have been published:

Publication 1 – F.L. Inambao and K. Cunden, "**Offshore Wind Resource Assessment Off the South African Coastline**" published in the International Journal of Mechanical Engineering and Technology (IJMET), Vol. 10, Issue 6, June 2019, pp 95-119.

Publication 2 – F. Inambao and K. Cunden, "**Offshore Vertical Axis Wind Turbine Simulation**" published in the International Journal of Mechanical and Production Engineering Research and Development (IJMPERD), Vol. 11, Issue 2, April 2021, pp 187-204.

Publication 3 – K. Cunden and F.L. Inambao, "**Design, Construction, and Testing of Low-Speed Wind Tunnel**" published in the International Journal of Mechanical and Production Engineering Research and Development (IJMPERD), Vol. 11, Issue 6, December 2021, pp 237-256.

The following articles will be published in South African Department of Higher Education accredited journals, SCOPUS indexed.

(a) Kumaresan Cunden and Professor Freddie Liswaniso Inambao, Offshore Wind Energy Review: The Potential for South Africa, Journal of Harbin Engineering University (JHEU), ISSN: 1006-7043, xxx (xxx) xxx

(Accepted for publication)

(b) Kumaresan Cunden and Prof. Freddie Inambao, Fabrication and Testing of Small-Scale Helical Wind Turbine, Journal of Harbin Engineering University (JHEU), ISSN: 1006-7043, xxx (xxx) xxx

(Accepted for publication)

(c) Kumaresan Cunden and Professor Freddie Liswaniso Inambao, Comparison of Helical VAWT to reference VAWT and HAWT for Offshore applications, Journal of Aeronautical Materials (JAM), ISSN: 1005-5053, xxx (xxx) xxx

(Accepted for publication)

In all the above-listed papers, the candidate is the main contributing author, while Prof. Freddie L. Inambao is the supervisor.

Signed: 

Acknowledgements

All my efforts are due to the blessings of the Lord who has provided me with the knowledge to assist and develop this project for the benefit of the people of this planet. God has provided me with the correct influences in my life to deal with the many high and low moments during my study.

My sincere gratitude also goes to my mother and father for all their support and patience during this study. An immense thank you to my supervisor, Professor Freddie L. Inambao, of the Discipline of Mechanical Engineering at the University of KwaZulu-Natal who has supervised the following research work. He has always made time to speak and guide me, not only on an academic level but also on a personal level. He has provided me with stimulating conversation and support during the tenure of my studies and will always be cherished by me. May God bless you and your family.

I also wish to show my deepest gratitude to all the administrative staff from the Faculty of Engineering of the University of KwaZulu-Natal who have always taken the time to guide and assist me through my administrative challenges.

ABSTRACT

Over the past decade, the renewable energy sector nationally and globally has experienced a large growth due to factors such as increases in government subsidies and cost reductions. One of the fastest-growing sectors within the renewable energy space is wind energy, however, the growth comprises mainly onshore wind farm developments but is limited by land availability. Typical wind turbine farms are large special deployments that accommodate large amounts of land. Offshore wind resources are normally higher density than that land-based resources due to fewer obstructions to the wind.

The resource available offshore along the eastern and western coastline of South Africa has significant potential which may be tapped with offshore wind turbines. Findings from the investigation found four potential sites along the coastline of South Africa which are viable for offshore wind turbine exploration. The results of the study found that these sites can be connected to onshore bulk substations and located in zones that are outside the areas of shipping traffic to not affect economic trade. These locations allow suitable access to coastal areas and ports which can reduce strain on the national electrical grid as well as reduce transmission losses from inland power stations. The sites which were investigated have a mean wind speed of 9.5 m/s with power densities between 500 W/m^2 and 1000 W/m^2. However, the ocean seafloor depth between 1km and 3km deep poses a challenge, new floating wind turbine concepts and wind farm configurations technologies indicate that these may be overcome to harness the large energy potential. The study indicates that the offshore potential sites are suitable for offshore wind turbine development and grid integration. The sites which are closer to the shoreline (between 10km and 50km from the shore) have short-medium term deployment potential.

The previously designed, vertical axis, ocean hydrokinetic turbine was optimized for wind conditions by evaluating a larger set of aerodynamic profiles. It was found that the symmetric profiles exhibited stable characteristics when under loading in the upwind and downwind side of the turbine resulting in a smoother transfer of torque to the rotor shaft. The results showed a smooth torque profile on the rotor with minimal main rotor vibration. Even though the aspect ratio of 1.5 has a larger operating range for large tip speed ratio (TSR) range, the aspect ratio of 1 has a higher coefficient of power range resulting in higher turbine power output.

The need for a suitable control volume for small scale testing led to the design and construction of a suitable wind tunnel for the small scale wind turbine testing. The wind tunnel was designed to accommodate a small scale vertical turbine at a velocity of 9 m/s to 9.3 m/s based on the mean wind speed of the potential sites. The turbulence intensity was examined and found to be minimum across the testing section.

A small scale wind turbine was fabricated based on the vertical axis helical blade which was designed at the optimum twist angle for an aspect ratio of 1, due to the nature of power and performance at selected TSR's. The study had proven that the results from the test are in good comparison to that of the simulation. For utility scale turbines with larger power outputs (5MW to 10MW) the rotor speed would be between 10 and 15 RPM for maximum power output.

The helical turbine, in comparison to reference HAWT and VAWT turbines within the market, show an improvement to the power curve efficiency. The helical blade profile shows positive results on the transmission of mechanical power from the blade to the rotor torque in comparison to other VAWT systems within the market. This allows for reduced impact on mechanical and electrical components of the turbine. When deployed in a standardised wind farm layout, the helical turbine outperforms the reference HAWT and VAWT turbines with respect to capacity factor and annual energy production.

The investigation found that there are suitable offshore wind farm locations along the coastline of South Africa which can provide suitable clean energy as well as diversify the country's energy mix as per the national development plan and long-term energy targets. The study concluded that the vertical axis turbine design can provide much needed power which may be fed into coastal regions at bulk point of supply or to offshore oil & gas rigs and possibly coupled with hydrogen technology in the future.

.

TABLE OF CONTENTS

LIST OF FIGURES

LIST OF TABLES

NOMENCLATURE

Chapter 3

A_H	Average element horizontal area (m^2)
b	Constant (-)
c	Scale parameter (m/s)
g	Gravitational Acceleration (m/s^2)
h	Element height (m)
k	Shape parameter (-)
$P(U, k, c)$	Weibull distribution for wind profiles
S	Cross-sectional surface facing the wind (m^2)
U	Mean wind speed velocity (m/s)
U_{Ref}	Reference wind speed (m/s)
U_*	Frictional Velocity (m/s)
z	wind speed target height (m)
z_0	Roughness length (m)
z_{Ref}	Reference height (m)
α	Empirical coefficient accounting for atmospheric stability (-)
$\psi(\zeta)$	Integrated stability function governing momentum (-)

Chapter 4

AR	Aspect Ratio (-)
B	Number of Blades (-)
c	Chord length of Blade (m)
C_D	Coefficient of Drag (-)
C_L	Coefficient of Lift (-)
D	Turbine Diameter (m)
H	Turbine Height (m)
Re_{Blade}	Blade Reynolds Number (-)
U_{Rel}	Relative incoming wind speed (m/s)
v	Kinematic viscosity of air at sea level (m^2/s)
σ	Solidity Ratio (-)
δ	Blade Helix Angle (°)
ώ	Blade Wrap (%)

Chapter 5

A	Hydraulic cross-section area (m^2)
A_{Fan}	Cross-section area of the fan (m^2)
$A_{Test\ Section}$	Cross-section area of the test section (m^2)
c	Speed of sound (m/s)
C_p	Specific heat at constant pressure (J/kg. K)
C_v	Specific Heat at constant volume (J/kg. K)
D_{tube}	Diameter of the laminar flow tube (m)
h	Static head (m)
k	Ratio of specific heats (-)
K	Turbulent kinetic energy (J/kg)
M	Mach Number (-)
$\dot{M}$	Mass flow rate (m^3/s)
P	Pressure (kPa)
P_0	Stagnation pressure (Pa)
R	Unique gas constant (J/kg mol K)
Re_{crit}	Reynolds number for laminar flow (-)
$s_1 - s_2$	Change in entropy (kJ/kg K)
T	Temperature of fluid (K)
$T.I.$	Turbulence intensity (%)
T_0	Stagnation Temperature (K)
U_∞	Mean flow velocity (m/s)
u_{RMS}	Root mean square of velocity fluctuations (m/s)
V	Flow velocity (m/s)
V_{tube}	Fluid velocity of the laminar tube (m/s)
α	Contraction angle (°)
ρ	Density of fluid (kg/m^3)
ρ_0	Stagnation density (kg/m^3)
μ	Dynamic viscosity (kg/m. s)

Chapter 6

AR	Aspect Ratio (-)
A_S	Surface Area of Turbine (m)
A_T	Wind Tunnel Test Section Area (m)
A_ω	Swept Area (m)

B	No. of Turbine Blades (-)
B_f	Blockage Factor (-)
B_R	Blockage Ratio (-)
c	Blade chord length (m)
C_P	Coefficient of Power (-)
D	Turbine Diameter (m)
H	Turbine Height (m)
P_f	Power of the fluid (W)
P_m	Mechanical Power (W)
T	Torque
U_c	Corrected Wind Speed (m/s)
U_f	Wind Speed without Turbine (m/s)
U_t	Wind Speed with Turbine (m/s)
U_∞	Freestream Wind Speed (m/s)
σ	Solidity Ratio (%)
δ	Helix Angle (°)
ρ	Density of Fluid (kg/m^3)
ω	Rotational Speed (rad/s)
ώ	Turbine Blade Wrap (%)

Chapter 7

A	Swept Area (m^2)
C_P	Coefficient of Power (-)
C_T	Thrust Coefficient (-)
D	Turbine Diameter (m)
I_u	Turbulence Intensity (%)
k	Wake rate of expansion ratio (-)
n_y , n_z	Wake spatial length exponents (m)
σ_{V_y} , σ_{V_z}	Wake velocity deficit distribution (-)
P	Power (kW)
P_r	Power Ratio (-)
P_γ	Misaligned Production (MWh)
P_{γ_0}	Yaw aligned production (MWh)
U_∞	Freestream Velocity (m/s)
$U_\varphi(x)$	Wake Velocity Deficit (m/s)

v	Wind Speed (m/s)
β_F	Wake cross sectional ratio after expansion (-)
β	Blade Pitch (°)
ξ	Aspect Ratio (-)
ε_{V_y} , ε_{V_z}	Initial Wake (-)
$\sigma(x)$	Wake width along streamwise path (m)
λ	Tip Speed Ratio (-)
δ_F	Wake Expansion Factor (-)
ρ	Density (kg/m^3)

CHAPTER 1 : INTRODUCTION

1.1 Background

The world is rapidly moving towards a shift from fossil fuels to renewable energy solutions. This has been spurred due to the changes in the global climate and the need to shift from carbon-intensive fuels. Energy is a key driver for any country to develop which aids social and economic developments. Recently, sustainable energy generation has also been a key factor in Sustainable Development Goals (SDGs) developed by the United Nations (UN) framework, [1], [2].

The electrical power generation within South Africa is mainly produced from coal-fired power stations, however, the developments in the Renewable Energy Independent Power Producer Procurement Programme (REIPPPP) have been changing the energy mix within the country. South Africa is abundant in coal resources [3]; however, the world is reducing its dependence on fossil fuel consumption as well as complying with the SDG meaning that South Africa is required to maintain a balanced energy mix consisting of cleaner sources of electrical energy generation, [4], [5].

Figure 1-1 shows the development of the REIPPPP for South Africa. The figure details the spread of the installed capacity of technologies over the country from bid windows 1 to 4. The figure shows that most of the wind turbine farms are located along the western and eastern coastlines of South Africa.

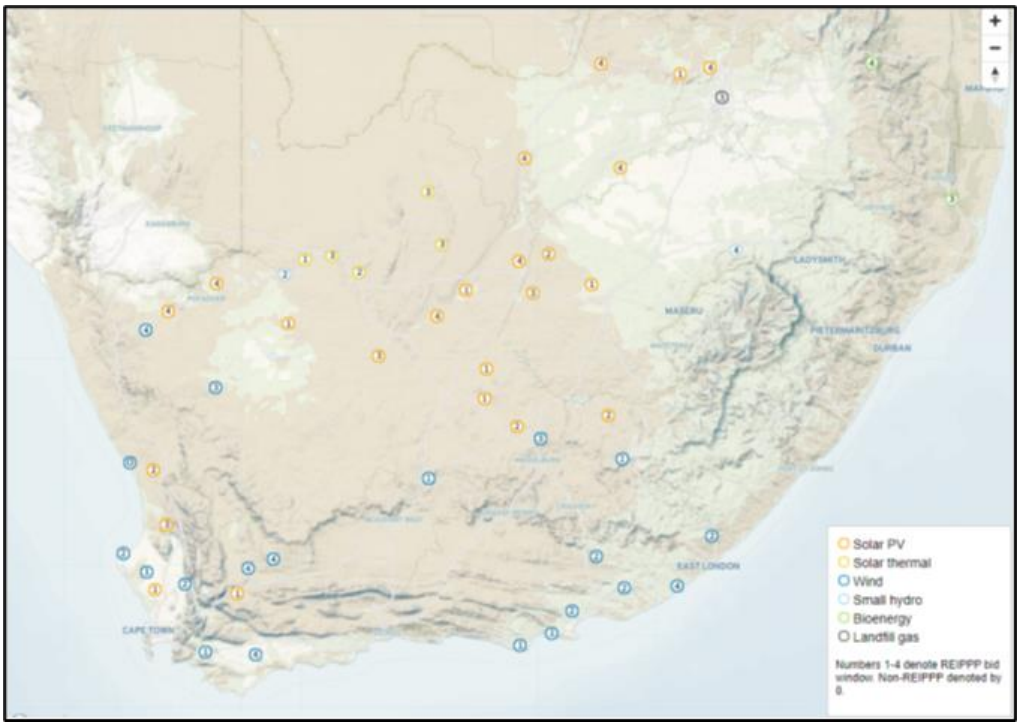

Figure 1-1: REIPPPP Location of Installed Power Plants, [6]

South Africa utilizes the REIPPP programme as an auctioning mechanism to attract foreign investment and mobilize the private industry in the development of various renewable energy technologies for the benefit of the country. This programme also aims to shift the balance from a centralised vertically integrated model of power generation and supply toward a diversified, independent model of power generation and distribution, [7], [8].

Figure 1-2 shows the installed wind capacity for the African continent, sourced and compiled from independent analysis from International Renewable Energy Agency (IRENA) Capacity Statistics 2021, [9]. The installed wind capacity is increasing over the last 2 decades due to multiple reasons such as growing demand, and policy changes within African nations incorporating the shift towards renewable energy resources. However, offshore wind provides significantly more potential due to the abundance of resources found offshore with minimal obstruction to the wind flow regime.

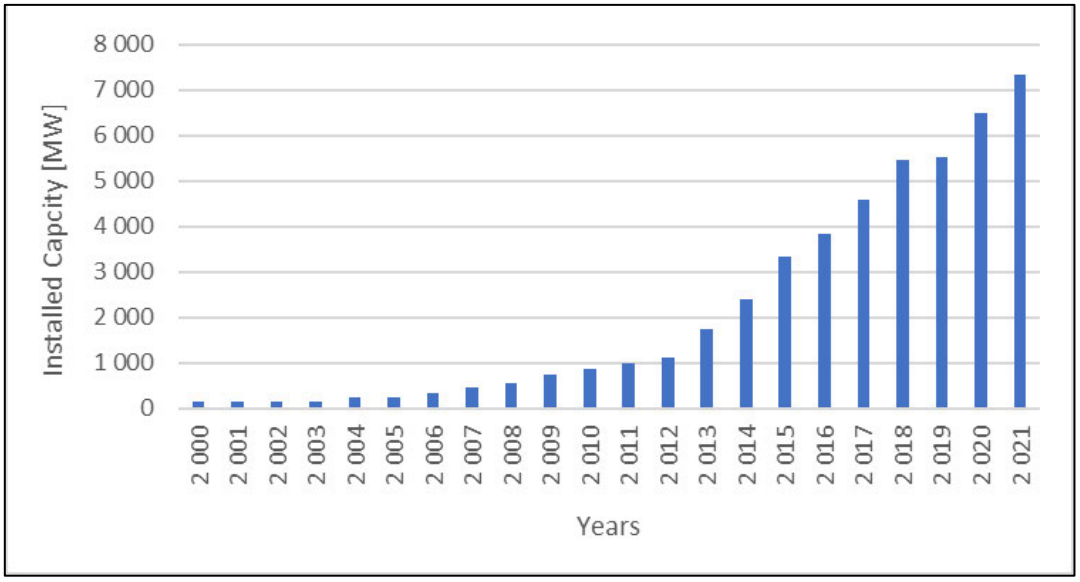

Figure 1-2: Installed Wind Capacity - Africa

Figure 1-3 below shows the leading countries which have contributed to the growth of the wind energy sector within Africa due to onshore wind. It can be seen that Egypt, Morocco, and South Africa are the leaders in installed capacity with South Africa being the highest-ranking country, mainly due to the success of the REIPPP programme highlighted in Figure 1-1 contributing to the high rate of deployment.

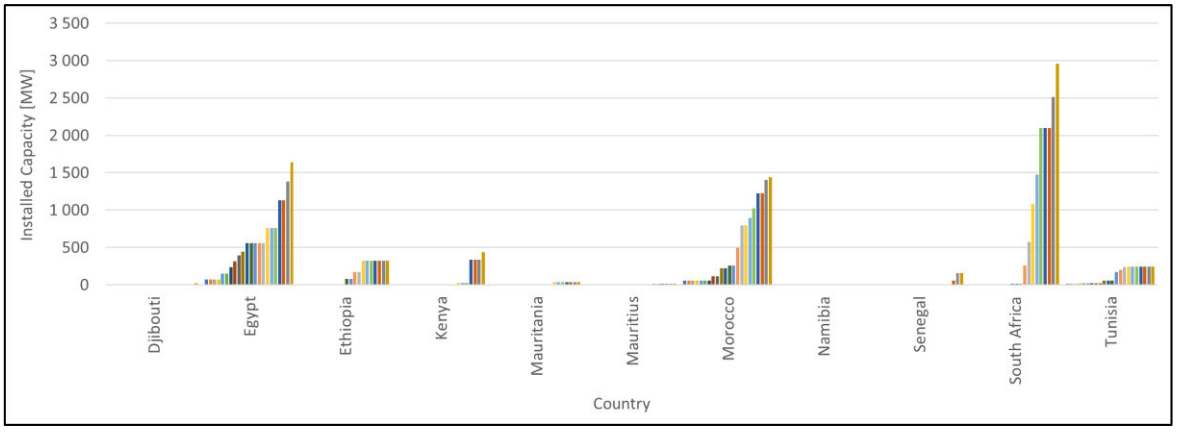

Figure 1-3: Installed Wind Capacity in Africa by country

However, as land becomes scarce and the economic potential of coastal land becomes more valuable for other economic contributions such as agriculture, and commercial and industrial trade, the incorporation of large wind farms will become challenging to develop and construct. Encroachment within residential zones may also pose its challenges due to aesthetic disputes and noise play a significant role, [10]–[13].

The offshore wind potential for wind farms is typically higher than that of the onshore counterparts due to the lack of obstructions such as trees, buildings, and uneven terrain, [14]–[17]. Offshore wind farms also lack the socio-economic challenges that the onshore wind farms, however, still require these impact assessments about marine life and other pertinent factors, [13], [18]–[20].

South Africa has recently had a challenging time about energy provisions from the current energy provider for the state. The energy providers from the Independent Power Producers (IPPs) may only provide energy when significant resources are available. As previously shown, the location of renewable generation, in particular onshore wind, is located in regions along the coast which are not spatially distributed to allow for the equal evacuation of generated power to inland regions.

The current orientation of onshore and offshore wind turbines is built on the traditional 3-bladed horizontal axis wind turbine design. The challenges with these types of turbines are the need for complex control systems which need to pitch the turbine blades and yaw the entire turbine towards best suited incoming wind relative to the main hub of the turbine. A vertical axis wind turbine, however, does not need such complex control architecture due to the cross-flow nature of the turbine that accepts wind flow from any horizontal direction. The use of such a turbine in offshore conditions has added the benefit of reduced support structure eccentricity conditions as the main generator is located at the base of the turbine. Large offshore wind turbine designs also reduce the need for gearboxes as permanent magnet generators are used to achieve large power outputs at lower rotational speeds.

The research conducted in this thesis highlights the energy which can be extracted by the offshore wind potential along the South African coastline in the eastern and western coastal regions. The proposed solution is developed based on previous research conducted by Cunden, K in [21] and [22] and is an adaptation of a hydrokinetic cross-flow turbine based on the Gorlov helical turbine concept. The wind turbine is envisioned to be coupled via a floating offshore platform to harness both ocean and wind resources simultaneously for maximum energy production.

1.2 Research Questions

The proposed doctoral project was to design and analyse a novel floating hybrid vertical axis wind turbine coupled with a vertical axis ocean current turbine. Cunden, K [22] had previously designed and simulated an offshore novel vertical axis ocean turbine to harness energy from the Agulhas current. It is proposed that the design of the ocean turbine be utilized, as a basis, for the design of the wind turbine. Both turbines would provide power to an offshore substation and transmit power to the onshore transmission connection point. This system would aid in the possible reduction of energy demand or supply-constrained South African coastal region networks.

The proposed research would aim to answer some critical questions which would shed light on possible energy solutions for the national and global energy sector. The following are the key research questions that are planned to be answered by the study:

1. What is the offshore wind resource potential along South Africa (> 100 km offshore)?
2. How far offshore would be acceptable for an offshore wind system?
3. What is the resultant rotor torque and potential energy output?
4. What are the possible transmission systems that may be used to evacuate power from the wind farm?

1.3 Aims and Objectives of the study

The renewable energy sector, nationally and globally, has experienced rapid growth due to various factors impacting government subsidies, the need for affordable energy, and new funding for sustainable energy creation.

Currently, the wind turbine market is dominated by the traditional Dutch Windmill type design which is known as the horizontal axis wind turbine (HAWT). These types of turbines exploit the aerodynamic lift generated as the wind passes over an airfoil turbine blade. These conventional systems are well-known engineering designs and robust by nature. Another type of wind turbine, which is becoming common in the sector as well as a growing area of research, is the vertical axis wind turbine (VAWT).

The proposed project could prove to be of significant benefit for the offshore renewable energy industry and the energy sector as a whole. As offshore wind turbines are still emerging into the energy space. The proposed design has the potential to offer a clean and effective source of power generation for the country and the global energy industry. The technology also could reduce the demand and a possible solution for electrifying coastal regions.

The thesis aimed to understand if a vertical axis wind turbine may be suitable for electrical power generation at offshore locations along the South African coastline.

The research objectives are in accordance with the aims set out for the study as follows:

1. To utilize literature reviews to gain an understanding of parameters and governing equations to be used in the numerical modelling
2. Obtain offshore wind and ocean velocity profile data for South Africa.
3. Locate the minimum offshore distance from the coast which would not disrupt existing marine traffic.
4. Analyse the results from the numerical simulations to understand each turbine's performance under offshore conditions.
5. To construct and test a prototype of the wind turbine in a wind tunnel.
6. Comparison of the results from testing with that of simulation.

1.4 Layout of the dissertation

The following thesis is set out to achieve the aims and objectives which are accomplished in 7 chapters. Each of the 7 chapter's content is summarized below.

Chapter 1 presents the background to the study which outlines the need for more sustainable energy solutions and explains the potential of offshore wind compared to onshore wind energy production. The contents of this chapter consist of research questions including the aims and objectives of the study, the layout of the dissertation, the scope of the study, the original contribution of the study to the renewable energy field, and lastly relevant contributing publications.

Chapter 2 consists of an in-depth literature review that investigates previous research which has been conducted in the same or similar field of study. This review consists of an examination of conference proceedings, international peer-reviewed journal articles, dissertations on a master's and doctoral level as well as reputable reports from international government agencies. The study elaborates on the types of wind turbines and compares the orientations, compares types of foundations including anchoring options, and elaborates on possible electrical transmission systems for grid connection.

Chapter 3 investigates and provides findings of a resource assessment of offshore wind locations identified and summarises the wind profile along various regions along the South African coastline. The evaluation utilizes synthetic meteorological wind resource data which was filtered considering shipping routes for development. The study highlights four possible sites which may be developed for far offshore wind farms.

Chapter 4 outlines the numerical simulation of the proposed vertical axis wind turbine design consisting of an investigation of various aerodynamic profiles and then comparing the lift and drag characteristics, turbine height to the radius, blade wrap, and turbine solidity. The objective was to understand the sensitivities of these parameters on the turbine rotor torque profile and power curve.

Chapter 5 elaborates on the design and fabrication of the wind tunnel which was used to test the fabricated scaled wind turbine. The wind tunnel was utilized to analyse various fabricated models of the vertical turbine. The wind tunnel was designed to have minimum turbulence intensity within the testing chamber to provide a laminar flow to the turbine.

Chapter 6 details the design and fabrication of the scaled vertical axis wind turbine. The results logged were the turbine speed and electrical output via a DC generator. The torque was calculated based on the relationship of the logged power and speed. The tested turbine results were compared to numerical simulations of the turbine incorporating correction factors due to blockage within the wind tunnel.

Chapter 7 compares the chosen turbine design to that of commercially available reference HAWT and VAWT configuration turbines. The chapter also investigates the predicted Annual Energy Production (AEP) in 3 different wind farm layout configurations.

Chapter 8 summarises the findings from the investigations and concludes the thesis and also includes recommendations for future work to be considered.

1.5 Scope of the study

The research within the thesis was focused on the design and evaluation of a vertical axis cross-flow turbine system aimed at extracting energy from the natural offshore wind resources and supplying coastal regions of the country.

The research consists of a resource assessment, numerical simulations of the vertical wind turbine, design and fabrication of a small-scale prototype of the turbine, fabrication of a suitable wind tunnel as well as testing of the scaled turbine.

1.6 Original contribution of the study

The concept of a vertical axis wind turbine for offshore energy production, off the coast of South Africa, has not been investigated for far offshore locations requiring floating platform configurations for harnessing the large potential. The thesis contributes to the scientific body of knowledge of the resource assessment and potential offshore, the results from the investigation of various aerodynamic profiles for the wind turbine.

1.7 References

[1] O. J. Ayamolowo, A. O. Salau, and S. T. Wara, "The Power Industry Reform in Nigeria: The Journey So Far," in 2019 IEEE PES/IAS PowerAfrica, 2019, pp. 12–17, doi: 10.1109/PowerAfrica.2019.8928657.

[2] O. J. Ayamolowo, P. T. Manditereza, and K. Kusakana, "South Africa power reforms: The Path to a dominant renewable energy-sourced grid," Energy Reports, vol. 8, pp. 1208–1215, 2022, doi: https://doi.org/10.1016/j.egyr.2021.11.100.

[3] O. N. Nobela, R. C. Bansal, and J. J. Justo, "A review of power quality compatibility of wind energy conversion systems with the South African utility grid," Renew. Energy Focus, vol. 31, pp. 63–72, 2019, doi: https://doi.org/10.1016/j.ref.2019.10.001.

[4] I. D. Ibrahim et al., "A review on Africa energy supply through renewable energy production: Nigeria, Cameroon, Ghana and South Africa as a case study," Energy Strateg. Rev., vol. 38, p. 100740, 2021, doi: https://doi.org/10.1016/j.esr.2021.100740.

[5] O. M. Akinbami, S. R. Oke, and M. O. Bodunrin, "The state of renewable energy development in South Africa: An overview," Alexandria Eng. J., vol. 60, no. 6, pp. 5077–5093, 2021, doi: https://doi.org/10.1016/j.aej.2021.03.065.

[6] Department of Mineral Resources and Energy, "Integrated Resource Plan (IRP2019)," 2019. [Online]. Available: http://www.energy.gov.za/IRP/2019/IRP-2019.pdf.

[7] H. Visser, G. A. Thopil, and A. Brent, "Life cycle cost profitability of biomass power plants in South Africa within the international context," Renew. Energy, vol. 139, pp. 9–21, 2019, doi: https://doi.org/10.1016/j.renene.2019.02.080.

[8] A. S. Oyewo, A. Aghahosseini, M. Ram, A. Lohrmann, and C. Breyer, "Pathway towards achieving 100% renewable electricity by 2050 for South Africa," Sol. Energy, vol. 191, pp. 549–565, 2019, doi: https://doi.org/10.1016/j.solener.2019.09.039.

[9] IRENA, “Renewable capacity statistics 2021,” International Renewable Energy Agency, 2021.

[10] J. M. Northrup and G. Wittemyer, “Characterising the impacts of emerging energy development on wildlife, with an eye towards mitigation,” Ecol. Lett., vol. 16, pp. 112–125, 2013, doi: 10.1111/ele.12009.

[11] R. Klæboe and H. B. Sundfør, “Windmill Noise Annoyance, Visual Aesthetics, and Attitudes towards Renewable Energy Sources,” International Journal of Environmental Research and Public Health , vol. 13, no. 8. 2016, doi: 10.3390/ijerph13080746.

[12] V. Vlami et al., “Residents’ views on landscape and ecosystem services during a wind farm proposal in an island protected area,” Sustain., vol. 12, no. 6, 2020, doi: 10.3390/su12062442.

[13] E. A. Virtanen et al., “Balancing profitability of energy production, societal impacts and biodiversity in offshore wind farm design,” Renew. Sustain. Energy Rev., vol. 158, p. 112087, 2022, doi: https://doi.org/10.1016/j.rser.2022.112087.

[14] J. Li and X. (Bill) Yu, “Onshore and offshore wind energy potential assessment near Lake Erie shoreline: A spatial and temporal analysis,” Energy, vol. 147, pp. 1092–1107, 2018, doi: https://doi.org/10.1016/j.energy.2018.01.118.

[15] F. L. Inambao and K. Cunden, “Offshore wind resource assessment off the South African coastline,” Int. J. Mech. Eng. Technol., 2019.

[16] D. C. A. Lima, P. M. M. Soares, R. M. Cardoso, A. Semedo, W. Cabos, and D. V Sein, “The present and future offshore wind resource in the Southwestern African region,” Clim. Dyn., vol. 56, no. 5, pp. 1371–1388, 2021, doi: 10.1007/s00382-020-05536-4.

[17] S. Peter, C. Xinyu, and M. Michael, “Offshore wind: An opportunity for cost-competitive decarbonization of China’s energy economy,” Sci. Adv., vol. 6, no. 8, p. eaax9571, Jul. 2022, doi: 10.1126/sciadv.aax9571.

[18] R. J. C. . Khumar, V. D. Kumar, D. Baskar, M. B. Arnnusi, R. Jenova, and M. A. Majid, “Offshore wind energy status, challenges, opportunities, environmental impacts, occupational health, and safety management in India,” Energy Environ., vol. 32, no. 4, pp. 565–603, 2020, doi: 10.1177/0958305X20946483.

[19] O. M. H. C, M. Shadman, M. M. Amiri, C. Silva, S. F. Estefen, and E. La Rovere, “Environmental impacts of offshore wind installation, operation and maintenance, and

decommissioning activities: A case study of Brazil," Renew. Sustain. Energy Rev., vol. 144, p. 110994, 2021, doi: https://doi.org/10.1016/j.rser.2021.110994.

[20] N. T. Xuan Son and P. Thi Gam, "Vietnam's Policy for Promoting Offshore Wind Power and Environmental Impact Assessment," Environ. Claims J., vol. 34, no. 2, pp. 156–169, Apr. 2022, doi: 10.1080/10406026.2021.1932335.

[21] F. L. Inambao and K. Cunden, "Design and Numerical Simulation of a Small Scale Helical Cross Flow Turbine," in 13th BIE Biennial Conference, 2013, pp. 23–32.

[22] K. Cunden, "Design of a Novel Hydrokinetic Turbine for Ocean Current Power Generation," University of Kwa-Zulu of Natal, 2015.

CHAPTER 2 : OFFSHORE WIND ENERGY REVIEW – THE POTENTIAL FOR SOUTH AFRICA

The following chapter of the study investigates the various different literature and reports which were published in international journals, reputable reports and articles as well as independent data analysis based on trusted sources of information. The results presented in this chapter provide a strong foundation for the further investigations conducted. The chapter highlight the evolution of the offshore wind industry and the different types of configurations of offshore wind turbine technology including reviews of offshore wind turbine foundations. The chapter concludes by assessing the potential of offshore wind farm power generation for South Africa.

OFFSHORE WIND ENERGY REVIEW – THE POTENTIAL FOR SOUTH AFRICA

Kumaresan Cunden and Professor Freddie Liswaniso Inambao

Department of Mechanical Engineering, University of Kwa-Zulu-Natal

Durban, South Africa

ABSTRACT

Over the past decades, the energy demand of the world has increased dramatically due to various contributing factors. Environmental impacts, policy, and wind resources impact the size of wind turbines located onshore. Offshore wind technology can play a key role in the decarbonization of coastal cities and assist the global transition towards cleaner electrical generation sources. The offshore wind energy industry has progressed significantly over the past decade due to a multitude of factors in the economic and technical sectors. Policy, regulations, and innovative financing aided the development of the offshore wind industry. Another contributing factor to the increase in deployment of offshore wind power has been the evolution of turbine size for the offshore wind turbine sector. The following study aims to review the key components of the offshore wind industry for a case study of South Africa. The study examines the differences between turbine configurations such as HAWT and VAWT designs of turbines, foundation types, and potential electrical network topologies for South Africa.

Keywords: Offshore Wind, Offshore wind foundations, HVDC, HVAC, South Africa.

2.1 Introduction

Over the past decades, the energy demand of the world has increased dramatically due to various contributing factors, [1]–[5]. According to the British Petroleum (BP) statistical review of global energy supply, the major contributor to energy supply stems from fossil fuel sources (i.e. Coal; Natural Gas, and Oil), [6]. However, there had been a decline in fossil fuel contribution and an increase in renewable energy contributions from 2019 to 2020 as shown in Table 2-1 below. It was found that the major fossil fuel contribution is natural gas and oil except for the Asia Pacific region which relies heavily on coal for electrical energy generation.

Table 2-1: Energy Statistics by Fuel

		Fossil	Nuclear	Hydro & Other	Renewables
Total World	**2019**	62.9%	10.4%	16.5%	10.3%
Total World	**2020**	61.3%	10.1%	16.9%	11.7%
% Change		-1.5%	-0.3%	0.4%	1.4%

Major countries, like Japan, the European Union, and China, have since announced ambitious decarbonization plans for the long-term to shift their respective states to a net-zero economy and achieve the respective carbon emission reduction goals. This was seen even through the Covid-19 pandemic which had minimum effect on the renewable energy policy targets or incentives, [10].

The policies which have been developed over the decades have been a key driver for large-scale renewable energy deployment globally as well as cost reductions and innovation in the renewable energy space. Countries across the world have slowly been moving away from feed-in tariffs (FiTs) and feed-in premiums (FIPs) towards more competitive set tariff options (competitive auctions, green certificates, corporate power purchase agreements (PPAs), etc.) for large-scale systems or portfolio based distributed generation projects. It is forecasted that in the next half-decade the policies and regulatory frameworks which enable competitive environments will make up 60% of all global renewable energy expansions, [7].

Figure 2-1 shows the major contributing policies which support wind deployment across the global markets of wind deployment. The support mechanisms and policies coupled with decreasing materials and other supply costs are attributed to the main key drivers of wind deployment over the next half-decade. Considering all of the wind capacity which is set to come online within the next five years, 40% are supported by FiTs and FIPs which are trailed by 35% which are supported by competitive auctions. Competitive auctions are prevalent in all regions except the United States of America and China, [7].

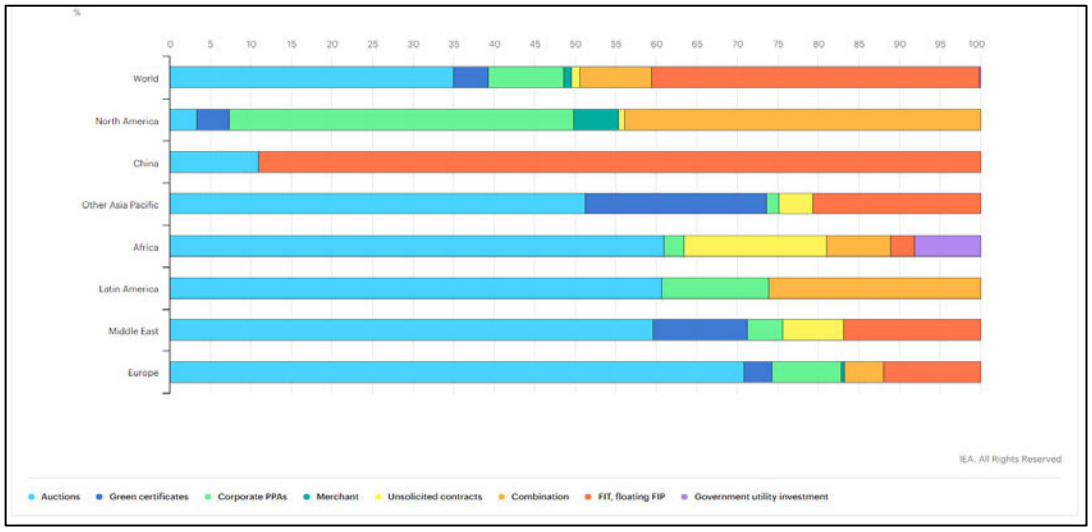

Figure 2-1: Supporting Policy Schemes for Wind Energy, [8]

2.2 Status of Offshore wind

Offshore wind technology can play a key role in the decarbonization of coastal cities and assist the global transition toward cleaner electrical generation sources,[6], [9]. Figure 2-2 shows a graphical representation of the statistics of onshore and offshore wind technology installed capacity from the year 2000 till the year 2020, [10]. The figure accounts for the global installed capacity over the two decades and it can be seen that the offshore capacity is slowly increasing and a steady rate.

This may be due to various factors such as an increase in energy yield in offshore sites as well as larger turbine capacities that can be deployed offshore which are not suitable for onshore integration, [9], [11]–[13]. Recent trends have also shown that deployments are increasingly moving further offshore

into deeper water depths forcing innovation in floating platform designs, [14]–[18]. In addition to these factors the offshore wind farms have minimal noise and visual negative impacts, however, considerations concerning marine ecosystems are still required when deploying these solutions, [17], [19]–[21].

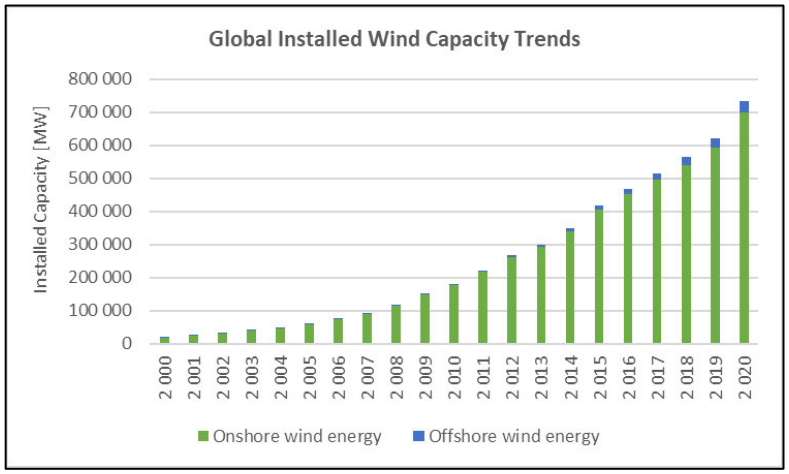

Figure 2-2: Onshore & Offshore Wind Installed Capacity 2021, [10]

H. Diaz and C. Guedes Soares analysed data from [22] which is shown in Table 2-2 indicating the major regions which have dominated the installation of offshore wind turbines. It can be seen both onshore and offshore that Asian and European markets have dominated the wind sector with the most installed capacity. The data depicts the dominance of the European and Asian markets in the aggressive installation of offshore wind farms. In the European sector, it was found that the United Kingdom (30 wind farms), Germany (19 wind farms), Denmark (13 wind farms), and the Netherlands (6 wind farms) have the most installed offshore capacity. In the Asian market, the leaders are China (21 wind farms) and Vietnam (2 wind farms), [17].

Table 2-2: Installed Offshore wind Capacity, [17]

Region	*Country*	*Installed Capacity [MW]*	*No. of Turbines*
Europe	Belgium	871.2	231
	Finland	84.4	18
	Denmark	1273.1	510
	Germany	5342.3	1167
	Ireland	25.2	7
	Netherlands	1117.8	365
	Sweden	191.2	79
	UK	7347.8	1796
Asia	China	2409.9	676
	Japan	41.3	22
	South Korea	35	15
	Taiwan	8	2
	Vietnam	183.2	102
America	United States	30	5

A contributing factor to the increase in deployment of offshore wind power has been the evolution of turbine size for the offshore wind turbine sector. Environmental impacts, policy, and wind resources

impact the size of wind turbines located onshore. Offshore wind energy about onshore wind energy does have many advantages concerning wind energy production, [23]–[25]. Larger turbines may be deployed offshore due to the lower impacts of terrain on the wind resource which normally translates to higher and more constant wind speeds as well as higher capacity factors, [25]–[28]. Figure 2-3 depicts the evolution of wind turbine size over the last three decades. The increase in turbine capacity usually is a result of an increase in rotor diameter. The benefits of larger rotor diameters can result in more energy being captured as well as a more consistent output over the year, [13], [29].

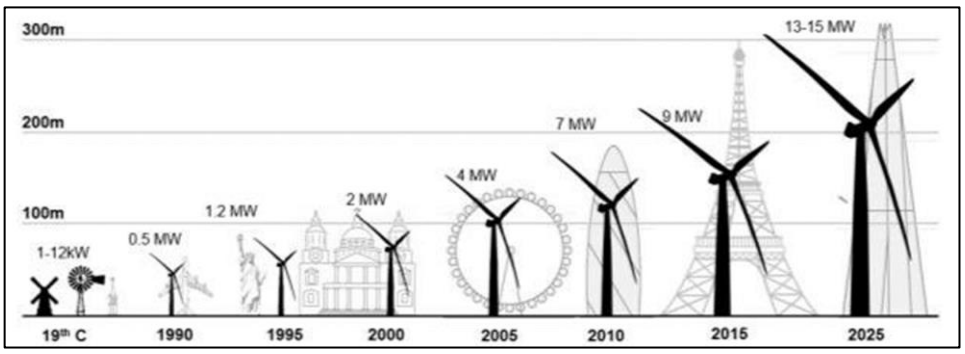

Figure 2-3: Evolution of wind turbine sizes, [30]

As mentioned in Table 2-2, Europe and Asia dominate the offshore wind industry currently with an installed capacity of 24.9 GW and 9.4 GW respectively, [10]. Figure 2-4 shows the trend of installation from the year 2000 to 2020 with Europe depicted in blue and Asia (predominantly China) highlighted in red. China consists of 8.99 GW of offshore wind capacity which constitutes 95.4% of Asia's offshore wind installed capacity, [10]. The figure shows an increasing trend of offshore wind energy deployment in the two major regions over the last ten years. It should be noted that the increases in turbine capacity, subsequently rotor diameter, have led to large wind farms being developed within the regions as seen in the figure.

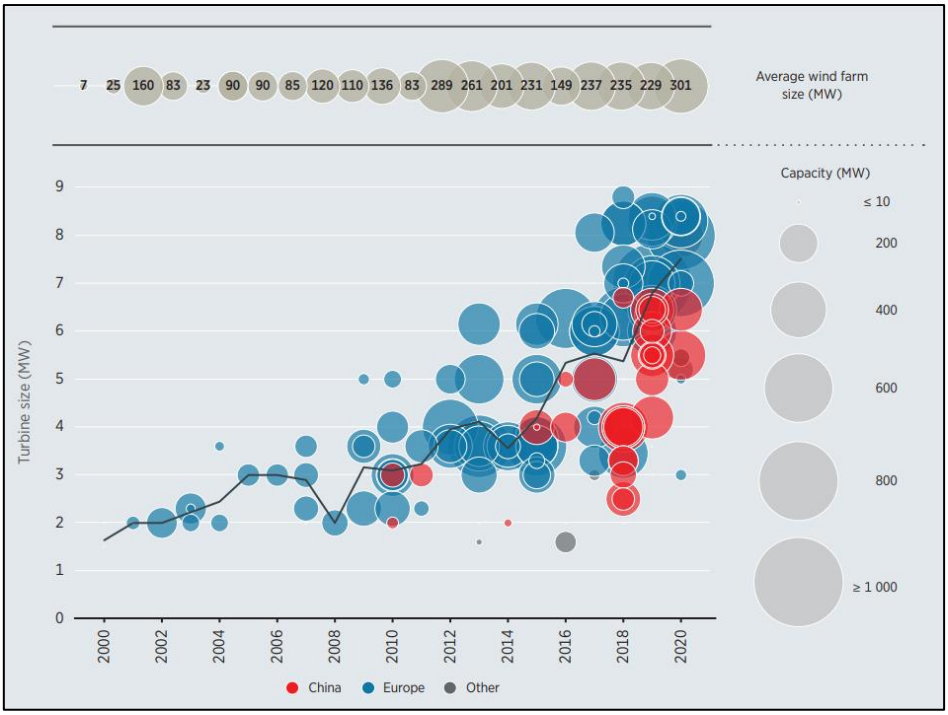

Figure 2-4: Average global offshore wind farm capacity and turbine size 2000 – 2020, [13]

It can be seen that the offshore wind energy industry has progressed significantly over the past decade due to a multitude of factors in the economic and technical sectors. Policy, regulations, and innovative financing aided the development of the offshore wind industry. This will continue as energy markets adapt and learn from one region to another but there are still some hurdles to overcome over the coming years, [31]–[33]. However, further decreases in costs are predicted as well as technology to allow for deeper sea deployment to harness more abundant wind resources, [34]–[36].

2.3 Types of Offshore wind Turbines

There are two main types of wind turbines which are grouped as Horizontal Axis Wind Turbines (HAWTs) and Vertical Axis Wind Turbines (VAWTs) and are recognized based on the axis of rotation of the turbine blades, [37]. The offshore wind industry adopted the HAWT type systems first due to years of existing research and the success of onshore HAWT systems, however, this was assumed and did not consider the variance in offshore environmental conditions, [38], [39].

Wind turbines are subject to a theoretical limit first identified by Joukowsky, Betz, and Prandtl during the early 1900s which defined the flow regime around an airfoil utilizing and integrating various mathematical models of the time, [40], [41]. Researchers use this in wind turbine design as a theoretical limit to which the turbine can extract energy from the wind resource. Airfoils are geometrical shapes that can either be symmetrical or asymmetrical to create a local pressure variance to create lift, much similar to that of an airplane wing, [42]–[44]. The design of the airfoil is of importance to maximize the power output from the wind turbine, [45].

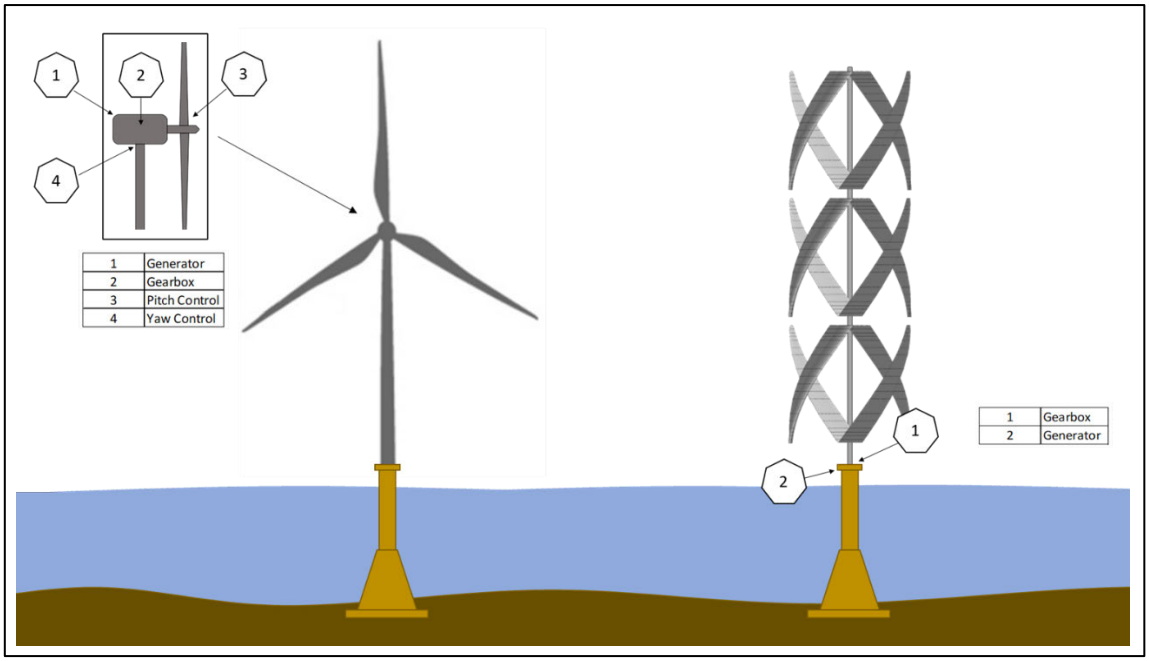

Figure 2-5: Comparison of HAWT and VAWT systems,

Research from [46] had initially indicated the investigations of VAWTs were low due to fatigue constraints, however, due to the need for systems to be deployed further offshore research has shown that VAWT systems are at an advantage over that of HAWTs, [38]. Researchers from Sandia laboratories have investigated the difference between HAWTs and VAWTs for deep offshore applications and some of the findings are shown in Figure 2-5. Results from the researchers show that the center of mass of the offshore VAWTs, compared to that of traditional HAWTs is lower which had led to a decrease in substructure costs, [47].

2.4 Offshore Wind Resource

The localised wind characteristics are required for the development of offshore wind farms, [48]. Due to the lack of existing offshore meteorological stations, synthetic data such as MERRA and MERRA-2 are used internationally as a trusted source of data for the initial feasibility investigation of the wind farm development. Various studies have been conducted on the validity of the utilisation of the MERRA datasets for onshore and offshore wind farms.

Olauson et al. had initially modelled the wind power potential in Sweden by using the MERRA-2 datasets, [49]. Staffell et al. were amongst the initial researchers that have used MERRA-2 and validated its use for the purpose of wind power generation for 23 European countries during 2016, [50]. Cali et al. had investigated and analysed the potential site locations for offshore wind farms in Turkey by using the MERRA dataset in 2018 with good correlation to the LiDAR measurement campaign, [51]. Hassoine et al. had used the MERRA-2 dataset to evaluate the optimal placement of the wind turbines for a large offshore wind farm and had shown that the dataset was a reliable source of information for

the energy prediction of the wind farm, [52]. The studies provide favourable conclusions on the use of the synthetic datasets for use of energy prediction of offshore wind farms.

2.5 Offshore wind Turbine Foundations

Offshore wind turbines gradually developed from the more known onshore-based turbines towards offshore locations for higher wind resources. A similar evolution had occurred with the foundations of these turbines as the systems progressed further from the shoreline. The depth in which the offshore wind farm system will be deployed is of importance when choosing a suitable foundation system because the typical cost of implementing the system increases significantly in proportion to depth, [53]. The sea depth may be classified into three regions: Shallow water depth (0 m – 30 m); transitional depth (30 m – 50 m) and deep water depth (50 m and greater), [54]. Offshore foundations for fixed systems are broken into six types of fixed foundations, shown in Figure 2-6, which are typically implemented in shallow and transitional depths, [54]–[56].

2.5.1 Gravity-Based Foundations

The gravity-based foundation systems were the first foundations to be used as wind turbines migrated from onshore to offshore. The systems are designed based on the self-weight of the turbine to be sufficiently able to resist the offshore forces and moments to allow for stability, [57]. The researchers from [58] also give a large review of the evolution of gravity-based foundation systems. This type of foundation is normally suited for shallow water depths, with the deepest wind farm being located in Blyth (UK) in a water depth of 35.5 m, [17], [59].

A comprehensive construction procedure was described in studies conducted by researchers in [59]. One of the deficiencies of the gravity-based foundation system is that the foundation requires identification of suitable bearing soil and levelling of the seabed soil before installation and the use of considerable scour protection around the substructure. The most recent generation of gravity-based foundations also requires a large onshore production and storage area including the required heavy lifting machinery to hoist the substructures for transportation and site installation, [56], [58], [60].

2.5.2 Monopile Foundations

Monopile foundations utilize a single large-diameter steel substructure that is anchored sufficiently in the seabed. The foundation is simple in design and manufacturing traditionally consists of joining circular steel sections onshore and more than one substructure can be transported on a single vessel. Due to the simplicity of the design, fabrication, transportation, and installation of the foundation; the monopile system has become the most common type of substructure which is being utilized in current offshore fixed base wind turbine farms. Connected to the substructure is another transitional cylinder

that carries secondary structures such as access ladders, work platforms, and boat landings. This type of foundation requires no prior preparation of the seabed and less scour protection, [56].

Monopile foundations are the most commonly used foundation methods for offshore wind farms in the European region and 63% of the operational offshore wind farms consist of these foundation systems as of 2018. Diaz and Soares also indicate that America utilizes this foundation method 100% of the time and Asia roughly 43%, however, it should be noted that this type of foundation method is best suited for shallow water depths, [17].

2.5.3 Suction Bucket Foundations

Suction bucket foundations or suction caisson foundations are sometimes divided into single and multiple designs, [57]. These systems are becoming increasingly used in offshore applications due to the convenience of transport and lower installation costs in comparison to the previous two foundation methods, [17]. The foundation represents an upside-down bucket that is gradually lowered into the soft seabed. The water is then pumped out creating a negative pressure which aids the mechanism to sink deeper into the seabed without too much external force being applied, [17], [57].

2.5.4 Tripod Foundations

The tripod foundation uses a central steel tube structure on top of a three-legged steel structure which is used to translate the loading of the wind turbine to the foundation. In comparison to that monopile foundations, Tripod foundations may be more stable in extreme weather conditions, [61], [17]. Oh, K.Y. et. Al. indicates that tripod foundations are more suited for transitional water depths as they provide the required bearing capacity which is needed for such systems, [53].

2.5.5 Lattice Jacket Foundations

The jacket foundation systems use a steel lattice jacket structure to support the top bearing load of a wind turbine. The lattice structure reduces the cross-sectional area of the foundations to reduce the impact of wave loading on the structure, [62], [63]. These types of structures are suitable for transitional water depths between 20 m and 50 m, [17], [62], [63]. This is the second most frequently used type of foundation structure for offshore wind turbines, [63].

2.5.6 High Rise Pile Cap (HRPC)

The response of the offshore structure is important when designing offshore wind farms. The soil properties of which fixed bottom offshore wind turbine structures are installed are also important concerning Poison's ratio; the shear modulus as well as the shear strength of the seabed soil, [53]. The HRPC system comprises a concrete top structure bearing the load and a configuration of steel piping that extends outwards as it descends into the depths of the [53] ocean, [17]. This type of offshore wind

foundation is predominantly located in Asia with all of Vietnam's offshore fleet utilizing these foundations, [64].

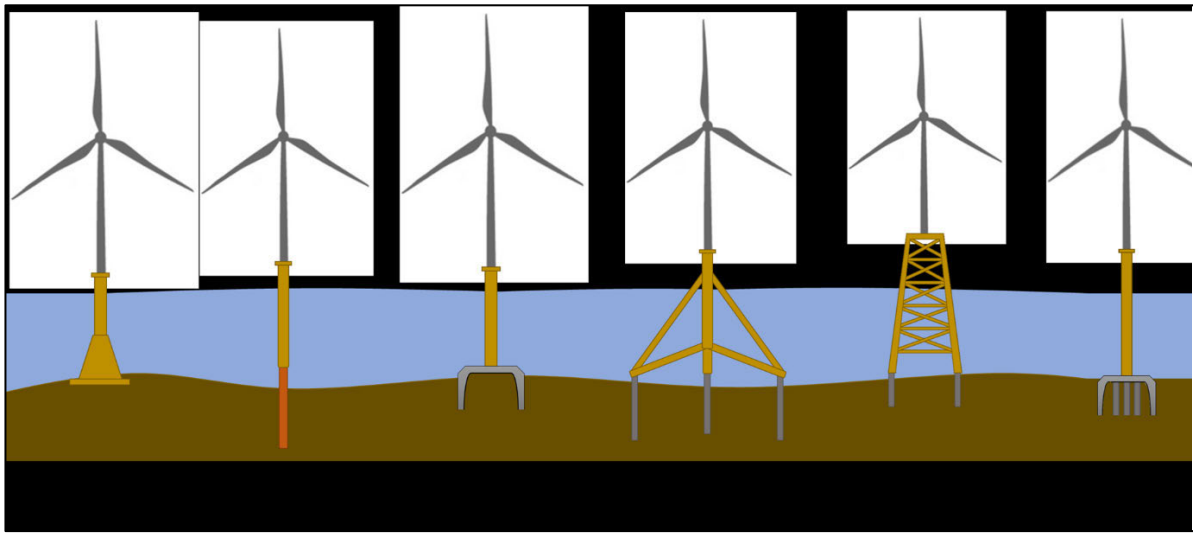

Figure 2-6: Fixed offshore foundations

The above foundations are suitable for shallow and transitional water depths and would be too costly to be developed for deeper waters due to the turbine requirements which would be higher than the highest wave height in the desired location, [57].

2.6 Floating Offshore Wind Platforms

Floating platforms are being investigated for deep water applications with water depths of greater than 100 m as some regions do not have suitable continental shelves for fixed bottom foundations as highlighted above. The developments are influenced by the oil and gas industry as it has made significant advancements for offshore platforms, however, there are some differences due to different aerodynamic and hydrodynamic loading forces of wind turbines on the platform structure.

Figure 2-7 illustrates the different types of floating offshore foundations available on the commercial market. The Dutch tri-floater consists of a semi-submersible tripod structure which achieves static stability by exploiting the buoyancy force mainly, which requires a large waterplane area. The spar buoy consists of a monopile structure that occupies a low waterplane area, which is ballasted with water or a solid ballast. This maintains the center of gravity below the center of buoyancy. Spar buoy floaters are traditionally stable due to the large draught. The tension leg platform (TLP) system consists of a submersible foundation that has a large buoyancy which is anchored via tension mooring lines. This creates the require restoring moment needed for stabilising the turbine during operation, [65].

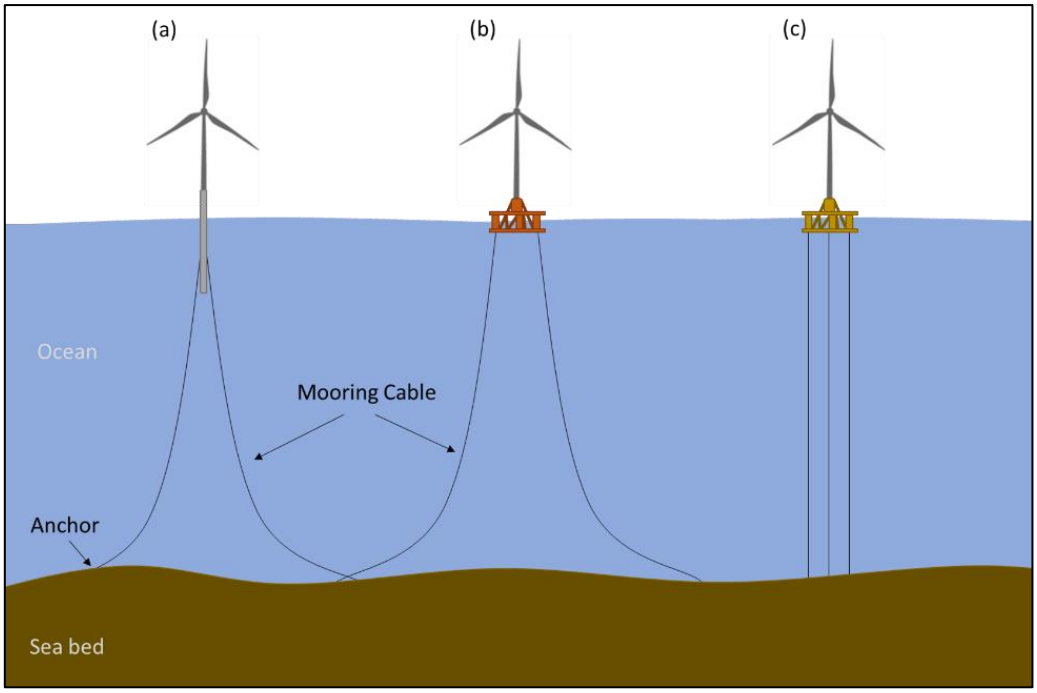

Figure 2-7: Floating offshore foundations: (a) Spar-Buoy; (b) Semi-submersible; (c) Tension leg

All of these types of foundations utilize mooring cables to the ocean floor with large mooring cables which are anchored to the sea floor. Some mooring lines are manufactured out of steel, some use a hybrid polyester or nylon line which may be taut or have slack allowing for natural movement in the ocean conditions, [66]. Figure 2-8 shows the different configurations of mooring lines that are used for floating offshore wind turbines. Figure 2-8 (a) shows a steel catenary configuration consisting of steel components, Figure 2-8 (b) is a taut configuration consisting of fibre and steel components and Figure 2-8 (c) is a hybrid configuration using counterweights and a buoy consisting of steel and fibre components. The steel components are usually steel wires or steel chains and the fibre components are usually polyesters or nylon fibres, [66].

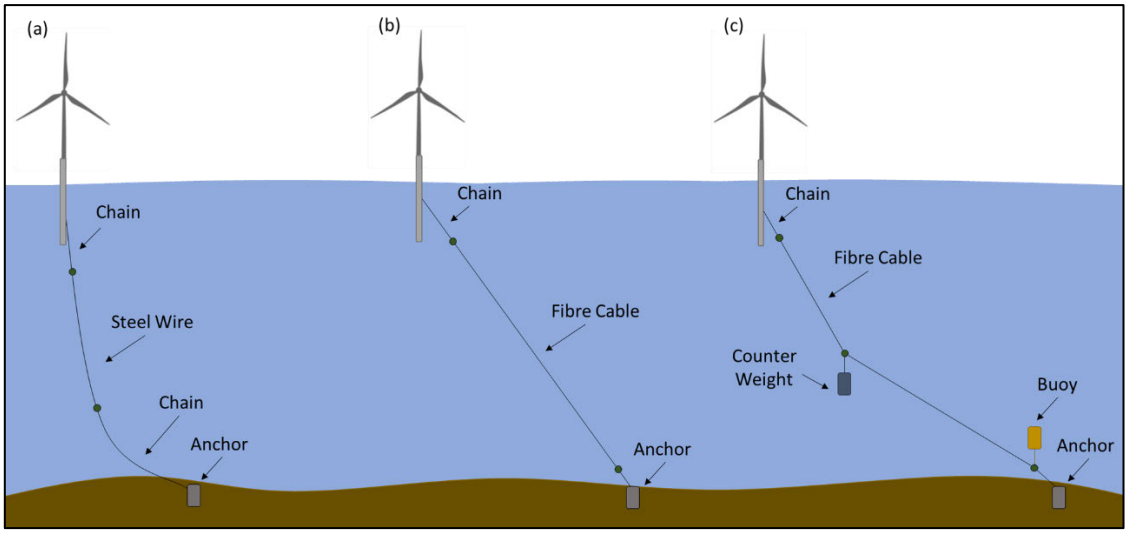

Figure 2-8: Mooring Line Configurations: (a) Catenary, (b) taut, (c) hybrid

For floating wind turbines, the cost and the stability of the systems as well as the scale of the farm are required to achieve a financially suitable solution for power generation in deep waters. As shown above, various mooring systems may be utilized for the tethering of the floating structure for stability, however, suitable anchors are also required for the entire system. There are traditional gravity-based anchors, anchor piles which are anchors that are piled into the seabed first, suction embedded anchors utilizing negative pressure with an anchor at the base of the system, dynamically installed torpedo anchors which are driven into the seabed, and drag embedded anchors which are also driven into the seabed and uses drag forces to maintain the stability of the floating structure, [57], [67], [68]. These are some of the many anchors which are used for floating applications within the oil and gas and floating wind turbine industry.

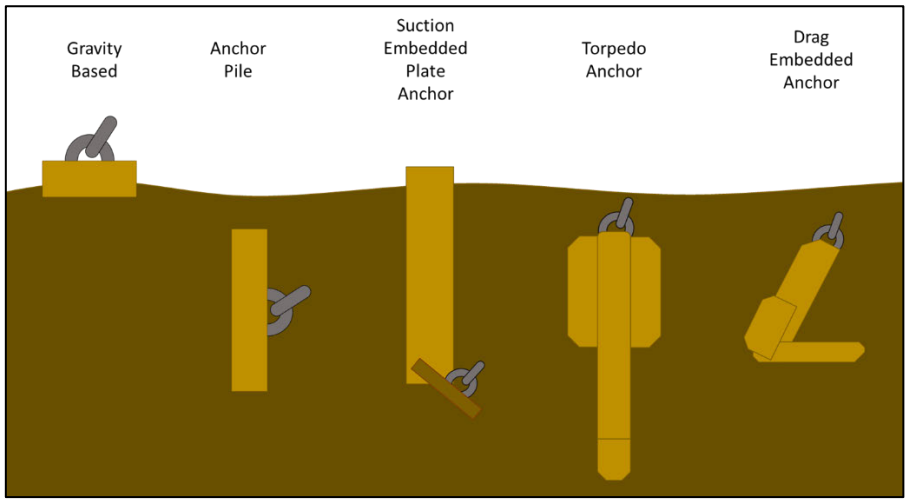

Figure 2-9: Types of Anchors for Floating Systems

2.7 Offshore Wind Energy Grid Integration Systems

The following section of the study highlights the different potential electrical collector components, systems, and configurations for offshore wind turbines to date. These types of systems are essential for evacuating the electrical power generation from the offshore site to onshore locations where it may be utilized within the respective electric grid.

Two main types of electrical transmission types exist for evacuation, both for onshore and offshore applications, of power generation. The following study aims to highlight a high-level overview of the offshore high voltage direct current (HVDC) and high voltage alternating current (HVAC) network architectures.

The individual wind turbines are interconnected via an internal reticulation network at lower alternating current (AC) voltages because the electrical output of each wind turbine is highly variable. The most common generator type of wind turbines, for offshore applications, is the doubly-fed induction generator (DFIG) due to its ability to operate under variable speeds, lower costs and losses in

comparison to other generator types, [69]. The stator of the offshore wind turbine generators is usually connected to a local rectifier which converts the power output to direct current (DC) and inverts the power back to AC at a stable network frequency within the local reticulation network, [70]. This configuration can be seen in Figure 2-10 below.

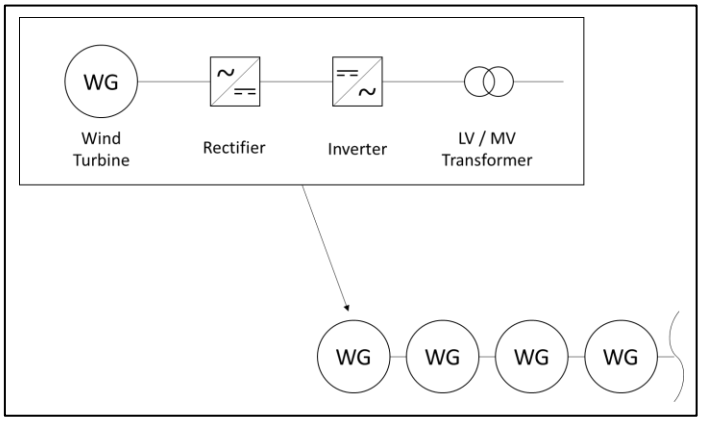

Figure 2-10: Wind Turbine Reticulation Network Architecture

2.7.1 HVAC

The HVAC system is the most traditional system being utilized for many years now for onshore applications as it allows for efficient transiting of electrical power from power generators (coal-fired power stations, nuclear stations, solar power stations, onshore wind power stations, etc.). Due to the mature nature of the system, connection to the onshore transmission grid may be achieved via traditional step-up transformers reducing the need for power electronic converters, [70]. The power is then transmitted to shore via subsea cables and collected at an onshore substation for grid integration as shown in Figure 2-11.

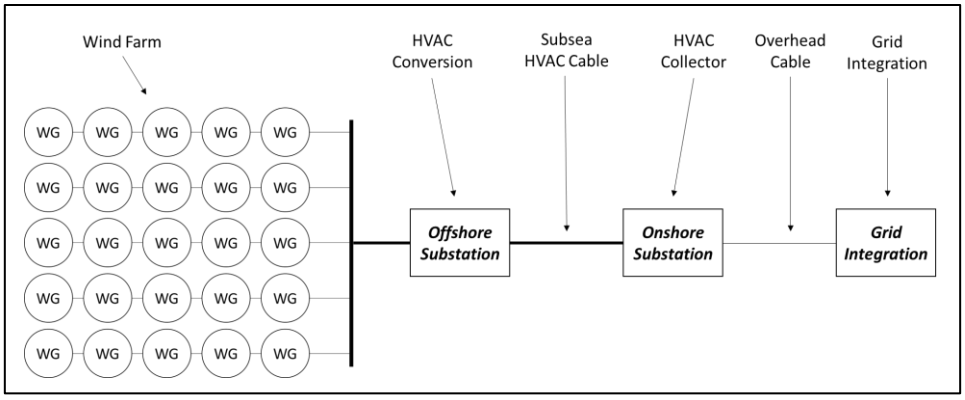

Figure 2-11: HVAC Grid Integration

The AC collection system works similarly to that of traditional AC grids onshore using an HVAC transmission network. At the point of the AC offshore substation, the power from the wind farm is collected and passes through a step-up transformer. The power is transmitted via HVAC subsea cables

to an onshore substation that collects and steps down the power to the same frequency and voltage of the electrical grid for integration.

2.7.2 HVDC

The HVDC system is a transmission method for evacuating power from the localized wind turbine farm to the onshore grid integration point. As offshore wind farms migrate further from onshore connection points, the HVDC transmission method becomes an attractive investment option, [71]. At an offshore substation, the AC collector uses a traditional step-up transformer, to step up the voltage, which is then converted to HVDC for power transmission to shore via subsea cables as shown in Figure 2-12.

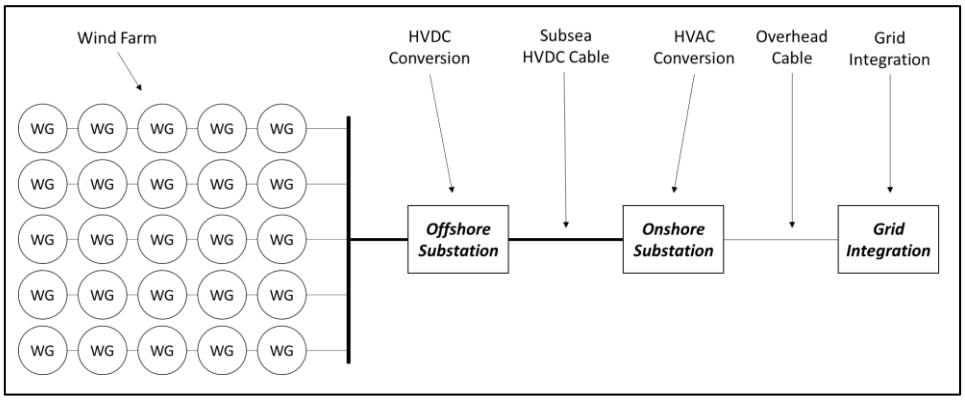

Figure 2-12: HVDC Grid Integration

The HVDC network architecture utilizes a step-up AC transformer at the offshore substation collector which then feeds into a controlled rectifier that transmits the HVDC power via subsea cable to an onshore substation collector. At this point, the HDVC passes through an inverter which is then collected into an AC step-down transformer which is integrated into the electrical grid.

There are two main types of HVDC transmission technology, the first which is the line commutated converter (LCC) and the second being voltage source converter (VSC). The LCC requires a compensator to support the voltage and reactive power that integrates to the offshore electrical common bus bar. The VSC though, does not need the reactive power compensation and has the added benefit of black-start capability, meaning it does not need conventional generation units to retrieve the electrical system, [72].

2.8 Offshore Wind Potential – South Africa

South Africa has undergone significant changes concerning renewable energy deployment in the country. The need for South Africa's energy diversification was conceived in the Department of Minerals and Energy (now Department of Mineral Resources and Energy – DMRE) White paper of 1998 which highlighted the need for primary energy diversification under objective 5 of the paper, [73].

This was further followed by the 2003 update to the paper which extended the diversification to cleaner energy generation in line with international commitments such as the Paris Accord, [74].

The Renewable Energy Independent Power Producer Procurement Program (REIPPPP) of South Africa, launched in 2011, has received international recognition for the program's success and lessons learned as a mechanism to stimulate private-public participation in the renewable sector, [75], [76]. Figure 2-13 depicts a map of the successful renewable energy plants from bid windows 1-4 of the REIPPP program, [77]. Concerning wind energy, the figure shows that the eastern and western cape regions have the most installed wind energy in the country.

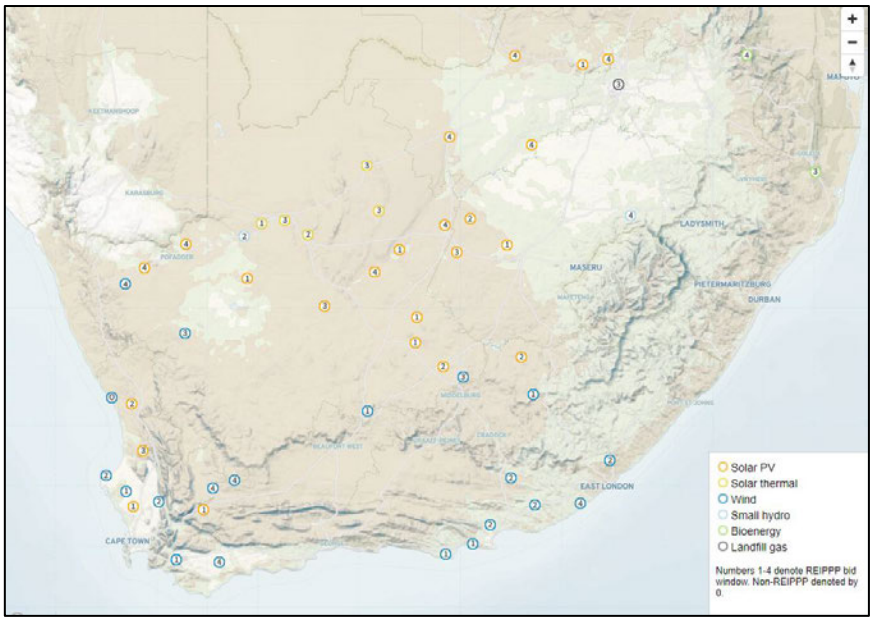

Figure 2-13: South African REIPPPP Technology Map, [77]

The REIPPPP and the Integrated Resource Plan (IRP) 2019 [78] do not yet accommodate offshore wind energy for South Africa as of yet. Cunden, K and Inambao, F.L had investigated the offshore wind resource potential for South Africa in [28] deep-sea locations. This was to understand the potential of floating offshore wind turbines and the benefits for coastal region energy supply.

The study had found that there is significant potential for the South African coastline along the eastern and western coasts shown as potential site locations in Figure 2-14. The ocean depth, of sites that were located 200 km to 500 km from shore, was found to be more than 2 km deep in some region which call for the need for floating offshore wind turbines. The deep water regions are due to the steep continental shelf which is found around South Africa. Studies conducted by researchers of [79] and [70] have shown that HVDC may be viable for grid integration of far offshore wind farms due to the advantages of HVDC compared to HVAC concerning the distance to shore.

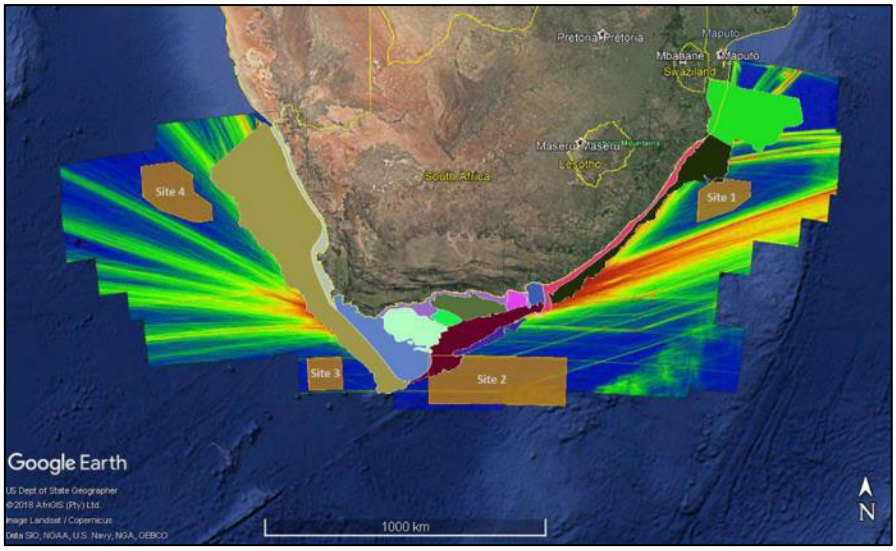

Figure 2-14: Identified Potential Site Locations, [28]

The site locations shown in Figure 2-14 have power densities ranging from 591 W/m^2 to a maximum of 1201 W/m^2 between hub height ranges of 100 m to 200 m, [28]. However, due to the current needs of the state, options that are roughly 100 km from the onshore connection may also be a suitable option for an offshore wind farm development. This would require permit clearance for the oil and gas blocks, clearance protocols for major shipping routes, existing fishing rights and environmental permitting required to name a few, [80], [81].

The turbines may lay along the coastal regions which can be coupled with the appropriate floating wind platforms as shown in Figure 2-7 and anchored to the ocean floor with a mooring system as shown in Figure 2-8 may assist in developing large-scale floating offshore wind farms. Choice of the best-suited anchor is required as shown in Figure 2-9 above. The study of the soil structure at various anchor levels is required to ensure the wind farm is harnessed to the seabed during rough sea conditions. This also requires a complex hydrodynamic study of the oceanic forces, induced resonance, and acoustic vibrations on the mounting structure and rotating body.

2.9 Conclusion

The following study aimed to review the key components of the offshore wind industry for a case study of South Africa. The study examined the differences between turbine configurations such as HAWT and VAWT designs turbines. The types of foundations were also examined for an offshore application for fixed and floating offshore wind turbines and the requirements for each of the configurations. The power evacuation network architecture was also investigated and comparisons of HVAC to HVDC were conducted. Studies conducted by [28] show the offshore wind resource potential for South Africa as well as potential sites along the eastern and western coastline of the country.

2.10 Future Work

Future work will include geotechnical research requires to be conducted per potential site to understand the grain structure, soil composition, and ocean hydrodynamics to design a suitable offshore platform and mooring system for the wind farm. The examination also is required of the onshore grid connection points and the availability of capacity of the regional network for grid integration of the offshore wind farm.

2.11 References

[1] M. L. Parry, O. F. Canziani, J. P. Palutikof, P. J. van der Linden, and C. E. Hanson, "IPCC, 2007: Climate Change 2007: Impacts, Adaptation and Vulnerability. Contribution of Working Group II to the Fourth Assessment Report of the Intergovernmental Panel on Climate Change," Cambridge, UK, 2007.

[2] J. Huang and M. B. McElroy, "A 32-year perspective on the origin of wind energy in a warming climate," *Renew Energy*, vol. 77, pp. 482–492, 2015, doi: https://doi.org/10.1016/j.renene.2014.12.045.

[3] W. Wang, X. Huang, L. Tan, J. Guo, and H. Liu, "Optimization design of an inductive energy harvesting device forwireless power supply system overhead high-voltage power lines," *Energies (Basel)*, vol. 9, no. 4, pp. 1–16, 2016, doi: 10.3390/en9040242.

[4] Y. Kumar *et al.*, "Wind energy: Trends and enabling technologies," *Renewable and Sustainable Energy Reviews*, vol. 53, pp. 209–224, 2016, doi: https://doi.org/10.1016/j.rser.2015.07.200.

[5] A. Benazzouz, H. Mabchour, K. El Had, B. Zourarah, and S. Mordane, "Offshore Wind Energy Resource in the Kingdom of Morocco: Assessment of the Seasonal Potential Variability Based on Satellite Data," *J Mar Sci Eng*, vol. 9, no. 1, 2021, doi: 10.3390/jmse9010031.

[6] British Petroleum (BP), "Statistical Review of World Energy 2021," 2021.

[7] IEA, "Renewables 2020 - Analysis and Forecast 2025," 2020.

[8] IEA, "Main remuneration schemes supporting forecast wind capacity additions 2020-2025," Paris, 2020.

[9] K. Umoh and M. Lemon, "Drivers for and barriers to the take up of floating offshore wind technology: A comparison of Scotland and South Africa," *Energies (Basel)*, vol. 13, no. 21, 2020, doi: 10.3390/en13215618.

[10] IRENA, "Renewable capacity statistics 2021," International Renewable Energy Agency, 2021.

[11] J. K. Kaldellis and M. Kapsali, "Shifting towards offshore wind energy—Recent activity and future development," *Energy Policy*, vol. 53, pp. 136–148, 2013, doi: https://doi.org/10.1016/j.enpol.2012.10.032.

[12] IRENA, "Renewable Power Generation Costs in 2018," Abu Dhabi, 2019.

[13] IRENA, *Renewable Power Generation Costs in 2020*. Abu Dhabi, 2021.

[14] R. James and M. C. Ros, “Floating Offshore Wind: Market and Technology Reveiw,” United Kingdom: Edinburgh, 2015.

[15] A. Moore, J. Price, and M. Zeyringer, “The role of floating offshore wind in a renewable focused electricity system for Great Britain in 2050,” *Energy Strategy Reviews*, vol. 22, pp. 270–278, 2018, doi: https://doi.org/10.1016/j.esr.2018.10.002.

[16] M. Hannon, E. Topham, J. Dixon, D. McMillan, and M. Collu, “Offshore Wind, Ready to Float? Global and UK Trends in the Floating Offshore Wind Market,” 2019. doi: 10.17868/69501.

[17] H. Díaz and C. Guedes Soares, “Review of the current status, technology and future trends of offshore wind farms,” *Ocean Engineering*, vol. 209, p. 107381, 2020, doi: https://doi.org/10.1016/j.oceaneng.2020.107381.

[18] S. Loughney, J. Wang, M. Bashir, M. Armin, and Y. Yang, “Development and application of a multiple-attribute decision-analysis methodology for site selection of floating offshore wind farms on the UK Continental Shelf,” *Sustainable Energy Technologies and Assessments*, vol. 47, p. 101440, 2021, doi: https://doi.org/10.1016/j.seta.2021.101440.

[19] B. Mendela *et al.*, “Operational offshore wind farms and associated ship traffic cause profound changes in distribution patterns of Loons (Gavia spp.),” *J Environ Manage*, vol. 231, pp. 429–438, 2019, doi: https://doi.org/10.1016/j.jenvman.2018.10.053.

[20] E. T. Methratta, “Monitoring fisheries resources at offshore wind farms: BACI vs. BAG designs,” *ICES Journal of Marine Science*, vol. 77, no. 3, pp. 890–900, 2020, doi: 10.1093/icesjms/fsaa026.

[21] S. S. Kulkarni and D. J. Edwards, “A bibliometric review on the implications of renewable offshore marine energy development on marine species,” *Aquac Fish*, 2021, doi: https://doi.org/10.1016/j.aaf.2021.10.005.

[22] TGS Company, “4C Offshore,” 2019. https://www.4coffshore.com/

[23] L. G. Morgan, E.C.; Lackner, M.; Vogel, R.M.; Baise, “Probability distributions for offshore wind speeds,” *Energy Convers Manag*, vol. 52, pp. 15–26, 2011.

[24] R. M. Pichugina, Y.L.; Banta, R.M.; Brewer, W.A.; Sandberg, S.P.; Hardesty, “Doppler lidar–based wind-profile measurement system for offshore wind-energy and other marine boundary layer applications,” *Applied Meteorological Climatology*, vol. 51, pp. 327–349, 2012.

[25] A. Fernández-Guillamón, K. Das, N. A. Cutululis, and Á. Molina-García, “Offshore wind power integration into future power systems: Overview and trends,” *J Mar Sci Eng*, vol. 7, no. 11, 2019, doi: 10.3390/jmse7110399.

[26] M. D. Esteban, J. J. Diez, J. S. López, and V. Negro, “Why offshore wind energy?,” *Renew Energy*, vol. 36, no. 2, pp. 444–450, 2011, doi: https://doi.org/10.1016/j.renene.2010.07.009.

[27] H. S. Bagiorgas, G. Mihalakakou, S. Rehman, and L. M. Al-hadhrami, “Offshore wind speed and wind power characteristics for ten locations in Aegean and Ionian Seas,” *Journal of Earth System Science*, vol. 121, no. 4, pp. 975–987, 2012, doi: 10.1007/s12040-012-0203-9.

[28] F. L. Inambao and K. Cunden, “Offshore wind resource assessment off the South African coastline,” *International Journal of Mechanical Engineering and Technology (IJMET)*, 2019.

[29] A. Badger, M.; Badger, J.; Nielsen, M.; Hasager, C.B.; Peña, “Wind class sampling of satellite SAR imagery for offshore wind resource mapping,” *Applied Meteorological Climatology*, vol. 49, pp. 2474–2491, 2010.

[30] F. Pisanò, “Input of advanced geotechnical modelling to the design of offshore wind turbine foundations,” in *XVII European Conference on Soil Mechanics and Geotechnical Engineering*, Reykjavik, 2019. doi: 10.32075/17ECSMGE-2019-1109.

[31] Z. O’Hanlon and V. Cummins, “A comparative insight of Irish and Scottish regulatory frameworks for offshore wind energy – An expert perspective,” *Mar Policy*, vol. 117, p. 103934, 2020, doi: https://doi.org/10.1016/j.marpol.2020.103934.

[32] Y. Wei, Q.-P. Zou, and X. Lin, “Evolution of price policy for offshore wind energy in China: Trilemma of capacity, price and subsidy,” *Renewable and Sustainable Energy Reviews*, vol. 136, p. 110366, 2021, doi: https://doi.org/10.1016/j.rser.2020.110366.

[33] D. MacKinnon, A. Karlsen, S. Dawley, M. Steen, S. Afewerki, and A. Kenzhegaliyeva, “Legitimation, institutions and regional path creation: a cross-national study of offshore wind,” *Reg Stud*, pp. 1–12, Jan. 2021, doi: 10.1080/00343404.2020.1861239.

[34] W. D. Musial and J. Beiter, Philipp C. Nunemaker, “Cost of Floating Offshore Wind Energy Using New England Aqua Ventus Concrete Semisubmersible Technology,” Orono, ME, 2020. doi: https://doi.org/10.2172/1593700.

[35] Wang, Zekun and Zhang, Fuxi, “The Development and Tendency of Current Off-Shore Wind Power Plant All over the World,” *E3S Web Conf.*, vol. 194, p. 2004, 2020, doi: 10.1051/e3sconf/202019402004.

[36] M. Shields, P. Beiter, J. Nunemaker, A. Cooperman, and P. Duffy, “Impacts of turbine and plant upsizing on the levelized cost of energy for offshore wind,” *Appl Energy*, vol. 298, p. 117189, 2021, doi: https://doi.org/10.1016/j.apenergy.2021.117189.

[37] S. Eriksson, H. Bernhoff, and M. Leijon, “Evaluation of different turbine concepts for wind power,” *Renewable and Sustainable Energy Reviews*, vol. 12, no. 5, pp. 1419–1434, 2008, doi: https://doi.org/10.1016/j.rser.2006.05.017.

[38] H. Akimoto, K. Tanaka, and K. Uzawa, “Floating axis wind turbines for offshore power generation{\textemdash}a conceptual study,” *Environmental Research Letters*, vol. 6, no. 4, p. 44017, Oct. 2011, doi: 10.1088/1748-9326/6/4/044017.

[39] M. Borg, A. Shires, and M. Collu, “Offshore floating vertical axis wind turbines, dynamics modelling state of the art. part I: Aerodynamics,” *Renewable and Sustainable Energy Reviews*, vol. 39, pp. 1214–1225, 2014, doi: https://doi.org/10.1016/j.rser.2014.07.096.

[40] V. L. OKULOV and J. N. SØRENSEN, “Maximum efficiency of wind turbine rotors using Joukowsky and Betz approaches,” *J Fluid Mech*, vol. 649, pp. 497–508, 2010, doi: DOI: 10.1017/S0022112010000509.

[41] P. Lecanu, J. Breard, D. Mouaze, and B. Smorgrav, “Theoretical Calculation of Wind (Or Water) Turbine: Extending the Betz Limit,” *Preprints (Basel)*, 2021.

[42] F. L. Inambao and K. Cunden, “Design and Numerical Simulation of a Small Scale Helical Cross Flow Turbine,” in *13th BIE Biennial Conference*, Gaborone, Botswana: Botswana Institution of Engieers, 2013, pp. 23–32.

[43] K. Cunden, “Design of a Novel Hydrokinetic Turbine for Ocean Current Power Generation,” University of Kwa-Zulu of Natal, 2015.

[44] F. L. Inambao and K. Cunden, “Offshore Vertical Axis Wind Turbine Simulation,” *International Journal of Mechanical and Production Engineering Research and Development*, vol. 11, no. 2, pp. 187–204, 2021.

[45] P. Sharma, B. Gupta, M. Pandey, A. K. Sharma, and R. Nareliya Mishra, “Recent advancements in optimization methods for wind turbine airfoil design: A review,” *Mater Today Proc*, vol. 47, pp. 6556–6563, 2021, doi: https://doi.org/10.1016/j.matpr.2021.02.231.

[46] H. J. Sutherland, D. E. Berg, and T. D. Ashwill, “A retrospective of VAWT technology,” California, 2012.

[47] D. T. Griffith *et al.*, “Design Studies for Deep-Water Floating Offshore Vertical Axis Wind Turbines,” Alburquerque, New Mexico, 2018.

[48] S. Balluff, J. Bendfeld, and S. Krauter, “Short term wind and energy prediction for offshore wind farms using neural networks,” in *2015 International Conference on Renewable Energy Research and Applications (ICRERA)*, IEEE, Nov. 2015, pp. 379–382. doi: 10.1109/ICRERA.2015.7418440.

[49] J. Olauson and M. Bergkvist, “Modelling the Swedish wind power production using MERRA reanalysis data,” *Renew Energy*, vol. 76, pp. 717–725, Apr. 2015, doi: 10.1016/j.renene.2014.11.085.

[50] I. Staffell and S. Pfenninger, “Using bias-corrected reanalysis to simulate current and future wind power output,” *Energy*, vol. 114, pp. 1224–1239, Nov. 2016, doi: 10.1016/j.energy.2016.08.068.

[51] U. Cali, N. Erdogan, S. Kucuksari, and M. Argin, “Techno-economic analysis of high potential offshore wind farm locations in Turkey,” *Energy Strategy Reviews*, vol. 22, pp. 325–336, Nov. 2018, doi: 10.1016/j.esr.2018.10.007.

[52] M. A. Hassoine, F. Lahlou, A. Addaim, and A. A. Madi, “Improved Design of a Large Offshore Wind Farm by Using Biogeography based Optimization,” *International Journal of Renewable Energy Research*, vol. 11, no. 2, Jun. 2021, doi: 10.20508/ijrer.v11i2.12036.g8199.

[53] K.-Y. Oh, W. Nam, M. S. Ryu, J.-Y. Kim, and B. I. Epureanu, “A review of foundations of offshore wind energy convertors: Current status and future perspectives,” *Renewable and Sustainable Energy Reviews*, vol. 88, pp. 16–36, 2018, doi: https://doi.org/10.1016/j.rser.2018.02.005.

[54] W. Musial and S. Butterfield, “Future for Offshore Wind Energy in the United States,” in *EnergyOcean*, Florida, USA: National Renewable ENergy Laboratory (NREL), 2004.

[55] B. C. O'Kelly and M. Arshad, "Offshore wind turbine foundations – analysis and design," C. Ng and L. B. T.-O. W. F. Ran, Eds., Woodhead Publishing, 2016, pp. 589–610. doi: https://doi.org/10.1016/B978-0-08-100779-2.00020-9.

[56] A. Mathern, C. von der Haar, and S. Marx, "Concrete support structures for offshore wind turbines: Current status, challenges, and future trends," *Energies (Basel)*, vol. 14, no. 7, 2021, doi: 10.3390/en14071995.

[57] X. Wu *et al.*, "Foundations of offshore wind turbines: A review," *Renewable and Sustainable Energy Reviews*, vol. 104, pp. 379–393, 2019, doi: https://doi.org/10.1016/j.rser.2019.01.012.

[58] M. D. Esteban, J.-S. López-Gutiérrez, and V. Negro, "Gravity-Based Foundations in the Offshore Wind Sector," *J Mar Sci Eng*, vol. 7, no. 3, 2019, doi: 10.3390/jmse7030064.

[59] P. Mengé, "Gravity Base Foundations for the Wind Turbines on the Thorntonbank@Belgium," 2008.

[60] M. D. Esteban, B. Couñago, J. S. López-Gutiérrez, V. Negro, and F. Vellisco, "Gravity based support structures for offshore wind turbine generators: Review of the installation process," *Ocean Engineering*, vol. 110, no. June 2018, pp. 281–291, 2015, doi: 10.1016/j.oceaneng.2015.10.033.

[61] D. Kwag, M. Oh, Os. Kwon, and S. Bang, "Field Installation Tests of Monopod Suction Pile and Tripod Suction Buckets," in International Conference on Offshore Mechanics and Arctic Engineering, vol. Volume 6: 2013. doi: 10.1115/OMAE2013-10100.

[62] K. E. Thomsen, *Offshore Wind: A comprehensive guide to successful offshore wind farm installation*, Second Edi. Tranbjerg, Denmark: Elsevier, 2014.

[63] O. M. H. C, M. Shadman, M. M. Amiri, C. Silva, S. F. Estefen, and E. La Rovere, "Environmental impacts of offshore wind installation, operation and maintenance, and decommissioning activities: A case study of Brazil," *Renewable and Sustainable Energy Reviews*, vol. 144, p. 110994, 2021, doi: https://doi.org/10.1016/j.rser.2021.110994.

[64] C. Y. Li *et al.*, "Construction technology of high-rise pile cap foundation of offshore wind power in Taiwan Strait," in *Earth and Environmental Science*, IOP Publishing, 2017, pp. 1–8. doi: doi:10.1088/1755-1315/93/1/012037.

[65] A. Ghigo, L. Cottura, R. Caradonna, G. Bracco, and G. Mattiazzo, "Platform Optimization and Cost Analysis in a Floating Offshore Wind Farm," *J Mar Sci Eng*, vol. 8, no. 11, p. 835, Oct. 2020, doi: 10.3390/jmse8110835.

[66] H. Haslum, "OW CoE and SubseaUK Mooring and Anchoring Systems Webinar," Global Underwater Hub, 2020.

[67] A. C. Lowmass, "Installation and keying of follower embedded plate anchors," University of Western Australia, 2006.

[68] Y. Ming, A. C. P., and M. J. D., "Behavior of Suction Embedded Plate Anchors during Keying Process," *Journal of Geotechnical and Geoenvironmental Engineering*, vol. 138, no. 2, pp. 174–183, Feb. 2012, doi: 10.1061/(ASCE)GT.1943-5606.0000582.

[69] D. Das, J. Pan, and S. Bala, "HVDC Light for large offshore wind farm integration," in *2012 IEEE Power Electronics and Machines in Wind Applications*, IEEE, Jul. 2012, pp. 1–7. doi: 10.1109/PEMWA.2012.6316363.

[70] S. Rahman, I. Khan, H. I. Alkhammash, and M. F. Nadeem, "A comparison review transmission mode for onshore integration of offshore wind farms: HVDC or HVAC—A comparison review," *Electronics (Switzerland)*, vol. 10, no. 12, pp. 1–15, 2021, doi: 10.3390/electronics10121489.

[71] Y. A. Sultan, S. S. Kaddah, and A. A. Eladl, "VSC-HVDC system-based on model predictive control integrated with offshore wind farms," *IET Renewable Power Generation*, vol. 15, no. 6, pp. 1315–1330, Apr. 2021, doi: 10.1049/rpg2.12109.

[72] N. Flourentzou, V. G. Agelidis, and G. D. Demetriades, "VSC-Based HVDC Power Transmission Systems: An Overview," *IEEE Trans Power Electron*, vol. 24, no. 3, pp. 592–602, Mar. 2009, doi: 10.1109/TPEL.2008.2008441.

[73] Department of Minerals and Energy, "White Paper on the Energy Policy of the Republic of South Africa," Pretoria, 1998.

[74] Department of Minerals and Energy, "White Paper on Renewable Energy," Pretoria, 2003.

[75] A. Eberhard, J. Kolker, and J. Leigland, "South Africa's Renewable Energy IPP Procurement Program: Success Factors and Lessons," Washington, DC., 2014.

[76] T. Z. Bischof-Niemz, C. Mushwana, and D. B. K. Milazi, "Success of the REIPPPP and potential future considerations," in *The Sustainability Energy Resource Handbook*, 2016, pp. 20–29.

[77] energyblog, “Utility-scale Renewable Energy Generation Sites - South Africa.” https://www.energy.org.za/map-south-african-generation-projects (accessed Dec. 01, 2021).

[78] Department of Mineral Resources and Energy, “Integrated Resource Plan (IRP2019),” 2019.

[79] M. P. ; Bahrman and B. K. Johnson, “The ABCs of HVDC transmission technologies,” *IEEE Power Energy Mag*, vol. 5, no. 2, pp. 32–44, 2007, doi: 10.1109/MPAE.2007.329194.

[80] R. C. Spijkerboer, C. Zuidema, T. Busscher, and J. Arts, “The performance of marine spatial planning in coordinating offshore wind energy with other sea-uses: The case of the Dutch North Sea,” *Mar Policy*, vol. 115, p. 103860, May 2020, doi: 10.1016/j.marpol.2020.103860.

[81] H. Obane, Y. Nagai, and K. Asano, “Assessing the potential areas for developing offshore wind energy in Japanese territorial waters considering national zoning and possible social conflicts,” *Mar Policy*, vol. 129, p. 104514, Jul. 2021, doi: 10.1016/j.marpol.2021.104514.

CHAPTER 3 : OFFSHORE WIND RESOURCE ASSESSMENT OFF THE SOUTH AFRICAN COASTLINE

The following chapter presents the offshore wind resource for South Africa. The article covers a literature review and methodology of meteorological analysis for the offshore resource including saliant factors such as shipping routes and oil and gas fields. The article shows consists of synthetic meteorological, from WAsP extrapolations, of data of 624 data points with three (3) hub heights of 0 m, 50 m and 200 m which was then refined down to the identified sites. The research also gives insight into possible grid connection points and the level of connection which requires to be considered.

CHAPTER 3 – **Cite this article:** F.L. Inambao and K. Cunden, "**Offshore Wind Resource Assessment Off the South African Coastline**" published in the International Journal of Mechanical Engineering and Technology (IJMET), Vol. 10, Issue 6, June 2019, pp 95-119.

Link to article:

https://iaeme.com/MasterAdmin/Journal_uploads/IJMET/VOLUME_10_ISSUE_6/IJMET_10_06_006.pdf

International Journal of Mechanical Engineering and Technology (IJMET)
Volume 10, Issue 06, June 2019, pp. 95-119 . Article ID: IJMET_10_06_006
Available online at http://www.iaeme.com/ijmet/issues.asp?JType=IJMET&VType=10&IType=6
ISSN Print: 0976-6340 and ISSN Online: 0976-6359

OFFSHORE WIND RESOURCE ASSESSMENT OFF THE SOUTH AFRICAN COASTLINE

Freddie L. Inambao and Kumaresan Cunden
School of Mechanical Engineering, University of Kwa-Zulu Natal
Durban, South Africa

ABSTRACT

The world is undergoing a paradigm shift as more people are becoming aware of energy consumption patterns, reinforcing the need for developing cleaner and more sustainable ways to generate electrical energy. Globally, the development of onshore wind farms is sometimes impeded by factors such as aesthetic impact, acceptance by the public, the threats to surrounding biodiversity, noise from the power plant and possible land use conflicts. Due to these concerns, offshore wind plants have been developed. Offshore wind energy is generally greater in comparison to that of onshore wind energy because the wind speeds offshore are generally higher and more constant with fewer obstructions to the wind resource. The offshore wind potential for South African coastal regions was investigated and analysed in this study. Various factors such as shipping routes, oil and gas exploration fields and possible transmission connection points were taken into consideration before selecting four data collection sites. The predominant wind direction, mean wind speed, wind shear and spatial geographic information was analysed for each site. The sites' wind direction did not have any similarities, with each site having its own prevailing wind directions. Within the 50 m hub height, Site 2 showed the best potential based on the power density. Site 1 and Site 3 showed similar power densities to each other with Site 4 showing the lowest power density. The distance to shore ranged from 200 km to 500 km with a steep continental shelf drop to a depth of approximately 3 000 m. The study conducted shows that there is offshore wind potential off the coast of South Africa. Energy generated by this method could assist South Africa to increase access to energy, reduce expensive transmission line losses to coastal provinces, and assist the country to transition towards a more sustainable future energy mix in line with developed nations.

Keywords: Offshore wind, Resource Assessment, WAsP.

Cite this Article: Freddie L. Inambao and Kumaresan Cunden, Offshore Wind Resource Assessment Off the South African Coastline, *International Journal of Mechanical Engineering and Technology*, 10(6), 2019, pp. 95-119.
http://www.iaeme.com/IJMET/issues.asp?JType=IJMET&VType=10&IType=6

1. INTRODUCTION

The world is undergoing a paradigm shift as more people are becoming aware of energy consumption patterns, reinforcing the need for cleaner ways to generate electrical energy. The International Renewable Energy Agency (IRENA) is an intergovernmental organisation which supports countries in their efforts to attain a more sustainable energy future. Figure 1 was constructed using IRENA's Renewable Energy Statistics databases [1]. The trend in Figure 1 indicates rapid growth in the installed renewable energy capacity over the past decade across all renewable resources.

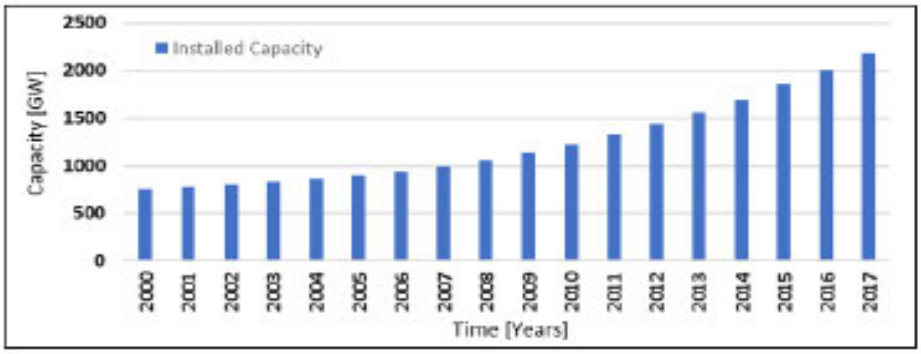

Figure 1 Total global renewable energy installed capacity

During the first five years of the millennium the European market dominated the renewable energy portfolio. However, the Asian and the North American markets have now gained significant market share. Figure 2 depicts the evolution of the renewable energy capacity market share across the major continents of the world. Asia has now taken the lead with the most installed renewable capacity comprising 39.85 % (204.6 GW) of the market in comparison to the Europeans with 33.2 % (170.6 GW) [1].

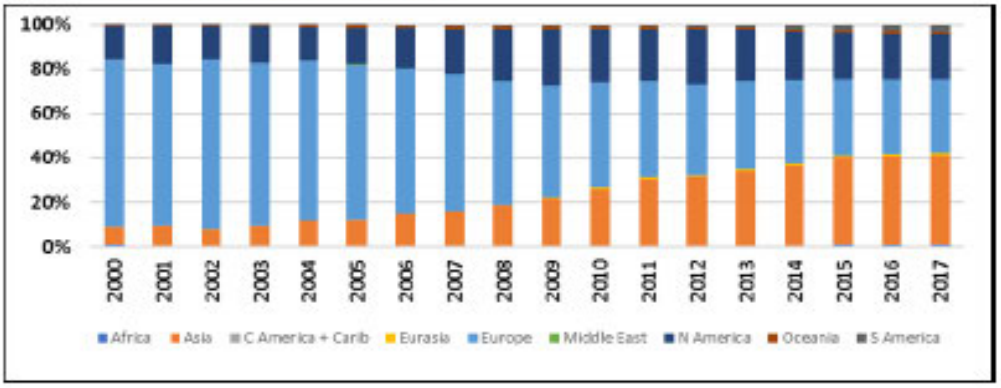

Figure 2 Market share of renewable capacity 2000-2016

Onshore wind and solar photovoltaic (PV) technologies have experienced the largest amount of growth over the last decade in relation to other renewable technologies, as seen in Figure 3 [1]. This can be attributed to the maturity of technologies and rapid advancements in the respective fields of study, as well as the ease of deployment in comparison to larger thermal plants such as bioenergy and geothermal power plants.

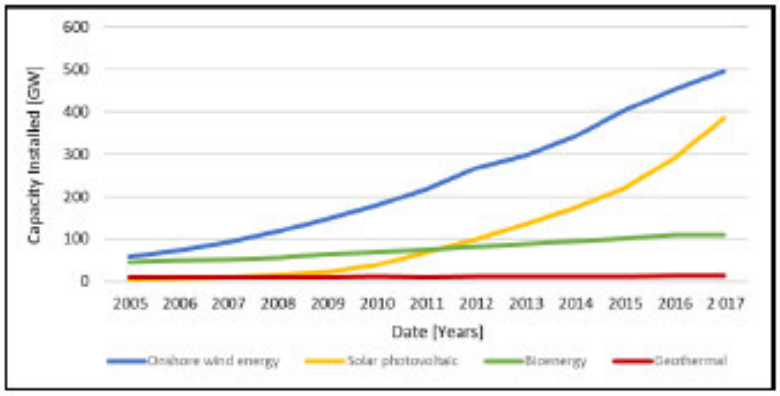

Figure 3 Renewable energy technology growth

In many regions of the world, the development of onshore wind farms are sometimes impeded by factors such as visual impact, acceptance by the public, threats to the surrounding biodiversity, noise from the power plant and possible land use conflicts [2]. The multiple permutations of these conflicts are likely to hinder the future development of onshore wind farms. Due to these possible future impacts, as well as the added benefit of increased specific production (1) (kWh/kWp), major developments in the world are moving towards offshore wind farms [3, 4].

The potential of offshore wind energy is greater than that of onshore wind energy. This is because the wind speeds found offshore are generally higher and more constant with less obstructions to the wind resource. Added to this, there are the fewer concerns regarding noise pollution, aesthetic imact and most other types of land-based turbine restrictions [5]. The development of offshore windfarms has led to an increase in turbine swept areas from larger turbine blades resulting in an increase in generator capacity harvesting more energy per square meter. Though the advantages are numerous, some of the disadvantages of offshore wind energy development include expensive marine foundations and the high costs of onshore electrical grid integration [3]. For the purpose of comparison, Figure 4 shows the contribution of energy produced by both areas of supply, normalised by the installed capacity during that period.

Europe contributes a large amount to the growth of offshore wind installations because of limited land area available for onshore developments [6], [7]. The largest offshore wind farm in the United Kingdom was commissioned in 2012 and is the London Array, consisting of a total of 630 MW of generation capacity. A further 370 MW is planned for phase 2 development [8]. China's first commercial offshore wind project is located close to the Donghai Bridge in Shanghai totalling 102 MW in capacity with grid supply since June 2010 [9], [10].

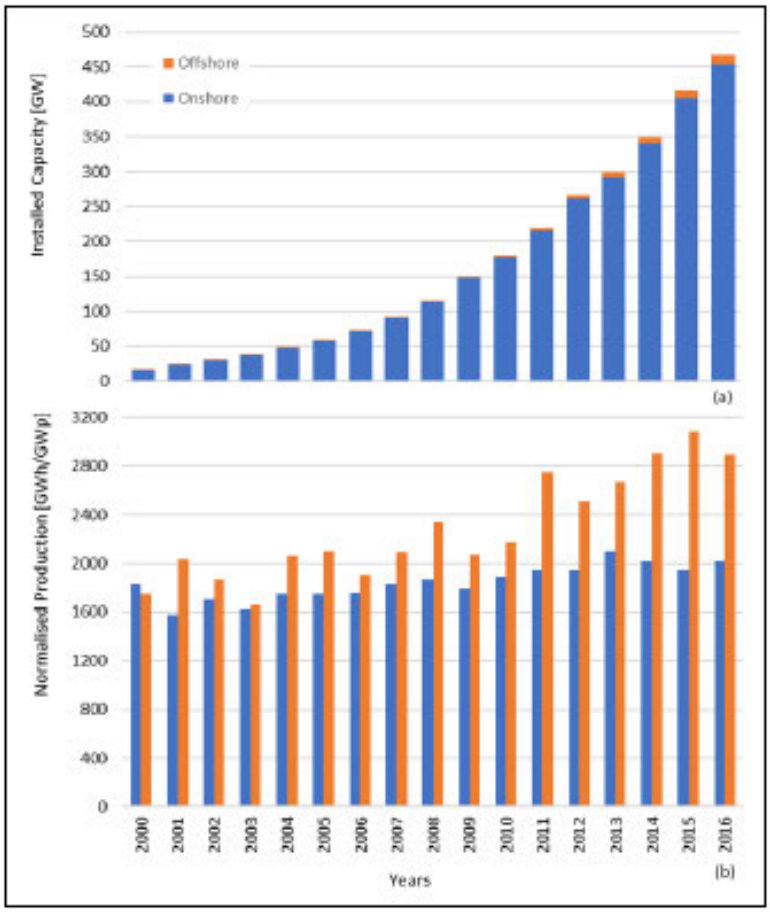

Figure 4 (a) Installed capacity; (b) Normalised production

This paper aims to evaluate offshore wind energy potential for the development of a conceptual offshore wind energy power plant facility off the South African coast. The investigation aims to understand the average wind speed, dominant wind direction and wind shear effects of particular locations in the region. Shipping routes and relevant bathymetry will be investigated to better understand the environmental conditions which need to be overcome before development of an offshore wind farm.

2. LITERATURE REVIEW

Before developing the methodology for the offshore wind resource evaluation, an understanding of best practice was required. Murthy and Rahi [11] conducted a review of offshore wind energy assessments regarding the main characteristics required for a resource assessment. Their work outlined the various methodologies used for wind power projects and the uncertainties associated with wind energy assessments. The paper gave a basic understanding of wind behaviour through periods of change (diurnal, seasonal, monthly and annual). The authors state that a minimum data log of 1 meteorological year is required for an assessment, however, more data would lead to a more accurate estimation of energy potential for the given region.

Sharma and Ahmed [12] conducted research on the wind energy potential for the Fiji islands of Kadavu and the Suva Peninsula. The authors gathered mean wind speeds and predominant wind directions for each site based on 18 month and 12 month investigation periods respectively. Wind shear effects were also investigated to understand the variation of shear

force with respect to height. The authors utilised the WAsP simulation tool to simulate a high resolution (5 km^2) resource map for both regions. The result of the simulations showed a good potential for wind energy production.

Lima et al. [13] sought to estimate the offshore wind energy potential for Ceara in Brazil in an effort to increase the maturity of the offshore wind energy sector. The study utilised the Regional Atmospheric Modeling System (RAMS) to estimate the average wind speed, direction and power density for the area. The study considered the bathymetry and the shipping traffic for the Ceara region. The authors evaluated the average wind speed for three periods consisting of El Nina, El Ninõ and Neutral years, each of which were evaluated through seasonal changes. The results showed an average wind speed of 8 m/s and a power density of roughly 720 W/m^2 no matter what the period.

Werapun et al. [5] conducted an offshore energy potential study for southern Thailand. The study followed a similar methodology to the previous authors' utilising a 120m high meteorological mast measuring data at different heights along the mast. The average wind speed was seemingly low (4.28 m/s) with the dominant wind direction stemming from the North which resulted in wind power density being 85 W/m^2. The area was simulated using the WAsP simulation tool for nine base cases for wind farm layout and the authors found that the capacity factors of the simulation ranged from 0.98 % to 2.68 %.

Kim et al. [14] investigated the potential for offshore wind farm site selection aimed at finding the feasibility of an offshore wind farm site around the coastal regions of the Jeju islands, South Korea. The evaluation categories in this study were: energy production and economics, protected areas, human marine activities, and the marine ecology of the area. The researchers concluded that the number of feasible areas for offshore deployment was low when utilising all factors of all the categories in comparison to just using the energy potential and economics of the region alone.

Mahdy and Bahaj [15] identified that there is a global gap regarding the assessment of offshore wind potential sites and thus proposed a new methodology of assessment for potential offshore sites. The methodology was based on the analytical hierarchy process in conjunction with spatial assessment within a GIS domain. The methodology was developed with the aim of assisting the scaling up of renewable energy from 1 GW to 7.5 GW in Egypt by 2020. The authors hypothesised that the increase in renewable energy would come from larger offshore wind installed capacity. Areas identified were potential sites around the Red Sea which was duly estimated to be able to accommodate 33 GW of installed capacity. The researchers concluded that the methodology which was developed could be applicable globally to produce adequate offshore wind suitability maps for potential wind power locations.

3. METHODOLOGY

The main aim of this study was to identify an ideal offshore location to situate a large floating offshore wind farm to supply coastal regions of South Africa with clean renewable energy. The conceptual assessment of this task was conducted based on methodologies found in the literature. The methodology was governed by three criteria for site selection: impact on shipping routes, spatial proximity to the electrical grid, and possible impact on future offshore oil and gas exploration.

Meteorological data set was obtained from the Global Wind Atlas which was developed by the Technical University of Denmark, Department of Wind Energy [16], in WAsP data file format. The data set consisted of 624 individual meteorological points containing wind resource data (Figure 5). The wind resource data was interpreted using WAsP simulation software. The data set contained wind resource data for 12 sectored wind roses at each location and associated wind profile frequency distributions at 3 hub heights of 0 m, 50 m and 200 m respectively.

The analysis of the wind vector data was first filtered by understanding the prevalent wind direction through evaluating the wind rose generated for the dataset. The wind rose along the eastern coastline of the country exhibited two distinct wind directions – either stemming from the north north east or from the south south west.

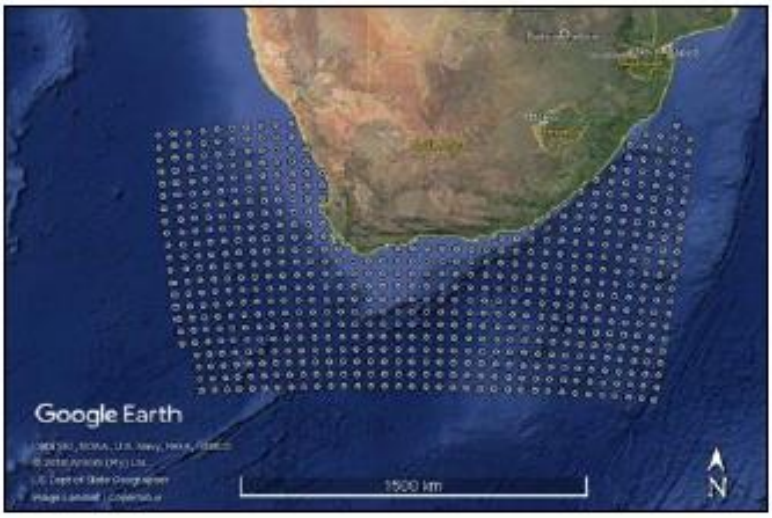

Figure 5 Meteorological data points

Once the resource data was obtained, the shipping routes were overlaid to gauge high and low-density shipping paths (Figure 6). The potential sites were located in positions where there was little to no marine traffic. The shipping routes were constructed using images obtained from the Marine Traffic website [17]. It is evident that the South African coast line experiences a high volume of marine traffic.

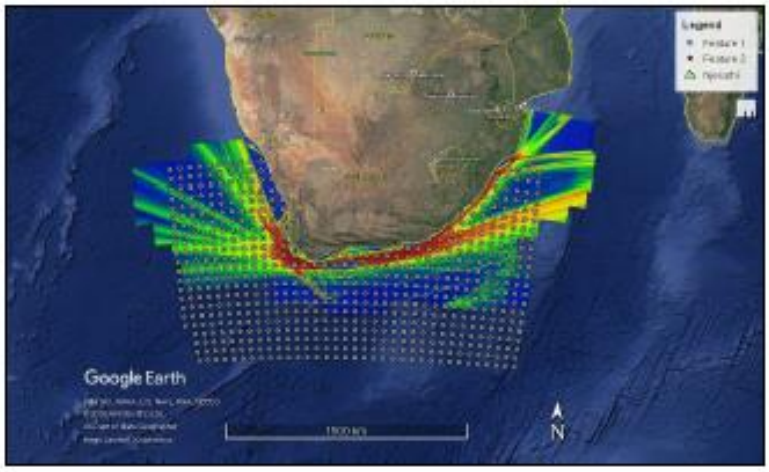

Figure 6 Shipping routes [17]

The second criterion was spatial proximity to the national electrical grid. The transmission electrical grid was sourced from the Africa Electrical Transmission Network (AICD) and implemented in Google Earth as shown in Figure 7 [18]. The coastal ports of South Africa are located at points a, b and c which represent the KwaZulu-Natal, Eastern Cape and Western Cape provinces respectively [19].

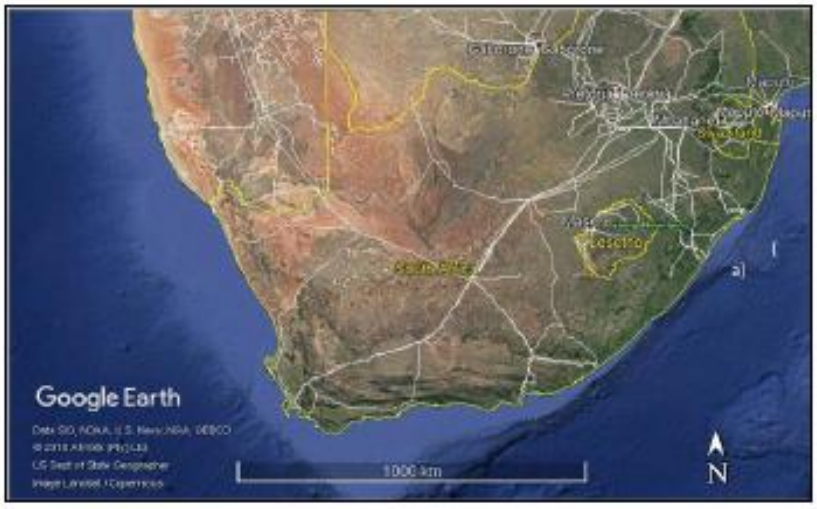

Figure 7 Transmission electrical grid South Africa [18]

From the Eskom transmission expansion plan 2016 to 2025 [19] it was found that point KwaZulu-Natal, Eastern Cape and Western Cape provinces in Figure 7 would increase by 841 MW, 609 MW and 656 MW respectively over the 10-year period. As the bulk of the power stations supplying the country are located inland, the transmission losses incurred while transmitting energy to coastal regions are high. It was hypothesised that an offshore wind farm would be able to minimise transmission losses by supplying energy to coastal regions. Added to this was the resultant decrease in the loading on the onshore electrical grid. This may allow for future capital to be transferred from many smaller distribution scale grid upgrades to prioritised transmission upgrades so as to address unserved customers or planned grid expansion.

The third criterion was the location of offshore oil and gas fields. Although countries are reforming to move away from fossil fuels, the commodity trading business around oil and gas of any particular country has significant benefit to that country's economy. Potential sites were identified in areas where there would be minimal impact on exploration of the area by interested organisations / companies. Figure 8 depicts the offshore oil and gas identified sites within the coastal region of South Africa [20].

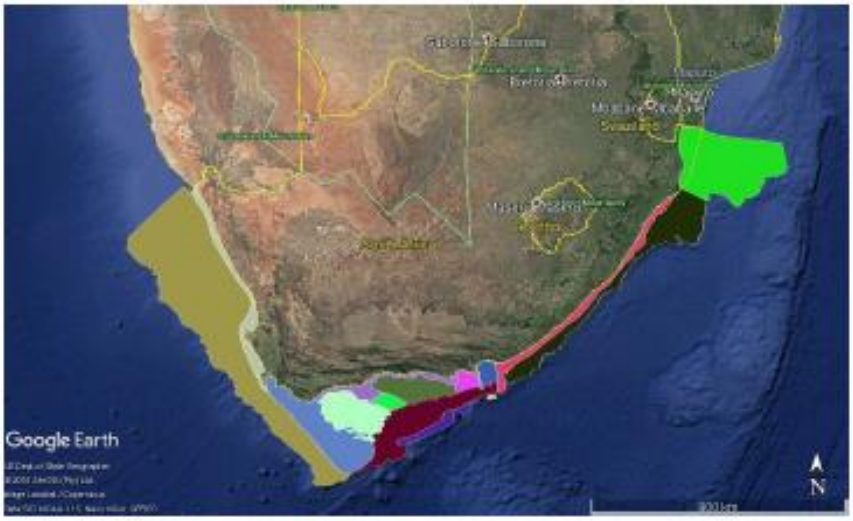

Figure 8 Offshore oil and gas – identified sites [20]

Potential sites for offshore wind farms were assessed based on all the above-mentioned criteria. Figure 9 shows the identified potential offshore sites. The meteorological points have a spatial resolution of roughly 50 km x 60 km. Site 1 and 2 slightly overlap with two of the identified oil and gas areas, however, this was only due to the nature of the resolution of meteorological data.

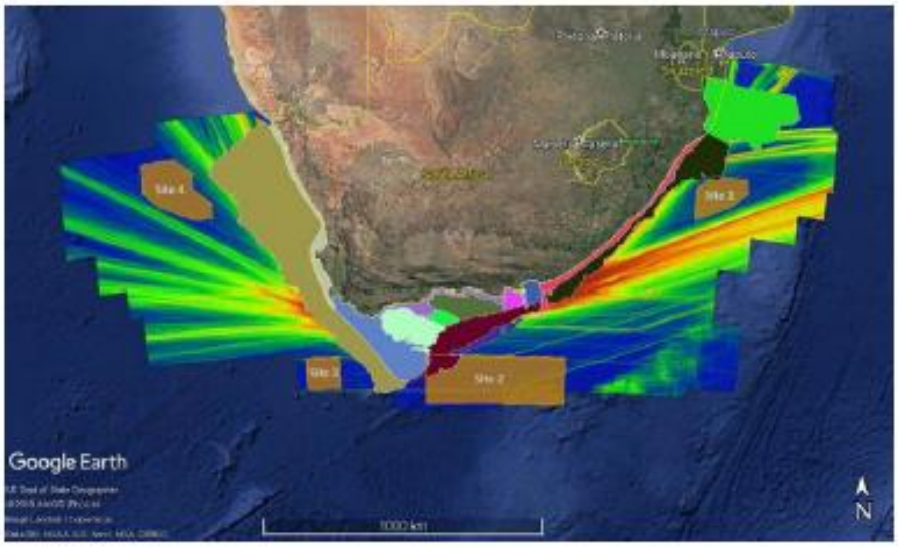

Figure 9 Identified potential sites

Once each site's simulated wind data was analysed from each of the meteorological points within the selected boundaries, an average wind speed for hub heights 50 m, 100 m and 200 m was calculated. Wind speed is a key factor in site analysis as it is indicative of the potential within the region for energy extraction.

4. SITE INVESTIGATION & ANALYSIS

This section of the investigation analyses each of the potential sites which were assumed based on the above methodology and depicted in Figure 9 above. Wind resource data was difficult to acquire. The use of satellite imagery tools (ASCAT, QuickSCAT, RapidSCAT etc.) did not contain relevant data which could be readily used for the analysis of the wind potential at the chosen sites. The International Renewable Energy Agency (IRENA) data was more suitable. Irena is a free, online portal for the high-level assessment of renewable energy resource potential at a chosen location / site [21].

The wind resource data was obtained from the Technical University of Denmark's (DTU) *Global Wind Atlas* portal which uses data from IRENA [16]. Data from this source was also used to develop the *Wind Atlas of South Africa – WASA* [16] which was developed for onshore wind analysis of the South African coastline by various South African research bodies such as the CSIR, South African Weather Services, University of Cape Town and the DTU Department of Wind Energy. The wind atlas was constructed using various onshore meteorological sites in conjunction with conventional forecasting tools such as the WAsP wind simulator.

The online portal allows for the rough selection of points for data collection. The potential sites were mapped as estimated polygon shapes based on the co-ordinates of each of the boundary points. The resultant wind statistical data was downloaded in WAsP format to be analysed further. Wind speed and wind direction were analysed for each of the sites depicted in Figure 9.

4.1. Wind Direction

4.1.1. Site 1

Site 1 is located off the eastern coast of Durban, roughly 200 km offshore from the Durban harbour in a south east direction or 115° bearing. The site has an estimated perimeter of 600 km and an estimated surface area of ± 21 000 km^2. Figure 10 is a graphical representation of Site 1. The site encompassed 11 of the meteorological data points obtained from DTU *Global Wind Atlas* [16].

Figure 10 Potential – Site 1

A wind rose is a vector plot which denotes direction and frequency respectively. A wind rose developed from the wind resource data comprises 12 sectors where Sector 1 encompasses a bearing of 345° to 15° and thus the midpoint for Sector 1 of the wind rose plots was 0° with a 15° arc span on either side (Figure 11). Once a common understanding of the demarcation of the sector boundaries was developed, the sectors within the wind rose were utilised as means of reference to establish which direction the wind stemmed from for all the potential sites under investigation.

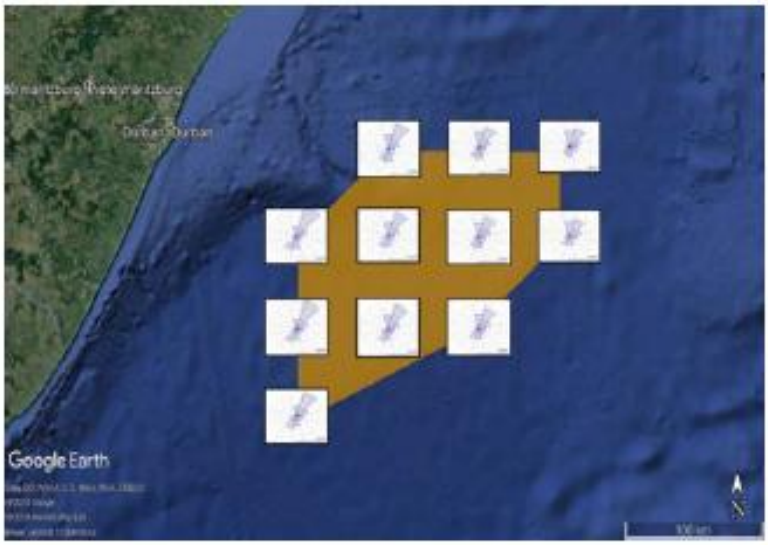

Figure 11 Site 1 – Wind rose plots

The most predominant wind directions were found to be Sectors 2 and 8 of each of the wind roses for Site 1. The average wind speed for the area was calculated based on the mean wind speeds of each of the meteorological stations analysed. The average wind speed for hub heights 50 m, 100 m and 200 m were 9.19 m/s, 9.25 m/s and 9.34 m/s respectively.

4.1.2. Site 2

Site 2 is a larger site than Site 1. It is located roughly 300 km south of Port Elizabeth. It has an estimated perimeter reading of 1 250 km and an estimated surface area of ± 79 000 km^2. The site is located in a potential retroflection zone (**2**) for ocean currents as found by Cunden [22]. Figure 12 is a graphic representation of the potential of Site 2. As seen in Figure 9, Site 2 has minimum shipping route impacts but may lie on a possible potential oil and gas field. From the meteorological data collected, the site comprised 36 individual meteorological data points which were analysed at various hub heights.

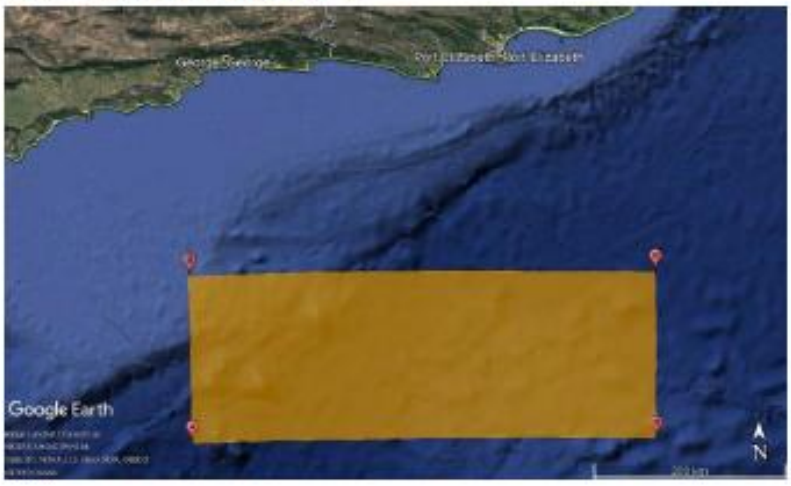

Figure 12 Potential – Site 2

Within Site 2, the prevailing wind direction was found to be in Sectors 3, 4, 9, 10, and 11 (Figure 13). This indicates that the wind direction changes through an annual cycle. The average wind speed for hub heights 50 m, 100 m and 200 m were 9.47 m/s, 9.55 m/s and 9.68 m/s respectively.

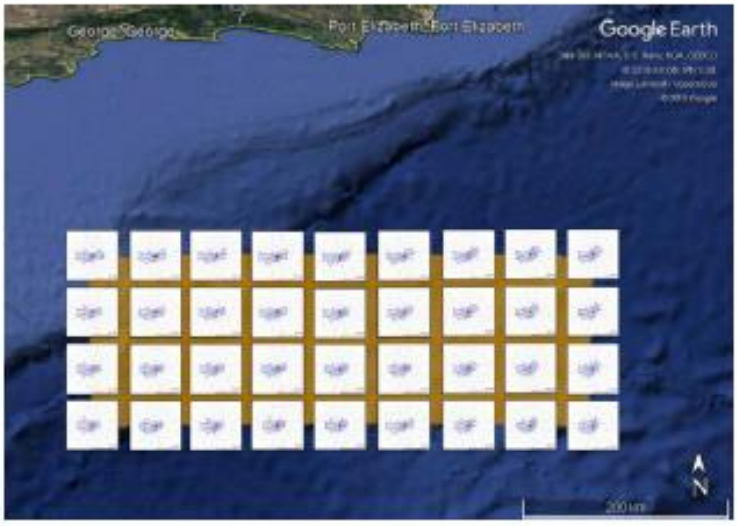

Figure 13 Site 2 – Wind rose plots

4.1.3. Site 3

Site 3 is located roughly 290 km south (± 188° bearing) of Cape Town (Figure 14). The site has an estimated perimeter of 463 km and an estimated surface area of ± 13 332 km^2. The site is the smallest of the four identified potential wind farm sites.

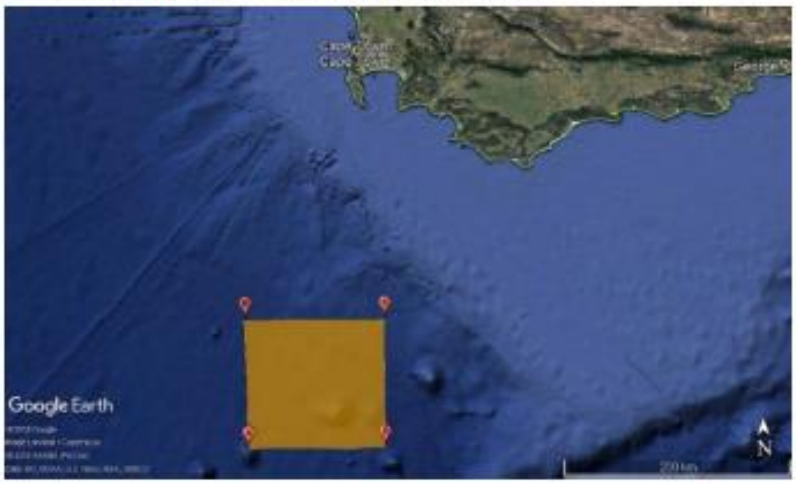

Figure 14 Potential – Site 3

At Site 3 the prevailing wind directions were in Sectors 5 to 11, with the highest occurring in Sectors 9, 10 and 11 (Figure 15). The distribution of wind over a span of 180° may be attributed to the convergence of two significant climate zones, namely, the Atlantic and Indian ocean zones, mixing in South Africa's southernmost region. The average wind speed for hub heights 50 m, 100 m and 200 m were 9.12 m/s, 9.12 m/s and 9.27 m/s respectively.

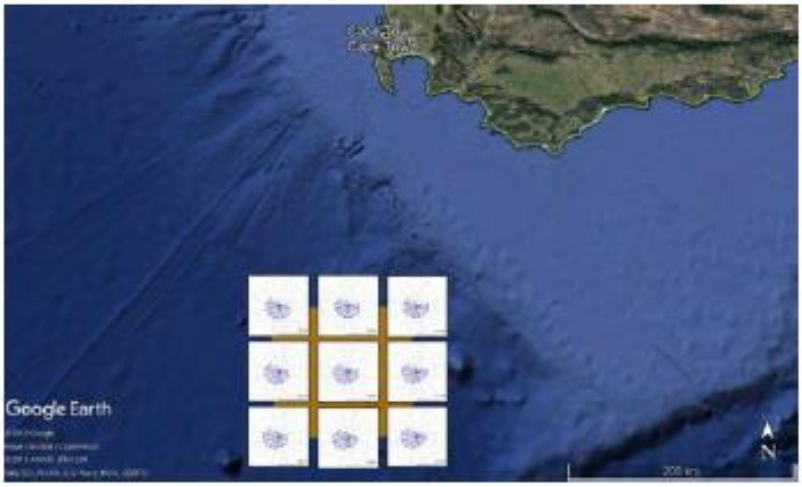

Figure 15 Site 3 – wind rose plots

4.1.4. Site 4

Site 4 is located an estimated 570 km north west (± 298° bearing) of Saldanha Bay and is the furthest potential site out of the four. The site has an estimated perimeter of 807 km and an estimated surface area of ± 37 419 km^2. The site has a minimum impact on oil and gas exploration sites and shipping routes as seen in Figure 16.

Figure 16 Potential – Site 4

Site 4's wind rose plot is depicted in Figure 17 where it can be seen that the predominant wind direction is south easterly (Sectors 6 and 7). This may be a result of the mixing climatic conditions further south leading to a retroflected mass of wind moving towards the north from the Cape peninsula region.

Figure 17 Site 4 - wind rose plots

4.2. Wind Speed

To gauge the wind speed potential in each of the site areas, each of the meteorological points were mapped for hub heights of 50 m, 100 m and 200 m and an average wind speed was calculated for each hub height respectively. It is known that wind shear profile has a logarithmic nature and may be approximated in mathematics by means of the log wind profile equation which takes into account factors such as surface roughness and atmospheric stability. The equation which governs the logarithmic nature of the wind profile is as follows:

$$U = \frac{u_*}{k}\left[\ln\left(\frac{z}{z_0}\right) - \psi(\zeta)\right] \quad (1)$$

Where:

U Mean wind speed (m/s)

z Height at which mean wind speed is located (m)

u_* Frictional velocity (m/s)

z_0 Surface roughness (-)

$\psi(\zeta)$ Integrated stability function governing momentum (-)

The integrated stability function comprises the Obukhov Length Scale which includes further parameters such as sea surface temperature, kinematic heat flux over the surface body as well as the cube of the frictional velocity [24]. However, these factors are not easily found in literature or readily available and for the analysis being conducted a more simplified version of the above was utilised in order to obtain a plausible understanding of the wind shear profile for the site areas.

To extrapolate the wind shear profile the more common Wind Power Law was used [25]:

$$U = U_R \left(\frac{z}{z_R}\right)^{\alpha} \quad (2)$$

Where:

U Mean wind speed (m/s)

U_R Reference wins speed (m/s)

z Height at the mean wind speed (m)

z_R Reference height (m)

α Empirical Coefficient accounting for the atmospheric stability (-)

Equation 2 has been found to be suitable to extrapolate wind shear for hub heights less than 100 m [23]. The 50 m hub height measurement was used as the first basis for extrapolation for each of the sites. An iterative solver was used to extract the atmospheric coefficient required.

Figure 18 depicts a possible representation of the different wind shear profiles for each of the sites. The extrapolation shows the changing wind shear at various hub heights below 100 m based on the arithmetic average of mean wind speeds located within the boundaries of each site. As expected, the mean wind speed located offshore is significantly higher that onshore with a gradual increase in wind shear gradient.

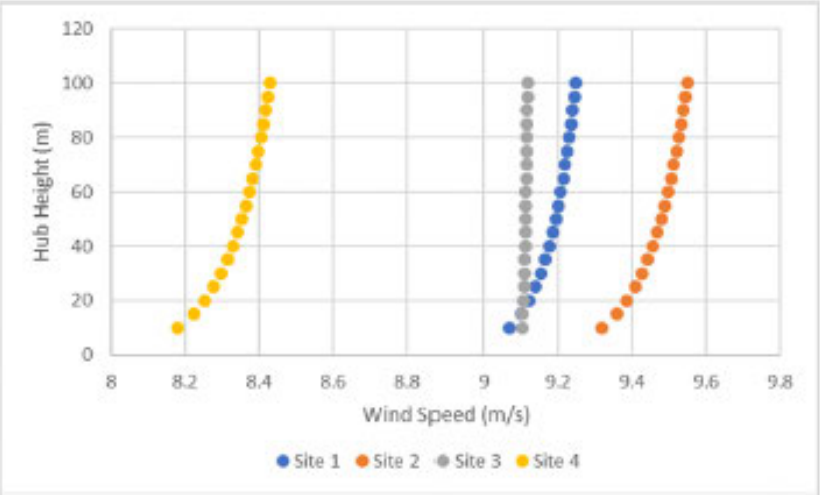

Figure 18 Extrapolated wind shear profiles

Wind resource is relatively unpredictable and erratic by nature; however, on consistent monitoring and investigation of terrestrial based meteorological stations, a best fit curve was found to adequately describe the wind resource which is based on the 2-parameter Weibull

distribution. As shown in literature, the 2-parameter Weibull statistical distribution is the most common way of understanding wind potential [26–28].

The Weibull distribution gives one an appreciation of the probability of wind speed occurrences at a chosen site. The function requires three parameter inputs, one being a variable and the two other parameters being static which define the distribution. The Weibull distribution is defined as follows:

$$P(U,k,c) = \frac{k}{c}\left(\frac{U}{c}\right)^{k-1} e^{-\left(\frac{U}{c}\right)^{k-1}} \quad (3)$$

Where:

U	Wind speed (m/s)
k	Shape parameter (-)
c	Scale parameter (m/s)

The shape parameter of the distribution defines how the probabilities of wind speed are spread throughout the distribution. It is generally found that the larger the shape parameter the closer the distribution tends towards becoming Gaussian in shape. The shape parameter for wind distributions is usually near 2 [29]. The scale parameter defines the most probable speed in the distribution (the mode value). Traditionally with regards to wind resource analysis, the larger the scale parameter is in value, the higher the mode of the distribution, which basically means that the probability of a random wind speed value is less likely to be lower than the mode of the distribution [29], [30].

In relation to the four offshore sites, the WAsP forecasted statistical parameters were used as a basis for defining wind resource dispersion over the site area. Each of the meteorological points from each site, as depicted in figures' 11; 13; 15 and 17, were analysed. WAsP gives an empirical relationship of roughness length and roughness elements taken from the description given by Lettau [31]. The simple description is given as follows [31]:

$$z_0 = 0.5\,\frac{(h.S)}{A_H} \quad (4)$$

Where:

z_0	Roughness length (m)
h	Element height (m)
S	Cross-sectional surface facing the wind (m^2)
A_H	Average element horizontal area (m^2)

The above is more suited for terrestrial based applications as it considers various vegetation and foliage effects in relation to the wind flow. Charnock [32] provides a description of surface roughness phenomena over water bodies and explains that the roughness length of different surfaces directly affects the wind speed which WAsP further defines as roughness classes. A full list of surface roughness guidelines is illustrated in Appendix A. Charnock [32] developed an equation which ignored the viscous effects and the surface tension of the water are ignored, as follows:

$$z_0 = b\,\frac{U_*^{\,2}}{g} \quad (5)$$

Where:

z_0	Roughness length (m)
b	Constant (-)

U_* Frictional Velocity (m/s)

g Gravitational acceleration (m/s^2)

The WAsP tool has defined a constant roughness length of 0.0002 m for wind resource over water bodies. During the development of the software both a constant value and equation 5 was used. The resultant constant value proved to give good results in comparison to equation 5 and hence maintained the constant roughness value over water bodies. The DTU Wind Energy project [33] used onshore high-resolution meteorological measurements taken over extensive periods to establish and develop WASA. The interpolation of results to offshore water bodies was conducted within the WAsP software based on the onshore readings and respective surface roughness in relation to water bodies. For the identified offshore sites, these results were used to determine the probability distribution of the resource based on the statistical parameters obtained from the data.

4.2.1. Site 1

Figure 19 shows the general wind characteristics for Site 1. The Weibull distribution for the two dominant sectors of the site's general wind direction was constructed using the wind statistic parameters obtained via the online wind atlas synthetic data. Sectors 2 and 8 proved to have the highest frequency and were analysed. It can be seen that Sector 2's distribution is more Gaussian in shape due to the k-shape factor being closer to 3. The skewness (close to 0) of both data sets indicates a more normally distributed dataset. The mean wind speed for both the sectors is 10.5 m/s at a 50 m hub height. It may be noted that Sector 2's probability density distribution depicts more probable wind speeds between 6 m/s and 15 m/s in comparison to Sector 8's distribution which depicts a higher probability of higher wind speeds over 15 m/s.

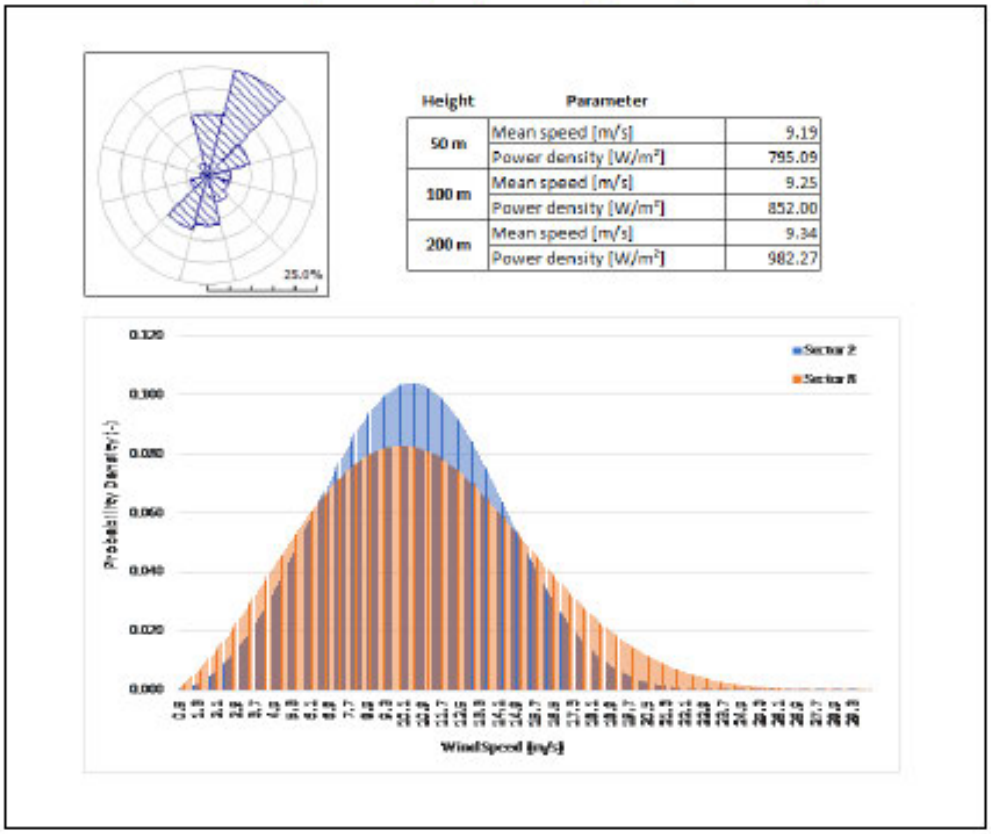

Height	Parameter	
50 m	Mean speed [m/s]	9.19
	Power density [W/m²]	795.09
100 m	Mean speed [m/s]	9.25
	Power density [W/m²]	852.00
200 m	Mean speed [m/s]	9.34
	Power density [W/m²]	982.27

Figure 19 General wind characteristics – Site 1

4.2.2. Site 2

The general wind characteristics for Site 2 are shown in Figure 20. It was found that Sectors 3 and 10 were the dominant wind directions for the site. The Weibull distributions of these sectors are shown. Sector 3 has a higher density for wind speeds of 5 m/s to 14 m/s and lower probabilities of higher wind speeds. The distribution of wind speed in Sector 10 shows a lower peak but higher density of probabilities between 6 m/s to 16 m/s, including higher probabilities of wind speeds greater than 15 m/s. The mean wind speed for Sectors 3 and 10 are 9.7 m/s and 11.1 m/s respectively at a 50 m hub height.

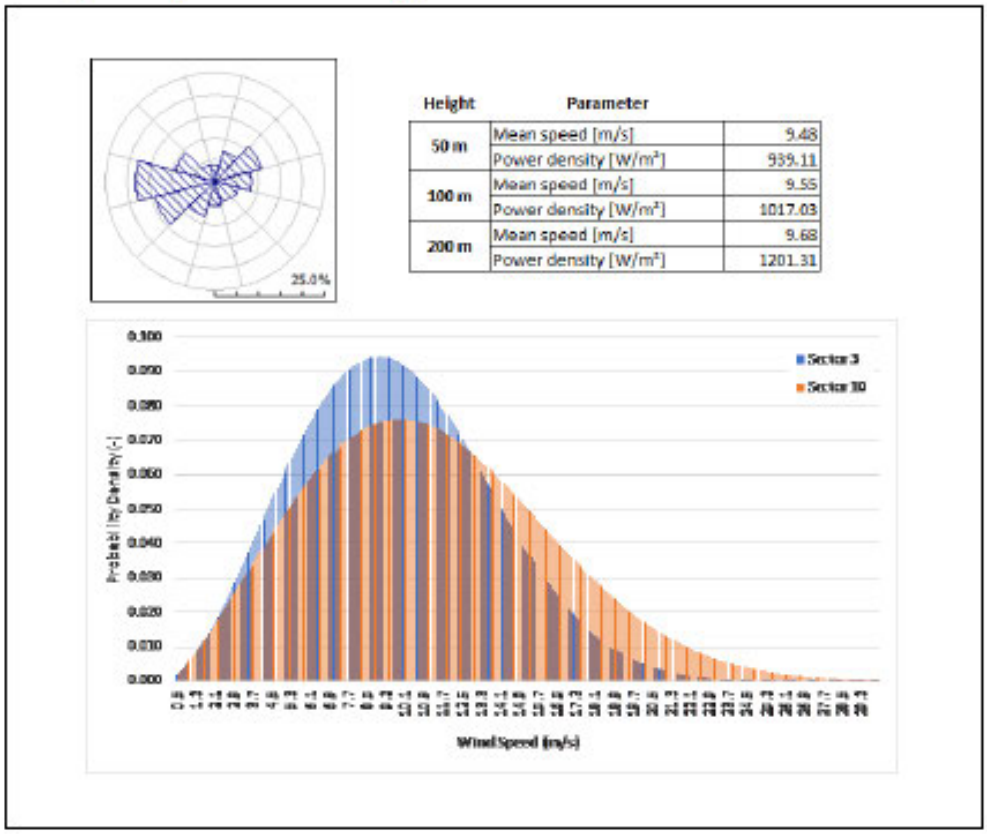

Figure 20 General wind characteristics – Site 2

4.2.3. Site 3

Site 3 is unique as it is located at the southern tip of the country. This region is known to have mixing of the warm Agulhas current (east coast) and the cold Benguela current (west coast). Along with the trade winds stemming from the South Pole towards the equator and the Coriolis effect from the planet's rotation, Site 3 would be expected to have cross-cutting winds. The wind rose shown in Figure 21 shows that the most frequent directions are from Sectors 9 and 10, although the span of wind directions in comparison to the other three sites is much larger with relatively equal frequencies which is assumed to possibly be due to the cross-winds occurring at the site's location. Sectors 6 and 9 were chosen for analysis. The mean wind speed for both sectors was relatively similar with Sector 6 having a mean value of 8.22 m/s and Sector 9 having a mean value of 9.2 m/s. Comparing the two probability distributions it can be seen that Sector 9 has higher probabilities of higher wind speeds especially between wind speeds of 12 m/s to 20 m/s, in relation to Sector 6.

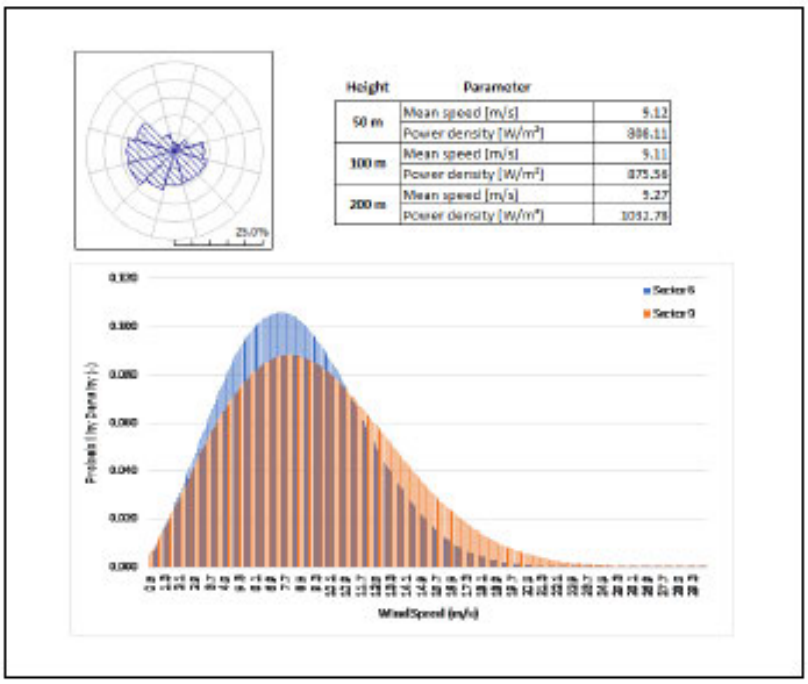

Figure 21 General wind characteristics – Site 3

4.2.4. Site 4

Figure 22 illustrates the general wind characteristics for Site 4 located west of the Northern Cape. The dominant wind directions are Sectors 6 and 7. Comparing the two probability density distributions, it is evident that Sector 6 experiences higher valued wind speeds compared to Sector 7. Both sectors have shape factors greater than 3 leading to the Gaussian shape of both distributions. The mean wind speed for Sector 6 is 9.8 m/s and Sector 7 is 7.8 m/s at 50 m hub height. In comparison to the previous sites, Sites 4 and 3 have lower mean wind speed values than Sites 2 and 1.

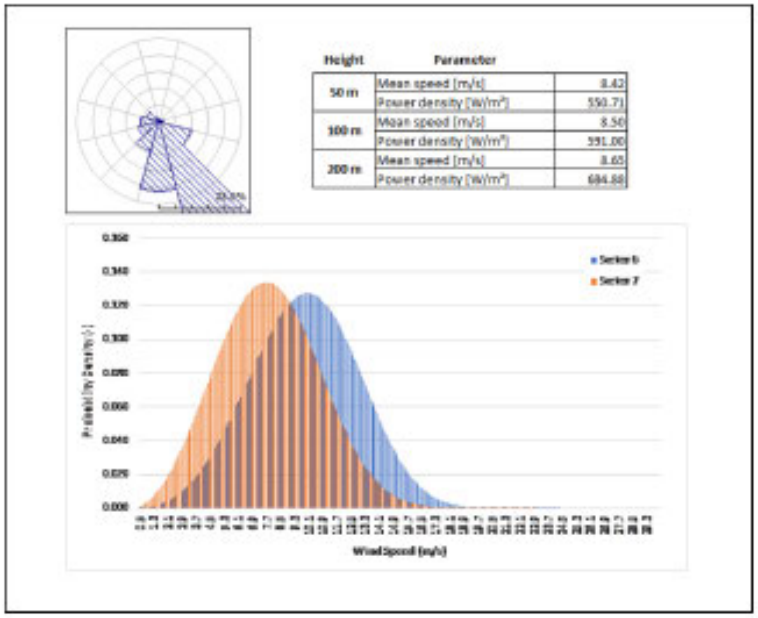

Figure 22 General wind characteristics – Site 4

Each of the above sites were evaluated and Table 1 below encapsulates each of the sites' wind mean speed and power density characteristics. It can be seen by evaluation of the data table that Sites 2 and 3 have good mean wind speeds and encapsulate the most power density of the four sites. There is a need to analyse each of the meteorological points within the area chosen as the mean wind speed and power density varies over large areas.

Table 1 Site wind and power characteristics

Height	Parameter	Site 1	Site 2	Site 3	Site 4
50 m	Mean speed [m/s]	9.19	9.48	9.12	8.42
	Power density [W/m²]	795.09	939.11	808.11	550.71
100 m	Mean speed [m/s]	9.25	9.55	9.11	8.50
	Power density [W/m²]	852.00	1017.03	875.56	591.00
200 m	Mean speed [m/s]	9.34	9.68	9.27	8.65
	Power density [W/m²]	982.27	1201.31	1032.78	684.88

4.3. Site Geographical Analysis

It is visualised that the energy which is produced offshore from any of the potential sites will be fed to the coastal regions. In order to be as cost effective as possible, utilisation of existing electrical integration points is advised initially (unless specific assets are required) for the most optimum power transfer to shore. To gauge this, the distance to the site sub-integration point (assumed to be the site central location) from the main feeder was investigated with regards to surface elevation in respect to the standard sea surface level.

4.3.1. Site 1

Site 1 is based off the coast of Durban and has an area of 21 000 km^2 as previously stated. There are two main power incomers as shown in Figure 23, namely, Klaarwater (a) and Illovo (b) with each having 275 kV lines respectively [18]. Figure 23 shows that the distance to the different tie in points is roughly 200 km with the elevation level to the centroid of the site area also included. It is noted that the deepest point is roughly 3 000 m from the ocean surface.

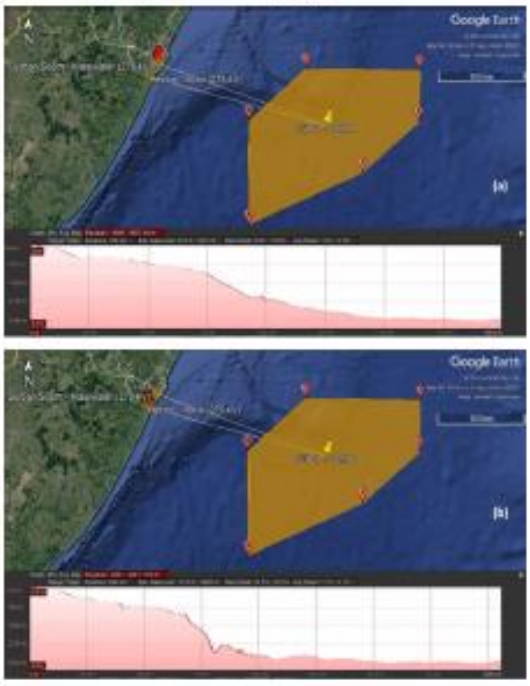

Figure 23 Location of possible points of connection – Site 1

4.3.2. Site 2

Figure 24 shows the distance from the various possible onshore connection points to the centre of Site 2 which is assumed to be the central integration point of harvested offshore wind energy for the site. The three potential connection points are Leeches Bay (132 kV), Poseidon (220 kV) and Proteus (400 kV), all of which are in the Eastern Cape. On average, the distance to onshore connections is 409 km with the shortest distance being in relation to the Poseidon substation. There is a distinct steep shelf drop off the Eastern Cape coastline.

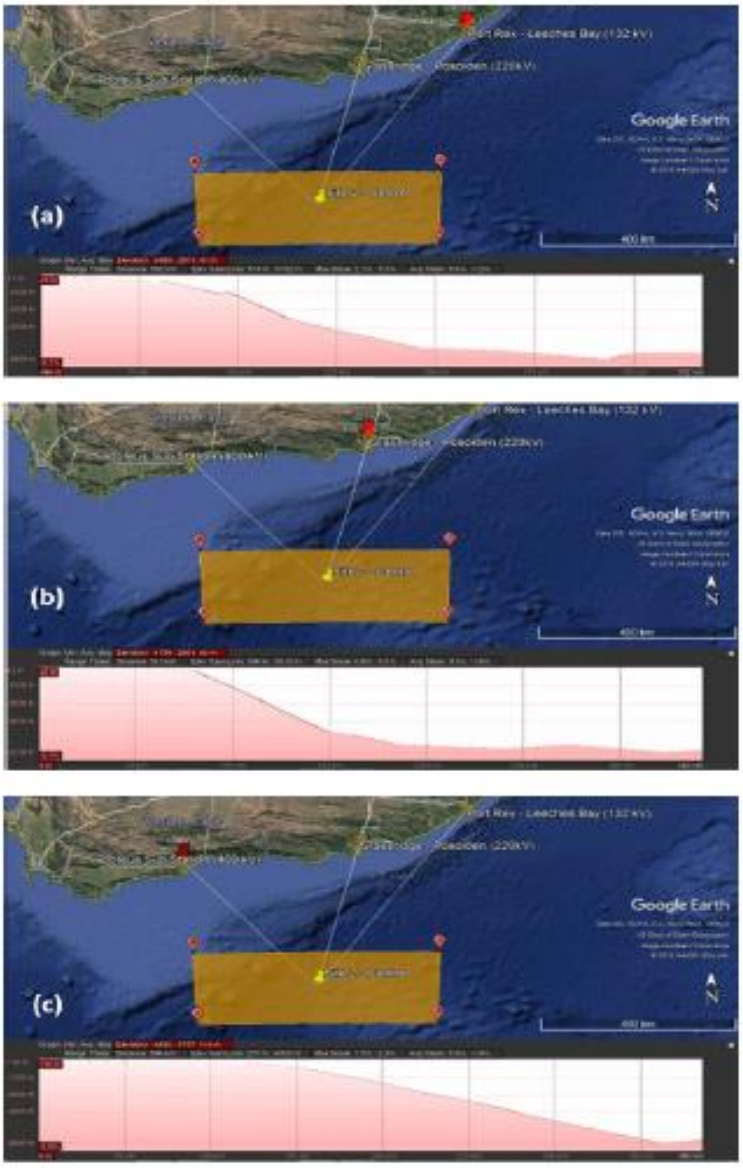

Figure 24 Location of possible points of connection – Site 2

4.3.3. Site 3

Figure 25 shows the two closest transmission substations, either of which could function as an integration point for Site 3, namely, Acacia (400 kV) and Palmeit (400 kV). On average the distance to an onshore integration point is 280 km with Palmeit being the closest at a distance of 275 km offshore. The diagram also indicates the coastal shelf declination which extends further out than the previous site declinations.

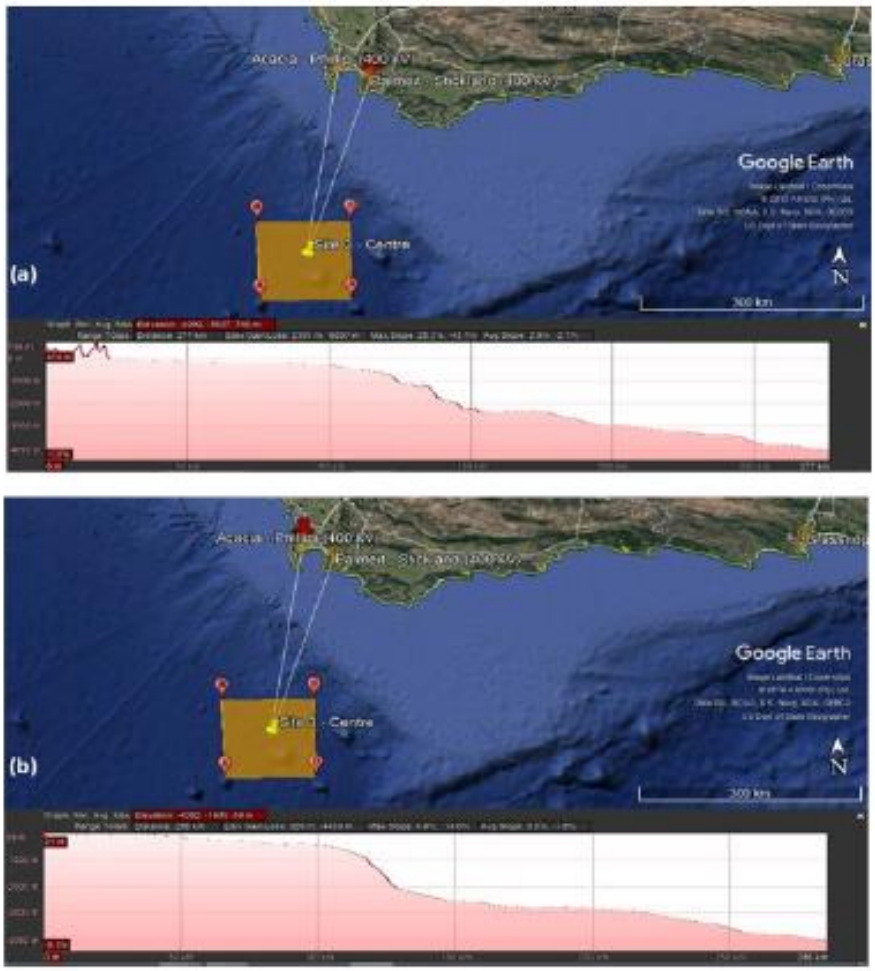

Figure 25 Location of possible points of connection – Site 3

4.3.4. Site 4

Site 4, as seen in Figure 26, is located 527 km on average from the western coastline of South Africa. The province/state which is closest to the site is the Northern Cape. The province is the largest in the country but has the lowest population in the country. Limited connection points are located along the western coast. Only two transmission connection points could be located but there may be smaller coastal distribution feeders where connection may be possible. The two transmission substations are Gromis (400 kV) and Juno (400 kV), each having a distance to site of over 450 km.

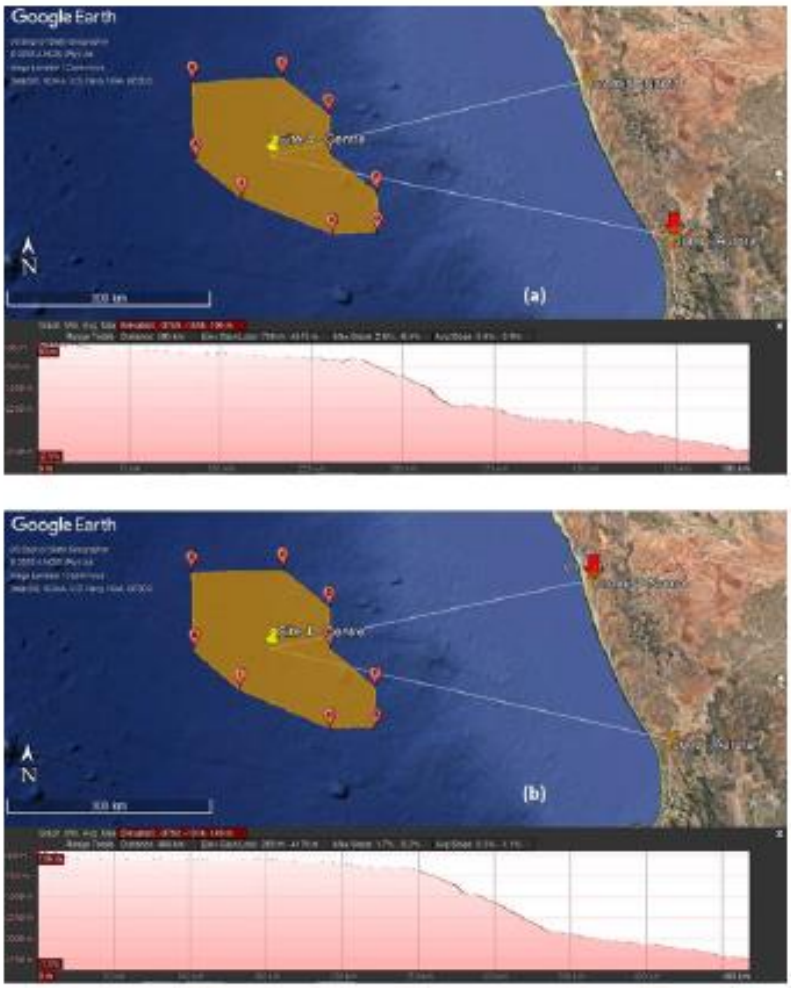

Figure 26 Location of possible points of connection – Site 4

The gradual evolution of offshore wind farms are a result of most regions already utilising most of the space onshore zoned for energy production structures as well as the higher resource potential located offshore [6]. As shown above, the depths at each of the sites are far deeper than what traditional offshore wind turbines are subjected to. For this reason, most of the wind farms located at such distances offshore would require a floating structure as depths in these regions are beyond conventional anchoring.

5. CONCLUSION

This article aimed to investigate the offshore wind potential for the South African coast. Various factors were taken into consideration before demarcating potential sites for investigation, such as shipping routes, potential exploration oil and gas fields and possible transmission connection points. Utilising this methodology, four potential sites were identified. The predominant wind direction, mean wind speed, wind shear and spatial geographic information was analysed for each site.

The wind direction for each of the sites were dependent on many factors which influence the wind resource such as cross-wind interference and ocean currents. The wind direction did not have any similarities between sites, with each site having its own predominant wind directions. Site 1 had a dominant wind direction from a north easterly direction and the polar opposite as well. Site 2's prevailing wind direction was from the west and occasionally from a

north easterly direction. Site 3 had a large span of wind direction as it is located in a high mixing zone of various strong wind forces. Site 4's principle wind direction was from the south east along the western coastline of the Northern Cape province.

Within the 50 m hub height, Site 2 showed the best potential based on the power density. In comparison, Site 1 and Site 3 showed similar power densities to each other and Site 4 depicted the lowest power density. The general wind speed characteristics were analysed for each of the sites and the average wind speed (taking into consideration all of the sites identified) was 9.5 m/s with large power densities between 500 W/m2 to over 1 000 W/m2.

The distance to shore ranged from 200 km to 500 km with a steep continental shelf drop to approximately 3 000 m deep. This means that the traditional means of offshore wind platforms would not be adequate for anchoring the plant, and a floating offshore structure would be more suitable. The use of a centrally located electrical energy collector hub within each site, with possibly N – 2 contingency measures, could be useful to connect to fewer feeder bays within the closest transmission substation onshore. This could also allow for the filtering out the power variations from widely spaced turbines.

The study conducted shows that there is offshore wind potential off the coast of South Africa. Energy generated by this method could assist South Africa to increase access to energy, reduce expensive transmission line losses to coastal provinces, and assist the country transition towards a more sustainable future energy mix in line with developed nations.

ACKNOWLEDGMENTS

We would like to acknowledge the assistance of government institutions for the assistance in information as well as our colleagues at the university for providing direction to research.

REFERENCES

[1] Whiteman, A., Esparrago, J., Rinke, T., Elsayed, S., Arkhipova, I., Strinati, C. et al. Renewable Energy Statistics 2018. (IRENA), Abu Dhabi, 2018.

[2] Green R. and Vasilakos, N. The Economics of Offshore Wind. *Energy Policy*, 39(2), 2011, pp. 496-502.

[3] Esteban Dolares, M., Javier Diez, J., Lopez Jose, S. and Negro, V. Why Offshore Wind Energy. *Renewable Energy*, **36**, 2011, pp. 444-450.

[4] Kaldellis J. and Kapsali, M. Shifting Towards Offshore Wind Energy – Recent Activity and Future Development. *Energy Policy*, **53**, 2013, pp. 136-148.

[5] Werapun, W., Tirawanichakul, Y., Kongnakorn, W. and Waewsak, J. An Assessment of Offshore Wind Energy Potential on Phangan Island by in Southern Thailand. *Energy Procedia*, **52**, pp. 2014, pp. 287-295.

[6] Breton S.-P. and Moe, G. Status, Plans and Technologies for Offshore Wind Turbines in Europe and North America. *Renewable Energy*, **34**, pp. 2009, 646-654.

[7] Bilgili, M., Yasar, A. and Simek, E. Offshore Wind Power Development in Europe and its Comparison with Onshore Counterpart. *Renewable and Sustainable Energy Review*, **15**, 2011, pp. 905-915.

[8] London Array Limited. London Array. n.d. Available: http://www.londonarray.com/the-project-3/phase-2/

[9] Da, Z., Xiliang, Z., Jiankun, H. and Qimin, C. Offshore Wind Energy Development in China: Current Status and Future Perspective. *Renewable and Sustainable Energy Reviews*, **15**, 2011, pp. 4673-4684.

[10] Sun, X., Huang, D. and Wu, G. The Current State of Offshore Wind Energy Technology Development. *Energy*, **41**, 2012, pp. 298-312.

[11] Murthy K. S. R. and Rahi, O. P. A Comprehensive Review of Wind Resource Assessment. *Renewable and Sustainable Energy Reviews*, **72**, 2017, pp. 1320-1342.
[12] Sharma K. and Ahmed, M. R. Wind Energy Resource Assessment for the Fiji islands: Kadavu Island and Suva Peninsula. *Renewable Energy*, **89**, 2016, pp. 168-180.
[13] Lima, D. K. S., Leão, R. P. S., dos Santos, A. C. S., de Melo, F. D. C., Couto, V. M., de Noronha, A. W. T. et al., Estimating the Offshore Wind Resources of the State of Ceará in Brazil. *Renewable Energy*, **83**, pp. 2015, 203-221.
[14] Kim, T., Park, J.-I. and Maeng, J. Offshore Wind Farm Site Selection Study Around Jeju Island, South Korea. *Renewable Energy*, **94**, pp. 2016, 619-628.
[15] Mahdy M. and Bahaj, A. S. Multi Criteria Decision Analysis for Offshore Wind Energy Potential in Egypt. *Renewable Energy*, **118**, 2018, pp. 278-289.
[16] Department of Wind Energy. Global Wind Atlas 1.0 [Online]. Available: http://science.globalwindatlas.info/index.html
[17] Marine Traffic. Density Plots 2017, March. Available: https://www.marinetraffic.com/
[18] Harvard College. (2017, March). Africa Electricity Transmission Network (AICD). Available: https://worldmap.harvard.edu/data/geonode:africa_electricity_transmission_network_o7k. 2017, March
[19] Eskom Holdings, Eskom – Transmission Development Plan 2016-2025, 2016.
[20] Petroleum Agency South Africa. Petroleum Agency SA. 2013, 23 July. Available: https://www.petroleumagencysa.com/
[21] International Renewable Energy Agency (IRENA), Average Wind Speed 1 km at 50m Height DTU 2015. In Global Atlas for Renewable Energy, Wind Map, IRENA, 2015.
[22] Cunden, K. Design of a Novel Hydrokinetic Turbine for Ocean Current Power Generation. Master of Science in Mechanical Engineering. Master's Thesis, Mechanical Engineering, University of Kwa-Zulu of Natal, Durban, South Africa, 2015.
[23] Pacheco, A., Gorbena, E., Sequeira, C. and Jerez, S. An Evaluation of Offshore Wind Power Production by Floatable Systems: A Case Study from SW Portugal. *Energy*, 131, 2017, pp. 239-250.
[24] Sanz Rodrigo, J., Cantero, E., Garcia, B., Borbon, F., Urigoyen, U. and Lozano, S. Atmospheric Stability Assessment for the Characterization of Offshore Wind Conditions. *Journal of Physics: Conference Series*, **625**, 2015.
[25] Hsu, S., Meindl, E. and Gilhousen, D. Determining the Power-Law Wind Profile Exponent under near Neutral Stability Conditions at Sea. *Journal of Applied Meteorology*, 33, 1994, pp. 757-765.
[26] Azad, A. K., Rasul, M. G., Islam, R. and Shishir. I. R. Analysis of Wind Energy Prospect for Power Generation by Three Weibull Distribution Methods. *Energy Procedia*, **75**, 2015, pp. 722-727.
[27] Ouarda, T. B. M. J., Charron, C., Shin, J. Y., Marpu, P. R., Al-Mandoos, A. H., Al-Tamimi, M. H. et al., Probability Distributions of Wind Speed in the UAE. *Energy Conversion and Management*, **93**, 2015, pp. 414-434.
[28] Wang, J., Qin, S., Jin, S. and Wu, J. Estimation Methods Review and Analysis of Offshore Extreme Wind Speeds and Wind Energy Resources. *Renewable and Sustainable Energy Reviews*, **42**, 2015, pp. 26-42.
[29] Patel, M. R. Wind and Solar Power Systems, 2nd ed. New York: CRC Press, 2005.
[30] Hodge, B. K. Alternative Energy Systems and Applications. New York: John Wiley & Sons, Inc, 2010.

[31] Lettau, H. Note on Aerodynamic Roughness-Parameter Estimation on the Basis of Roughness-Element Description. *Journal of Applied Meteorology*, 8, 1969, pp. 828-832,.
[32] Charnock, H. Wind Stress on Water Surfaces. *Quarterly Journal of the Royal Meteorological Society*, **81**, 1955, pp. 639-640.
[33] DTU Wind Energy. WAsP 11.2. Technical University of Denmark, 1987.

APPENDIX

Appendix A

Physical z_0 [m]	Terrain surface characteristics	Roughness Class	z_0 specified in WAsP [m]
1.5		4 (1.5 m)	1.5
> 1	tall forest		> 1
1.00	city		1.00
0.80	forest		0.80
0.50	suburbs		0.50
0.40		3 (0.40 m)	0.40
0.30	shelter belts		0.30
0.20	many trees and/or bushes		0.20
0.10	farmland with closed appearance	2 (0.10 m)	0.10
0.05	farmland with open appearance		0.05
0.03	farmland with very few buildings/trees	1 (0.03 m)	0.03
0.02	airport areas with buildings and trees		0.02
0.01	airport runway areas		0.01
0.008	mown grass		0.008
0.005	bare soil (smooth)		0.005
0.001	snow surfaces (smooth)		0.003
0.0003	sand surfaces (smooth)		0.003
0.0002	(used for water surfaces in the Atlas)	0 (0.0002 m)	0.0
0.0001	water areas (lakes, fjords, open sea)		0.0

"It should be noted, that in general the roughness length as applied in WAsP has to be considered as a climatological parameter because the roughness of an area changes with foliation, vegetation, snow cover and so on. The energy production of a wind turbine must be determined on the basis of climatology, primarily because of the variations of the weather; however, the seasonal variations in the local terrain characteristics can also have a profound influence.

It is recommended that land surfaces are not assigned roughness lengths smaller than 0.003 m (3 mm); this is especially important when met. masts, reference masts or turbines are located in such terrain with anemometer heights / heights / hub-heights more than 80 m."

NOTES

(1) Specific production is a factor which normalises an electrical generation plant's production by comparing the actual generated energy with that of the installed nameplate capacity of the generator(s). The units of measurement are kWh/kWp.

(2) A retroflection zone is an area in which the flow in question encounters specific obstacles which cause the flow to diverge from the original path and turn on itself, either clockwise or anticlockwise in direction.

CHAPTER 4 : OFFSHORE VERTICAL AXIS WIND TURBINE SIMULATION

The following chapter presents the simulation of the vertical axis wind turbine for the sites which were identified in and presented in Chapter 3. The paper shows the scaling the turbine and effect on turbine parameters such as chord length. The research was conducted based on a parametric approach of changing chord length, solidity ratio, and aspect ratio turbine parameters. The initial sites were presented and the corresponding Reynolds numbers were calculated and applied to the simulations. The simulations compares the previous NACA blade profiles with a Selig blade profile. The results, conclusions and future work are also presented in the article.

CHAPTER 4 – **Cite this article:** F.L. Inambao and K. Cunden, "**Offshore Vertical Axis Wind Turbine Simulation**" published in the International Journal of Mechanical and Production Engineering Research and Development (IJMPERD), Vol. 11, Issue 2, April 2021, pp 187-204.

Link to article:

http://www.tjprc.org/publishpapers/2-67-1616049303-15IJMPERDAPR202115.pdf

International Journal of Mechanical and Production Engineering Research and Development (IJMPERD)
ISSN (P): 2249–6890; ISSN (): 2249–8001
Vol. 11, Issue 2, Apr 2021, 187–204

Original Article

OFFSHORE VERTICAL AXIS WIND TURBINE SIMULATION

FREDDIE INAMBAO & KUMARESAN CUNDEN

Department of Mechanical of Engineering, University of KwaZulu-Natal, Durban, South Africa

ABSTRACT

The world is undergoing a paradigm shift as more people are becoming aware of energy consumption patterns, reinforcing the need for developing cleaner and more sustainable ways to generate electrical energy. Globally, the development of onshore wind farms is sometimes impeded by factors such as aesthetic impact, acceptance by the public, the threats to surrounding biodiversity, noise from the power plant and possible land use conflicts. Vertical Axis Wind Turbines (VAWTs) are now being developed and tested for offshore and far offshore power generation. The following paper aims to test a helical turbine design for sites identified off the coast of South Africa. The paper investigates multiple blade profiles under the equivalent blade Reynolds number for the identified sites. Each of the blades' characteristic profiles were analysed to understand the lift and drag characteristics under various Reynolds conditions. The Selig series S1046 blade profile showed good results in comparison to the other blade profiles. The results showed that the lift and drag coefficients are not significantly affected by the level of ambient disturbance. The performance curves under low solidity ratios showed that the S1046 profile was preferable in comparison to the NACA23018 and NACA0015 blade profiles. With respect to torque distribution on the turbine rotor, the S1046 profile depicted stable output over a larger range of tip speed ratio. The turbine results also show that an aspect ratio of 1.5 proved to have a larger operating range than that of the higher aspect ratio of 2.5.

KEYWORDS: *VAWT, South Africa, NCrit, Aspect Ratio& Eskom*

Received: Jan 03 2021; **Accepted:** Jan 23, 2021; **Published:** Mar 09, 2021; **Paper Id.:** IJMPERDAPR202115

1. INTRODUCTION

The world is undergoing a paradigm shift as more people are becoming aware of energy consumption patterns, reinforcing the need for cleaner ways to generate electrical energy. The use of coastal wind turbine farms is increasing globally, as offshore wind conditions are more favourable than terrestrial based sites due to the wind profiles located offshore [1], [2].

South Africa's power supply consists of predominantly coal based power stations located inland. This poses technical challenges to deliver power to the coastal regions and losses are incurred [3].

Figure 1: Power Stations in South Africa [4]

The addition of offshore wind farms can assist South African coastal regions by offsetting central power generation. Offshore wind farms can provide clean energy to the coastal regions based on the sites shown in Inambao and Cunden[2].

A suitable wind turbine configuration is required for investigation of the estimated power production and annual energy yield for the investigated sites. Building on the work conducted by Cunden [5], a vertical axis wind turbine orientation was investigated within this study.

2. LITERATURE REVIEW

Islam et al. [6] conducted an investigation into the growing trends within the wind industry and compared the traditional Horizontal Axis Wind Turbines (HAWT) to the Vertical Axis Wind Turbines (VAWT). The researchers investigated many aspects including the suitability for wind classes; control systems implemented; the aerodynamics of each system and the comparison of the respective energy production. The authors indicated the need for energy storage systems to be coupled with the wind facility due to the intermittent nature of wind energy. An interesting result in the study was that the VAWT could out-produce the HAWT system by 10 times for the same spatial area. This was because the HAWT systems require larger spacing between turbines as a result of inherent wake interference compared to that of VAWT based systems.

Óskarsdóttir[7] conducted research which looked at the general comparison of the HAWT and VAWT systems. The main distinction between HAWT and VAWT systems are related to the aerodynamics of the turbine. The HAWT system traditionally exploits the lift effect on the turbine blade which is similar to that of an aeroplane,while the VAWT system isa

drag-based design. This changed recently with modification of the VAWT to also utilise the lift effect. A major advantage of the VAWT is that it can accept incoming flow from any direction and is less hindered with wake effects from nearby turbines if orientated appropriately. If the VAWTs are placed in the opposite direction as the neighbouring turbine, the resultant efficiency of the turbine increases. The assumption is that the opposing spins form a control volume around both turbines, reducing the drag interreference of the flow.

Colmenar-Santos et al. [1] conducted research on the status, challenges and future impacts of Spanish offshore wind developments. The article focused mainly on the electrical components of the system from the generator to the transmission systems. The paper investigated the foundation options for offshore wind turbine facilities as well as local challenges which hinder offshore development,and proposed solutions. The main issues highlighted were environmental restrictions due to policy and regulations and that the offshore shelf depth was inadequate for the traditional offshore systems.

Arrambide et al. [8] noted that there are various technical challenges for offshore wind turbines,including the type of turbine model to be utilised in the power generation scheme. Wind farm designers consider several factors such as: the wind speed and designated wind class of the chosen site(s); the wake effects and electrical losses; the respective environmental impacts and restrictions; and power capacity and energy production for the chosen type of turbines.This data is also used to understand the cost per unit produced of the offshore facility. The researchers found that there was higher energy production for lower power density turbines. The study concluded that this parameter is more reliable than the selected capacity factor for a chosen wind turbine based on the site.

3. METHODOLOGY

The main objective for this study was to utilise the sites which were studied in [2] for the design of a helical cross-wind vertical wind turbine. The design was based on the investigations conducted by [5] as a basis for the design of a suitable offshore wind turbine. Each of the investigated sites' approximate area was used to determine the energy density with respect to the proposed conceptual wind turbine design at that site.

Each of the 4 sites' wind analysis data which were determined in [2] were used in the current study to understand the effect on the rotor torque of the turbine. The investigation methodology for the above-mentioned investigation objectives was as follows:

- Combined analysis of [2] to gauge the absolute minimum, mean and maximum wind speeds with respect to a chosen standard deviation for optimising the turbine design
- Parametric study of the proposed turbine design in [5]
- The effect of varying the turbine performance parameters on turbine rotor torque and the turbines power curve
- Analysis of blade profiles and effect on rotor torque and power curve
- The turbine's respective power coefficient curves based on selected turbine airfoil profiles
- The effect on power curves was found at various turbine aspect ratios

The numerical processing software called QBlade [9] was utilised in the analysis of the turbines in this study. The simulation software was first used in the investigation of a hydrokinetic turbine studied in [5]. The study showed a good

correlation with other computer fluid dynamic (CFD) software and empirical results obtained from other researchers. The same software was used with the addition of a lifting line model which was added to the package in 2019. This resulted in understanding the effect of the wake field on the turbine spacing configuration as recommended in [5]. Since the effect of stacking was done in this study, the mean and standard deviation resultant wind speeds were taken for all hub heights (50m, 100m, 200m) which were researched in [2]. This proved useful as each site had a unique dispersion of wind speed.

4. SITE INVESTIGATION AND ANALYSIS

This section of the investigation analyses each of the potential sites based on the above methodology. Wind resource data was difficult to acquire. The use of satellite imagery tools (ASCAT, QuickSCAT, RapidSCAT etc.) did not contain relevant data which could be readily used for the analysis of the wind potential at the chosen sites. The International Renewable Energy Agency (IRENA) data was more suitable. IRENA is a free, online portal for the high-level assessment of renewable energy resource potential at a chosen location / site [9].

The wind resource data was obtained from the Technical University of Denmark's (DTU) *Global Wind Atlas* portal which uses data from IRENA [10]. Data from this source was also used to develop the *Wind Atlas of South Africa – WASA*[10] which was developed for onshore wind analysis of the South African coastline by various South African research bodies such as the CSIR, South African Weather Services, University of Cape Town and the DTU Department of Wind Energy. The wind atlas was constructed using various onshore meteorological sites in conjunction with conventional forecasting tools such as the WAsP wind simulator.

The online portal allows for the rough selection of points for data collection. The potential sites were mapped as estimated polygon shapes based on the co-ordinates of each of the boundary points. The resultant wind statistical data was downloaded in WAsP format to be analysed further.

4.1 Site Overview

4.1.1 Site 1

Site 1 (Figure) is located off the eastern coast of Durban, roughly 200 km offshore from the Durban harbour in a south east direction or 115° bearing. The site has an estimated perimeter of 600 km and an estimated surface area of ± 21 000 km^2.

Figure 2: Site 1

4.1.2 Site 2

Site 2 is a larger site than Site 1. It is located roughly 300 km south of Port Elizabeth. It has an estimated perimeter reading of 1 250 km and an estimated surface area of ± 79 000 km^2. The site is located in a potential retroflection zone[1] for ocean currents as found by Cunden [5]. Figure 12 is a graphical representation of the potential of Site 2. From the meteorological data collected, the site comprised 36 individual meteorological data points which were analysed at various hub heights. The average wind speed for hub heights 50 m, 100 m and 200 m were 9.47 m/s, 9.55 m/s and 9.68 m/s respectively.

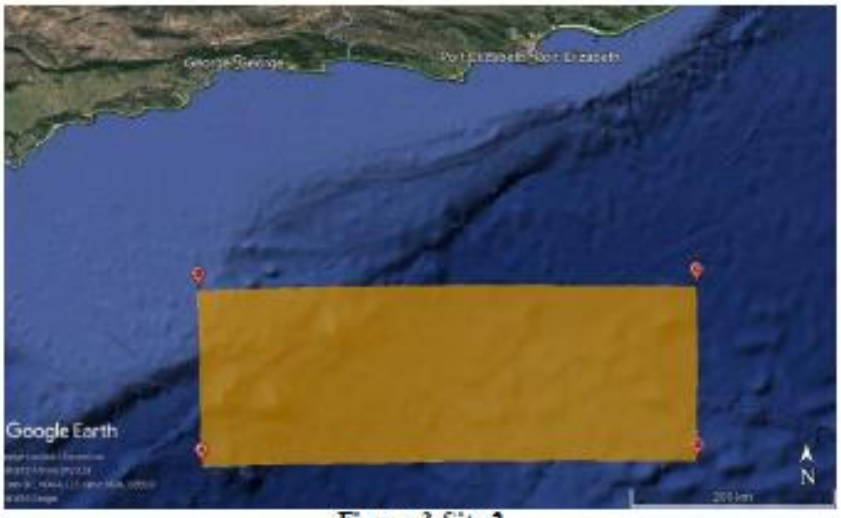

Figure 3:Site 2

4.1.3 Site 3

Site 3 is located roughly 290 km south (± 188° bearing) of Cape Town (Figure 4). The site has an estimated perimeter of 463 km and an estimated surface area of ± 13 332 km^2. The site is the smallest of the four identified potential wind farm sites. The average wind speed for hub heights 50 m, 100 m and 200 m were 9.12 m/s, 9.12 m/s and 9.27 m/s respectively.

Figure 4: Site 3

[1] A retroflection zone is an area in which the flow in question encounters specific obstacles which cause the flow to diverge from the original path and turn on itself, either clockwise or anticlockwise in direction.

4.1.4 Site 4

Site 4 is located an estimated 570 km north west (± 298° bearing) of Saldanha Bay and is the furthest offshore of the four potential sites. The site has an estimated perimeter of 807 km and an estimated surface area of ± 37 419 km^2.

Figure 5: Site 4

Table 1 describes the wind speed regime for each site in totality. This means that the mean wind speeds at the various hub heights reflect the overall wind speed effect at that point of measurement. In the case of synthetic data, as which was used in [2] to obtain Table 1 the mathematical equivalent is found as the sum of the effect of the wind profiles from all wind directions.

Table 1: Wind Speed Potential Profile of each Site

Height	Parameter	Site 1	Site 2	Site 3	Site 4
50 m	Mean speed [m/s]	9.19	9.48	9.12	8.42
	Power density [W/m^2]	795.09	939.11	808.11	550.71
100 m	Mean speed [m/s]	9.25	9.55	9.11	8.50
	Power density [W/m^2]	852.00	1017.03	875.56	591.00
200 m	Mean speed [m/s]	9.34	9.68	9.27	8.65
	Power density [W/m^2]	982.27	1201.31	1032.78	684.88

4.2 Simulation Parameters

4.2.1 Wind Speed

Each of the four sites have unique wind profile regimes with independent wind profiles and distributions. Table 2 indicates the minimum, mean and maximum wind speeds used for the simulation of offshore wind turbine design.

Table 2 shows the post analysis for each of the sites for the predominant wind directions as per the distributions found in Appendix A.

Table 2: Post site analysis - Wind Speed

	Sites			
Wind Speed [m/s]	1	2	3	4
Min	7.8	6.1	4.9	7.9
Mean	10.3	9.0	7.4	10.0
Max	13.0	12.0	10.1	12.0

4.2.2 Turbine Parameters

The turbine which was used for the simulation was based on the research conducted by [5] and was further investigated to understand if a hydrokinetic turbine design may be used for a wind turbine application.

The solidity ratio (σ) of a turbine represents the circumferential blade area in comparison to the void area of the turbine. The solidity ratio can be represented as follows [5].

$$\sigma = \frac{Bc}{\pi D} \tag{1}$$

where:

σ	Solidity Ratio (-)
B	Number of Blades (-)
c	Chord length of the blade (m)
D	Turbine Diameter (m)

Initially a 1 MW turbine was designed for as a single VAWT which may be seen in Appendix B.However, the blade chord lengths were too high for construction and the structural stability of this turbine was thought to be impractical. As chord length was the limiting parameter, a parametric investigation was conducted by varying the turbine diameter and solidity ratio to find a suitable chord length for the turbine.

Table 3 shows the effect on the turbine chord length based on variation of the solidity ratio and turbine diameter to obtain suitable blade chord lengths to work with.

Table 3: Effect on Blade Chord Length

		Solidity Ratio (σ)				
		15%	20%	25%	30%	35%
Turbine Diameter (m)	5	0,59	0,79	0,98	1,18	1,37
	10	1,18	1,57	1,96	2,36	2,75
	15	1,77	2,36	2,95	3,53	4,12
	20	2,36	3,14	3,93	4,71	5,50
	25	2,95	3,93	4,91	5,89	6,87

The investigations conducted in [11] indicated that an Aspect Ratio (AR) of 1 was the most stable through all blade Reynolds numbers. The current investigation aimed to understand the effects of AR on the turbine rotor toque as well as performance based on the turbine design.

The turbine which was designed in [5] forms the basis for investigation. The investigation found that a 4 bladed

turbine resulted in steady torque loading on the turbine rotor in comparison to a 3 bladed VAWT in the same category. This paper investigates the effect of varying the blade number on the rotor torque and turbine performance.

Blade wrap was used to understand the effect of helix angle on the turbine's performance. Blade wrap is defined as the percentage of a turbine's radial circumference which is occupied by the collective amount of blades [5]. In simple terms, this is the understanding of how much of the turbine's blades are in contact with the incoming flow. In the case of 100% blade wrap this would indicate that the turbine always has a blade in contact with the freestream incoming flow. Less than a 100% would indicate regions of voids which results in periodic vibrations on the rotor torque. Blade wrap is represented as shown:

$$\dot{\varphi} = \frac{BH}{\pi D \tan\delta} \tag{2}$$

where:

$\dot{\varphi}$	Blade Wrap (-)
B	Number of Blades (-)
H	Turbine Height (m)
D	Turbine Diameter (m)
δ	Blade Helix Angle (^{o})

QBlade v.963 software was used to simulate the turbine configurations and obtain blade rotor torque [12]. The following were chosen as turbine parameters to be investigated in the numerical simulations:

σ	Solidity Ratio (%)	20% / 25% / 30%
c	Blade Chord Length (m)	1.57 / 1.96 / 2.36
D	Turbine Diameter (m)	10
AR	Aspect Ratio (-)	1 / 1.5 / 2.5
B	Number of Blades (-)	4
$\dot{\varphi}$	Blade Wrap (%)	100%

4.2.3 Blade Profile Analysis

There are various types of blade profiles which may be used for turbine design. Various types of cambered and symmetrical profiles exist, and each has unique properties which directly affect the performance of a turbine. Cambered blades result in trailing edges which have negative effects on turbine output for a VAWT type turbine. Symmetrical blade profiles were chosen arising from investigations in [5] which found that the downwind effect on blade tangential torque was minimised with a symmetrical profile in comparison to a cambered profile. Simulations of NACA 4 series, NACA 5 series and Selig profiles on a 3 bladed VAWT was conducted by [11]. The results gave an indication of how various

turbine blades behaved under low to relatively high blade Reynolds numbers. From these results 3 blades were chosen from each of the airfoil profile groups which exhibited good power curve characteristics through the changing Reynolds domains. The chosen blade profiles are depicted in Figure 6.

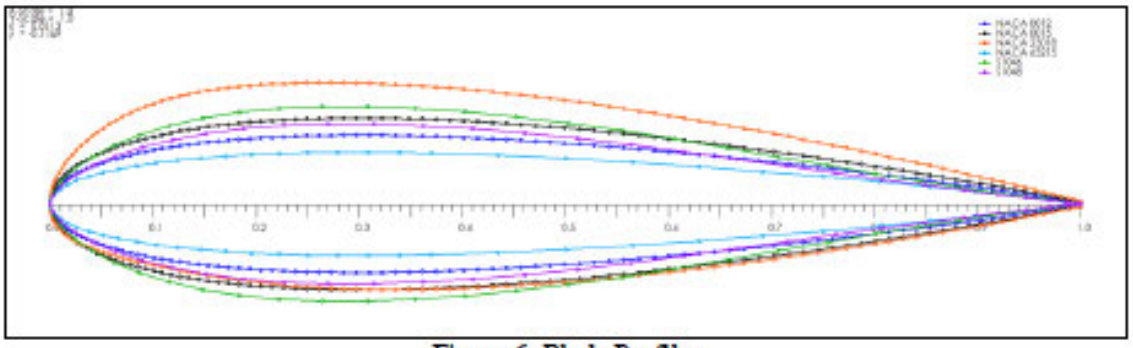

Figure 6: Blade Profiles

The blade Reynolds number is the comparison of the fluid flow velocity over the blade chord length in relation to the prevalent wind speed entering the blade circumferential path as it moves through a single rotation, [5].

$$Re_{Blade} = \frac{U_{Rel}\, c}{v} \tag{3}$$

where:

Re_{Blade}	Blade Reynolds Number (-)
U_{Rel}	Relative incoming wind speed (m/s)
c	Chord length of the blade (m)
v	Kinematic Viscosity of air at Sea Level (m^2/s)

Each site had its own respective wind speeds as previously mentioned. The results from Table 4 were used for various turbine aspect ratios and radii to determine the blade Reynolds numbers per site, respectively.

Table 4: Blade Reynolds Numbers

	Site 1	Site 2	Site 3	Site 4
Min	5,035,155	3,937,750	3,163,110	5,099,709
Mean	11,834,767	10,651,290	8,870,696	11,189,234
Max	25,175,777	23,239,179	19,559,642	23,239,179

In order to obtain the respective characteristic curves for each blade profile the blade Reynolds number is required accompanied by the respective Mach number for numerical analysis. Added to the numerical solver are the site ambient conditions as a factor which is then included in the interpolation calculations.

The initial polar plots were obtained using Xflr5 XFOIL software [13] for the Min, Mean and Max blade Reynolds numbers for all sites. The software has two methods of analysing transition over the blade profile,namely, forced

and free transition. Forced prediction occurs over the trailing edge of the blade. Free transition is predicted using the simplified envelope method to predict the growth of two-dimensional Tollmein-Schlichting waves [14]. The user defined input of NCrit in the simulation allows the user to affect the envelope method based on real case scenarios [14].

The NCrit factor is a scale factor in the XFOIL simulation extrapolating the ambient physics conditions over the blade profile. The number represents the amount of ambient condition interference where 9 is the closest to a clean wind tunnel and 1 represents a large amount of interference or a dirty wind tunnel [14], [15]. In a real scenario this was considered to represent the particulate conditions which may be experienced offshore from airborne water through waves or sand clouds moving across the oceans. The studies conducted by [14], [16] indicate that the operating range for NCritis generally between 4 and 6.

Table 5 shows the parameters taken for the initial simulations of the polar characteristic curves of each blade.

Table 5: Blade XlfrPolar Parameters

	Re	Mach	Ncrit	
Min	3 163 110	0,02	1	9
Mean	10 051 993	0,02	1	9
Max	25 175 777	0,02	1	9

Figure 7 shows the ratio of lift to drag versus the blade's angle of attack (AoA) ranging from -25^0 to 25^0. It can be seen that the NACA23018 blade profile had higher performancecurves under more controlled ambient conditions taken as NCrit 9. The NACA63215 profile seems to underperform at a lower Reynolds number, however, all blade profiles seem to exhibit stable performance for both NCrit 1 and NCrit 9.

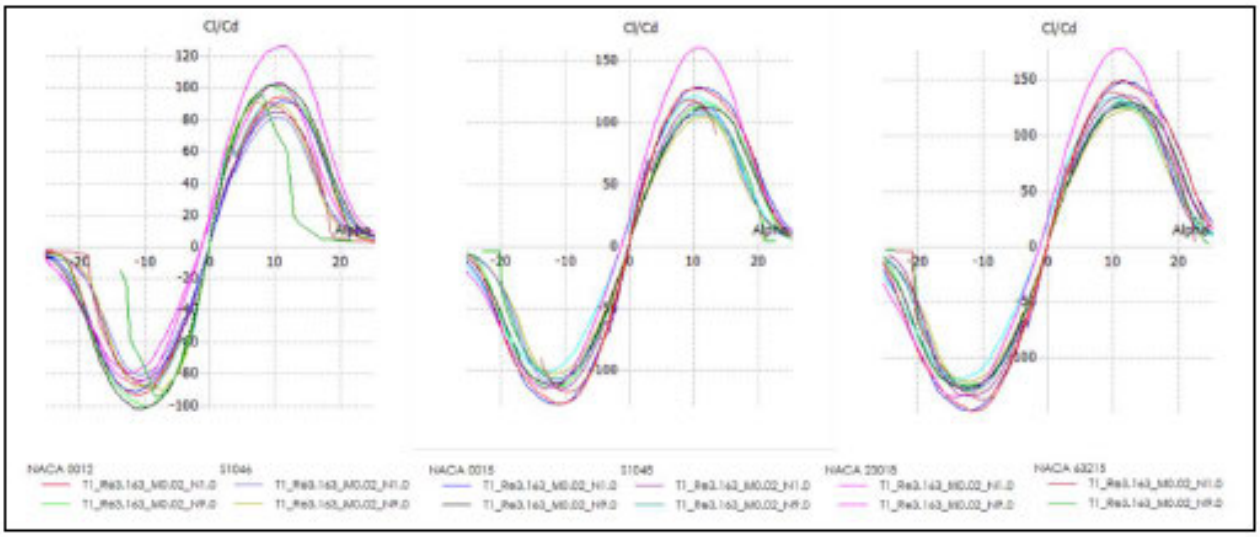

Figure 7:Lift/drag Coefficients vsAoA

Figure 8 shows the ratio of lift versus the blades' angle of attack (AoA) over the 3 blade Reynolds number scenarios shown in Table 5 above. As shown in [15], the profiles which were thicker performed better throughout the Reynolds distribution. Based on these findings the blade profiles chosen for turbine simulations in this study were NACA0015,NACA23018 and Selig S1046 due to their thicker profiles

and initial characteristic lift and drag characteristic curves.

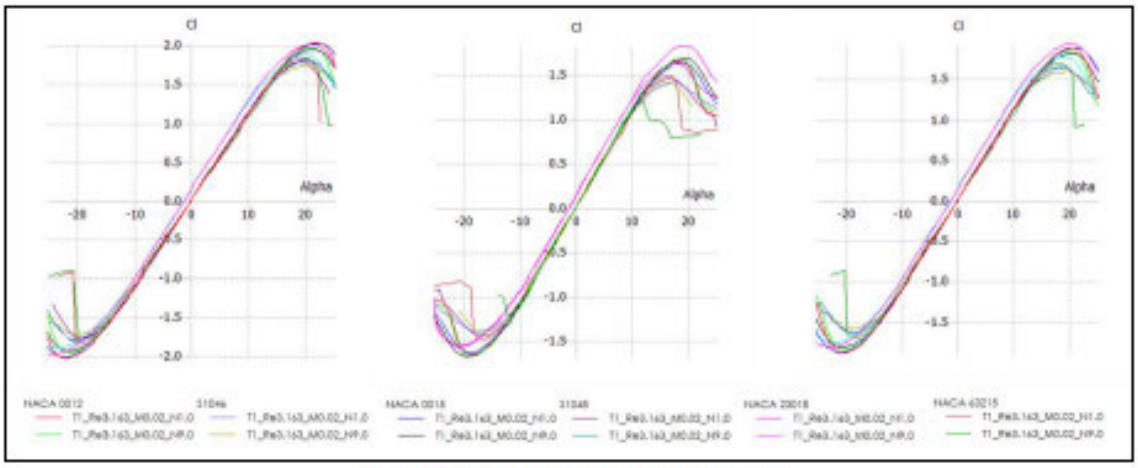

Figure 8: Lift/dragCoefficient vsAoA

Since the initial polar plots only predict for a limited AoA range, an extrapolation is required. Two types of extrapolation methods exist for aerodynamic / hydrofoil blade profile polar plots. Investigations conducted by [17] gave deeper insight into the extrapolation methods and the basic assumptions used for each.

Viterna Method

The Viterna method is the most commonly used method of extrapolation of blade profiles, [17]. The Viterna method relies on the initial polar plots to extrapolate the data from α_{stall} to 90^0 using the following [18]:

$$C_L = A_1 \sin 2\alpha + A_2 \frac{\cos^2 \alpha}{\sin \alpha} \tag{4}$$

$$C_D = B_1 \sin^2 \alpha + B_2 \cos \alpha \tag{5}$$

where:

$$C_D \approx 1.11 + 0.018AR \tag{6}$$

$$A_1 = \frac{C_{Dmax}}{2} \tag{7}$$

$$B_1 = C_{Dmax} \tag{8}$$

$$A_2 = (C_{LStall} - C_{Dmax} \sin \alpha_{Stall} \cos \alpha_{Stall}) \frac{\sin \alpha_{Stall}}{\cos^2 \alpha_{Stall}} \tag{9}$$

$$B_2 = \frac{C_{DStall} - C_{Dmax} \sin^2 \alpha_{Stall}}{\cos^2 \alpha_{Stall}} \tag{10}$$

The affect or Aspect Ratio (AR) has little effect on the result as it is only a small fraction in obtaining the drag coefficient for the method. The Viterna method does not, however, consider the pressure or skin friction force distribution of the profile. However, with reasonable assumptions in relation to the simulation the Viterna method provides reasonable

estimates for early design considerations [17], [19].

Montgomerie Method

The Montgomerie method is formulated around the assumption that there is some potential flow around the airfoil at AoA of 0^0. At higher angles of attack the assumption is that the airfoil behaves like a basic thin plate under flow conditions. For intermediate AoA a transformation function f is introduced to simulate the flow physics behaviour over the profile. The interpolation occurs between the thin plate behaviour (s) and the potential flow curve (t) which can be represented as follows [20]:

$$C_L = ft + (1 - f)s \tag{11}$$

Where the line function (t) is a tangent to the C_L curve at AoA = 0. The transformation function is determined from the initial polar plots of C_L vs α. The function is calculated as follows [20]

$$f = \frac{1}{(1 + k\Delta\alpha^4)} \tag{12}$$

Where:

$$k = (\frac{1}{f_2} - 1)\frac{1}{(\alpha_2 - \alpha_m)^4} \tag{13}$$

The introduction of α_m into the solving of the variable (k) is defined as the angle where the C_L starts to deviate from the potential curve (t) [17]. This angle can be computed using the following formula:

$$\alpha_m = \frac{\alpha_1 - G\alpha_2}{(1 - G)} \tag{14}$$

And the G variable is described as the function [17], [20]:

$$G = \sqrt[4]{\frac{\frac{1}{f_1} - 1}{\frac{1}{f_2} - 1}} \tag{15}$$

The investigations conducted by [17] indicated that for a detailed understanding of the flow physics in the numerical solver, the Montgomerie method produces a closer result than that of the Viterna due to the iterative transformation function that is incorporated in the Montgomerie method. This was the basis of choosing the Montgomerie method for extrapolating the polar plots for the chosen blade profiles shown in Figure 9.

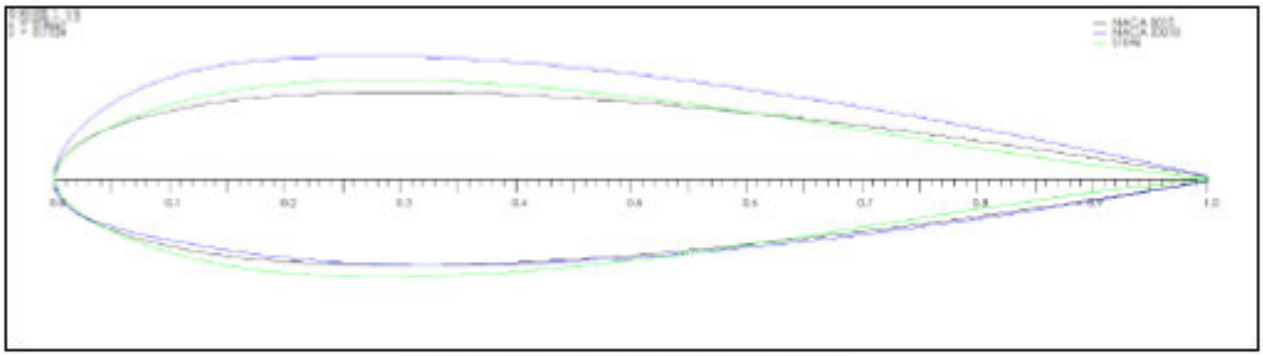

Figure 9: Final Selected Airfoil Profiles

5. RESULTS

The extrapolated blade profile data was used in the double multiple streamtube model as described in [5], [21]. It was found in [5] that a higher discretisation of the initial turbine blade results in more reasonable results. Figure 10 shows the blade discretisation which was refined to be used for each blade simulation. The discretisation allows for a higher resolution of understanding on the performance curves for the turbine.

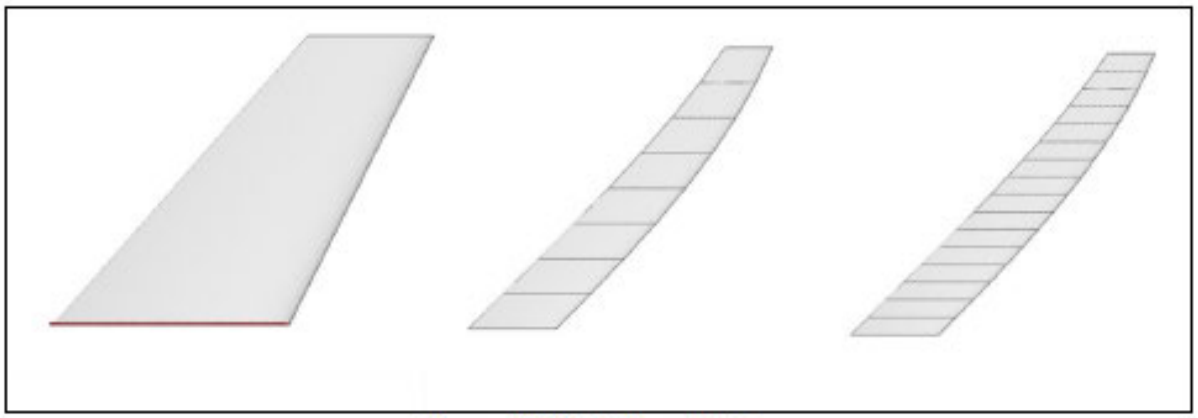

Figure 10: Blade Discretisation

Figure 11 depicts the results from the simulation for all 3-blade Reynolds number scenarios mentioned earlier in comparison to varying solidity ratio by changing the blade chord length. It can be seen from the results that the high solidity ratio favours the turbine performance curve as the turbine can maintain performance over a larger tip speed ratio (TSR) range. The results also show that the symmetrical profiles of NACA0015 and Selig S1046 have a higher performance curve thanNACA23018.

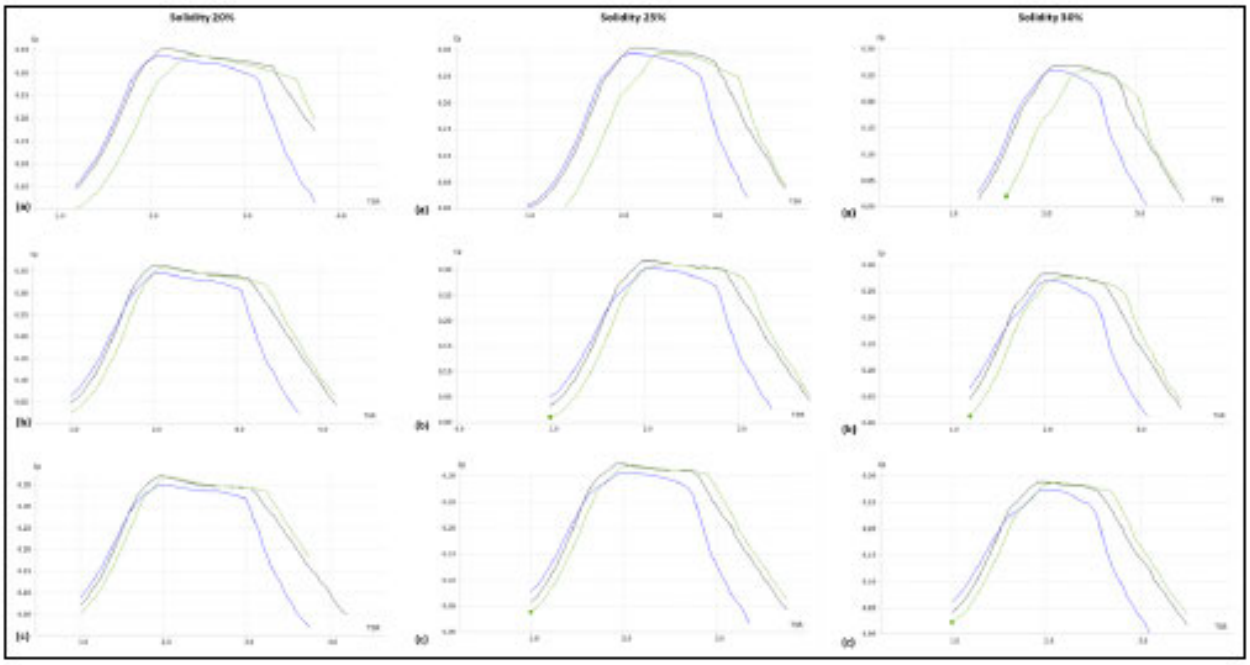

Figure 11: CP Curves for Varying Solidity Ratios
Blade Reynolds No. - (a) Min, (b) Mean, (c) Max

Figure 12 shows the point at which the NACA23018 profile starts to show signs of instability as the tangential force on the blade seems to peak slightly through the TSR of 2.8. This is not yet evident on the torque output on the rotor Figure 13 shows the torque assessment at TSR 3.4 of the blade profiles. It is seen that both the NACA23018 and the NACA0015 profiles start to become unstable which is evident in the torque profile on the rotor, whereas the S1046 profile seems to be more stable.

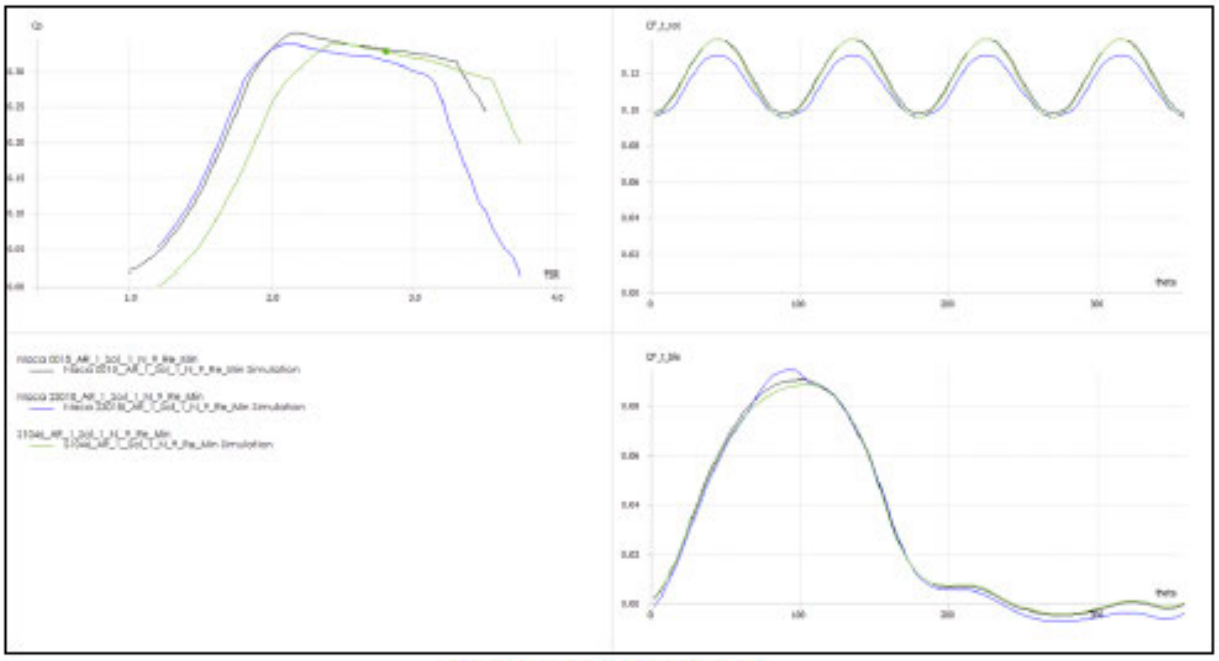

Figure 12:CP Assessment 1

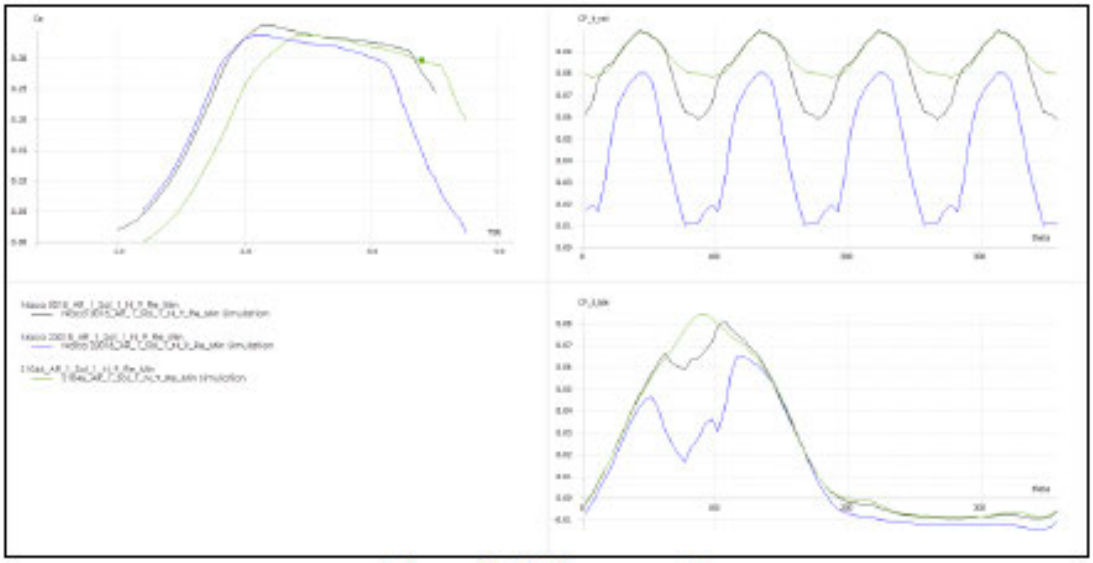

Figure 13:CP Assessment 2

The above results show the effect of thicker symmetric blade profiles on the torque output of a helical VAWT design according to [5]. Based on these results the S1046 profile was chosen for the helical VAWT design as it exhibits a larger TSR operating range with relatively steady torque profile on the turbine shaft through these ranges.

Figure 13 shows the tangential force on the blade as it moves through its circumferential path of the turbine on the bottom right corner. It can be seen that in comparison to the previous TSR in Figure 12 above, the forces on the NACA0015 and NACA23018 profiles seem to undergo some stall or fluctuation on the blade which gets translated back to the turbine rotor.

Figure 14 depicts the variation of the performance curve due to the change in AR while using the S1046 profile and a solidity ratio of 20% by utilising a chord length of 1.57m. The results show that an AR of 1.5 outweighs that of 2.5. The operating range of the turbine has been extended to ±3.75 which allows the turbine to operate longer at a stable output in comparison to to the ARs of 1 and 2.5.

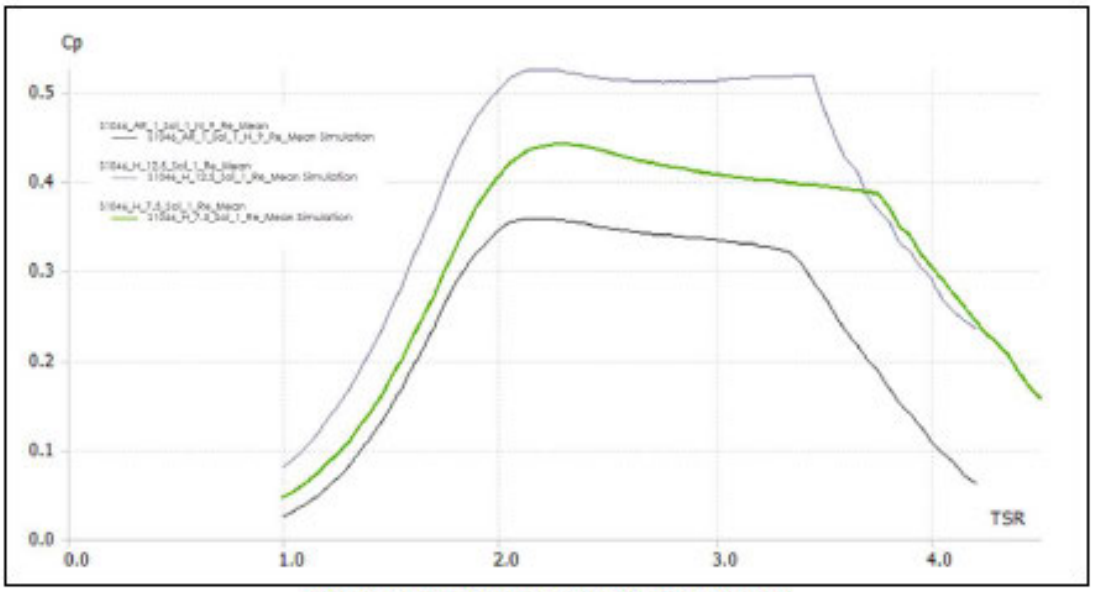

Figure 14:CP Assessment with Varying AR

Figure 15 shows the analysis of the torque profile of the different aspect ratios. The results show a TSR of 2.2 with all profiles showing stable conditions on the turbine rotor. At TSR 3.45 the AR of 1 becomes unstable first and is seen with the black line in the torque profile. For a TSR of 3.75 the results show that both the AR of 1 and 2.5 become unstable which is reflectedin the torque profile of the turbine. This shows that an AR of 1.5 seems suitable for further investigation as the operating range of the turbine with respect to tip speed ratio is larger than that of the compared ARs.

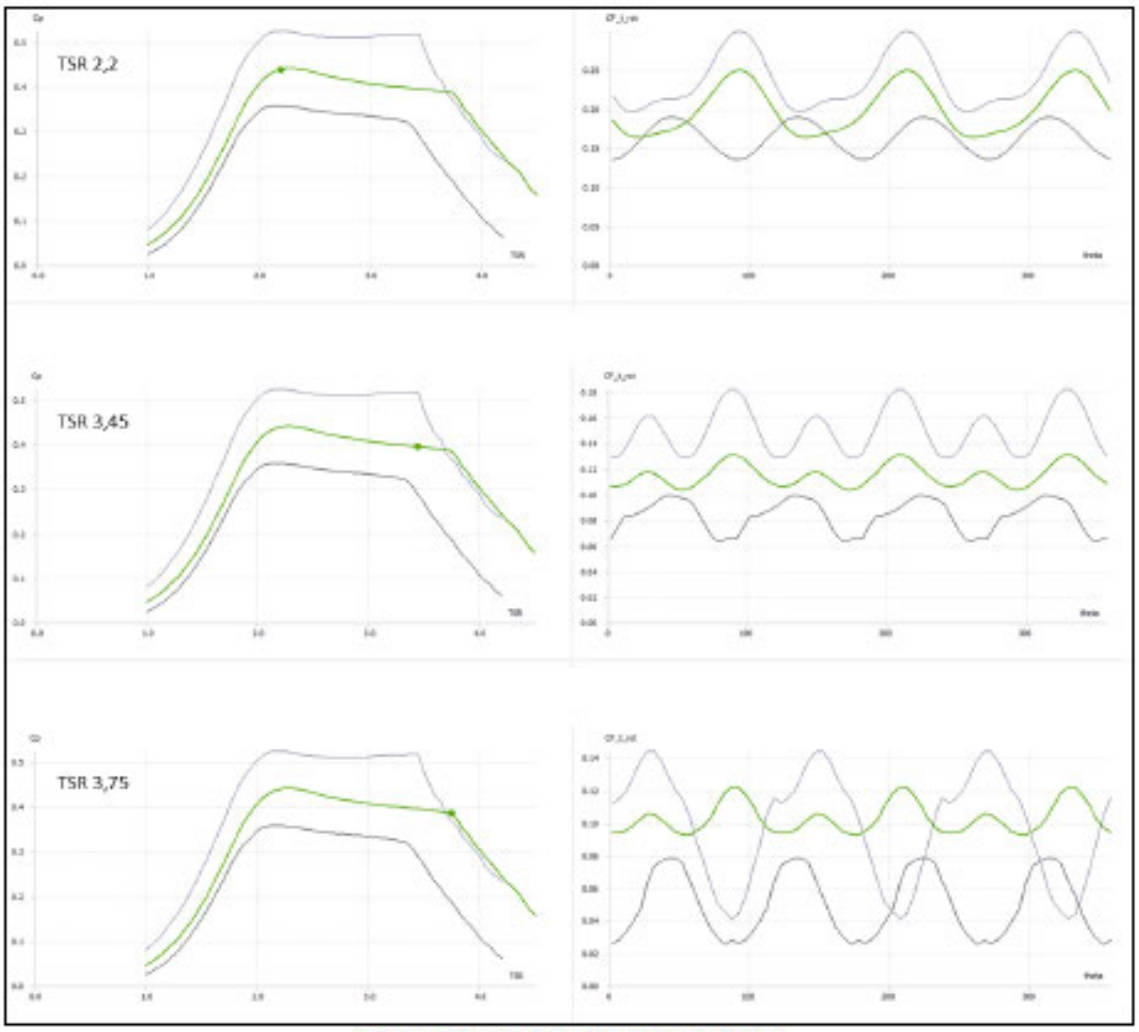

Figure 15:Analysis of Torque Profile

6. CONCLUSIONS

This article aimed to investigate the turbine design investigated in [5]in the context of similar characteristics to those found in the sites identified in [2]. The paper investigated multiple airfoil profiles which were narrowed down to a single symmetric blade profile. The blade profiles were examined across the minimum, mean and maximum wind speeds of the sites. This was translated to equivalent blade Reynolds numbers which were used in the simulations. Post assessment of the initial performance curves allowed for reduction of turbine parameters to solidity ratio and blade profile which were favourable for the turbine output. The torque profiles were examined over the TSR operating range as well as the effect of aspect ratio on the turbine's performance.

The Selig series S1046 displayed favourable results for an offshore turbine in comparison to the other blade

profiles examined via the numerical simulations. The performance of this profile is shown in Figure 7 which compares the performance curves in the min, mean and maximum wind speeds translated to blade Reynolds numbers. It was evident that an increase in solidity ratio decreased turbine performance by narrowing the operating TSR range of the turbines as shown in Figure 7 comparing the curves across the Reynolds distribution. The results show that the S1046 profile exhibits a stable torque on the turbine rotor at high TSRs compared to the NACA23018 and NACA0015 profiles. The aspect ratio shifts the turbines performance curve vertically; however, the performance result is not scaled linearly. The results depict that an aspect ratio of 1.5 has a larger TSR operating range than a lower aspect ratio of 1 and a higher aspect ratio of 2.5. Comparison of the torque profiles also shows more stability with the aspect ratio of 1.5.

6. FUTURE WORK

Future work is planned to assess the turbine design in a farm layout to be further assessed on the sites mentioned in Table 2. The next part of the series of work will investigate a S1046 bladed helical turbine with an aspect ratio of 1.5 under the site conditions mentioned in [2] and in the post analysis of the sites conducted in this investigation. The turbine will also be tested under NCrit values of between 4 and 6 as recommended by [14], [16].

ACKNOWLEDGMENTS

We would like to acknowledge the assistance of government institutions for the assistance with information as well as our colleagues at the university for providing direction to the research.

REFERENCES

1. *A. Colmenar-Santos, J. Perera-Perez, D. Borge-Diez, C. DePalacio-Rodríguez, "Offshore wind energy: A review of the current status, challenges and future development in Spain". Renewable&Sustainable Energy Reviews, vol. 64, 2016, 1–18.*
2. *F. L. Inambao, K. Cunden, "Offshore wind resource assessment off the South African coastline". International Journal of Mechanical Engineering & Technology, Vol. 10, No. 6, 2019, 95-119.*
3. *Eskom, "Eskom - Transmission Development Plan 2016 - 2025". 2016.*
4. *Eskom, "Map of Eskom Power Stations". 2013.*
5. *K. Cunden, "Design of a novel hydrokinetic turbine for ocean current power generation," Master's dissertation, University of Kwa-Zulu of Natal, 2015. http://hdl.handle.net/10413/12499*
6. *M. R. Islam, S. Mekhilef, R. Saidur, "Progress and recent trends of wind energy technology".Renewable & Sustainable Energy Reviews, Vol. 21,2013, 456–468.*
7. *M. M. Moh Saad, N. Asmuin, and M. Ó. Óskarsdóttir, "A general description and comparison of horizontal axis wind turbines and vertical axis wind turbines". IOSR J. Eng. www.iosrjen.org ISSN, vol. 04, no. 08, pp. 2250–3021, 2014, [Online]. Available: https://skemman.is/bitstream/1946/19859/1/Margrét Ósk Óskarsdóttir.pdf?60Ahttp://www.iosrjen.org/Papers/vol4_issue8 (part-2)/E04822730.pdf.*
8. *I. Arrambide, I. Zubia, A. Madariaga, "Critical review of offshore wind turbine energy production and site potential assessment," Electric Power Systems Research, vol. 167, 2019, 39–47, 2019. https://doi.org/10.1016/j.epsr.2018.10.016.*
9. *International Renewable Energy Agency, "Average wind speed 1 km at 50m height DTA 2015," Global Atlas for Renewable Energy - Wind Map, 2015. https://irena.masdar.ac.ae/gallery/#gallery.*

10. Department of Wind Energy, "Global WInd Atlas 1.0." http://science.globalwindatlas.info/index.html.

11. S. Roy, H. Branger, C. Luneau, D. Bourras, B. Paillard, "Design of an offshore three-bladed vertical axis wind turbine for wind tunnel experiments," Proc. Int. Conf. Offshore Mech. Arct. Eng. - OMAE, vol. 10, 2017, doi: 10.1115/OMAE2017-61512.

12. Hermann Föttinger Institute of TU Berlin, "QBlade wind turbine design & simulation - open source software for HAWT &VAWT Simulations." 2020, [Online]. Available: http://www.q-blade.org/#welcome.

13. M. Drela, H. Youngren, M. Scharrer, A. Deperrois, "Xflr5." 2018, [Online]. Available: http://www.xflr5.com.

14. N. A. Cancelli, T. W. Von Backstrom, T. S. A. Denton, "Aerodynamic optimisation of a small-scale wind turbine blade for low windspeed conditions," 5th South African Conference on Computational and Applied Mechanics 2006, 177–185..

15. M. Caboni, E. Minisci, A. Riccardi, "Aerodynamic design optimization of wind turbine airfoils under aleatory and epistemic uncertainty," Journal of Physics: Conference Series, Vol. 1037, No. 4, 2018, doi: 10.1088/1742-6596/1037/4/042011.

16. J. Bosman, "The Aerodynamic & Structural Design of a 1kW Turbine Blade," WWEA Conference Paper, 2003.

17. F. Mahmuddin, S. Klara, H. Sitepu, S. Hariyanto, "Airfoil Lift and Drag Extrapolation with Viterna and Montgomerie Methods," Energy Procedia, vol. application to Aerodynamics for Blades on Wind Turbines and Propellers.pdf," no. June, p. 53, 2004.105, 2017, 811–816, 2017, doi: 10.1016/j.egypro.2017.03.394.

18. L. Viterna D. Janetzke, "Theoretical and experimental power from large horizontal-axis wind turbines," Clearvland, 1982. doi:doi:10.2172/6763041.

19. M. Brown, "Computational method for determining distributed aerodynamic loads on planforms of arbitrary shape in compressible subsonic flow," Master,s dissertation, University of Kansas, 2013.

20. B. Montgomerie, "Methods for root effects, tip effects and extending the ANgle of Attack Range to +- 180, with application to aerodynamics for blades on wind turbines and propellers". Swedish Research Defence Agency, 2004.

21. S. Roy et al., "Critical review of offshore wind turbine energy production and site potential assessment," Electric Power Systems Research, vol. 167, 2017, 39–47, doi: https://doi.org/10.1016/j.epsr.2018.10.016.

CHAPTER 5 : DESIGN, CONSTRUCTION AND TESTING OF LOW-SPEED WIND TUNNEL

The following chapter presents the design, construction and testing of a low-speed wind tunnel for the purpose of testing a small scale version of the vertical axis wind turbine. Simulation of turbines normally utilise input parameters which are based on assumptions leading to approximated results. The results are required to be verified against scaled model testing usually conducted in wind tunnels. The wind tunnel was based on an open circuit design to minimise the space requirements. The method of construction, design wind flow speed requirements, testing results and conclusions were documented within the article.

CHAPTER 5 – **Cite this article:** K. Cunden and F.L. Inambao, "**Design, Construction and Testing of Low-Speed Wind Tunnel**" published in the International Journal of Mechanical and Production Engineering Research and Development (IJMPERD), Vol. 11, Issue 6, December 2021, pp 237-256.

Link to article:

http://www.tjprc.org/publishpapers/2-67-1639046376-15IJMPERDDEC202115_Corrected_No_Formatting_08.12.2021.pdf

International Journal of Mechanical and Production Engineering Research and Development (IJMPERD)
ISSN (P): 2249–6890; ISSN (E): 2249–8001
Vol. 11, Issue 6, Dec 2021, 237–256

DESIGN, CONSTRUCTION AND TESTING OF A LOW-SPEED WIND TUNNEL

KUMARESAN CUNDEN & PROFESSOR FREDDIE L. INAMBAO

School of Mechanical Engineering, University of KwaZulu-Natal, Durban, South Africa

ABSTRACT

The increase in wind energy over the last decade has depicted a significant development in onshore and offshore wind turbine designs. Wind turbine designs are highly dependent on aerodynamic properties of lift and drag. There is normally an iterative process consisting of numerical design, prototype construction, testing and optimisation, calibration of computational flow models on the path to commercialisation. Theoretical turbine models are usually validated or optimised by the assessment of scaled models tested in a wind tunnel. The aim of this paper was to design and manufacture a small-scale low-speed wind tunnel for the testing and optimisation of novel wind turbines. An open circuit design was chosen instead of a closed system to save space. The wind tunnel was to achieve maximum flow speed of 9m/s in alignment to average wind speeds located off the South African coastline as investigated in previous studies. The conditions within the testing area of the design were required to maintain steady flow conditions. A hot wire wind anemometer was used to measure the flow speeds at different points of the wind tunnel for the validation of the design. The results showed that each section of the wind tunnel complied to the design conditions with minimum error. The turbulence intensity was also investigated and depicted across the circuit. The results have shown that the design philosophy which was chosen was sound and the system may be pursued for the testing of novel scaled wind turbines and scaled aerodynamic profiles for validation and optimisation purposes.

KEYWORDS: South Africa, Wind Tunnel & Offshore Wind Turbines

Received: Aug 24, 2021; **Accepted**: Sep 14, 2021; **Published**: Nov 06, 2021; **Paper Id.**: IJMPERDDEC202115

Original Article

1. INTRODUCTION

The current versions of wind tunnels have been in existence for roughly 150 years. Prior to this, the best approach was to attach a scaled model to a whirling arm as first utilised by Benjamin Robins (1707 – 1751) which made a large contribution to the early study of fluid mechanics [1], [2].

There are many different wind tunnel design types depending on the application. Wind tunnels which are classified based on the velocity of the fluid in the test chamber are known as subsonic, transonic, supersonic and hypersonic [3]. The Mach number can be used as a simplified way of understanding the type of wind tunnel being used. The subsonic wind tunnel ($M < 3$) can vary in cross-sectional area of the test section from less than 1 m x 1 m to systems large enough to encompass a full scale industrial truck or large aircraft models [4]. The testing of scaled wind tunnel models is tested in subsonic wind tunnels.

There are various aerodynamic phenomena which can occur at low speeds and low Reynolds numbers, one being a laminar separation bubble which may lead to a decrease in lift as well as an increase in drag leading instability, and unintended vibrational response [5]–[8]. Computational models are usually conducted and validated or optimised via wind tunnel testing and such models are used throughout research facilities, universities, governmental organisations and industry [4]. Some studies have been conducted in the past decades which have

proved some of the capabilities of robust mathematical models for simulations of aerofoils at both high and low Reynolds numbers which can be found in [9]–[11].

Wind tunnels are widely used to conduct aerodynamic tests for full or scaled versions of components [12]–[15]. These systems assist engineers to make appropriate design decisions and aid researchers in understanding thermo-fluid systems. Wind tunnels provide an appropriate means for researchers, engineers, and scientists to investigate complex thermo-fluid dynamic problems which are not always adequately captured by computational models and numerical simulations.

This study aimed to design a wind tunnel capable of being used to test a small-scale vertical axis wind turbine which was designed and elaborated in [16]–[18]. An open circuit design was chosen as this type of wind tunnel design has shown reliable results in previous researchers investigations [19], [20]. This research paper consists of the methodology used, the design methods applied, the phased construction of the wind tunnel system, and the results from the system.

2. METHODOLOGY

The wind tunnel was designed and fabricated for the purpose of testing a novel wind turbine airfoil design as described in [16], [18]. The wind tunnel was required to have suitable scaled contraction, with test and diffuser sections being capable of developing a 9 m/s fluid velocity within the testing chamber. This value was based on the average wind speed observed in [21] for potential offshore wind sites. The following methodological factors were applied to design, calibrate and test the wind tunnel system:

- A maximum turbine diameter (Φ) and height of 150 mm
- A maximum target fluid speed of 9 m/s in the testing chamber
- Selection of appropriate axial fan DC fan controller
- Calibration of wind tunnel axial fan
- Calibration of test chamber incremental steps
- Measure flow speeds at each section
- Evaluate the turbulence intensity of each section

3. DESIGN OF WIND TUNNEL

The axial fan was obtained first as the wind tunnel design constraints were dependent on the maximum wind speed of the fan chosen. A market scan was conducted of both DC and AC powered fans. The price was also a factor in choosing an appropriate cost-effective axial fan. A light 12 V DC fan was chosen and sourced from a light vehicle radiator unit. This led to obtaining a 300 mm, 12 V, 80 W radiator fan with a 30 A AC to DC power supply to meet the electrical demand of the fan. A market scan was conducted for various DC motor controllers with a variable potentiometer for controlling the pulse width modulation (PWM) waveform output to the motor by varying the resistance to effectively change the DC voltage supply.

Fluid flow in piping or ducting requires movement of fluid for the desired result of the system being utilised (i.e., refinery piping, water reticulation networks, power station cooling networks etc.). All these systems experience some form

of losses – major and minor. Major losses are normally due to frictional effects in fully developed flow which is dependent on the area of the duct. Minor losses are normally the result of inlets and exits due to area changes in the ducting system [22].

The selected wind tunnel system was split into four major sections, namely, the settling chamber, contraction (inlet), testing (middle) and diffuser (exit) sections with an open circuit wind tunnel design. The first part of the system was responsible for taking air from a natural atmospheric state and developing the flow to achieve laminar conditions via the settling chamber. The contraction nozzle was designed to accelerate the flow to desired speeds with minimum losses and turbulence to the flow entering the testing section of the system. The testing section was required to have a fluid speed of 9m/s to meet the mean wind speed conditions investigated in [21]. The diffuser section of the wind tunnel was designed based on the constraint of the axial fan maximum speed.

3.1 Settling Chamber

The settling chamber has a uniform cross-sectional area over its length [8] as its function was to stabilise the flow entering the system. The settling chamber was designed to achieve laminar conditions within the testing region of the wind tunnel. This is normally done by utilising some form of laminar flow element (LFE) [23] which resembles a group of straws covering the inlet flow area. Each straw element was narrow enough to achieve a Reynolds Number less than R_{crit} ($R_{crit} \approx 2300$) shown in equation (1) below [22].

$$Re_{Crit} = \frac{\rho V_{tube} D_{tube}}{\mu} \tag{1}$$

where: Re_{Crit} - Reynolds number for laminar flow (Crit ≈ 2300); ρ - Fluid density (kg/m^3); V_{tube} - Fluid Velocity (m/s); D_{tube} - Diameter of tube (m); μ - Dynamic viscosity of air (kg/m·s)

The minimum diameter of the tube elements was found to be ≈ 34 mm when setting the Reynolds number to 2300. The straws being used had a diameter of 5 mm resulting in a Reynolds number of 338.39 which was suitable to develop stable flow for the test section of the wind tunnel. The plastic straws, which were grouped in bundles of 55 to 60 individual straws, were utilised as laminar flow elements. Figure 1 is a graphical representation and layout of the planned settling chamber.

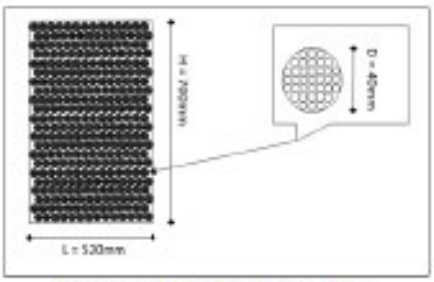

Figure 1: Settling Chamber

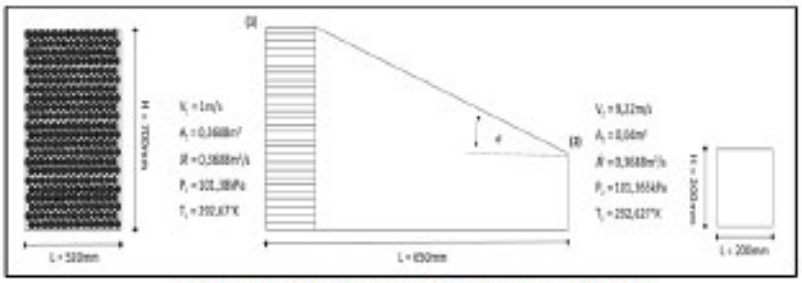

Figure 2: Settling and Contraction Section

The straws were stacked vertically, as shown in Figure 1, so as to cover the entire inlet of the contraction section. By arranging the straws in this way, the incoming flow was segmented into various stream tubes to develop the flow to a laminar state through a smaller hydraulic area. The flow rate for the entire hydraulic area equates to the sum of the flow rates of each laminar flow element as well as the linear pressure drop relationship to achieve laminar flow [22].

3.2 Contraction Section

The contraction section of the wind tunnel was directly coupled to the settling chamber. The purpose of this section of the wind tunnel was to accelerate the fluid flow to the testing section by gradually reducing the cross-sectional area per a unit distance from the settling chamber. The contraction angle (α) was designed at ≈ 20° from a height of 700mm reducing to 200mm over a length of 500mm.

The fan output was assumed to be 4 m/s based on initial testing of the fan without completion of the full wind tunnel, as the fan induces flow through the system. The mass flow rate was calculated based on the continuity equation (2) [22], [24] and taking the density of air to be constant throughout the system. The mass flow rate was calculated to be 0.3688 m^3/s using an area of 0.09 m^2 for the fan. Using this the inlet and exit velocities of the contraction section were found to be 1 m/s and 9.22 m/s respectively.

$$\dot{M} = \rho V A \tag{2}$$

where: $\dot{M}$ - Mass flow rate (m^3/s); V - Flow velocity (m/s); A - Hydraulic cross section area (m^2); ρ - Flow density (kg/m^3)

For systems where the flow rate is relatively low resulting in subsonic conditions, the fluid behaves as if it is an incompressible fluid. For the purpose of calculating initial gas states at key points of the wind tunnel, it was assumed that the flow was isentropic since the changes in flow variables across the entire system were gradual and not significantly large. The isentropic process allows for changes in the thermodynamic variables of a gas, although the heat capacity of the substance is required to be constant [25]. For this design, the heat capacity of the system was assumed constant resulting in the ratio of specific heats (equation 3) being constant [24].

$$k \equiv \frac{C_p}{C_v} \tag{3}$$

where: k - Ratio of specific heats (-); C_p . Specific heat at constant pressure (J/kg K); C_v- Specific heat at constant volume (J/kg K)

To check if the entire wind tunnel can be classified as a subsonic system, a Mach number is needed. If the Mach number is less than 1 the flow regime is classified as subsonic and if the Mach number is greater than 1 the flow regime is classified as supersonic. The Mach number is defined in equation (4) and is the relationship of the fluid velocity to the speed of sound of the same fluid:

$$M = \frac{V}{c} \tag{4}$$

where: M - Mach number (-); V - Fluid velocity (m/s); c - Speed of sound at fluid state (m/s)

Since the fluid is air and is modelled around the ideal gas equation, the speed of sound is a function of specific heats and temperature of the fluid. The speed of sound of the fluid can be calculated with equation (5) to attain the Mach number.

$$c = \sqrt{kRT} \tag{5}$$

where: c - Speed of sound (m/s); k - Ratio of specific heats (-); R - Unique gas constant (J/kg mol K); T - Fluid temperature (K)

The speed of sound corresponding to the fluid velocity found at the exit of the contraction section was 343.11 m/s at a temperature of 20 °C. The Mach number for the test section was calculated to be 0.027 which was significantly lower than 1, classifying the wind tunnel system as a subsonic system. As stated above, for subsonic conditions the flow regime may be treated as incompressible flow throughout the system, taking heat capacities as constant [22], [24], [25]. The Bernoulli equation (6) is commonly used to determine the static pressure of the system by understanding the dynamic pressure via the velocities as calculated above and illustrated in Figure 2. This was reduced to equation (7) taking that the static head differential between all points of the system is 0 m as the system is horizontally orientated.

$$P_1 + \frac{1}{2}\rho {V_1}^2 + \rho g h_1 = P_2 + \frac{1}{2}\rho {V_2}^2 + \rho g h_2 \tag{6}$$

$$P_1 + \frac{1}{2}\rho {V_1}^2 = P_2 + \frac{1}{2}\rho {V_2}^2 \tag{7}$$

where: P - Pressure (kPa); V - Flow velocity (m/s); ρ - Flow density (kg/m^3); h - Static head (m)

Equation (7) was a suitable method for calculating the pressure of each section of the wind tunnel. However, incorporation of the specific heat capacities of the fluid resulted in more accurate calculations, so stagnation equivalents were used as the enthalpy and internal energy components were also catered for. The stagnation state values are equivalent state variables as if the flow was adiabatically reduced to stationary [24].

$$\frac{T_o}{T_{ref}} = 1 + \frac{k-1}{2} {M_{Ref}}^2 \tag{8}$$

$$\frac{\rho_o}{\rho_{ref}} = \left[1 + \frac{k-1}{2} {M_{Ref}}^2\right]^{k/(k-1)} \tag{9}$$

$$\frac{P_o}{P_{ref}} = \left[1 + \frac{k-1}{2} {M_{Ref}}^2\right]^{k/(k-1)} \tag{10}$$

where: T_o, ρ_o, P_o - Stagnation state variables (temperature – K, density – kg/m^3, pressure – Pa); , T_{ref}, ρ_{ref}, P_{ref}

Temperature – (K), density – (kg/m^3), Pressure – (Pa); M - Mach number (-); k - Ratio of specific heats (-)

The surrounding ambient thermodynamic air state was used as initial reference gas properties which was applied to equations (8) to (10). Taking the reference gas state conditions shown at the inlet of the contraction section in Figure 2 above, the Mach number was 0.003, and the stagnation pressure (P_o) and stagnation temperature (T_o) were 101.38 kPa and 292.67 °K, respectively. These values were used to compute the outlet pressure (P_2) of the contraction section and local temperature (T_2) which were found to be 101.365 kPa and 292.627 °K, respectively.

Equation (11) was used as a standard thermodynamic method for determining the change in entropy from the contraction inlet to outlet. The change of entropy was 0.0409 kJ/kg·K which may be an indication of friction in the system

not factored in previously.

$$s_2 - s_1 = C_p \ln\frac{T_2}{T_1} - R \ln\frac{P_2}{P_1} \quad (11)$$

where: s_2- s_1 - Change in entropy (kJ/kg·K); C_P . Specific heat at constant pressure (J/kg K); T - Fluid temperature (K); R - Unique gas constant (J/kg mol K); P - Fluid pressure (kPa)

The contraction section is a nozzle which accelerates the fluid flow to the testing chamber and can also be assessed by understanding the relationship between the inlet cross-sectional area to the outlet of the contraction section which is referred to as the nozzle area ratio. This parameter should be large enough to attain maximum fluid acceleration and low total pressure losses in the upstream settling chamber [8]. Studies from [26] indicate that a nozzle contraction ratio which is in the range of 6 to 10 is adequate. Ratios below 6 results in higher pressure losses in the upstream sections typically at the screens used for laminar development, while ratios higher than 10 are not beneficial to the system fluid mechanics and is wasteful. The nozzle ratio of the current system was found to be 9.17 which is in line with the findings of [26].

The values calculated for the settling and contraction sections seemed to have been adequate to achieve the desired results at the test section of the wind tunnel. The states from the output of the contraction section were used as input for the test section of the wind tunnel.

3.3 Test Section

The turbine which was designed in [16], [17] and was further developed and numerically assessed in [18], utilised a Selig S1046 blade profile with the centre of mass at roughly 30 % of the blade profile. The turbine was constrained based on the maximum width of the testing chamber ± 180 mm considering clearance and tolerances for the turbine in the section. Figure 3 illustrates the testing chamber for the turbine, where the turbine was located on axis (a).

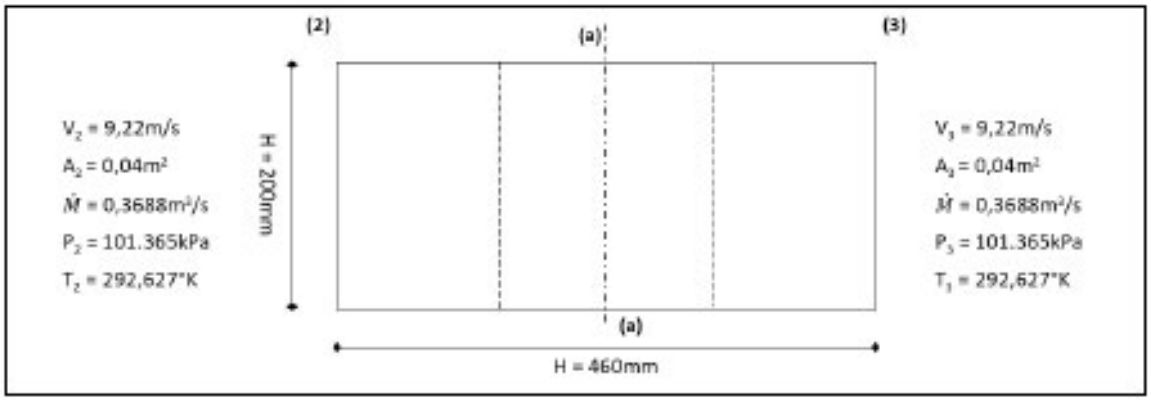

Figure 3: Testing Section.

The test section of the wind tunnel was designed to encompass one turbine to test torque and potential output power from the design in an effort to validate designs presented in [18] which was an adaptation from the designs of [16]. The testing section was assumed to be frictionless for the design phase to have negligible pressure drop over the length of the section.

Findings which were reported in [27] indicate that the testing chamber length would be best suited in a range of 0.5 to 3 times that of the inlet cross-sectional area. This was because of the flow requiring a minimum of 0.5 times that of

the cross-sectional area to develop the flow from the contraction section and avoid boundary layer separation. If lengths of the test section exceed 3 times the length of the inlet cross-sectional area, boundary thickness may occur. The test section which was designed had a length which was 2.3 times that of the hydraulic inlet area, which was acceptable.

3.4 Diffuser Section

Since the chosen wind tunnel system was based on an open circuit design the position of the fan was chosen to be located at the end of the diffuser to have an induced fluid flow field. This allowed the fluid to be pulled through the system passing through the settling chamber for flow straightening, entering the contraction section for accelerating the flow to the test section and finally recovering the flow via the diffuser and out the system from the work done by the axial fan.

Within the diffuser section of the wind tunnel there is a relationship between the cross-sectional area of the fan to that of the testing section outlet area or inlet of the diffuser. As shown in [26] an aspect ratio range is imposed on the relationship between the fan and testing outlet cross-sectional areas which is shown in equation (12):

$$2 \leq \frac{A_{Fan}}{A_{Test\ Section}} \leq 3 \tag{12}$$

where: A_{Fan} - Cross-sectional area of Fan (m^2); $A_{Test\ Section}$ - Cross-sectional area of test section (m^2)

The aspect ratio of the diffuser section was found to be 2.83 which was adequate as ratios above 3 results in irregular fan inlet flow speeds and lower than 2 causes an increase in wind tunnel dimension and fabrication costs. Figure 4 shows the fluid flow states from the inlet to the outlet of the diffuser and through the axial fan. The thermodynamic states were achieved by using equations (8) to (10) with reference values because of the testing chamber analysis.

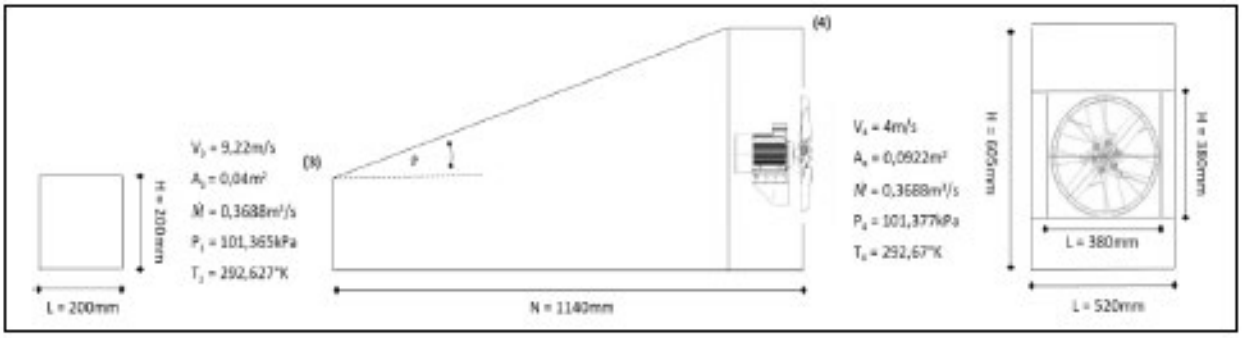

Figure 4: Diffuser Section.

A 12 V DC radiator fan was sourced (80 W) for the system which can generate a flow velocity of 4 m/s to 5 m/s. However, the fan required an appropriate controller to control the flow speed whilst testing the turbine over fluid velocities from 0 m/s to 9 m/s in increments of 0.5 m/s steps of analysis. The hydraulic area of the fan was 0.0962 m^2 utilising a hydraulic radius of 350 mm. The diverging angle of the diffuser (θ) was found to be 18.43° from the horizontal over a length of 1,14 m. The state equation (10) was used to find the outlet diffuser pressure, shown above, which shows suitable recovery through the diffuser section.

4. CONSTRUCTION

This section shows the construction of the wind tunnel system. Simple materials were used based on ease of supply and affordable prices. Each section of the wind tunnel was constructed separately and then joined via the section bases.

Table 1: Materials List – Settling Chamber and Contraction Section

Section	Materials	Size (L x B x W)	Qnt.
Settling chamber	Pine wood	700 mm x 22 mm x 22 mm	2
	Pine wood	520 mm x 22 mm x 22 mm	2
	Masonite	80 mm x 520 mm x 3 mm	1
	Steel straight bracket	45 mm x 45 mm x 15 mm	8
	Steel L bracket	40 mm x 15 mm x 3 mm	4
	Wood screw	3.5 mm x 16 mm	19
	Mesh	3.5 mm x 16 mm	1
	Plastic straws	530 mm x 720 mm	± 15,000
Contraction section	Pine wood	5 mm x 100 mm	2
	Pine wood	700 mm x 22 mm x 22 mm	2
	Pine wood	520 mm x 22 mm x 22 mm	2
	Pine wood	460 mm x 22 mm x 22 mm	1
	Pine wood	230 mm x 22 mm x 22 mm	4
	Masonite	650 mm x 22 mm x 22 mm	2
	Masonite	500 mm x 520 mm x 3 mm	1
	Wood screw	3.5 mm x 16 mm	10

The materials used for the construction were pine wood, Masonite, wood screws, masking tape, rubber sealer and glue. The exterior aesthetic of the system did not affect the performance of the wind tunnel, so this was not considered as a priority in the design. The construction of the wind tunnel also catered for key testing points in the system for the testing of wind speed and temperature.

Table 1 shows the material list for the construction of the settling chamber and contraction section. The mesh served as an extra layer of hydraulic refinement after the laminar flow elements and as a screen to hold the bundles of straw in place as flow was induced through the system.

Figure 5 shows the front and top view of the settling (a) and combined settling and contraction section (b) of the wind tunnel. The points highlighted in (b) as (1) and (2) are testing sections which corresponds to Figure 2. Test holes were drilled with a diameter of 20 mm to allow for the anemometer used for measuring wind velocity.

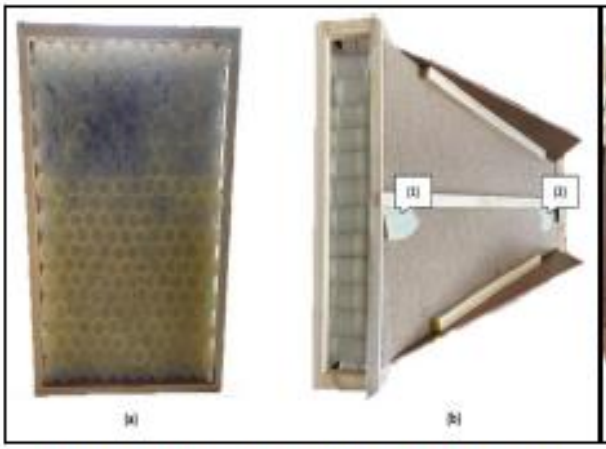

Figure 5: Constructed Settling Chamber and Contraction Section – (a) Side View, (b) Top View

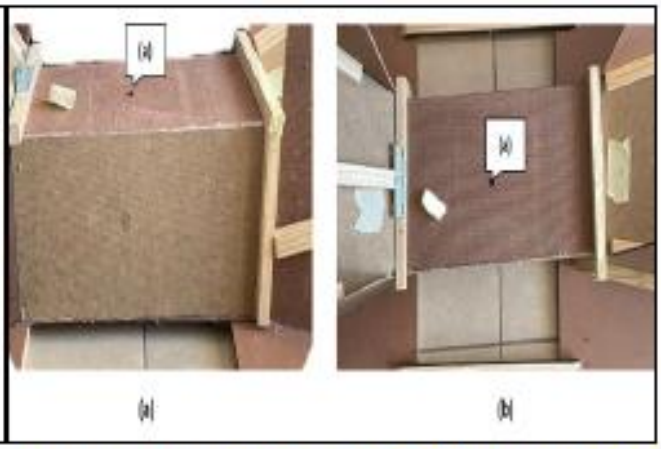

Figure 6: Testing Section – (a) Front View, (b) Top View of Testing Section.

The materials used for this section of the wind tunnel was Masonite board as shown above and rubber seal which was used to ensure minimum leakage. Masonite was chosen for each of the sections due to the smooth profile of one side reducing friction losses in the system. Table 2 shows the material list for the testing section of the tunnel.

Table 2: Materials List – Testing Section

Section	Materials	Size (L x B x W)	Qnt.
Testing Section	Masonite	460mm x 210mm x 3mm	4
	Rubber seal	840mm x 15mm x 3mm	2

Figure 6 shows the constructed testing section of the tunnel where the turbine would be subjected to aerodynamic loading. Figure 6 (a) depicts the side view and (b) the top view of the section of the system. The point indicated (a) in both pictures corresponds to the axis shown in Figure 3 above.

Figrue 7 shows the top view (a), side view (b) and the front view of the fan (c). The points labelled (3) and (4) correspond to the points indicated in Figure 4 above. The materials list for the diffuser section and fan section are reflected in Table 3.

Table 3: Materials List – Diffuser and Fan Section

Section	Materials	Size (L x B x W)	Qnt.
Diffuser section	Pine wood	850 mm x 22 mm x 22 mm	2
	Pine wood	700 mm x 22 mm x 22 mm	2
	Masonite	1000 mm x 650 mm x 3 mm	2
	Masonite	1000 mm x 520 mm x 3 mm	1
	Steel straight bracket	45 mm x 45 mm x 15 mm	2
	Steel L bracket	40 mm x 15 mm x 3 mm	4
	Wood screw	3.5 mm x 16 mm	30
Fan section	Pine wood	700 mm x 22 mm x 90 mm	2
	Pine wood	500 mm x 22 mm x 90 mm	2
	Pine wood	650 mm x 22 mm x 22 mm	1
	Pine wood	230 mm x 22 mm x 22 mm	4
	Masonite	1000 mm x 500 mm x 3 mm	1
	Masonite	650 mm x 500 mm x 3 mm	2

Figure 7: Diffuser Section and Fan – (a) Diffuser Top View, (b) Diffuser Side View, (c) Fan.

The system was joined together via the base of each section of the tunnel. The fan required DC power for operation so a 12 V AC to DC power supply was sourced (Figure 8). The fan was set to operate on constant full load rating if connected to the power supply directly. To control the fluid flow within the test section, proper control of the fan was required.

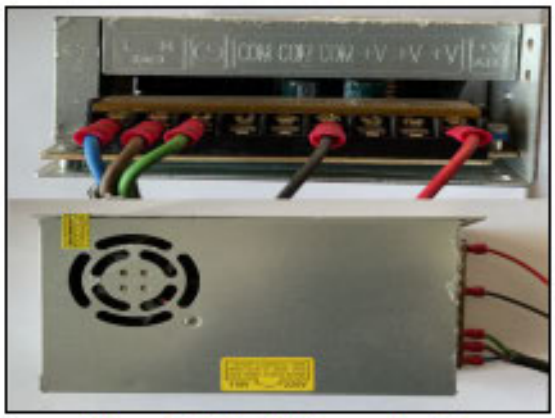

Figure 8: AC to DC Power Supply

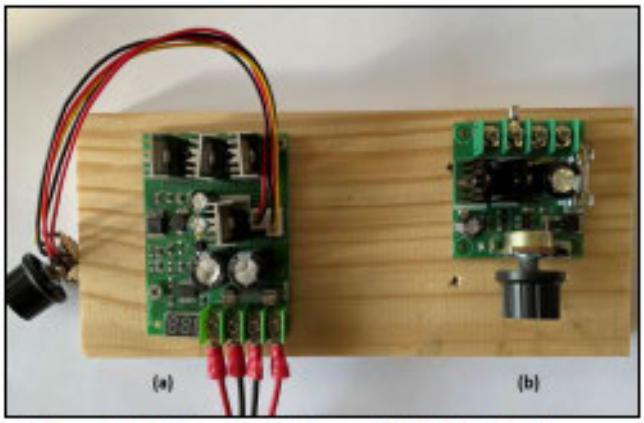

Figure 9: Motor Controllers – (a) 30 A, (b) 8 A.

Currently motor controllers are pulse width modulation (PWM) controllers. By adjusting the potentiometer on the device, the duty cycle of the motor is changed resulting in speed control via controlling the voltage. Initially an 8 A PWM controller was sourced but on testing it was not sufficient to control the motor stably at full load. This led to obtaining a larger 30 A PWM motor controller which ran the fan at full load without any fluctuations in output as experienced by the 8 A motor controller. Both motor controllers are shown in Figure 9.

Figure 9 (a) shows the controller which was chosen which has a linear relationship with the DC output voltage in relation to the percentage output of the LED when using the potentiometer to control the PWM output. This led to the mapping of the fan speed to the testing section speed which will be elaborated upon in the next section.

5. CONTROL AND INSTRUMENTATION

The following section of the paper explains the different tools and devices used for the control and instrumentation of the system to measure suitable variables in the wind tunnel. The major instruments which were used was a wind anemometer for flow speed and temperature and the motor controller for induced flow control. The methodology applied was to map the controller percentage output, reflected on the LCD shown in Figure 9 (a), with the test section speed in increments of 0.5 m/s.

A portable handheld sensor was used for measuring flow speed so as not as to cause major disturbances to the flow. A hot wire anemometer was chosen. This device also had telescopic capability which resulted in ease of measurement at the extremities of the contraction and diffuser inlet and out sections respectively. Figure 10 shows the anemometer which was used to measure the flow and temperature of the system. The devices' data was logged in per second readings in comma separated value format (.csv) which was exported and analysed in Microsoft Excel. However statistical data cleaning was required to the logged data which is further explained in the results section of the article.

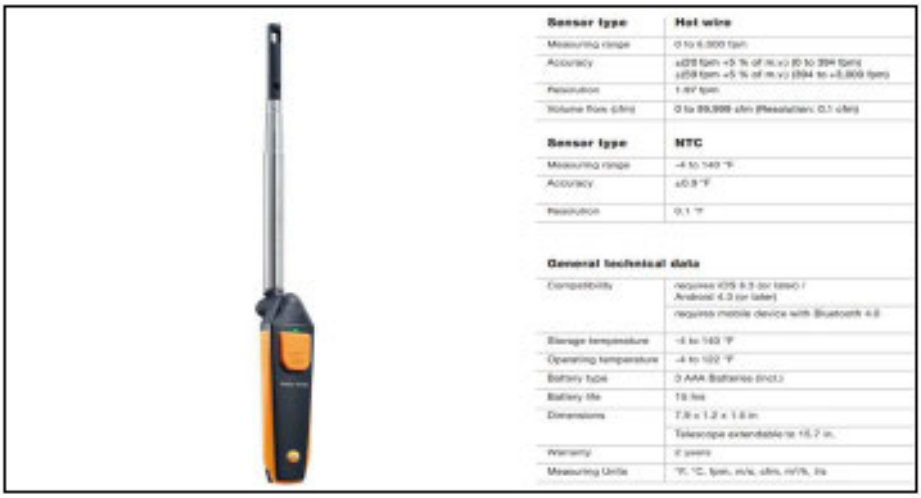

Figure 10: Hot Wire Wind Anemometer.

As shown in Figure 9, a motor control was used to control the fan speed. The motor controller chosen also had a linear relationship with the output DC voltage being regulated by the potentiometer to control the motor. Table 4 shows the mapping of the controller output to the 0.5 m/s increments for flow speed in the testing chamber of the wind tunnel system.

Table 4: Mapping of DC Controller to Test Section Flow Speed

Percentage	Voltage [DC]
0%	0,00
5%	0,58
10%	1,15
15%	1,73
20%	2,30
25%	2,88
30%	3,45
35%	4,03
40%	4,60
45%	5,18
50%	5,75
55%	1,00
60%	6,90
65%	7,48
70%	8,05
75%	8,63
80%	9,20
85%	9,78
90%	10,35
95%	10,93
100%	11,50

Test Section Speed	Percentage	Voltage [DC]
0,50	15%	1,73
1,00	19%	2,17
1,50	22%	2,53
2,00	29%	3,34
2,50	33%	3,80
3,00	38%	4,37
3,50	43%	4,95
4,00	48%	5,52
4,50	51%	5,87
5,00	57%	6,56
5,50	61%	7,02
6,00	66%	7,59
6,50	71%	8,17
7,00	76%	8,74
7,50	81%	9,32
8,00	86%	9,89
8,50	91%	10,47
9,00	96%	11,04
9,50	99%	11,39

6. RESULTS AND DISCUSSIONS

This section of the research shows the results from the testing points reflected in Table 4 to validate the design of the wind tunnel system. The data from the anemometer is read as comma separated values and processed in Microsoft Excel. To evaluate the system at various testing points on the wind tunnel, the tests were conducted for a period of 5 minutes resulting in 300 data points for sampling. However, for the incremental changes and calibrating the fan, the testing period was 1 minute per increment with a settling time of 45 seconds. The wind tunnel results were taken from testing the system

at full load conditions as the assumption was the conditions below full load would be valid based on the results from full loading of the fan.

There were five key testing points on the wind tunnel which started at the entrance of the contraction section (outlet of the settling chamber) towards the exit of the contraction chamber then onto the testing section and followed by the diffuser inlet and diffuser exit readings. The average flow speed, the stagnation pressure and the turbulence intensity were investigated from the data gathered. The researchers in [28] utilised the root mean square (RMS) method to post process the measured hot wire anemometer data to understand the turbulence intensity. The turbulence intensity is defined in equation (13) as the ratio of velocity fluctuations from the mean freestream velocity [8], [29], [30].

$$T.I. = \frac{u'_{RMS}}{U_\infty} \tag{13}$$

where: $T.I.$ - Turbulence intensity (%); u'_{RMS} - Root mean square of the velocity fluctuations (m/s); U_∞ - Mean flow velocity (m/s)

The RMS is normally used when the distribution is known and typically Gaussian in shape, however, the distribution of the sample set was not known in this instance. Researchers in [31] demonstrated that the standard RMS formula should be corrected with the variance being considered and applied. The term u'_{RMS} was defined as the amount of velocity fluctuation from the mean velocity for the measured sample in the total population size. After applying this correction, the turbulence intensities were resolved as per equation (13) above.

The turbulence intensity at each point of measurement in the system was calculated based on empirical readings as this is an input parameter in the computation fluid dynamic (CFD) model within the two turbulence transport equations being k-ε and k-ω respectively. The k term of the transport equation defines the turbulent kinetic energy and the ε term represents the dissipation of the turbulent energy. The ω term can be taken as the specific turbulence dissipation and is the rate at which the fluid is converted into internal thermal energy [32]. Equation (14) shows the relationship between k and turbulence intensity.

$$k = \frac{3}{2}(IU)^2 \tag{14}$$

where: k - Turbulent kinetic energy (J/kg); I - Turbulence intensity (%); U - Mean flow velocity (m/s)

6.1 Settling Chamber

Pre- and post-construction of the settling section measurements were conducted at the test chamber of the system to gauge the flow regime with and without a settling chamber. The measurement was based on incremental changes to the fan speed resulting in roughly 0.5 m/s velocity intervals for a 30 second duration. The following results show the change in stability of the flow shown in Figure 11.

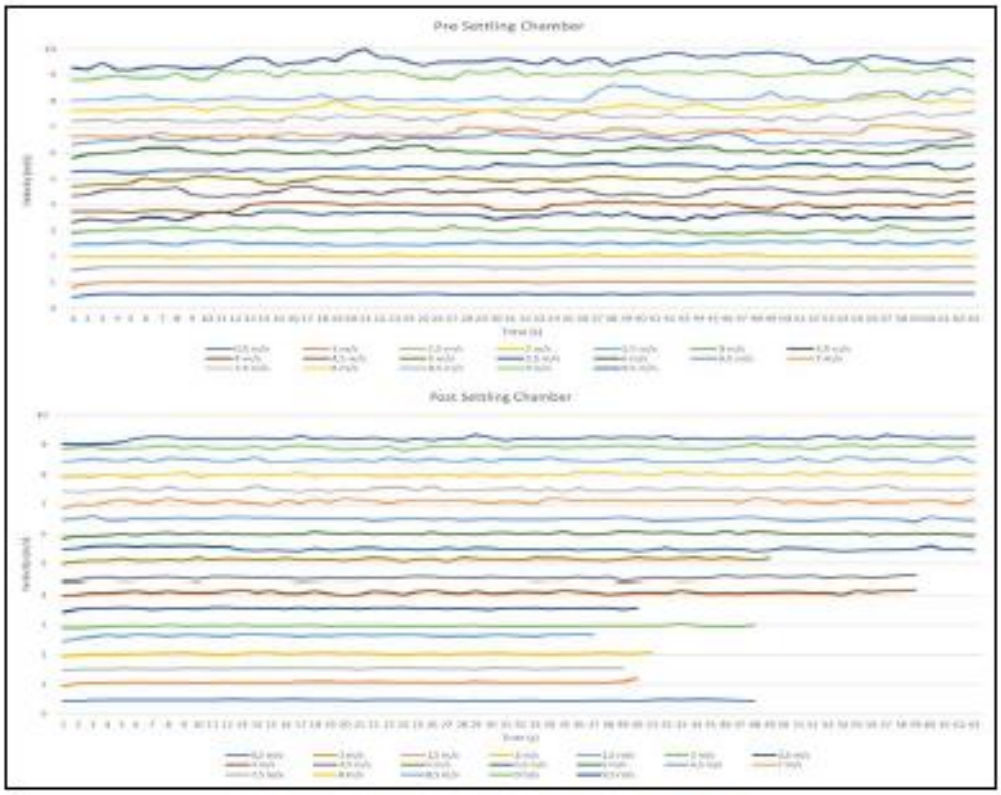

Figure 11: Pre-Settling and Post-Settling Chamber Results.

Figure 11 also depicts the results after the addition of the settling chamber laminar flow elements. There was a significant change in the stability of the flow after testing section speeds increased passed 3 m/s. The introduction of the laminar flow elements proved the settling chamber flow straightening capabilities at the testing section, demonstrating adequate testing conditions when varying flow speed range incrementally. There are signs of instability over speeds of 7 m/s, however, the disturbance did not significantly affect the testing conditions.

From the settling chamber the fluid enters the contraction section of the system for flow acceleration. During the accelerating process of the flow the fluid experiences minor changes in flow uniformity due to friction and seam joins between sections. Figure 12 shows the results of the instantaneous velocity and turbulence intensity for the inlet of the contraction nozzle. The inlet of the contraction chamber was located at point (A) as shown in Figure 12 and was taken as the resultant output of the settling chamber. The results show a stable velocity profile at full load of the system which is what was required. The averaged state velocity, temperature, Mach number and pressure were found to be 1.096 m/s, 292.67 °K, 0.00319 kPa and 101.38 kPa respectively. The turbulence intensity was calculated to be 0.84 % for the section showing that the settling chamber had successfully developed the flow to a laminar state.

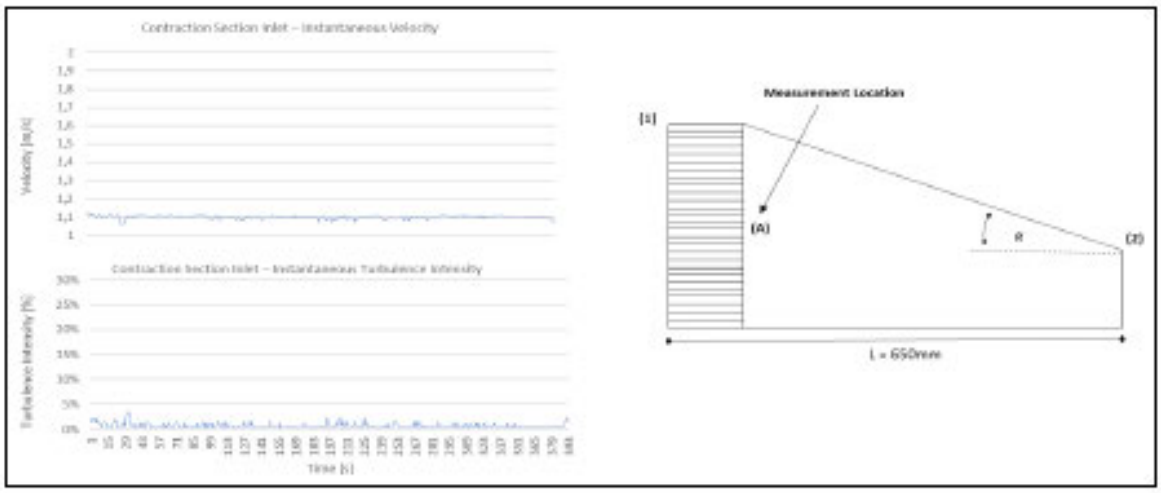

Figure 12: Contraction Nozzle Inlet – Velocity and Turbulence Intensity.

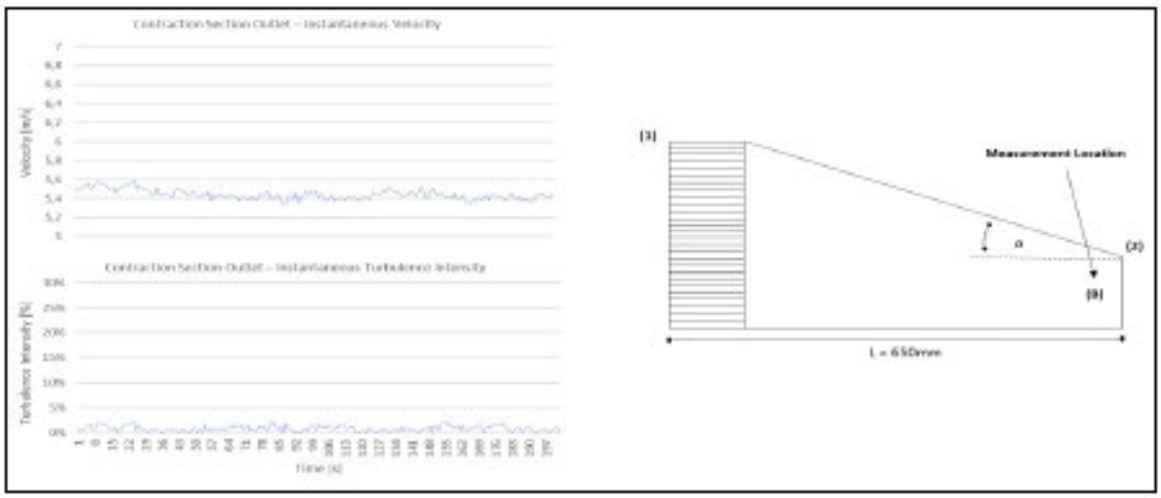

Figure 13: Contraction Nozzle Outlet – Velocity and Turbulence Intensity.

Figure 13 shows the results from the measurements taken at point (B) shown in the figure for the outlet of the contraction nozzle. The average accelerated flow velocity at (B) was found to be 5.44 m/s, an increase of 4.9 x that of the inlet speed of 1.096 m/s. The averaged state variables were 5.44 m/s, 293.25 °K, Mach number of 0.016 and 101.37 kPa taken as inlet conditions for the test section of the system. The turbulence intensity was 0.98 %.

The testing section results are shown in Figure 14 below which were measured at point (C). As stated in [27] the flow requires a minimum of 0.5 times the hydraulic diameter or length for the flow to fully develop from the contraction nozzle outlet. This was taken into consideration and the test results were recorded at a distance equivalent to the hydraulic length (200 mm) from the outlet of the contraction section. This measurement location was also taken to be adequate for the testing of the turbine as proposed in [16]–[18] for future experiments.

The results shown in Figure 14 show that the fluid accelerated adequately to meet the desired fluid velocity of 9 m/s with the section reaching an average speed of 9.23 m/s with a turbulence intensity of 0.76 %. This proved that the testing section had adequate stable developed flow for the testing of turbine designs. The average temperature within the section was measured to be 292.59 °K, 101.38 kPa and the Mach number was calculated to be 0.0269 and operated at

subsonic conditions.

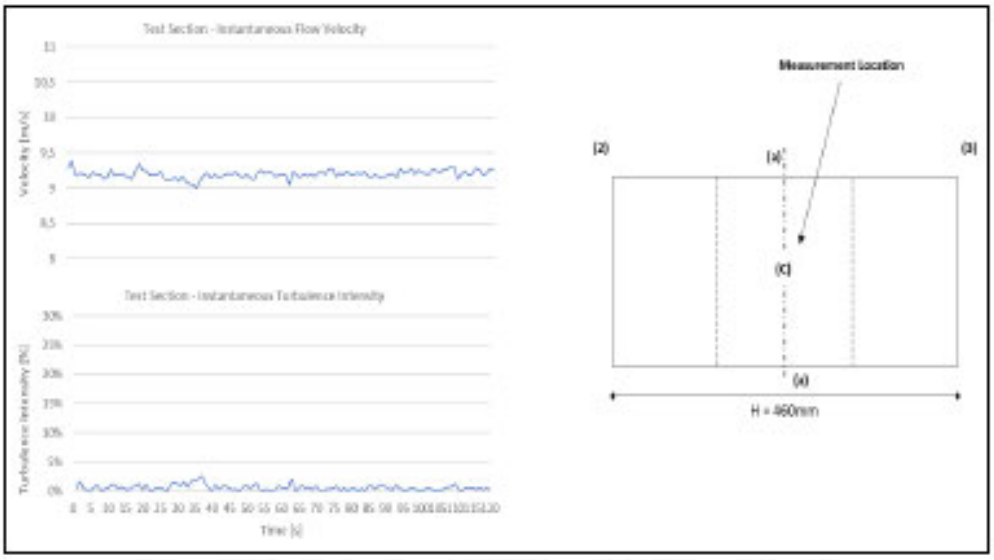

Figure 14: Testing Section – Velocity and Turbulence Intensity.

The diffuser inlet receives fluid flow from the test section was required to recover appropriately before merging back to atmospheric conditions of the large control volume. The results of the inlet sampling points are shown in Figure 15 measured at point (D). It can be seen from the results that the instantaneous velocity measured at the diffuser inlet of the system transitions into an unstable profile in comparison to the previous sections of the system. The averaged state variables for the measured locations for fluid velocity, temperature, Mach number and pressure were 7.67 m/s, 294.18 °K, Mach number of 0.022 and a pressure of 101.28 kPa. The turbulence intensity at this point was calculated to be 0.76 % which was stable and regarded as non-turbulent with a non-steady velocity profile.

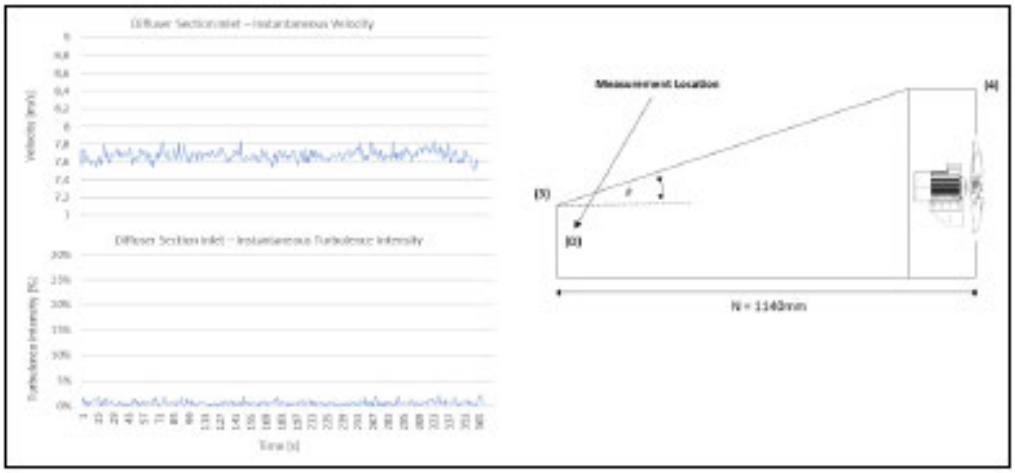

Figure 15: Diffuser Section Inlet – Velocity and Turbulence Intensity.

Figure 16 shows the results which were obtained from measurements at point (E) of the diffuser section. The instantaneous velocity profile was found to be unstable as this was relatively close to the axial fan. The state variables for this location were 3.81 m/s mean velocity, fluid temperature of 294.03 °K, a Mach number of 0.011 and pressure of 101.378 kPa. The turbulence intensity for the region was calculated to be 7.91 % which was roughly 9 x higher than the

previous sections of the wind tunnel system.

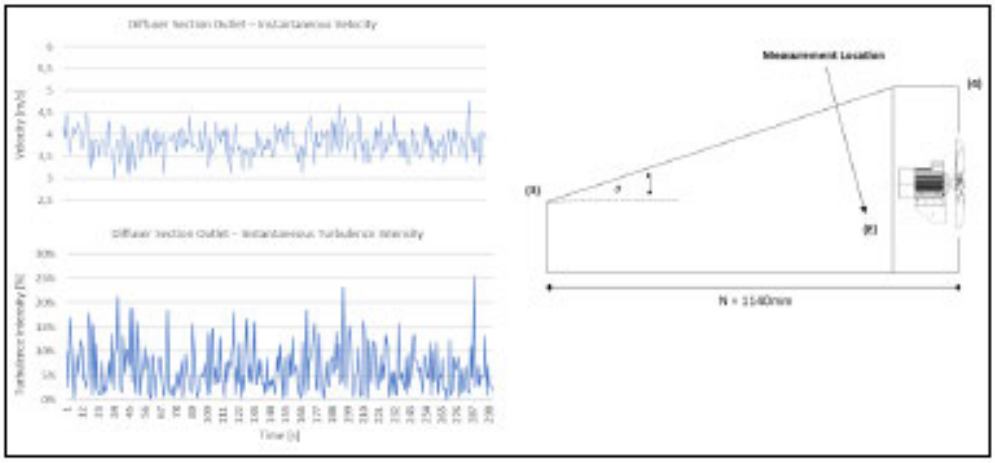

Figure 16: Diffuser Section Outlet – Velocity and Turbulence Intensity.

Table 5 shows the aggregated state variable results for all the sampling points identified above in Figure 2, Figure 3 and Figure 4 respectively. Analysing the results, the state variables are in good agreement with the design requirements as stated above which proves that the wind tunnel system would be suitable to perform tests on the chosen wind turbine.

Table 5: Results from Sampling Points

	[1]	[2]	[3]	[4]	[5]
Mean Velocity [m/s]	1,09	5,44	9,24	7,67	3,81
Stagnation Pressure [kPa]	101,379	101,375	101,365	101,37	101,38
Average Temperature [°K]	292,67	293,25	292,6	294,17	294,03
Mach No.	0,032	0,01585	0,02693	0,02232	0,01109
Turbulence Intensity [%]	0,84	0,98	0,76	0,76	7,91

Table 6: Turbulence Classification

Turbulence	Turbulence Intensity
Very Low	0,05 % - 1 %
Medium	1 % - 5 %
High	5 % - 20 %

Table 5 also shows the turbulence intensity of each of the sampling points. It was evident that the laminar flow elements accomplished the desired function of flow straightening from the contraction chamber to the point of entering the diffuser section of the wind tunnel. The high turbulence intensity experienced at point (E) was attributed to the flow fully recovering to atmospheric conditions as well as the influence of the induced draft from the fan. Table 6 shows the turbulence classification as a function of turbulence intensity [33].

Using this as a benchmark it can be seen that the turbulence profile was very low from the outlet of the settling chamber to the inlet of the diffuser section of the system. These conditions were shown to be in good relation to those of the numerical calculated state variables which proves that this wind tunnel design can be utilised for the testing of novel wind turbines and aerofoils for validation and optimisation.

7. CONCLUSIONS

The research conducted in the study aimed to investigate the design of a low-speed wind tunnel for the purpose of testing novel wind turbines and aerofoil designs. The system was designed in accordance with best practice from industry in the fields of thermodynamics and fluid dynamics. The wind tunnel was split into four major sections for design purposes, being the settling chamber, the contraction nozzle, the testing section and the diffuser section. Each section was designed and fabricated individually and assembled as a complete system for testing.

The testing of the system was conducted at various points through the operational length of the wind tunnel and measurements were recorded for evaluation and validation of state variables. It was found that the state variables at each measurement location were in good correlation to those of the numerical methods used for the design, thus proving that the design and fabricated wind tunnel was adequate for the testing of wind turbines and aerofoils elaborated in [18], [21].

8. FUTURE WORK

The current system design is planned to be utilised to calculate the potential of the turbine which was designed in [17], [18]. The addition of a microcontroller to simulate meteorological measured conditions is being investigated to understand the turbine's response and electrical output to fluctuating wind loading.

REFERENCES

1. *D. D. Baals and W. R. Corliss, Wind Tunnels of NASA, 1st ed. Washington D.C: Scientific and Technical Information Branch, National Aeronautics and Space Administration, 1981.*
2. *J. D. Jaramillo, "Design and construction of a low speed wind tunnel," Houghton College, 2017.*
3. *T. H. Yong and S. S. Doi, "Design and development of low-cost wind tunnel for educational purpose," 2015, doi: 0.1088/1757-899X/78/1/012039.*
4. *L. Cattafesta, C. Bahr, and J. Mathew, "Fundamentals of wind-tunnel design," Encyclopedia of Aerospace Engineering. John Wiley & Sons, 2010, doi: 10.1002/9780470686652.eae532.*
5. *R. Ricci and S. A. Montelpare, "Quantitative IR thermographic method to study the laminar separation bubble phenomenon," Int. J. Therm. Sci., vol. 44, pp. 709–719, 2005, doi: 10.1016/j.ijthermalsci.2005.02.013.*
6. *R. Ricci, S. A. Montelpare, and E. Silvi, "Study of acoustic disturbances effect on laminar separation bubble by IR thermography," Exp. Therm. Fluid Sci., vol. 31, pp. 349–359, 2007, doi: 10.1016/j.expthermflusci.2005.08.007.*
7. *W. Zhang, R. Hain, and C. J. Kahler, "Scanning PIV investigation of the laminar separation bubble on a SD7003 airfoil," Exp. Fluids, vol. 45, pp. 725–743, 2008, doi: 10.1007/s00348-008-0563-8.*
8. *S. Mauro, S. Brusca, R. Lanzafame, F. Famoso, A. Galvagno, and M. Messina, "Small-scale open-circuit wind tunnel: Design criteria, construction and calibration," Int. J. Appl. Eng. Res., vol. 12, no. 23, pp. 13649–13662, 2017.*
9. *C. P. Mellen, J. Frohlich, and W. Rodi, "Lessons from lesfoil project on large-eddy simulation of flow around an airfoil," AIAA J., vol. 41, pp. 573–581, 2003, doi: 10.2514/2.2005.*
10. *L. Davidson, LESFOIL: Large eddy simulation of flow around a high lift airfoil: Results of the project LESFOIL supported by the European Union 1998-2001. 2003.*
11. *A. Uranga, P. O. Persson, M. Drela, and J. Peraire, "Implicit large eddy simulation of transitional flows over airfoils and wings.," 19th AIAA Computational Fluid Dynamics, 22-25 June, San Antonio, Texas, USA, 2009.*
12. *J. M. Rainbird, J. Peiró, and J. M. R. Graham, "Blockage-tolerant wind tunnel measurements for a NACA 0012 at high angles of attack," J. Wind Eng. Ind. Aerodyn., vol. 145, pp. 209–218, 2015, doi: 10.1016/j.jweia.2015.06.006.*
13. *H. Sarlak, T. Nishino, J. N. Sørensen, Simos T., and C. Tsitouras, "Urans simulations of separated flow with stall cells over an nrel s826 airfoil," in AIP Conference, 2016, pp. 30–39, doi: 10.1063/1.4951795.*
14. *B. Celis and H. H. Ubbens, "Design and construction of an open-circuit wind tunnel with specific measurement equipment for cycling," Procedia Eng., vol. 147, pp. 98–103, 2016, doi: 10.1016/j.proeng.2016.06.196.*

15. I. Bayati, M. Belloli, L. Bernini, and A. Zasso, "Aerodynamic design methodology for wind tunnel tests of wind turbine rotors," J. Wind Eng. Ind. Aerodyn., vol. 167, pp. 217–227, 2017, doi: 0.1016/j.jweia.2017.05.004.

16. F. L. Inambao and K. Cunden, "Design and numerical simulation of a small scale helical cross flow turbine," in 13th BIE Biennial Conference, 2013, pp. 23–32.

17. K. Cunden, "Design of a novel hydrokinetic turbine for ocean current power generation," Master's dissertation, University of KwaZulu-Natal, 2015.

18. F. L. Inambao and K. Cunden, "Offshore vertical axis wind turbine simulation," Int. J. Mech. Prod. Eng. Res. Dev., vol. 11, no. 2, pp. 187–204, 2021.

19. J. Rajadas and B. Rogers, "Design, fabrication and testing of a low-speed wind tunnel laboratory," ASEE Annu. Conf. Expo. Conf. Proc., 2007, doi: 10.18260/1-2--2150.

20. N. Kumar Maurya, M. Maurya, A. Tyagi, and S. P. Dwivedi, "Design & Fabrication of low speed wind tunnel and flow analysis," Int. J. Eng. Technol., no. December, pp. 381–387, 2018, [Online]. Available: https://www.researchgate.net/publication/329872818.

21. F. L. Inambao and K. Cunden, "Offshore wind resource assessment off the South African coastline," Int. J. Mech. Eng. Technol., vol. 10, no. 6, pp. 95-119, 2019.

22. R. Fox W., P. Pritchard J., and A. McDonald T., "Internal incompressible viscous flow," in Introduction to Fluid Mechanics, John Wiley & Sons, 2009, pp. 328–337.

23. G. Millar H, "Laminar flow element and flow meter," US3349619A, 1967.

24. R. Fox W., P. Pritchard J., and A. McDonald T., "Introduction to compressible flow," in Introduction to fluid mechanics, John Wiley & Sons, 2009, pp. 582–604.

25. National Aeronautics and Space Administration (NASA), "Calorically perfect gas," Isentropic Flow. https://www.grc.nasa.gov/www/BGH/isentrop.html (accessed Apr. 15, 2021).

26. J. H. Bell and R. D. Mehta, "Contraction design for small low-speed wind tunnels," 1988. doi: 19890004382.

27. J. B. Barlow, W. H. Rae, and A. Pope, Low speed wind tunnel testing, 3rd ed. New York: Wiley-Interscience, 1999.

28. K. Pascioni, . Roger, A. Edstrand, and L. Cattafesta, "Characterization of an aeroacoustic wind tunnel facility," INTERNOISE, 43rd International Congress on on Noise Control Engineering: Improving the World through Noise Control, 2014.

29. M. Itoh and M. Kobayashi, "Turbulent structure in the three-dimensional boundary layer on a swept wing," in 4th International Symposium on Engineering Turbulence Modelling and Measurements, 1999, pp. 699–708, doi: https://doi.org/10.1016/B978-008043328-8/50067-9.

30. A. F. Molland and S. R. Turnock, "6 - Theoretical and numerical methods," in Marine Rudders and Control Surfaces, A. F. Molland and S. R. B. T.-M. R. and C. S. Turnock, Eds. Oxford: Butterworth-Heinemann, 2007, pp. 233–311.

31. T. Chai and R. R. Draxler, "Root mean square error (RMSE) or mean absolute error (MAE)?," Geosci. Model Dev., vol. 7, pp. 1525–1534, 2014, doi: 10.5194/gmdd-7-1525-2014.

32. D. Apsley, "Computational hydraulics - lecture notes." University of Manchester, 2021, [Online]. Available: https://personalpages.manchester.ac.uk/staff/david.d.apsley/lectures/comphydr/turbmodel.pdf.

33. *F. Jouse, "Defining turbulent boundary conditions," SimScale CAE Forum, 2016. https://www.simscale.com/forum/t/defining-turbulent-boundary-conditions/80895 (accessed Apr. 10, 2021).*

34. *Pittala, Suresh, and T. Diriba. "Computational Fluid Dynamics Analysis of Impeller Design For A Pump." International Journal of Mechanical Engineering (IJME) 5.4.*

35. *Alrobaian, Abdulrahman A., et al. "A new approach to low-cost open-typed subsonic compressible flow wind tunnel for academic purpose." International Journal of Mechanical and Production 8.6 (2018): 383-394.*

36. *Govardhan, D., and B. Praveen. "Design and Analysis of Two Throat Wind TunneL." International Journal of Mechanical and Production Engineering Research and Development (IJMPERD) 8. 1, Feb 2018, 513 520.*

37. *Prasad, U. Shiva, et al. "Design and analysis of two throat wind tunnel." International Journal of Mechanical and Production Engineering Research and Development 7.4 (2017): 381-388.*

CHAPTER 6 : FABRICATION OF TURBINE NOVEL SMALL SCALE TURBINE

The following chapter constitutes the fabrication of a small scale vertical axis turbine. The turbine was designed based on the principles which were highlighted in Chapter 4. The turbine was then modelled in a 3 dimensional (3D) landscape and exported to be post processed in a 3D printer processing software to create suitable print slices resulting in a smooth finish on the turbine blades. The blades were constructed in sections which were connected to form a single turbine helix blade. The blades were assembled to create a turbine which was tested in the constructed wind tunnel. A DC motor was used to measure the turbine output and a hall effect sensor was used to measure the turbine speed via a microcontroller used to process the data. The results had shown that the turbine design in comparison to the simulation results had a good correlation. This shows the potential for a scale version of the turbine for offshore power generation.

FABRICATION AND TESTING OF SMALL SCALE HELICAL WIND TURBINE

Kumaresan Cunden and Prof. Freddie Inambao

Department of Mechanical Engineering, University of KwaZulu-Natal

Durban, South Africa

ABSTRACT

Wind energy is one of the most abundant resources being exploited with wind turbines having the traditional horizontal axis wind turbine configuration. Traditional horizontal axis configurations are being utilized in onshore and offshore wind farms; however, the investigation of vertical axis wind turbine configurations has been increasing. The following study aims to investigate the design of a helical vertical axis wind turbine. A small-scale helical vertical axis wind turbine was designed based on previous investigations and research. The turbine was tested at wind speeds ranging from 7.5 m/s to 9.5 m/s. The results showed that the wind turbine was in good agreement with numerical simulations under typical environmental conditions.

Keywords: Vertical Axis Wind Turbine, Helical Wind Turbine, Small Scale Wind Turbine Blade Design

NOMENCLATURE AND ABBREVIATIONS

AR	Aspect Ratio	P_m	Mechanical Power
A_S	Surface Area of Turbine	RPM	Revolutions per Minute
A_T	Wind Tunnel Test Section Area	T	Torque
A_ω	Swept Area	VAWT	Vertical Axis Wind Turbine
B	No. of Turbine Blades	U_c	Corrected Wind Speed
B_f	Blockage Factor	U_f	Wind Speed without Turbine
B_R	Blockage Ratio	U_t	Wind Speed with Turbine
c	Blade chord length	U_∞	Freestream Wind Speed
C_P	Coefficient of Power	σ	Solidity Ratio
D	Turbine Diameter	δ	Helix Angle
DC	Direct Current	ρ	Density of Fluid
H	Turbine Height	ω	Rotational Speed
P_f	Power of the fluid	ώ	Turbine Blade Wrap

6.1 Introduction

Wind energy is one of the most abundant resources being exploited with wind turbines having the traditional horizontal axis wind turbine configuration. The onshore turbines have been in commercial operation globally in many electrical grids for many years, [1], [2]. Recently wind turbines have been migrating to offshore locations to harness greater resource availability and potential due to a lack of environmental obstructions, [3]–[5].

Traditional horizontal axis configurations are being utilized in onshore and offshore wind farms; however, the investigation of vertical axis wind turbine configurations has been increasing. One of the main advantages of vertical axis turbines, in comparison to horizontal axis turbines, is that they are not as limited to the direction of wind flow and can operate under crosswind conditions.

The following study aims to investigate the design of a helical vertical axis wind turbine that was described in [6]. The study was conducted to determine the characteristics of the turbine when subjected to wind loading forces within a controlled environment. The empirical investigation aimed to identify the start up wind speed as well as how the simulation results compared to a small scale model test of the design. The stud provides an overview of the fabrication process and the materials used for the construction of the small scale turbine which included support struts.

The following study aims to investigate the design of a helical vertical axis wind turbine. The layout of this article consists of the methodology, the turbine design parameters, the fabrication process of the small-scale turbine, a numerical simulation of the turbine, the experimental configuration followed by the results, discussions, and conclusions of the findings of the investigation.

6.2 Methodology

The following small-scale helical axis wind turbine was designed based on investigations and finds from the research conducted by Cunden and Inambao in [1] and [2]. The design has focused on a Selig 1406 17% thickness blade profile which is an asymmetrical blade profile. The results from [6] investigations showed that the profile had performed favourably in comparison to the NACA symmetrical profiles which were assessed. The fabrication of the turbine is detailed in Section 6.4.

The turbine was constructed and tested in the wind tunnel which was designed and constructed in [8]. The power was measured using a DC motor which was logged with a ChipKit uC32 microcontroller configured to log the current, voltage, and electrical power of the turbine at the rotor. A tachometer was developed with the aid of a digital hall effect sensor to measure the turbine rotational speed. The description of the experimental setup is detailed in Section 6.5. This experimental setup was used to

assess the rotational speed of the direct drive wind turbine and relate the rotational speed to that of the power output of the scaled modelled turbine which provided insight into the larger scale wind turbine.

6.3 Turbine Design

Horizontal axis wind turbines (HAWT) represent the most common wind turbine design which is found globally. These turbines traditionally consist of three blades with complex blade geometry and design, however, they also have a relatively high generation performance, [9]. One of the disadvantages of these turbines is that they have limited the direction of wind incoming from the turbine. A vertical axis wind turbine (VAWT), in comparison to the HAWT, has a simpler blade geometry and has the advantage of being a cross-flow turbine and is not limited to the lateral direction of incoming wind flow.

Figure 6-1 represents a basic discretization of a helical axis wind turbine which was used as the basis for the fabrication of the small-scale wind turbine evaluated for this study.

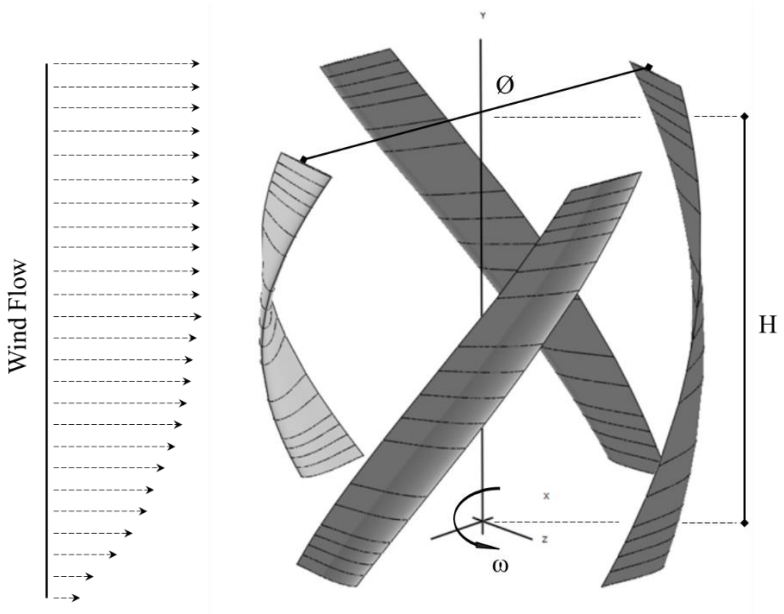

Figure 6-1: Helical Vertical Axis Wind Turbine

The turbine was designed based on the constraints of the wind tunnel which was designed and constructed by Cunden, K, [8] to test the small-scale helical wind turbine. Further investigation results indicate that the aspect ratio (AR) relationship to solidity directly affects the turbine power output. The following study utilizes an AR or 1 to maximize the swept area (A_ω) of the turbine.

The turbine was limited based on the wind tunnel testing chamber height. Equation (1) shows the relationship of the turbine height in comparison to the turbine radius known as the turbine's aspect ratio.

The resultant turbine radius is 87.5 mm and the diameter (D) is 175 mm using a turbine height of 175 mm.

$$AR = \frac{H}{2R} \tag{1}$$

Using a solidity ratio (σ) of 25% from the results of the study which was conducted in [6] the blade chord length (c) was calculated based on Equation (2) resulting in a blade chord length of 34.5 mm.

$$\sigma = \frac{Bc}{\pi D} \tag{2}$$

The blade wrap of a VAWT describes the number of the turbine's blades that are in contact with the fluid. The results from [7] indicated that four turbine blades with a 100% blade wrap had resulted in a smoother torque profile on the rotor shaft. Using the above constraints and results the helix angle (δ) was calculated to be 51.85°.

$$ώ = \frac{BH}{\pi D \tan \delta} \tag{3}$$

The tip speed ratio (λ) is the relationship of the turbine rotational speed (ω) in comparison to the fluid velocity (V) shown in Equation (4). This parameter is used to evaluate the turbine's parameters in the numerical solver from the results obtained from the testing of the small-scale turbine within the wind tunnel.

$$\lambda = \frac{R\omega}{V} \tag{4}$$

The power in the fluid (P_f) is described in Equation (5) where the power is a function of the density (ρ) of the fluid, the wetted area (A_ω), the freestream fluid velocity (U_∞).

$$P_f = \frac{1}{2}\rho A_\omega {U_\infty}^3 \tag{5}$$

The mechanical power (P_m) is described in Equation (6) which can be related to Equation (5). Using the relation of the two equations and understanding the rotational speed of the turbine by using Equation (4) the torque can be calculated.

$$P_m = T\omega \tag{6}$$

The coefficient of power (C_P) for a wind turbine is the ratio of the mechanical power which is extracted by the turbine is about the amount of power within the fluid shown in Equation (7). The turbine

maximum C_P is constrained by the Betz limit which is the theoretical maximum limit a turbine may extract from the fluid, [7].

$$C_P = \frac{P_m}{P_f} \tag{7}$$

Usually, turbine rotors are tested within wind tunnels and are near the test section walls which is not the case when operating in natural environments. This challenge arises from a blockage effect that has two main components the solid blockage and the wake blockage. The solid blockage is a result of the turbine's projected blade area impeding the wind tunnel flow and the wake blockage is the wake effect of the turbine which may not dissipate the wake energy as would be in natural conditions, [10].

When testing the VAWT within a wind tunnel the blockage ratio (B_R) was needed to correct the freestream fluid velocity (U_∞) due to the effect of the projected surface area of the wind turbine (A_S) impeding the wind flow through the wind tunnel test section (A_T). The relationship is represented in Equation (8), [11].

$$B_R = \frac{A_S}{A_T} \tag{8}$$

Research conducted by [11] notes where the blockage ratio exceeds 10% the results which are found are required to be corrected by the blockage factor. Various methods have been developed to calculate the blockage effect for wind tunnel testing. The research conducted by [12] derived correction factors related to drag and pressure coefficients to develop a semi-empirical factor whereas [13] suggested a simple method using 25% of B_R to correct the freestream velocity. Methods that were proposed by [14] had successfully built on the finds of [12] to a Savonius drag-type turbine. Investigations from [15] proposed correction methods based on utilizing the actuator disk theory and correcting the tip speed ratio (λ) and coefficient of power (C_P) as shown in Equation (4) and Equation (7) respectively by using the blockage factor (B_f) shown in Equation (9).

$$B_f = \frac{U_t}{U_f} \tag{9}$$

The blockage factor proposed by [15] relates the wind tunnel flow velocity with the turbine rotor (U_t) to the wind tunnel flow velocity without the turbine rotor (U_f)

Methods proposed by [13] were also adopted to correct the wind velocity incoming the turbine rotor with Equation 10. The factor (ε_t) is described as 25 % of the blockage ratio described in Equation (8). These factors were used in the correction of the test results data detailed in Section 6.6 of the study.

$$U_c = U_\infty(1 + \varepsilon_t) \tag{10}$$

Table 6-1 shows the final turbine rotor specifications used for the fabrication of the helical turbine based on the consolidation of the above design parameters.

Table 6-1: Turbine Specifications

Design Parameters	Detail
Aspect Ratio (AR)	1
Turbine Diameter (D)	175 mm
Turbine Height (H)	175 mm
Solidity (σ)	25 %
No. of Blades (B)	4
Blade Chord Length (c)	34.5 mm
Blade Wrap (ώ)	100 %
Helix Angle (δ)	51.85°

The specifications from Table 6-1 and the correction factors were used in the fabrication of the turbine and the analysis of the results from the wind tunnel testing.

6.4 Fabrication Process

The following section of the study details the fabrication process of the helical VAWT highlighting the blade discretization and strut design for the turbine. One of the challenges experienced when fabricating the turbine was blade manufacturing. Due to the twist angle of the helical profile, the turbine blade was segmented.

A three-dimensional (3D) printer was used to fabricate the turbine blades, couplings, bearing mountings, and upper and bottom struts. The fabrication process of a turbine blade is described in [16]–[18] of traditional HAWT blades. The turbine blades are hollow and consist of an outer shell that forms the aerodynamic shape to produce a resultant lift force. The helical blade which was designed to have a total helix angle of 51.85° was sectioned into five pieces of the same height and interlocked resulting in a piecewise helix angle of 10.37°

Figure 6-2 depicts one of the five designed blade segments and Figure 6-3 depicts a partial and fully fabricated blade segment. The partially fabricated blade segment was captured to illustrate the hollow nature of the turbine blade.

Figure 6-2: Blade Segment

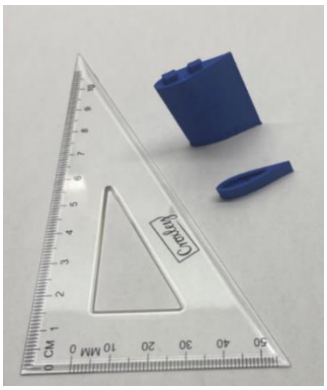

Figure 6-3: Blade Segment

The blades were sectioned into 5 interlocking pieces which were stacked on top of one another to form a full turbine blade as shown in Figure 6-4. The interlocking of the blade segments was fabricated to have a tolerance of ±0.1 mm to ensure a tight fit when assembled which is shown in Figure 6-5.

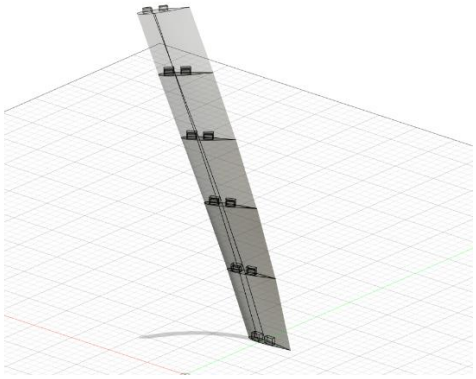

Figure 6-4: Turbine Blade Assembly

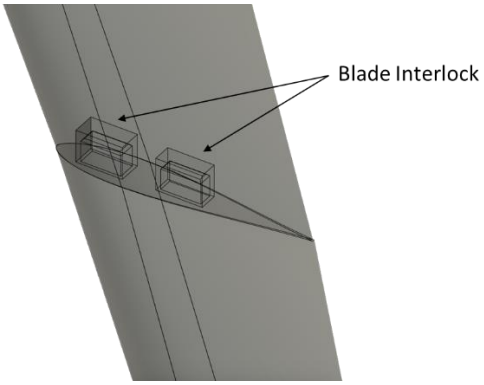

Figure 6-5: Blade Interlock

The blades were assembled and fixed to an upper and lower strut with a center tube shaft which was used to stabilize the turbine and transfer the extracted energy to be useful mechanical energy for power generation. Figure 6-6 depicts the fully assembled turbine prototype for testing.

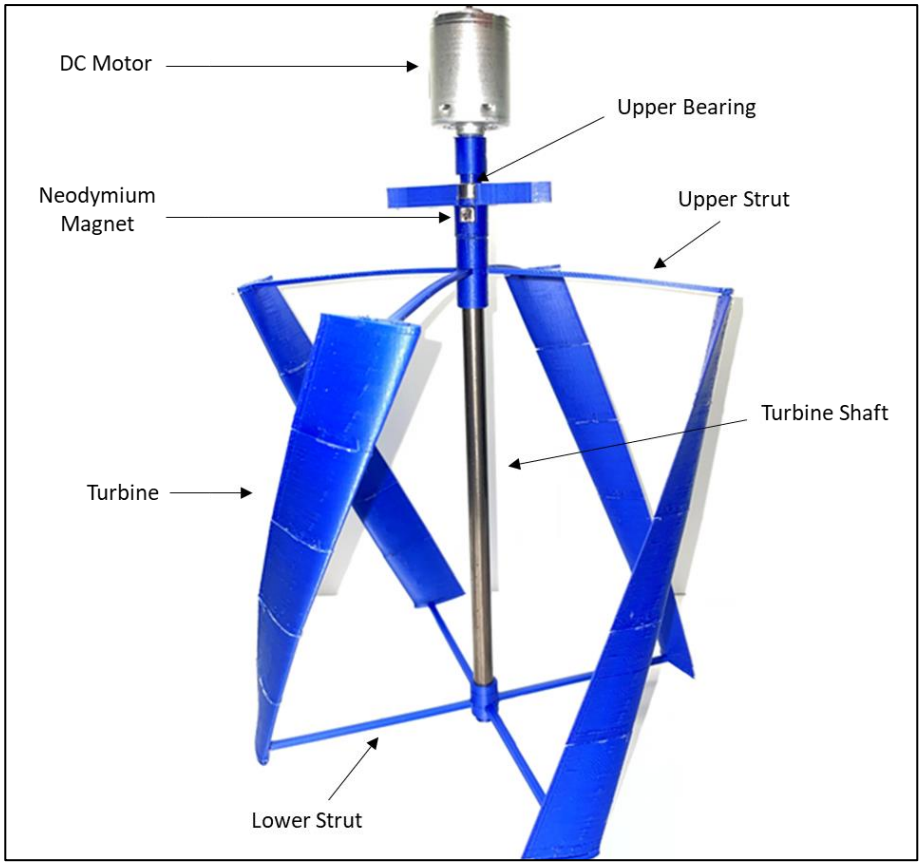

Figure 6-6: Turbine Assembly

The turbine and coupling components were assembled and tested within a wind tunnel at wind speeds of 7.5 m/s to 9.5 m/s.

6.5 Experimental Configuration

The following section of the study elaborates on the configuration of the experimental setup as well as the instrumentation used for the investigation of the VAWT in the wind tunnel setup. Figure 6-7 illustrates the experimental set-up of the VAWT within the wind tunnel as well as the DC motor coupling used to measure the power output from the turbine.

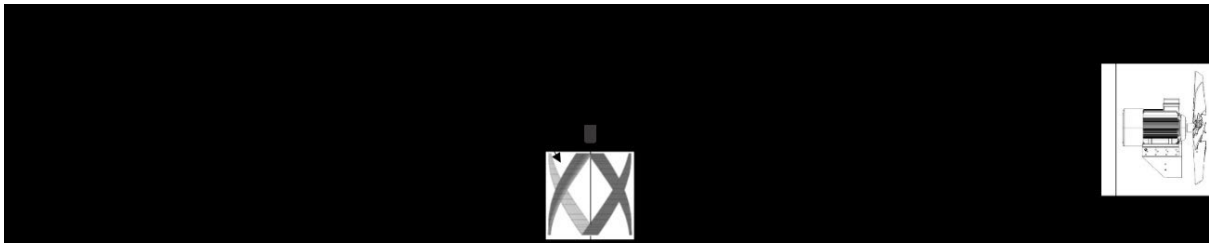

Figure 6-7: Experimental Set-up

Figure 6-8 shows the instrumentation and other devices used to log the experimental data from the designed VAWT. The turbine was connected to the DC motor using a hexagonal socket and a tight-fit connection to the DC motor shaft. This was where some losses occurred as a result of inertia and torque of the DC motor as well as frictional losses through the coupling system to the motor shaft. The voltage sensor was sued to determine the output voltage and current to calculate the power output of the turbine. The Hall effect sensor was used to measure the rotational speed of the turbine shaft by counting the pulses generated by the Neodymium magnet. The readings were processed and logged by the ChipKit uC32 microcontroller and saved to the PC for post-processing.

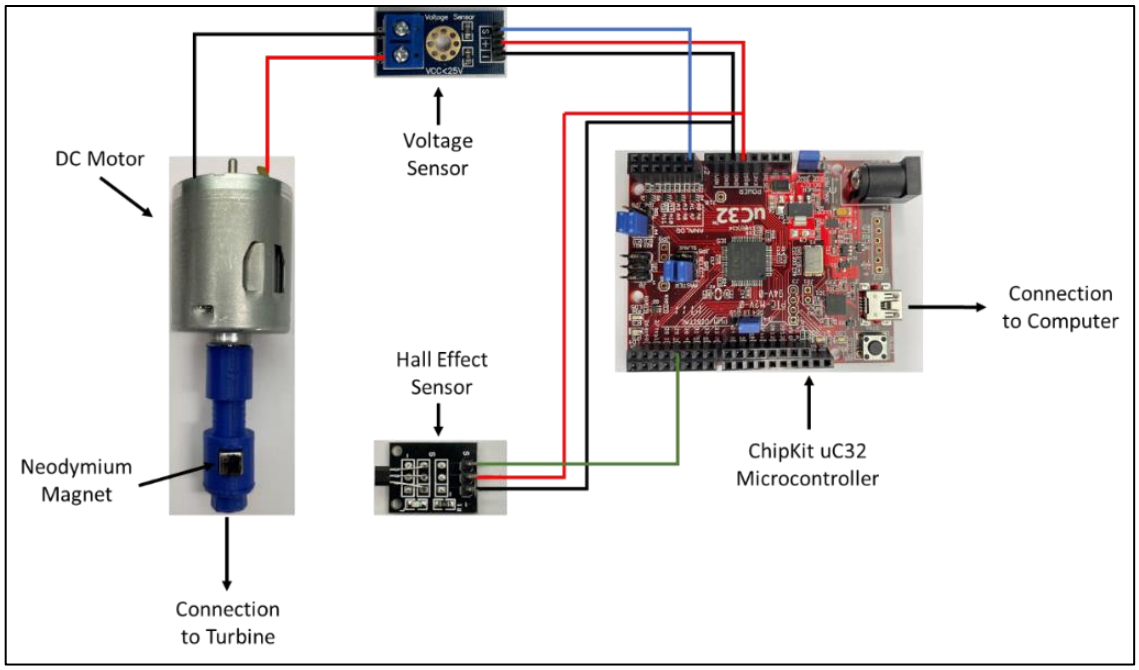

Figure 6-8: Instrumentation

The above instrumentation was interfaced with a computer via a serial communication cable. The results were logged in 5-second intervals to average out instantaneous fluctuations at the rotor shaft which may have not been accurately captured due to feedback and resolution from sensors.

6.6 Results and Discussion

The following section of the study elaborates on the results of the wind tunnel testing for the designed VAWT. Three tests were conducted by varying the wind tunnel wind speed by 0.5 m/s and the results were logged in 5-second intervals and allowed to settle for 5 minutes.

Figure 6-9 below shows the power measurements, of the three averaged tests which were conducted, in comparison to the rotational speed (RPM) at the rotor of the turbine.

A numerical simulation was performed for the turbine utilizing a double multiple stream tube analysis. The numerical simulation had the specifications which are shown in Table 6-2 below.

Table 6-2: Simulation Parameters

Simulation Parameters	Detail
Temperature	20 °C
Density of Air	1.204 kg/m^3
Mach Number	0.028
Dynamic Viscosity	1.825 x 10^{-5} kg/ms
Wind Speed	7.5 / 8 / 8.5 / 9 / 9.5 m/s

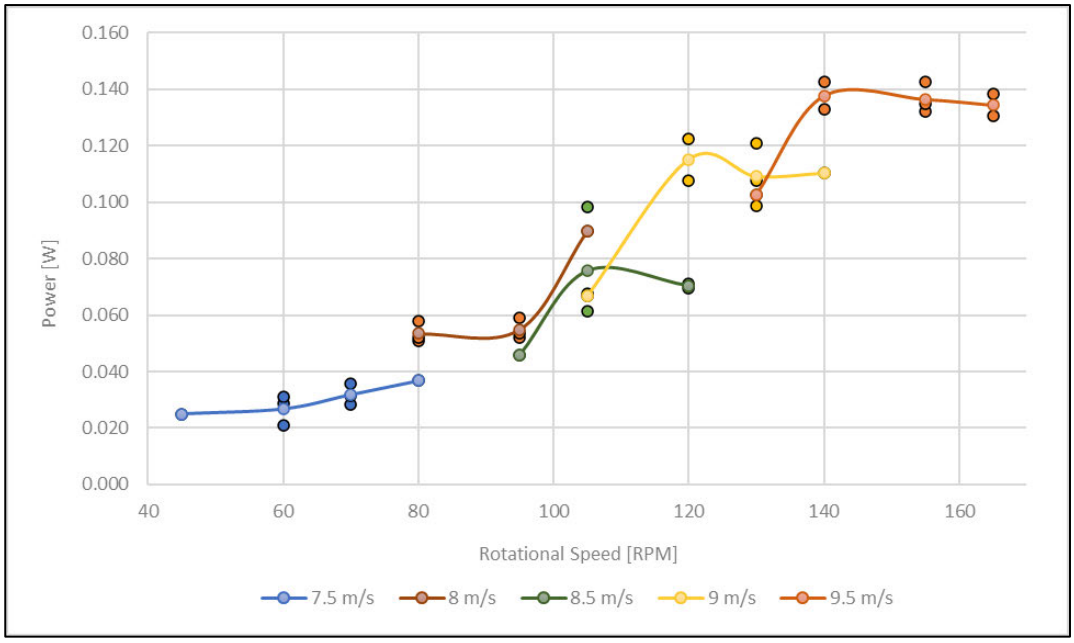

Figure 6-9: Experimental Results

Figure 6-10 represents the corrected values of the power measurements considering Equations (9) and (10) factoring in the blockage effects of the turbine in the wind tunnel. The freestream wind speed and the corrected power were used to calculate and plotted against the measured data.

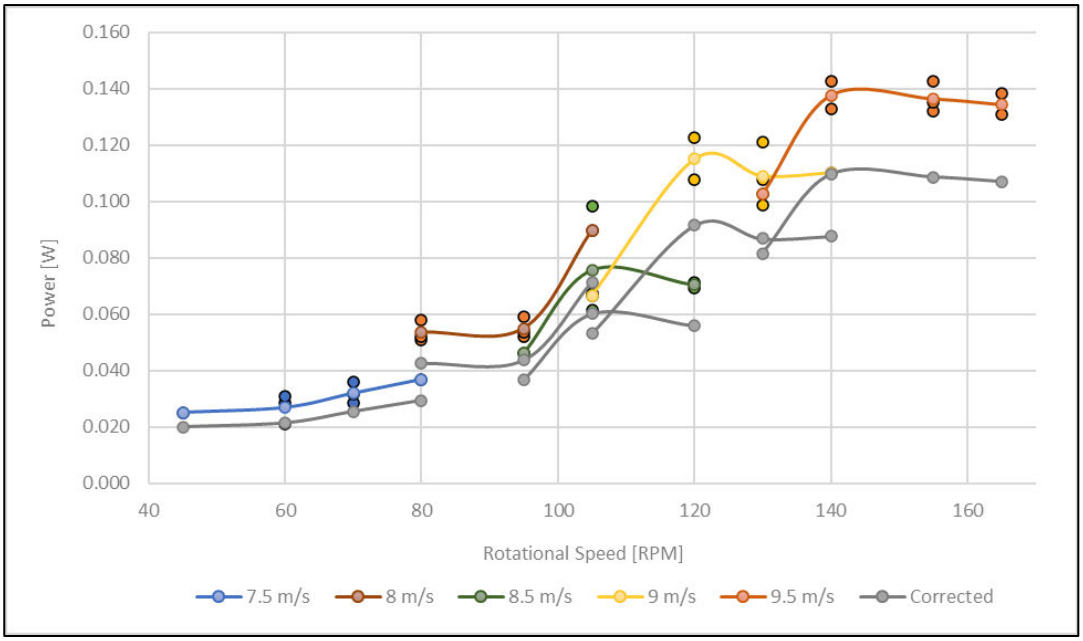

Figure 6-10: Experimental Results Corrected

Figure 6-11 shows the results of the wind tunnel test in comparison to a numerical simulation performed for the turbine. The measured results are in good relation to that of the freestream numerical solver results after utilizing the correction methods. The variations shown may be a result of vibration due to misalignment of turbine bearings and vibrations of the motor used whilst in operation.

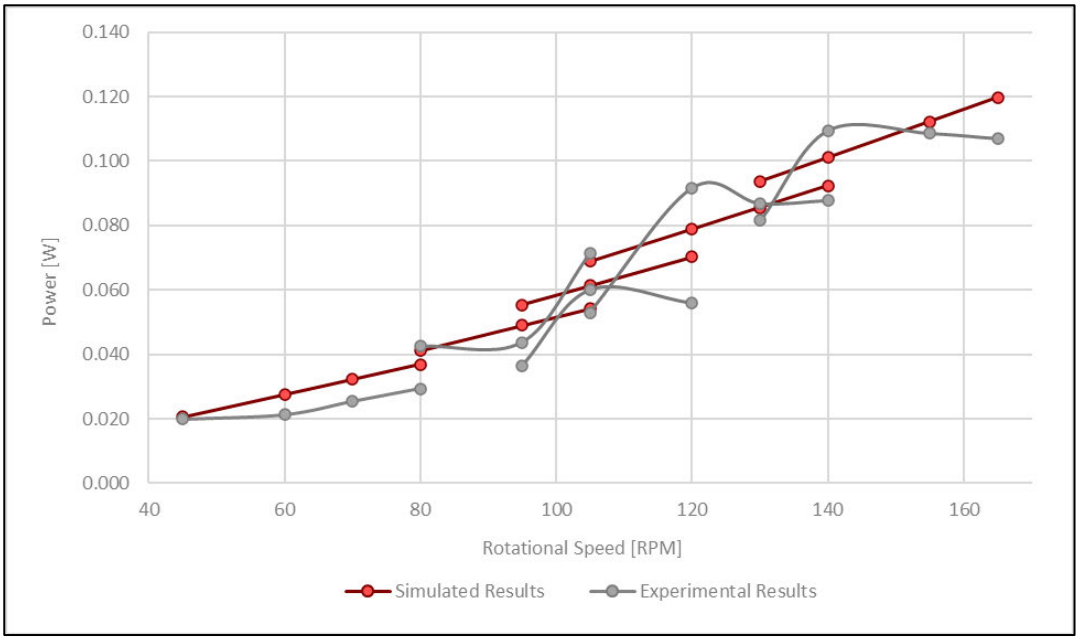

Figure 6-11: Measured compared to Simulation

The above results illustrate the turbine design may be developed for practical operations onshore and offshore for wind speeds having a mean of 9 m/s. Challenges may arise from turbine blade

manufacturing as the helical VAWT requires a twist angle which may be challenging for casting a single blade. One of the solutions may be to fabricate the blade in segments. Further investigations should be conducted into the fabrication of large-scale VAWTs.

6.7 Conclusions

A small-scale turbine rotor was designed using the formula described and was tested in a wind tunnel over a varying speed of 7.5 m/s to 9.5 m/s. The turbine blades were fabricated in sections due to the helical nature of the blade. The turbine output power and rotational speed were measured at each wind speed. A numerical simulation was performed considering an unbounded condition of flow which were in good comparison to the measured results after utilizing the appropriate correction factors. The torque profile of the turbine may be calculated, at different wind speeds, by utilizing the measured power and turbine rotational speed. Further research should be considered on varying strut designs and positions as well larger turbines with smaller segments for the turbine blades.

6.8 References

[1] K. Umoh and M. Lemon, "Drivers for and barriers to the take up of floating offshore wind technology: A comparison of Scotland and South Africa," *Energies (Basel)*, vol. 13, no. 21, 2020, doi: 10.3390/en13215618.

[2] British Petroleum (BP), "Statistical Review of World Energy 2021," 2021.

[3] M. Hannon, E. Topham, J. Dixon, D. McMillan, and M. Collu, "Offshore Wind, Ready to Float? Global and UK Trends in the Floating Offshore Wind Market," 2019. doi: 10.17868/69501.

[4] H. Díaz and C. Guedes Soares, "Review of the current status, technology and future trends of offshore wind farms," *Ocean Engineering*, vol. 209, p. 107381, 2020, doi: https://doi.org/10.1016/j.oceaneng.2020.107381.

[5] S. Loughney, J. Wang, M. Bashir, M. Armin, and Y. Yang, "Development and application of a multiple-attribute decision-analysis methodology for site selection of floating offshore wind farms on the UK Continental Shelf," *Sustainable Energy Technologies and Assessments*, vol. 47, p. 101440, 2021, doi: https://doi.org/10.1016/j.seta.2021.101440.

[6] F. L. Inambao and K. Cunden, "Offshore Vertical Axis Wind Turbine Simulation," *International Journal of Mechanical and Production Engineering Research and Development*, vol. 11, no. 2, pp. 187–204, 2021.

[7] K. Cunden, “Design of a Novel Hydrokinetic Turbine for Ocean Current Power Generation,” University of Kwa-Zulu of Natal, 2015.

[8] K. Cunden and F. L. ; Inambao, “Design, Construction and Testing of a Low-Speed Wind Tunnel,” *International Journal of Mechanical and Production Engineering Research and Development*, vol. 11, no. 6, pp. 237–256, 2021.

[9] D. Han, Y. G. Heo, N. J. Choi, S. H. Nam, K. H. Choi, and K. C. Kim, “Design, fabrication, and performance test of a 100-W helical-blade vertical-axis wind turbine at low tip-speed ratio,” *Energies (Basel)*, vol. 11, no. 6, pp. 1–17, 2018, doi: 10.3390/en11061517.

[10] J. B. ; Barlow, W. H. ; Rae, and A. Pope, *Low-Speed Wind Tunnel Testing*, Third. Toronto: John Wiley & Sons, 1999.

[11] E. Bešlagić, S. Lemeš, and F. Hadžikadunić, “Procedure for Determining the Wind Tunnel Blockage Correction Factor,” in *New Technologies, Development and Application III*, I. Karabegović, Ed., Cham: Springer International Publishing, 2020, pp. 331–339. doi: 10.1007/978-3-030-46817-0_38.

[12] E. C. ; Maskell, “A Theory of the Blockage Effects on Bluff Bodies and Stalled Wings in a Closed Wind Tunnel,” London, 1963.

[13] A. Pope and J. . J. ; Harper, *Low-Speed Wind Tunnel Testing*. New York: John Wiley & Sons, 1966.

[14] A. J. Alexander and B. P. Holownia, “Wind tunnel tests on a savonius rotor,” *Journal of Wind Engineering and Industrial Aerodynamics*, vol. 3, no. 4, pp. 343–351, 1978, doi: 10.1016/0167-6105(78)90037-5.

[15] A. S. ; Bahaj, A. F. ; Molland, J. R. ; Chaplin, and W. M. J. ; Batten, “Power and thrust measurements of marine current turbines under various hydrodynamic flow conditions in a cavitation tunnel and a towing tank,” *Renew Energy*, vol. 32, no. 3, pp. 407–426, 2007, doi: 10.1016/j.renene.2006.01.012.

[16] C.-H. Ong and S. Tsai, “Design, Manufacture andTesting of A Bend-Twist D-spar,” Stanford CA, 1999.

[17] P. S. ; Veers *et al.*, “Trends in the Design, Manufacture and Evaluation of Wind Turbine Blades,” *Wind Energy*, vol. 6, pp. 245–259, 2003, doi: 10.1002/we.90.

[18] D. Murray, Robynne E.; Snowberg, D. Berry, R. Beach, S. Rooney, and D. Swan, "Manufacturing a 9-Meter Thermoplastic Composite Wind Turbine Blade," in *American Society for Composites*, West Lafayette, Indiana: National Renewable Energy Laboratory (NREL), 2017.

CHAPTER 7 : COMPARISON OF HELICAL VAWT TO REFERENCE VAWT AND HAWT FOR OFFSHORE APPLICATIONS

The offshore wind energy market has experienced a recent boom in demand due to a global need of cleaner sources of energy production. The trend of investments, within the renewable energy technology basket, have been dominated by private sector investment due to the commercial viability and competitive nature of the sector. Vertical Axis Wind Turbines (VAWT) for offshore wind farms have good potential in comparison to the traditional Horizontal Axis Wind Turbines HAWT designs. The following study compares the designed helical VAWT to that of available VAWT and HAWT reference turbines which are constructed for offshore wind deployment. The study compares the power curve of each of the respective turbines, the impact of torque fluctuations on the rotor and the impact of torque fluctuations on the rotor and the wake impacts on energy production. The potential Annual Energy Output (AEP) of each of the respective turbines was also determined by exploring 3 types of wind farm turbine arrangements. The results proved favourable towards the helical turbine due to the nature of VAWT systems and the ability to be located closer together than that of HAWT systems. The results also show that the capacity factor is higher, and the wake losses are lower for the helical VAWT system, even under tightly spaced conditions.

COMPARISON OF HELICAL VAWT TO REFERENCE VAWT AND HAWT FOR OFFSHORE APPLICATIONS

Kumaresan Cunden and Professor Freddie Liswaniso Inambao

Department of Mechanical Engineering, University of Kwa-Zulu-Natal,

Durban, South Africa

The offshore wind energy market has experienced a recent boom in demand due to a global need of cleaner sources of energy production. The trend of investments, within the renewable energy technology basket, have been dominated by private sector investment due to the commercial viability and competitive nature of the sector. Vertical Axis Wind Turbines (VAWT) for offshore wind farms have good potential in comparison to the traditional Horizontal Axis Wind Turbine (HAWT) designs. The following study compares the designed helical VAWT to that of available VAWT and HAWT reference turbines which are constructed for offshore wind deployment. The study compares the power curve of each of the respective turbines, the impact of torque fluctuations on the rotor and the wake impacts on energy production. The potential Annual Energy Output (AEP) of each of the respective turbines was also determined by exploring 3 types of wind farm turbine arrangements. The results proved favourable towards the helical turbine due to the nature of VAWT systems and the ability to be located closer together than that of HAWT systems. The results also show that the capacity factor is higher, and the wake losses are lower for the helical VAWT system, even under tightly spaced conditions.

Keywords: Offshore Wind, Offshore Wind Turbines, Helical VAWT, HAWT.

7.1 Introduction

The offshore wind energy market has experienced a recent boom in demand due to a global need of cleaner sources of energy production. The market is driven by climate change commitments of various nations as well as various governmental subsidies and other financing mechanisms within the public and private sectors respectively, [1]. The trend of investments, within the renewable energy technology basket, have been dominated by private sector investment due to the commercial viability and competitive nature of the sector. Onshore and offshore wind technologies have also seen a large contribution of public sector investment which aid in the promotion of these technologies, [2]. The various government subsides and drive of nations to achieve net zero ambitions by 2050 has been one of the many drivers for investor confidence, especially within the offshore wind market, [3]. Various nations are now investigating the potential of offshore wind technologies to achieve these targets, [4]–[7].

Currently, there are a number of developments being undergone with respect to floating offshore wind farms which are located across Europe. There a few prototype floating offshore wind farms that are in operation which are the Hywind Scotland [8] and Kincardine [9] wind farms in Scotland and the WindFloat Atlantic [10] wind farm in Portgual. Recently, China has also deployed its first floating offshore wind prototype off the coast of Yanjiang city, [11]. These prototypes consist of traditional Horizontal Axis Wind Turbine (HAWT) systems with a tri-based semisubmersible floating platform. The Hywind Tampen wind farm also uses a HAWT, however, utilises a concrete ballast spar buoy system and is the largest operational floating wind farm (88 MW) to date, located more than 140 km offshore from Norway [12].

The cost of offshore wind turbines are expected to decrease as the turbine capacity increases. However, the HAWT system faces structural integrity challenges as blade sizes and subsequent support structures continuously increase. Larger rotor diameters result in higher cyclic loading on the main rotor and blades due to gravitational loads, [13]. Other fluid dynamic loads, such as wind shear and localised turbulence intensity, can affect Annual Energy Production (AEP) if not accounted for as well as structural loading on the blade root, [14]. The buoyancy and requirements for stability of floating offshore HAWT systems also have unique engineering requirements as the traditional HAWT system poses challenges such as eccentric moments increasing complexity of the semisubmersible structure, [15].

Vertical Axis Wind Turbines (VAWT) for offshore wind farms have good potential in comparison to the traditional HAWT designs. The HAWT design turbine have an operational wind speed up to a maximum of 25 m/s until which the turbine would have to be shut down to protect itself from damage. The VAWT system, however, has a much higher theoretical threshold for wind speed cut-off and can

withstand more extreme weather conditions in comparison to the HAWT design, [16]. Notably, VAWT wind farms can have denser turbine packing in comparison to HAWT wind farms due to the positive effect of wake interference and the recovery of internal wakes of VAWT designs, [16]–[18]. As previously highlighted, the HAWT design undergoes cyclic structural loading on the turbine blades due to gravity, but the conventional VAWT system experiences cyclical torque fluctuations at the rotor level which may have adverse effects for both mechanical and electrical transmission and control systems, [16].

The study which was conducted had the aim of investigating the potential of offshore wind farms to be installed far offshore from the South African coastline at various selected regions. The study had focused the technical investigation on a helical bladed, vertical axis wind turbine (VAWT) for the application in deep sea locations. A helical VAWT design was chosen due advantages such as lower recovery moment, lower centre of gravity, omnidirectional operation reducing yawing requirements and reduced cyclical rotor torque.

7.2 Current Status of Commercial VAWT Design

The two aerodynamic classifications of VAWTs comprise of drag and lift based designs. The Savonious design is based on a drag based aerodynamic system which is commonly found on wind anemometers used for measuring wind speed on meteorological stations. The lift based VAWT designs have three main types that are the Darrieus, H-Type Darrieus or straight bladed Darrieus and helical turbines.

There are some VAWTs which were developed for onshore applications; however, these are at a small scale in the order of 100 kW or less, [18]. There has since been numerous research and development of floating VAWT concepts and prototypes. Some notable concepts are summarised in Table 7-1.

Table 7-1: Summary of VAWT Research and Development

Turbine Name	Turbine Type	Country	Reference
NOVA	V-Shaped VAWT	United Kingdom	[19], [20]
Deepwind	Curved Darrieus	Denmark	[21], [22]
Floating Axis	Straight Darrieus	Japan	[21], [23]
Vertiwind	Helical Rotor	France	[24], [25]
SeaTwirl	Straight Darrieus	Sweden	[26]

Table 7-2 shows the available reports and data of National Renewable Energy Laboratories (NREL) reference HAWT and Sandia National Laboratories VAWT. It should be noted that the C_P of a turbine is dependent on the solidity of the turbine and the Reynolds number experienced by the turbine blades, [27]. Solidity rations of less than 10 % tend to decrease the C_P and increases the corresponding λ of the turbine and conversely, higher solidity ratio, greater than 40 %, tend to increase the C_P and decrease the

corresponding λ of the turbine, [18], [27]. From Table 7-2, it can be seen that the C_P values for both turbines are similar based on existing literature and results.

Table 7-2: HAWT and VAWT Characteristics

Turbine	Power Rating	Type	C_P (Max)	Reference
NREL	5 MW	HAWT	0.48	[28]
Sandia	100 kW	VAWT	0.4	[29]

Another factor which is used to compare the HAWT and VAWT systems are that of the swept area of turbines. The swept area is generally viewed as the area which is exposed to the free stream wind velocity used to extract energy from the flow. For HAWT systems the swept area is calculated based on the area of a circle (πr^2) where *r* denotes the blade length. For VAWT systems the area is based on the area of a rectangle (*H* x *D*) where *H* represents the total blade / turbine height and *D* represents the turbine diameter. Figure 7-1 is a graphical representation of the variance between swept area of the HAWT and VAWT turbines respectively.

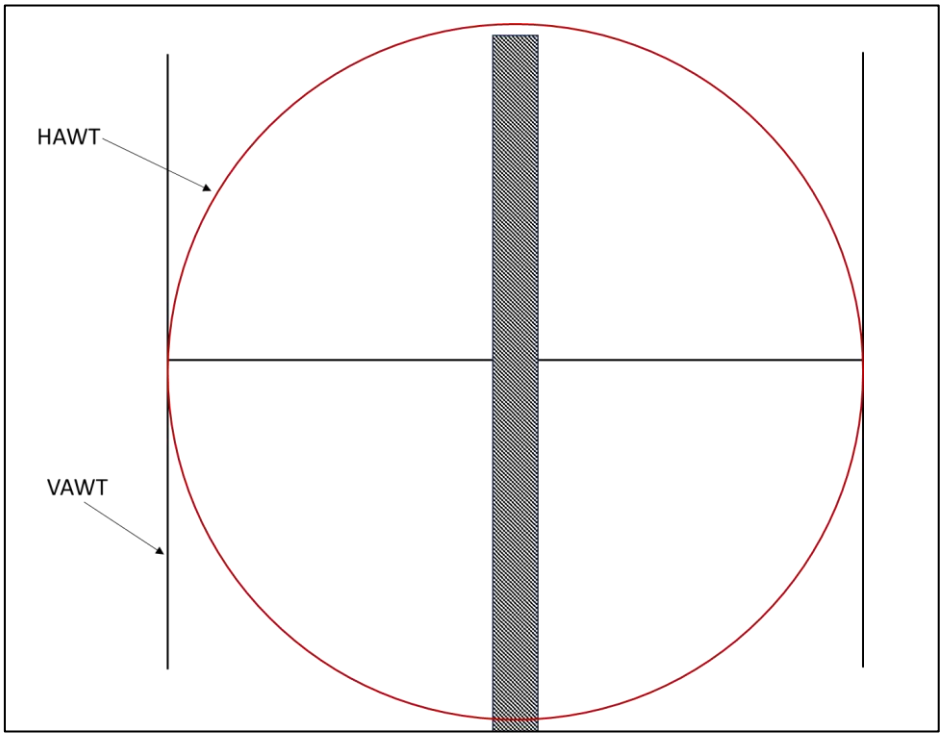

Figure 7-1: HAWT and VAWT Swept Area

The VAWT in comparison to the HAWT also has the additional benefits of the ability to convert wind energy from any direction due to the crosswind functionality, but with a HAWT this is not the case. The HAWT requires additional control and equipment to control the turbine yaw angle to direct the turbine in the predominant direction of the wind flow. Research which was conducted by [30] indicate the relationship of power production of HAWT's and yaw misalignment. The yaw misalignment (γ) is

the angle in which the rotor swept area of the HAWT is not perpendicular to that of the wind resource. This results in a reduction of power which was found to be proportional to the following equation:

$$P_r = \frac{P_\gamma}{P_{\gamma_0}} \approx \cos^{P_p}(\gamma) \quad (1)$$

The above equation approximates the power ratio (P_r) which is the relationship between the yaw misaligned production (P_γ) and the yaw aligned production (P_{γ_0}) which also may be modelled via utilising a cosine function. The variable P_p varies however, research indicates that this is between $1.88 < P_p < 5.14$ for offshore wind turbine applications, [31]–[33]. Figure 7-3 is a comparison of HAWT and VAWT power reduction based on the power ratio which is derived from the yaw misalignment. It should be noted that the VAWT system has theoretically no reduction of power due to the crosswind capabilities.

Table 7-3: HAWT and VAWT Characteristics, [18]

Yaw Angle	**HAWT corrected by Howland et al.** [30]	**Theoretical VAWT**
γ (°)	$P_r = \cos^2(\gamma)$	$P_r = 1$
± 5	0.99	1
± 10	0.97	1
± 15	0.93	1
± 20	0.88	1
± 25	0.82	1
± 30	0.75	1

7.3 Designed VAWT compared to Reference HAWT

The NREL 5 MW HAWT turbine was used as the initial reference for comparing the designed helical VAWT. The scaling and sizing of the VAWT was on the basis of swept area of the HAWT. The NREL turbine has rated power of 5 MW, rotor diameter of 126 m and is pitched regulated as a control mechanism, [34]. This resulted in a swept area of 12,462 m^2. The VAWT design was upscaled by changing the turbine diameter, keeping the aspect ratio constant at 1 and maintaining a solidity ratio of 20 %. SeaTwirl uses a Darrius straight bladed turbine design, so a similar type of turbine was created with the same swept area, aspect for the comparison of the two VAWT systems.

Figure 7-2 shows the comparison of the power coefficient curves of the helical VAWT and NREL reference turbine. The figure depicts that the HAWT turbine has a larger tip speed operational range, however, the power coefficient is lower in comparison to that of the VAWT turbine. This means that the HAWT has a higher rotational speed to that of the VAWT during operation. This may lead to an

increase in mechanical fatigue for various transmission components of the machine. The higher power coefficient of the VAWT indicates that advantage of the machine to extract energy from the incoming flow.

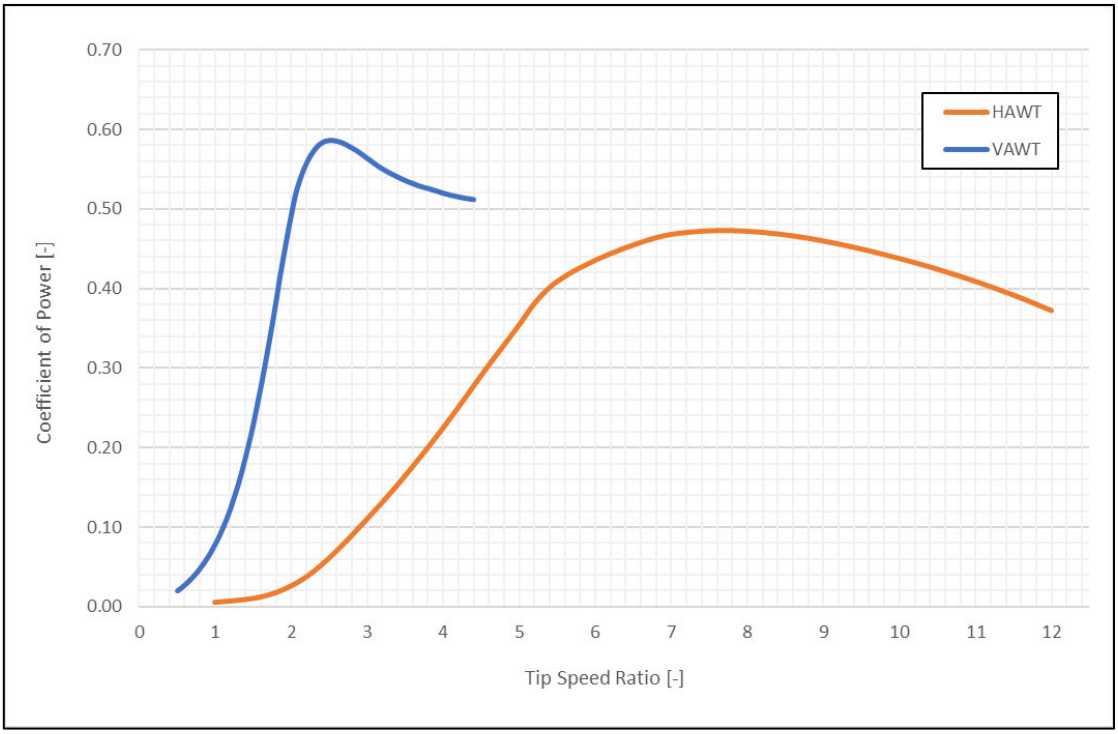

Figure 7-2: Power Coefficient - VAWT and HAWT

The power curve of a wind turbine is relationship of the freestream wind speed, at the turbine's hub height, and the corresponding active power generated by the turbine [35]–[37]. The relationship between the wind speed and power output (P) of the turbine is non-linear and may be approximated by the following equation:

$$P = \frac{1}{2}\rho A C_P(\lambda, \beta) v^3 \tag{2}$$

Where ρ is the air density, A is the swept area of the turbine, C_P is the coefficient of power for the turbine, v is the velocity of the wind. It should be noted that the coefficient of power is a function of the tip speed ratio denoted by λ and the blade pitch denoted by β. The power curve of a turbine has different zones of which the turbine operates.

Figure 7-3 shows the zones of the wind turbine with respect to the power curve. Zone 1 is where no power is generated and the turbine requires to overcome inertial and aerodynamic forces to start rotating. Zone 2 is when the turbine starts generating power ($v_{Cut\ in}$) at an increased rate, with respect to increasing wind speed. Zone 3 is where the turbine operates at the rated wind speed (v_{Rated})

generating constant power output at the rated power of the turbine. Zone 4 is when the turbine stops generating power at the cut off wind speed ($v_{Cut\ off}$) to protect the machine from failure.

It can also be seen that a power curve which has a gradient shift to the left indicates an improved efficiency and gradient shift towards the left indicates a reduced efficiency. Power curve efficiency can decrease due to wear and deterioration of the turbine blades and upgrades to the turbine blades may restore or increase the efficiency of the turbine, [37], [38].

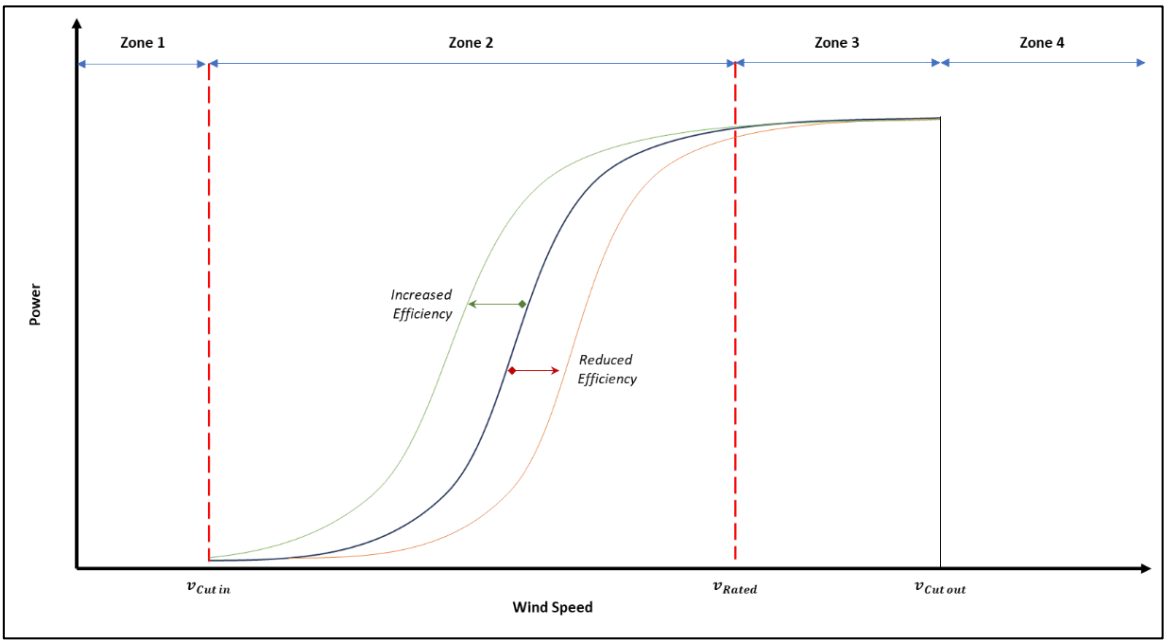

Figure 7-3: Power Curve

Figure 7-4 shows the comparison of the NREL reference wind turbine and the designed helical VAWT. Figure 7-4 compliments that of Figure 7-2 and depicts the added efficiency of the VAWT to that of the HAWT. This shows that the VAWT design has an added advantage to that of the HAWT for power generation. The VAWT operates at a lower rotational speed, does not require pitch control, can operate under extreme weather conditions and does not require yaw control due to its inherent cross wind capabilities.

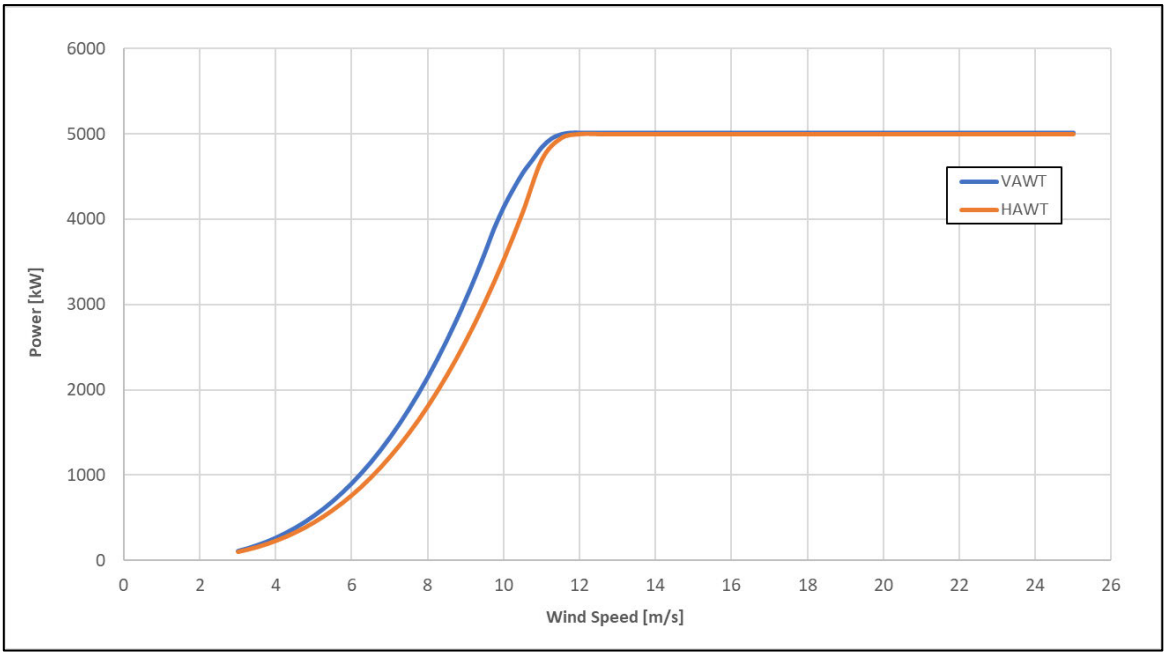

Figure 7-4: Power Curve - VAWT and HAWT

7.4 Designed VAWT compared to Reference VAWT

The next comparison of the helical turbine was to the Sandia 34-meter two bladed wind turbine and three bladed VAWT which is currently being investigated for offshore wind applications by SeaTwirl, a Swedish company as shown in Table 1 [26]. The Sandia turbine consists of two troposkin / curved blades and was designed to have a rated power output of 500 kW. The helical and straight bladed turbines were also scaled to produce a power of 500 kW.

Figure 7-5 shows the comparison of the two turbine's power coefficient curves in relation to the tip speed ratio It can be seen that the helical turbine has a higher C_P to that of the Sandia turbine and operates at a lower rotational speed. This is because of the increased solidity of the helical and straight bladed turbine's to that of the Sandia turbine, due to the number of turbine blades. The Sandia turbine also has a shorter chord length by a factor of roughly 2 and has a non-uniform aerofoil distribution along the blade length.

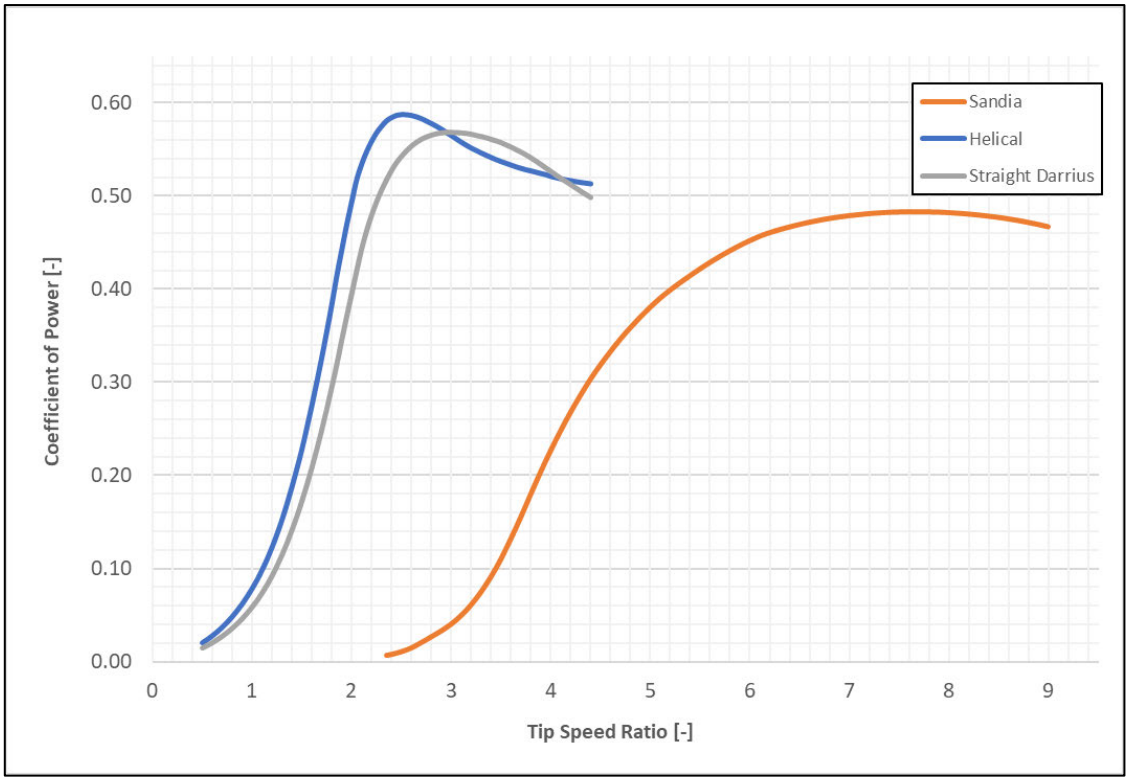

Figure 7-5: Power Coefficient - Helical vs Sandia vs Straight Darrius

To understand the benefits of the helical turbine in comparison to an existing VAWT of Darrius straight bladed design, the power coefficient and torque coefficient was also examined in the analysis. The results of the analysis are in Figure 7-6 below and show the increase in efficiency of the helical turbine design to that of the straight bladed turbine design. The torque coefficient is based on the quotient of the power coefficient (C_P) and tips speed ratio (TSR). This can lead to the optimum point of the power coefficient curve to define the limits of the power curve for the turbine.

The low TSR and high torque results in the turbine operating under a lower rotational speed. This can result in less turbine noise production and lower cyclic fatigue and stress on the turbine blades in comparison to traditional HAWT systems. The lower TSR and higher torque coefficient can also lead to the wake recovery being shorter in length in comparison to the HAWT counterpart. This can lead to shorter spacing of turbines in the inter-row and transverse directions leading to a more densely packed turbine farm resulting in a potentially larger energy production per square kilometre. The wake modelling which was used to predict the Annual Energy Production (AEP) is shown further in section 7.5.

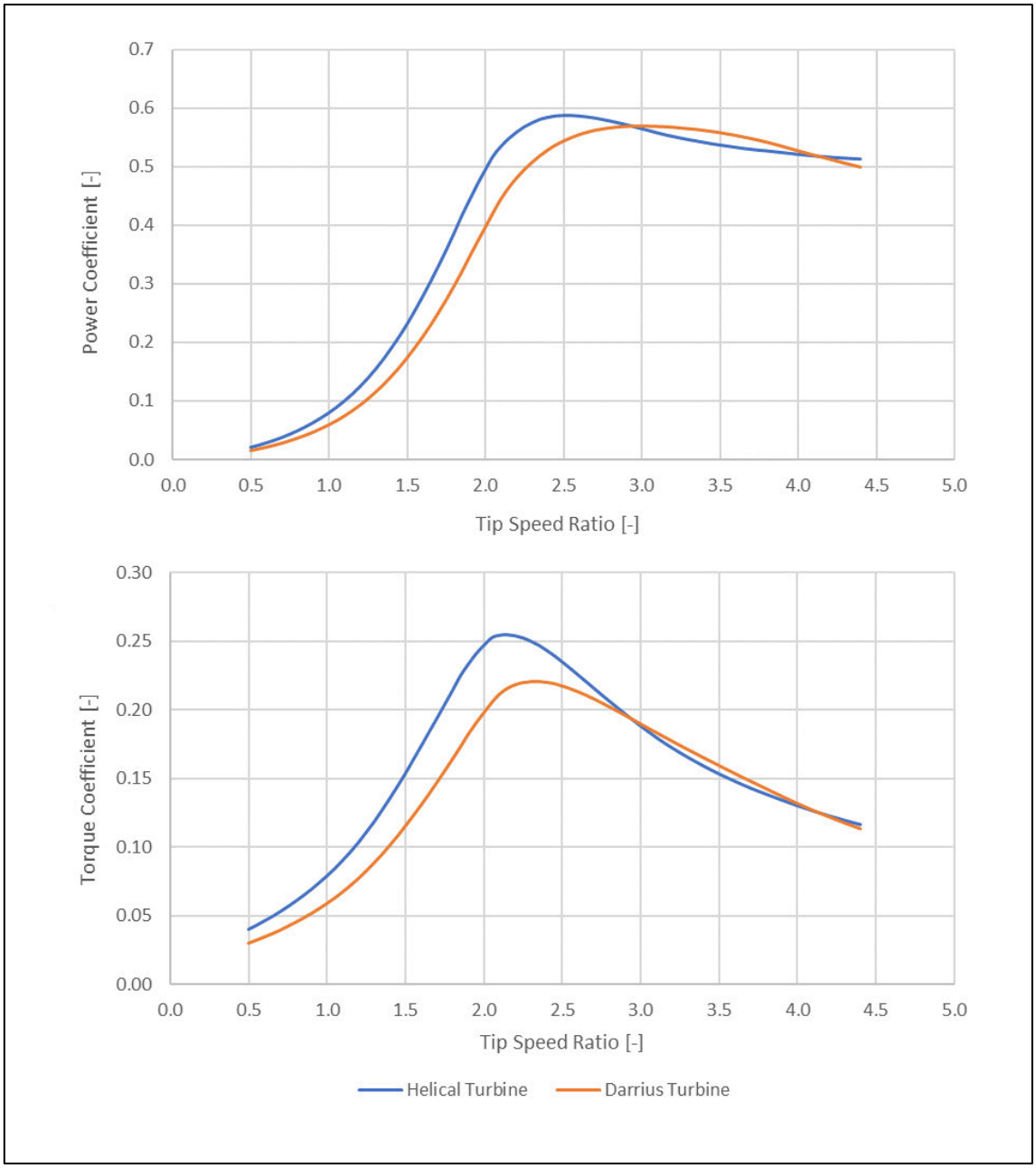

Figure 7-6: Power Coefficient and Torque Coefficient – Helical vs Straight Darrius

Figure 7-7 shows the torque profiling of the two vertical turbines (Helical and straight bladed Darrius turbine). The figure shows that at low wind speeds to high wind speeds, the helical turbine has a smoother more consistent torque profile on the turbine rotor. This results in a smoother transmission of mechanical power and lower fatigue and cycle loading on mechanical components of the machine. The analysis also shows the stability of the turbine at higher wind speeds allowing for a relatively constant power output. This is desirable for offshore applications as wind shear coefficient is lower than onshore sites with higher wind speeds.

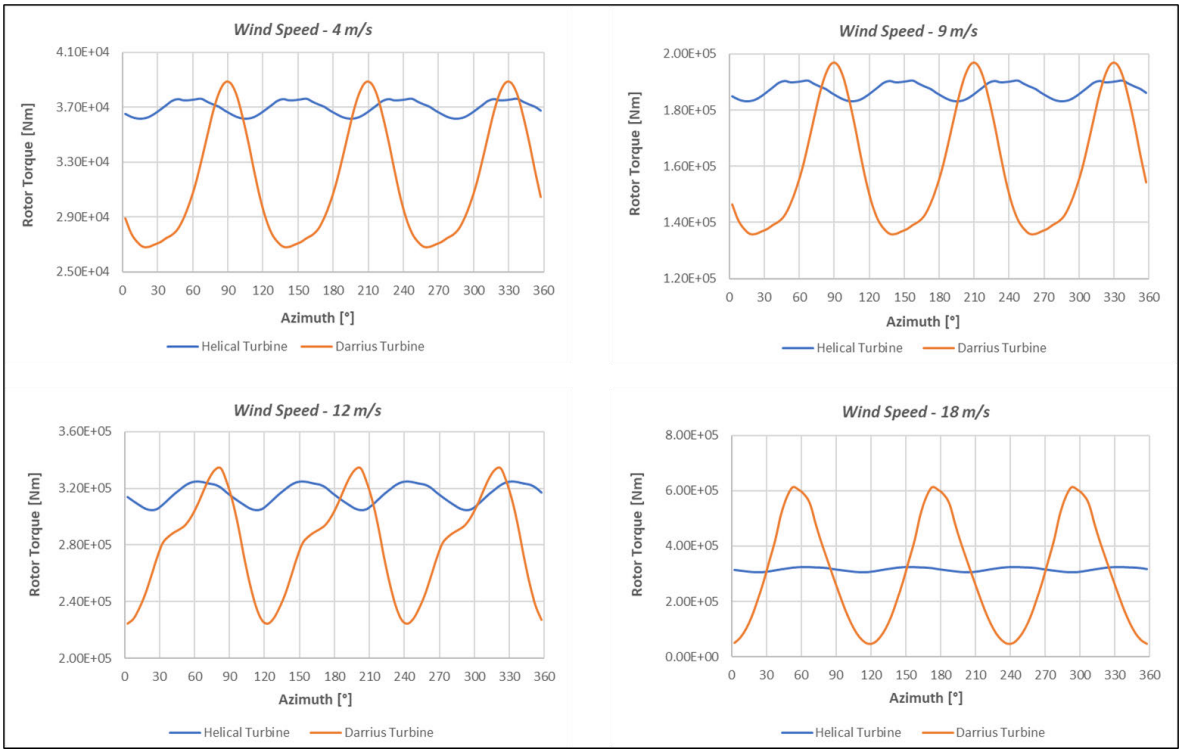

Figure 7-7: Torque Profile of Helical vs Darrius Straight Blade Turbine

The rotor torque profile is of significance as this affects the mechanical and electrical power output of the turbine. The mechanical power output has direct effects on the mechanical systems such as bearings and gearbox which has a direct result on the electrical output from the generator. The rotor torque was compared at wind speeds of 4 m/s, 9 m/s, 12 m/s and 18 m/s respectively based on approximations of the operating zones shown in Figure 7-3.

Figure 7-8 shows the power curves of both VAWT's and it can be noted that the helical turbine has a higher efficiency to the Sandia turbine resulting in a larger energy production. However, in comparison to the straight bladed design (such of that of SeaTwirl) the power curves are almost identical. This shows the potential of both helical and straight bladed VAWT systems to that of previous research and commercially available large scale turbines. However, to understand the true potential of helical turbines, the rotor torque was also evaluated for each of the helical and straight bladed turbine respectively.

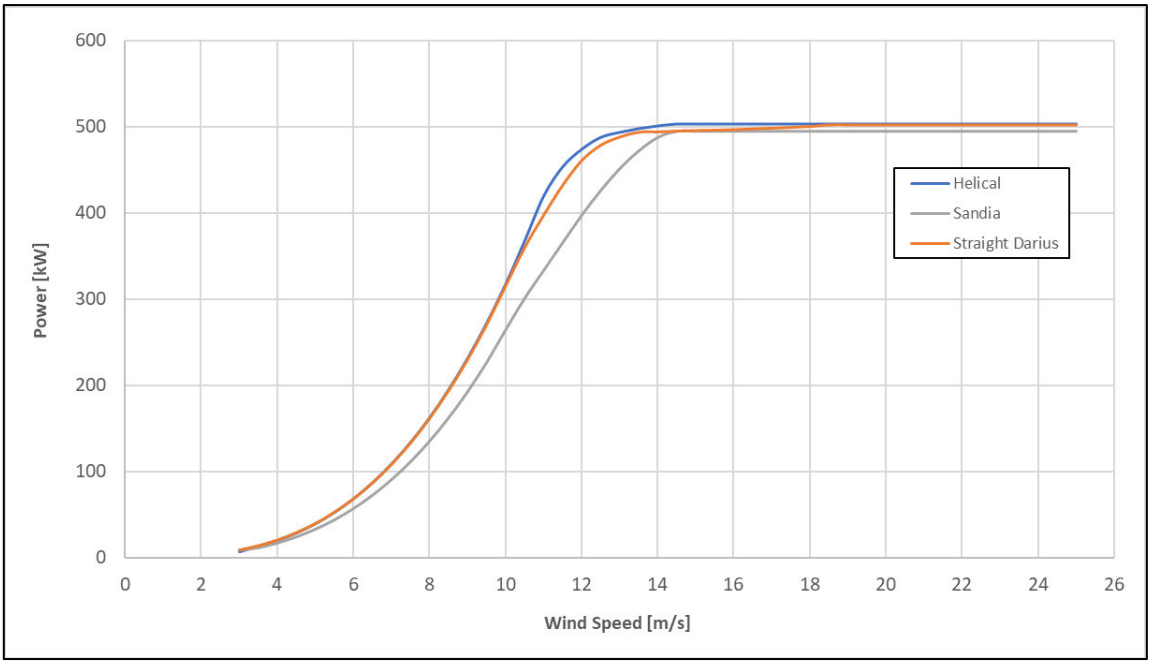

Figure 7-8: Power Curve – Helical vs Sandia vs Straight Darrius

The above analysis of turbines depicts the potential of the helical wind turbine in comparison to a reference large scale HAWT and reference VAWT turbines from two reputable research laboratories (NREL and Sandia). However, there is the need for understanding the Annual Energy Production (AEP) of farm of turbines at a specific site. Wind turbine spacing is a key factor when sizing a wind farm. HAWT systems and VAWT systems have different requirements for turbine spacing when it comes to optimising a wind farm potential site.

7.5 Wake Modelling

One of the main factors in spacing analysis is the wake development for HAWTs and VAWTs. The rationale behind the spacing of wind turbines is due to the recovery of the wake which is formed due to the turbine operation in the streamwise and crosswind directions. The HAWT systems typically have 3 to 5 diameters spacing in the crosswind direction and between 6 to 10 diameters in the streamwise direction which is aimed to achieve roughly 90% to 95% of the power output of an isolated wind turbine, [39].

The most common used wake model which is used to assume the predicted wake is the model which was proposed by Jensen [40] that assumed a top-hat shape for the velocity deficit and also a linear wake expansion rate which had typical values of 4% to 5% for offshore wind turbine systems and 7.5% for onshore wind turbine systems, [41], [42].

Commercially available wind simulation software, which is used to determine the AEP of a proposed wind farm, utilises the Jensen wake model to understand the losses within the wind farm. However, this

model tends to underestimate the deficit velocity because of the top hat profile assumption due the derivation solely being based on the conservation of mass, [43]. Additional research which was conducted by [44] had considered the conservation of mass and momentum within the control volume of analysis surrounding the turbine. The following equation shows the normalised wake deficit velocity that assumes as top hat profile as proposed by [44]:

$$\frac{\Delta U(x)}{U_\infty} = \frac{1}{2}\left(1 - \sqrt{1 - \frac{2C_T}{\beta_F + \left[{}^{\delta_F}/_{D}\right]}}\right) \tag{3}$$

Where U_∞ is the freestream velocity of the incoming wind, C_T is the thrust coefficient of the turbine, D is the turbine rotor diameter, $\Delta U(x)$ is the difference of the freestream velocity U_∞ and $U_\varphi(x)$, where $U_\varphi(x)$ is defined as the wake velocity that is in the streamwise direction of the turbine. Within the above equation the factor δ_F is taken as the expansion factor of the wake and β_F is the ratio of the cross-sectional area of the wake after the initial wake expansion to the swept area of the turbine blades and is represented by the following:

$$\delta_F = \frac{1}{2}\frac{\left(1 + \sqrt{1 - C_T}\right)}{\sqrt{1 - C_T}} \tag{4}$$

The conclusions of the investigations by [43] explain that the assumption of a top hat profile on wake velocity deficit can lead to substantial errors because of the underestimation of the deficit velocity at the wake centre and also the overestimation at the wake edges within wind farm predictions.

Following this, predictions of a Gaussian distribution can better represent the wake deficit velocity of the turbines within the wind farm. Studies which were based on numerical and experimental analysis by [45], [46] which was then followed by [43] including conservation of momentum and mass had led to the representation of a Gaussian model as shown in the equation below:

$$\frac{\Delta U(x)}{U_\infty} = \frac{1}{2}\left(1 - \sqrt{1 - \frac{2C_T}{8\left[{}^{\sigma(x)}/_{D}\right]^2}}\right) \times \exp\left(-\frac{r^2}{2\,\sigma(x)^2}\right) \tag{5}$$

Where, within this representation of the distribution, $\sigma(x)$ is the wake width that is assumed to expand linearly. The wake width is represented as follows:

$$\sigma(x) = k(x - x_{Nw}) + {}^{D}/_{\sqrt{8}} \tag{6}$$

Where k is the expansion rate of the wake and x_{Nw} is the distance at the end of the near wake. The variable k would have to be estimated which was based on the freestream velocity of the region and the turbulence intensity of the resource represented by I_u. The function of $\sigma(x)$ is dependent on the turbulence intensity of turbulence within the streamwise direction. An empirical linear relationship between wake expansion rate and streamwise turbulence intensity was proposed by [47] which was based on large-eddy simulations under neutral atmospheric conditions as shown in the equation below:

$$k = 0.38I_u + 0.004 \tag{7}$$

It is important to note that the wake expansion growth is linear function which is directly proportional to k. This results in a direct relationship top the turbulence intensity. Thus, higher turbulence intensity, which usually occurs at lower wind speeds, normally lead to a faster wake recovery through the downstream direction. Figure 7-9 (a) and (b) shows the wake deficit distribution of a HAWT along the downstream distance for both the horizontal and vertical planes based on equation (5).

The above wake functions are representative of the deficit velocity in the x-y plane (top / horizontal plane). The main contributors to the horizontal plane stems from the blade inducted vortices as found by [48]. The wake within the x-z plane (vertical plane) is similar to that of the horizontal plane of the HAWT but for VAWT the vertical plane wake recovery is different as the wind shear layers are impacted by the turbine tip vortices [49]. The blade induced vortices are in no way identical which results in a complete three dimensional wake, [50]. For the wake representation of a VAWT, due to the shape of the turbine, [51] had proposed a modification of equation (5) to produce a super Gaussian wake over two spatial planes, that consider horizontal and vertical planes.

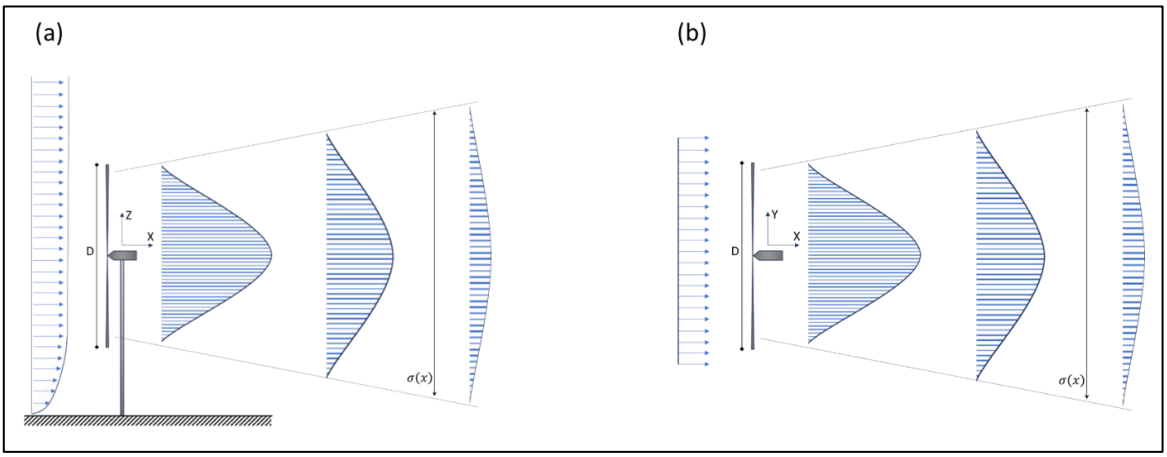

Figure 7-9: Wake velocity deficit distribution downstream - HAWT (a) Vertical Plane, (b) Horizontal Plane

The super Gaussian model considers the two spatial planes being the horizontal and vertical planes which affect the VAWT downstream wake deficit velocity. The work which was conducted by [51]

shows the uneven expansion of the wake in the horizontal and vertical planes of the VAWT. The following equation is a representation of the super Gaussian model:

$$\frac{\Delta U(x)}{U_\infty} = C_U(x) \times \exp\left(-\frac{y^{n_y}}{2\,{\sigma_{V_y}}^2}\right) \times \exp\left(-\frac{z^{n_z}}{2\,{\sigma_{V_z}}^2}\right) \tag{9}$$

The function $C_U(x)$ is defined below as follows:

$$C_U(x) = \left(2^{\gamma-2} - \sqrt{2^{\gamma-2} - \frac{C_T}{8\,{\sigma_{V_y}}^{2/n_y}\,{\sigma_{V_z}}^{2/n_z}\,\Gamma\left(1/n_y\right)\,\Gamma\left(1/n_z\right)}}\right) \tag{10}$$

Where the function $C_U(x)$ represents the local scale velocity function of the wake in both planes and spatial lengths which account for exponents n_y and n_z that define the three dimensional wake according to the Gaussian function. A full derivation of the super Gaussian wake function can be found in [51]. The variables σ_{V_y} and σ_{V_z} are terms which govern the distribution of the velocity deficit through both planes for the VAWT system. They are both dependent on the turbulence intensity of the flow within those planes similar to that of equation (7). The aspect ratio of the VAWT ($\xi = H/D$) has a direct relationship with σ_{V_z} and both terms are shown below:

$$\begin{aligned} \sigma_{V_y} &= k_{V_y} x + \varepsilon_{V_y} \\ \sigma_{V_z} &= k_{V_z}\, x/\xi + \varepsilon_{V_z} \end{aligned} \tag{11}$$

Considering the that the initial wake width is equal and the terms n_y and n_z are the values where $x = 0$ as ε_{V_y} and ε_{V_z} are evaluated as the initial wake. Figure 7-10 (a) and (b) show the velocity deficit distribution along the streamwise direction of the wake in the vertical and horizontal planes, respectively. It can be seen that the top hat nature of the wake is noticeable in the VAWT system along the vertical plane, however, typically develops to a more Gaussian shape around 10 diameters downstream. The wake becomes more complex when exposed to higher Reynolds numbers as the wake tends to meander through the streamwise direction.

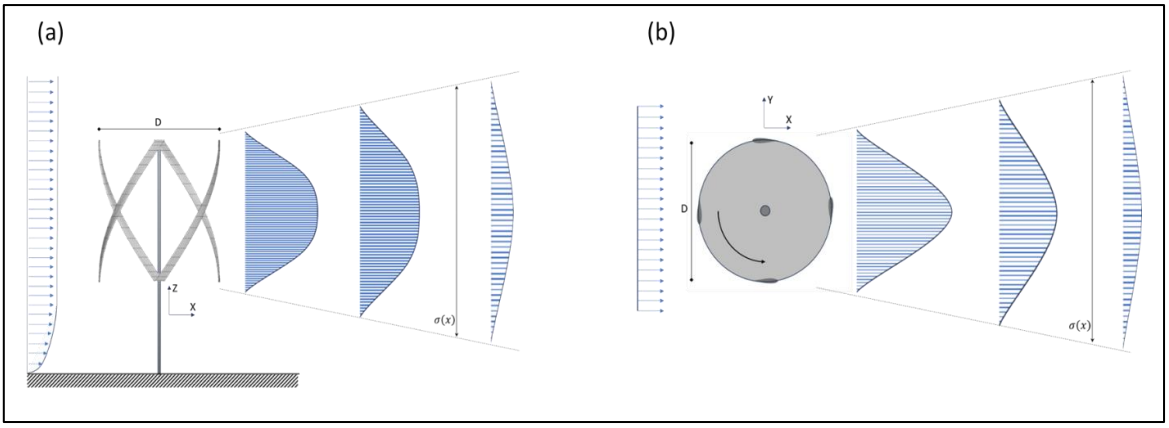

Figure 7-10: Wake velocity deficit distribution downstream - VAWT (a) Vertical Plane, (b) Horizontal Plane

For the HAWT systems the initial spacing was 10 diameters in the downstream direction and 8 diameters in the crosswind direction as found by [52]. Literature suggests that the wake recovers within 6 diameters crosswind and 7 diameters downstream which was taken for the VAWT systems, [50], [53], [54]. Research also suggests that VAWT farms may have a denser turbine layout to that of HAWT farms due to the positive influence of wake on the downstream turbine performance, [55]–[57]. However, to understand the comparison between the turbines, 3 sets of spacing configurations were chosen as shown in Table 7-4.

Table 7-4: Wind Farm Spacing Assumptions

Turbine Type	Crosswind Spacing	Downwind Spacing
Tight Spacing	3	5
Short Spacing	6	7
Large Spacing	8	10

Research conducted by [58] shows 4 potential sites which may be suitable for offshore wind deployment. Figure 7-11 shows the potential aggregated wind rose and wind speed distribution for the site (Site 4) which was chosen for the investigation of turbine layouts. The aim of the investigation was to understand the effect of spacing of the designed turbine to that of a similar turbine in both HAWT and VAWT configurations.

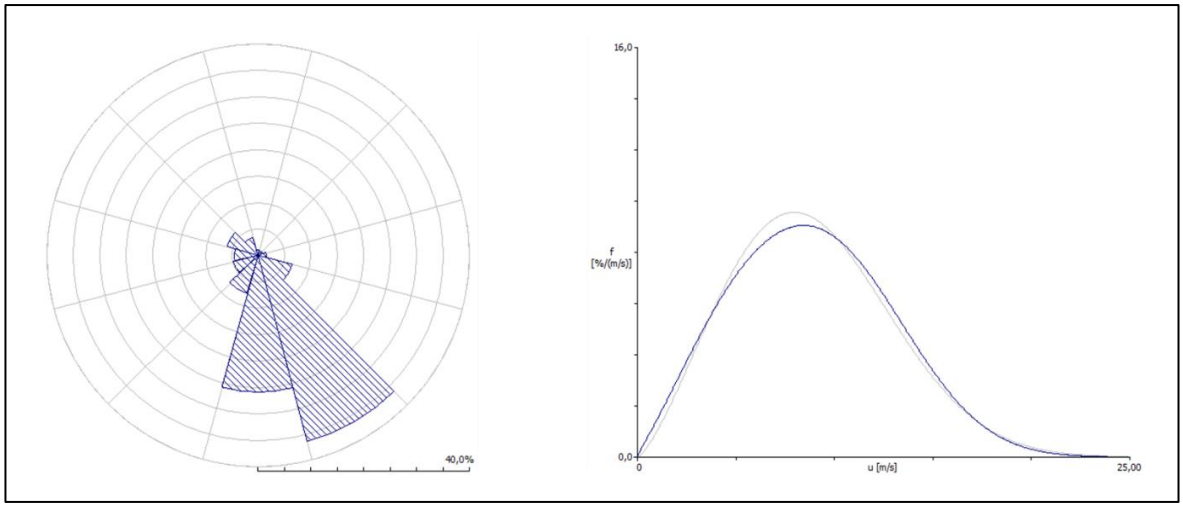

Figure 7-11: Wind Rose and Wind Distribution for potential Site

Figure 7-12 shows the possible wind farm layouts as per the assumptions in Table 7-4 above. Each of the respective simulations had considered a straight bladed Darrius turbine to estimate what existing commercially available VAWT systems can produce, a HAWT configuration turbine based on the NREL offshore reference turbine all of which are compared to the designed helical turbine. All of the turbines were sized to a capacity of 5 MW. The simulations were also adjusted to accommodate the wake characteristics as shown above.

The results of the simulations have shown that for the tight spacing of each of the turbines, the helical turbine has 7.7% and 14.2% increase in AEP in comparison to the straight Darrius turbine and NREL offshore reference turbine respectively. When considering the short and large spacing options the helical turbine had an increase of 7.7% and 13.5% increase in AEP respectively. On average the wake loss decreases from an average of 11.3%, 5.2% and 3.5% for the 3 spacing options respectively. Figure 7-13 shows a comparative loss of energy, in comparison to the helical design, per a month of operation.

Figure 7-14 shows the monthly energy output of the helical turbine, for the 3 spacing options shown in Table 7-4, and the average wind speed per month. The results show that even at low wind speeds the turbine performs well and has good production. In comparison to the HAWT and VAWT reference energy production, the helical turbine has 9.7% and 22% respectively increase in energy production, during the low wind speed months, on average.

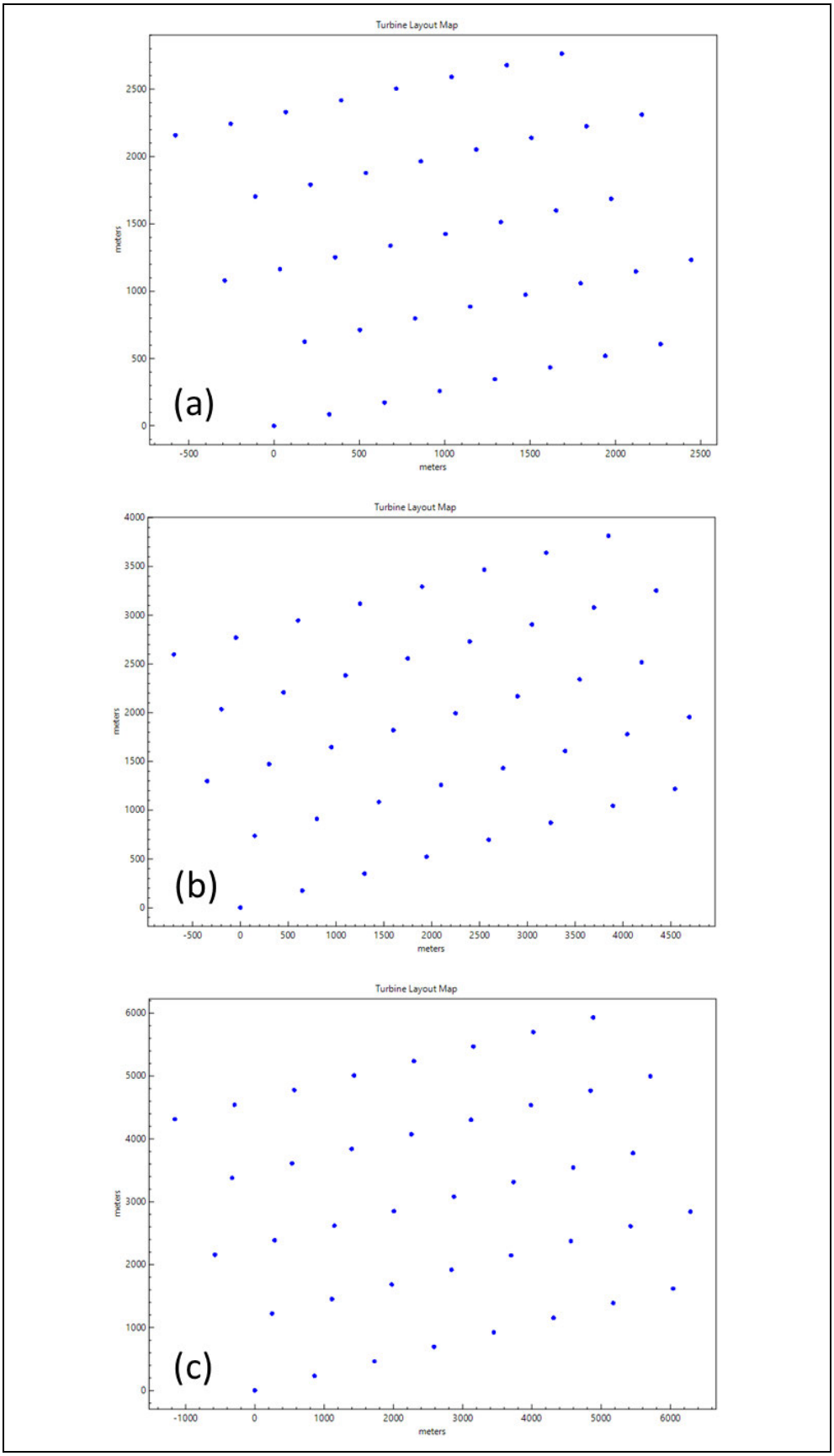

Figure 7-12: Wind Farm Layout (a) Tight Spacing (b) Short Spacing (c) Large Spacing

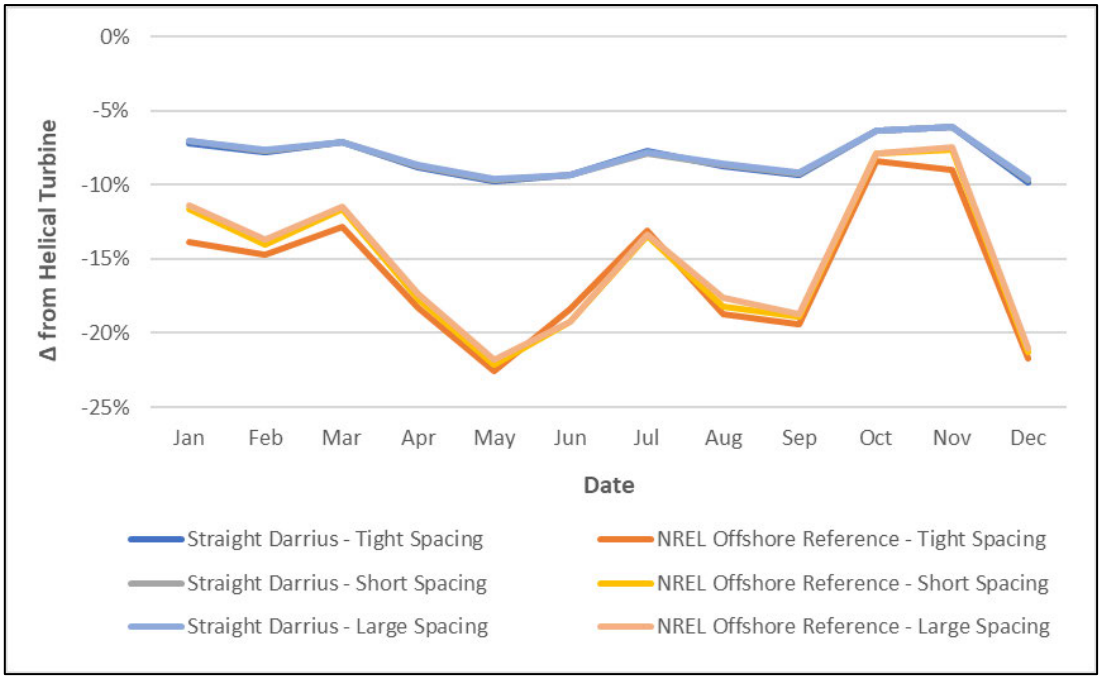

Figure 7-13: Annual Energy Production (AEP) Loss compared to Helical Turbine

The results show the helical VAWT has an increase in power production in comparison to the available VAWT and HAWT reference turbines respectively. The turbine also has favourable results when it comes to wind farm layout as the VAWT systems can be packed closer together in comparison to HAWT systems. Comparing the results of the 2 VAWT systems, the helical turbine is favourable as the impact on rotor torque shows that the helical turbine provides a smoother torque profile than that of the straight blade Darrius option. This allows for smoother transfer of mechanical power through the transmission system.

The helical system indicate that it may be useful for far offshore regions in a tightly spaced configuration so as to create an area which is dense enough for large power evacuation to an offshore substation. The positive benefits of using HVDC transmission systems with this turbine configuration in a wind farm is the black start capability of the system. For island areas and areas where coastal region energy demand is projected to grow, the option of offshore wind farms can prove to a viable source of clean energy

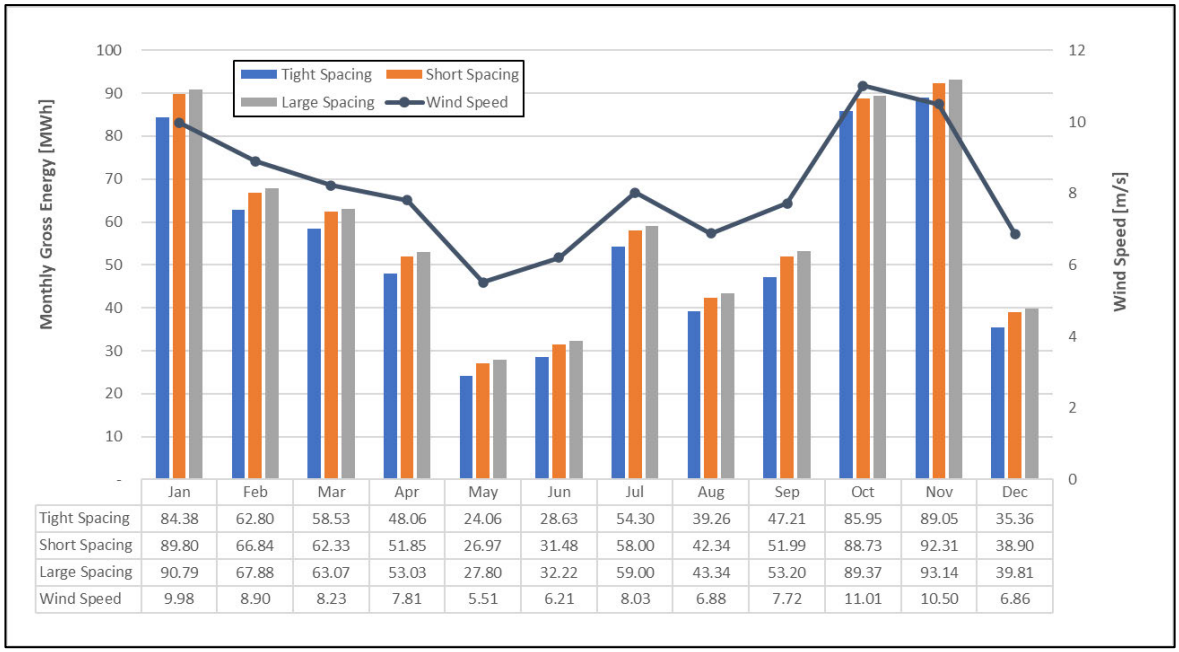

	Jan	Feb	Mar	Apr	May	Jun	Jul	Aug	Sep	Oct	Nov	Dec
Tight Spacing	84.38	62.80	58.53	48.06	24.06	28.63	54.30	39.26	47.21	85.95	89.05	35.36
Short Spacing	89.80	66.84	62.33	51.85	26.97	31.48	58.00	42.34	51.99	88.73	92.31	38.90
Large Spacing	90.79	67.88	63.07	53.03	27.80	32.22	59.00	43.34	53.20	89.37	93.14	39.81
Wind Speed	9.98	8.90	8.23	7.81	5.51	6.21	8.03	6.88	7.72	11.01	10.50	6.86

Figure 7-14: Helical Turbine monthly production profile

The increase in energy output of the turbine can lead towards a cheaper option for energy production in offshore locations. This requires future economic modelling to consolidate the transmission system which is to be used in relation to the distance from shore and the water depth.

7.6 Advantages of Helical VAWT

The helical turbine which is designed and explained in Chapter 4 was compared to that of existing commercially available reference vertical and horizontal axis turbines of utility scale. The following section of the study summarises the advantages of the helical VAWT to the reference HAWT and VAWT chosen:

a) A clear advantage of a VAWT system compared to a HAWT system is the ability to accept wind flow from all directions or cross-flow. Table 7-3 shows the correction which is required when using a HAWT configuration from the ratio of yaw misalignment production to yaw aligned production. This is because the HAWT system does not have cross-flow ability and needs to yaw in the direction of the freestream flow. The VAWT system has a theoretical ratio of 1 due to the configuration not needing a yaw system and the cross-flow ability of VAWTs.

b) The VAWT had incorporated the helical blade orientation utilizing four blades based which incorporated 100 % blade wrap. The blade wrap was significant due to the lower fluctuation of torque on the turbine rotor. It was found, from the simulation results, that the use of a symmetric Selig aerodynamic blade profile had preferable results in comparison to the NACA symmetric aerofoil. The Selig blade profile exhibited better rotor torque characteristics than that of the NACA profiles when the turbine experiences higher tip speed ratios (TSRs). Other VAWT systems do not

explicitly declare the aerofoil profile due to company Intellectual Property, however, comparing results from literature which state that NACA profiles are used for VAWT's, the Selig symmetrical profile shows positive results for the use in the helical VAWT resulting in a better performing power curve as shown in Figure 7-2 and Figure 7-5 of HAWT and VAWT comparisons, respectively

c) The turbine blades of HAWT configurations are subjected to gravitational loading and stresses along the blade profile due to wind shear changes resulting in cyclic loading and fatigue on the turbine blade roots. The reversing stress which occurs at the root of HAWT blades are not apparent in VAWT configurations which is another added advantage. The VAWT blades do undergo larger bending moment stresses along the blade which can be resolved with in-line blade stiffeners designed to provide aerodynamic stability in the heave and roll motion. The mechanical stress along the span of the turbine blade is reduced due to mechanical stiffeners and modular blade design and construction. The VAWT design has reduced cyclic fatigue along the root of the turbine blade due to these stiffeners and supports on both ends of the blades. The shape of the stiffeners can be designed to support the turbine in the heave and roll motion aiding in turbine stability.

d) The comparison of a helical VAWT to the reference HAWT shows that the VAWT has a lower tip speed operating range resulting in lower rotational speed. The VAWT configuration and power curve vs TSR (Figure 7-2 and Figure 7-5) show that the VAWT optimal operational point occurs at a TSR within a range of 2 and 2.2 meaning that the turbine has a lower operational rotational speed. This means that the turbine would experience lower environmental impacts and create less noise compared to the HAWT counterpart. Lower rotational speed of the turbine also leads to lower environmental impact losses such as leading edge erosion resulting in a potential lower operational and maintenance (O&M) budget on leading edge and blade trailing edge maintenance.

e) HAWT systems usually have a constant torque profile on the rotor with the aid of pitch control and blade design. The choice of helical blade design with a 100 % blade wrap ensures that the blade profile is always within the flow, to reduce the torque ripple on the rotor which is usually experienced by other VAWT configurations. Figure 7-7 shows the comparison of torque profile on the rotor of a straight bladed Darrius VAWT, which is currently available, to that of the designed turbine at various operating wind speeds. The results show a clear advantage of helical turbine blade design to that of the straight bladed design, with a smoother torque profile allowing for smoother mechanical power transmission.

f) Initial wake modelling considered a top-hat profile which was proposed in the late 1980's by Jensen. Developments in the wake modelling of turbines have shown that a Gaussian profile is more representative of the wakes generated by the turbines when operational. The HAWT configuration has larger wake profiles and thus requires larger inter-row spacing and transverse turbine spacing. The wake dissipation factor also varies between the two configurations. A comparison was done of tight spacing, short spacing and large spacing of both types of turbines, accommodating for wake dissipation factors respectively. The results in Figure 7-13 show the deviation of the existing VAWT

and HAWT turbines to that of the helical blade design. The results clearly show that the helical turbine design produces more energy than the other two counterparts. This can be attributed to the increase in efficiency reflected in the turbine power curve vs TSR shown in Figure 7-4 and Figure 7-8 respectively.

7.7 Selection of Helical VAWT

Based on the above advantages, the helical VAWT was chosen for the application for the potential offshore wind farm. In order to understand the potential of the wind farm, the turbine power curve was used to conduct a high level Annual Energy Production (AEP) for one of the sites described in Chapter 3. The wind speed and wind direction were obtained via online satellite date used for the simulation on an hourly profile.

The choice of a helical VAWT system result in larger AEP due to higher efficiency power curve compared to existing HAWT and VAWT systems (Figure 7-4 and Figure 7-8) and denser turbine spacing in farm configurations. The larger AEP and denser packing of turbines within a given offshore area, with an optimal electrical reticulation architecture and electrical transmission system can lead to a lower levelized cost of energy (LCoE) of the farm in comparison to existing HAWT based farm systems.

7.8 Conclusion

The study had aimed to investigate the designed helical turbine to that of a reference HAWT and VAWT turbine respectively, each of which are available in the commercial market. The investigation consisted of comparing the turbine's power curves, torque profiles, wake modelling, wind farm layout and energy output for each turbine and turbine layout.

The findings have shown that the helical turbine had an increased efficiency based on power curve comparison of both the HAWT and VAWT references. The torque profiling on the turbine rotor also had positive advantages with a helical design when compared to a straight bladed turbine. The torque fluctuations decrease allowing for a smoother transfer of mechanical power to the generator.

Wake modelling of the turbines has shown that the Gaussian profile has a stronger prediction compared to commonly used wake techniques. The eddy-viscosity modelling was chosen when simulating the turbines which represents as a Gaussian profile. The wake decay for VAWT and HAWT are different and when comparing results, the VAWT had favourable results in comparison to the reference VAWT and HAWT turbines.

The study found that the helical VAWT had a larger AEP and could accommodate a denser packing of turbines within a given offshore area. With the appropriate choice of inter turbine electrical reticulation

architecture and electrical transmission system to shore, the entire wind farm concept can lead to a lower levelized cost of energy (LCoE) of the farm in comparison to existing HAWT based farm systems.

In conclusion, the study shows the benefits of using a helical VAWT in comparison to the straight blade VAWT and reference HAWT. This shows the potential for a helical VAWT in an offshore environment for power production and shows potential for use in far offshore floating applications.

7.9 References

[1] S. Rodrigues, C. Restrepo, E. Kontos, R. Teixeira Pinto, and P. Bauer, "Trends of offshore wind projects," *Renewable and Sustainable Energy Reviews*, vol. 49, pp. 1114–1135, Sep. 2015, doi: 10.1016/j.rser.2015.04.092.

[2] IRENA and CPI (2023), "Global landscape of renewable energy finance," Abu Dhabi, 2023.

[3] M. Hannon, E. Topham, J. Dixon, D. McMillan, and M. Collu, "Offshore Wind, Ready to Float? Global and UK Trends in the Floating Offshore Wind Market," 2019. doi: 10.17868/69501.

[4] K. Jost and G. Xydis, "Offshore wind acceleration in the U.S. Atlantic coast and the 30 GW by 2030 target," *Proceedings of the Institution of Civil Engineers - Energy*, pp. 1–8, Mar. 2023, doi: 10.1680/jener.22.00045.

[5] L. M. Robertson, M. J. Dorreen, and M. A. Raza, "Harnessing Offshore Wind in Canada: The Regulatory Landscape for Offshore Wind Development and Lessons Learned from the United Kingdom, Denmark, and the United States," *Ocean Yearbook Online*, vol. 37, no. 1, pp. 276–310, May 2023, doi: 10.1163/22116001-03701014.

[6] P. Gristo, "President's Page: Energy transition as an opportunity for Latin American geoscientists, companies, and the people," *The Leading Edge*, vol. 42, no. 4, pp. 234–235, Apr. 2023, doi: 10.1190/tle42040234.1.

[7] J. G. Rueda-Bayona, A. Guzmán, J. J. C. Eras, R. Silva-Casarín, E. Bastidas-Arteaga, and J. Horrillo-Caraballo, "Renewables energies in Colombia and the opportunity for the offshore wind technology," *J Clean Prod*, vol. 220, pp. 529–543, May 2019, doi: 10.1016/j.jclepro.2019.02.174.

[8] Equinor, "Hywind Scotland remains the UK's best performing offshore wind farm," Mar. 23, 2021. https://www.equinor.com/news/archive/20210323-hywind-scotland-uk-best-performing-offshore-wind-farm (accessed Jun. 01, 2023).

[9] NS Energy, "Kincardine Floating Offshore Wind Farm, Scotland." https://www.nsenergybusiness.com/projects/kincardine-floating-offshore-wind-farm-scotland/ (accessed Jun. 01, 2023).

[10] WindFloat Atlantic, "WindFloat Atlantic." https://www.windfloat-atlantic.com/the-wind-farm/#history (accessed Jun. 01, 2023).

[11] A. Durakovic, “China’s First Floating Wind Turbine Heads Offshore.” https://www.offshorewind.biz/2021/07/13/chinas-first-floating-wind-turbine-heads-offshore/ (accessed Jun. 01, 2023).

[12] Equinor, “Hywind Tampen.” https://www.equinor.com/energy/hywind-tampen (accessed Jun. 01, 2023).

[13] M. Borg, A. Shires, and M. Collu, “Offshore floating vertical axis wind turbines, dynamics modelling state of the art. part I: Aerodynamics,” *Renewable and Sustainable Energy Reviews*, vol. 39, pp. 1214–1225, 2014, doi: https://doi.org/10.1016/j.rser.2014.07.096.

[14] L. Li, Y. Liu, Z. Yuan, and Y. Gao, “Wind field effect on the power generation and aerodynamic performance of offshore floating wind turbines,” *Energy*, vol. 157, pp. 379–390, Aug. 2018, doi: 10.1016/j.energy.2018.05.183.

[15] A. Ghigo, L. Cottura, R. Caradonna, G. Bracco, and G. Mattiazzo, “Platform Optimization and Cost Analysis in a Floating Offshore Wind Farm,” *J Mar Sci Eng*, vol. 8, no. 11, p. 835, Oct. 2020, doi: 10.3390/jmse8110835.

[16] M. R. Islam, S. Mekhilef, and R. Saidur, “Progress and recent trends of wind energy technology,” *Renewable and Sustainable Energy Reviews*, vol. 21, pp. 456–468, May 2013, doi: 10.1016/j.rser.2013.01.007.

[17] M. Kinzel, Q. Mulligan, and J. O. Dabiri, “Energy exchange in an array of vertical-axis wind turbines,” *Journal of Turbulence*, vol. 13, p. N38, Jan. 2012, doi: 10.1080/14685248.2012.712698.

[18] A. Arredondo-Galeana and F. Brennan, “Floating Offshore Vertical Axis Wind Turbines: Opportunities, Challenges and Way Forward,” *Energies (Basel)*, vol. 14, no. 23, p. 8000, Nov. 2021, doi: 10.3390/en14238000.

[19] A. Shires, “Development and Evaluation of an Aerodynamic Model for a Novel Vertical Axis Wind Turbine Concept,” *Energies (Basel)*, vol. 6, no. 5, pp. 2501–2520, May 2013, doi: 10.3390/en6052501.

[20] M. Collu, F. P. Brennan, and M. H. Patel, “Conceptual design of a floating support structure for an offshore vertical axis wind turbine: the lessons learnt,” *Ships and Offshore Structures*, vol. 9, no. 1, pp. 3–21, Jan. 2014, doi: 10.1080/17445302.2012.698896.

[21] H. Akimoto, K. Tanaka, and K. Uzawa, “Floating axis wind turbines for offshore power generation—a conceptual study,” *Environmental Research Letters*, vol. 6, no. 4, p. 044017, Oct. 2011, doi: 10.1088/1748-9326/6/4/044017.

[22] U. S. Paulsen *et al.*, “DeepWind-from Idea to 5 MW Concept,” *Energy Procedia*, vol. 53, pp. 23–33, 2014, doi: 10.1016/j.egypro.2014.07.212.

[23] H. Akimoto, K. Iijima, and Y. Takata, “Feasibility Study of the Floating Axis Wind Turbine: Preliminary Model Experiments,” in *Volume 10: Ocean Renewable Energy*, American Society of Mechanical Engineers, Jun. 2017. doi: 10.1115/OMAE2017-61944.

[24] M. Cahay, E. Luquiau, C. Smadja, and F. Silvert, “Use of a Vertical Wind Turbine in an Offshore Floating Wind Farm,” in *All Days*, OTC, May 2011. doi: 10.4043/21705-MS.

[25] W. Tjiu, T. Marnoto, S. Mat, M. H. Ruslan, and K. Sopian, “Darrieus vertical axis wind turbine for power generation II: Challenges in HAWT and the opportunity of multi-megawatt Darrieus VAWT development,” *Renew Energy*, vol. 75, pp. 560–571, Mar. 2015, doi: 10.1016/j.renene.2014.10.039.

[26] “SeaTwirl.” https://seatwirl.com/ (accessed Mar. 02, 2023).

[27] A. Rezaeiha, H. Montazeri, and B. Blocken, “Characterization of aerodynamic performance of vertical axis wind turbines: Impact of operational parameters,” *Energy Convers Manag*, vol. 169, pp. 45–77, Aug. 2018, doi: 10.1016/j.enconman.2018.05.042.

[28] A. Zanon, M. De Gennaro, and H. Kühnelt, “Wind energy harnessing of the NREL 5 MW reference wind turbine in icing conditions under different operational strategies,” *Renew Energy*, vol. 115, pp. 760–772, Jan. 2018, doi: 10.1016/j.renene.2017.08.076.

[29] T. Ashwill, “Measured Data for the Sandia 34-Meter Vertical Axis Wind Turbine,” Albuquerque, New Mexico, 1992.

[30] M. F. Howland *et al.*, “Influence of atmospheric conditions on the power production of utility-scale wind turbines in yaw misalignment,” *Journal of Renewable and Sustainable Energy*, vol. 12, no. 6, p. 063307, Nov. 2020, doi: 10.1063/5.0023746.

[31] J. Jonkman, S. Butterfield, W. Musial, and G. Scott, “Definition of a 5-MW Reference Wind Turbine for Offshore System Development,” Golden, CO, Feb. 2009. doi: 10.2172/947422.

[32] P. M. O. Gebraad *et al.*, “A data-driven model for wind plant power optimization by yaw control,” in *2014 American Control Conference*, IEEE, Jun. 2014, pp. 3128–3134. doi: 10.1109/ACC.2014.6859118.

[33] P. Hulsman, C. Sucameli, V. Petrović, A. Rott, A. Gerds, and M. Kühn, “Turbine power loss during yaw-misaligned free field tests at different atmospheric conditions,” *J Phys Conf Ser*, vol. 2265, no. 3, p. 032074, May 2022, doi: 10.1088/1742-6596/2265/3/032074.

[34] J. Jonkman, S. Butterfield, W. Musial, and G. Scott, “Definition of a 5-MW Reference Wind Turbine for Offshore System Development,” Colorado, Feb. 2009.

[35] M. Lydia, A. I. Selvakumar, S. S. Kumar, and G. E. P. Kumar, “Advanced Algorithms for Wind Turbine Power Curve Modeling,” *IEEE Trans Sustain Energy*, vol. 4, no. 3, pp. 827–835, Jul. 2013, doi: 10.1109/TSTE.2013.2247641.

[36] M. Lydia, S. S. Kumar, A. I. Selvakumar, and G. E. Prem Kumar, “A comprehensive review on wind turbine power curve modeling techniques,” *Renewable and Sustainable Energy Reviews*, vol. 30, pp. 452–460, Feb. 2014, doi: 10.1016/j.rser.2013.10.030.

[37] F. Bilendo, A. Meyer, H. Badihi, N. Lu, P. Cambron, and B. Jiang, “Applications and Modeling Techniques of Wind Turbine Power Curve for Wind Farms—A Review,” *Energies (Basel)*, vol. 16, no. 1, p. 180, Dec. 2022, doi: 10.3390/en16010180.

[38] G. Lee, Y. Ding, L. Xie, and M. G. Genton, “A kernel plus method for quantifying wind turbine performance upgrades,” *Wind Energy*, vol. 18, no. 7, pp. 1207–1219, Jul. 2015, doi: 10.1002/we.1755.

[39] M. Kinzel, Q. Mulligan, and J. O. Dabiri, “Energy exchange in an array of vertical-axis wind turbines,” *Journal of Turbulence*, vol. 13, p. N38, Jan. 2012, doi: 10.1080/14685248.2012.712698.

[40] N. O. Jensen, *A note on wind turbine interaction*, Riso-M-2411. Risoe National Laboratory, 1983.

[41] R. J. Barthelmie *et al.*, “Modelling and measuring flow and wind turbine wakes in large wind farms offshore,” *Wind Energy*, vol. 12, no. 5, pp. 431–444, Jul. 2009, doi: 10.1002/we.348.

[42] T. Göçmen, P. van der Laan, P.-E. Réthoré, A. P. Diaz, G. Chr. Larsen, and S. Ott, “Wind turbine wake models developed at the technical university of Denmark: A review,” *Renewable and Sustainable Energy Reviews*, vol. 60, pp. 752–769, Jul. 2016, doi: 10.1016/j.rser.2016.01.113.

[43] M. Bastankhah and F. Porté-Agel, “Experimental and theoretical study of wind turbine wakes in yawed conditions,” *J Fluid Mech*, vol. 806, pp. 506–541, Nov. 2016, doi: 10.1017/jfm.2016.595.

[44] S. Frandsen *et al.*, “Analytical modelling of wind speed deficit in large offshore wind farms,” *Wind Energy*, vol. 9, no. 1–2, pp. 39–53, Jan. 2006, doi: 10.1002/we.189.

[45] L. P. Chamorro and F. Porté-Agel, “A Wind-Tunnel Investigation of Wind-Turbine Wakes: Boundary-Layer Turbulence Effects,” *Boundary Layer Meteorol*, vol. 132, no. 1, pp. 129–149, Jul. 2009, doi: 10.1007/s10546-009-9380-8.

[46] Y.-T. Wu and F. Porté-Agel, “Atmospheric Turbulence Effects on Wind-Turbine Wakes: An LES Study,” *Energies (Basel)*, vol. 5, no. 12, pp. 5340–5362, Dec. 2012, doi: 10.3390/en5125340.

[47] A. Niayifar and F. Porté-Agel, “Analytical Modeling of Wind Farms: A New Approach for Power Prediction,” *Energies (Basel)*, vol. 9, no. 9, p. 741, Sep. 2016, doi: 10.3390/en9090741.

[48] H. Kadum, S. Friedman, E. H. Camp, and R. B. Cal, “Development and scaling of a vertical axis wind turbine wake,” *Journal of Wind Engineering and Industrial Aerodynamics*, vol. 174, pp. 303–311, Mar. 2018, doi: 10.1016/j.jweia.2018.01.004.

[49] G. Tescione, D. Ragni, C. He, C. J. Simão Ferreira, and G. J. W. van Bussel, “Near wake flow analysis of a vertical axis wind turbine by stereoscopic particle image velocimetry,” *Renew Energy*, vol. 70, pp. 47–61, Oct. 2014, doi: 10.1016/j.renene.2014.02.042.

[50] P. Ouro, S. Runge, Q. Luo, and T. Stoesser, “Three-dimensionality of the wake recovery behind a vertical axis turbine,” *Renew Energy*, vol. 133, pp. 1066–1077, Apr. 2019, doi: 10.1016/j.renene.2018.10.111.

[51] P. Ouro and M. Lazennec, “Theoretical modelling of the three-dimensional wake of vertical axis turbines,” *Flow*, vol. 1, p. E3, May 2021, doi: 10.1017/flo.2021.4.

[52] W. Musial, “Offshore wind energy facility characteristics,” in *BOEM’s Offshore Wind and Maritime Industry Knowledge Exchange Workshop*, Baltimore, Mar. 2018.

[53] M. Abkar, “Theoretical Modeling of Vertical-Axis Wind Turbine Wakes,” *Energies (Basel)*, vol. 12, no. 1, p. 10, Dec. 2018, doi: 10.3390/en12010010.

[54] P. Ouro and M. Lazennec, “Theoretical modelling of the three-dimensional wake of vertical axis turbines,” *Flow*, vol. 1, p. E3, May 2021, doi: 10.1017/flo.2021.4.

[55] H. Y. Peng, H. J. Liu, and J. H. Yang, “A review on the wake aerodynamics of H-rotor vertical axis wind turbines,” *Energy*, vol. 232, p. 121003, Oct. 2021, doi: 10.1016/j.energy.2021.121003.

[56] L. Kuang *et al.*, “Characterization of wake interference between two tandem offshore floating vertical-axis wind turbines: Effect of platform pitch motion,” *Energy Convers Manag*, vol. 265, p. 115769, Aug. 2022, doi: 10.1016/j.enconman.2022.115769.

[57] Z. Toor, H. Bahaidarah, and S. Rehman, “Aerodynamic Interference of Vertical Axis Wind Turbines in Array Configuration,” in *8 th Thermal and Fluids Engineering Conference (TFEC)*, University of Maryland, May 2023.

[58] F. L. Inambao and K. Cunden, “Offshore wind resource assessment off the South African coastline,” *International Journal of Mechanical Engineering and Technology (IJMET)*, 2019.

CHAPTER 8 : CONCLUSION

8.1 Conclusion

This thesis aimed to investigate the suitability of vertical axis wind turbines (VAWTs) to extract the vast potential wind energy resource off the coast of South Africa. The study examined the existing developments within the offshore wind industry by examining journal articles and leading industry reports. The investigations then considered the offshore wind energy potential using synthetic wind resource data extrapolated to hub heights of 50 m, 100 m, and 150 m.

The VAWT systems used for offshore wind applications are unique and the use of a helical blade profile has significant benefits for the industry. One of the challenges with traditional offshore wind turbines is the use of complex control systems for the pitch and yaw systems allowing for the best extraction of the resource. The use of a VAWT allows for cross-flow power generation which results in cost reductions and increased turbine availability. The helical VAWT was designed by examining various aerodynamic blade profiles at different turbine aspect ratios which were then prototyped and tested. The results were obtained from the simulations and tests were found to complete the objectives of the study and the following conclusions were drawn:

1. There initial resource assessment had identified potential sites for South Africa examining the eastern and western coastline of the country. Avoiding the busy shipping trade routes and understanding the oil and gas plots allowed for the selection of five potential offshore wind farm sites. The five sites are located roughly 200 km offshore of the coast and have significant potential for wind farms with a mean wind speed of 9 m/s which is more than typical onshore requirements which are in the range of 6 m/s to 7 m/s.
2. The turbine was fabricated and prototyped to be tested, on a small scale, within a wind tunnel. The test results confirmed the simulation results; however, the tests had indicated that an aspect ratio of 1 provided more favourable results in comparison to the aspect ratio of 1.5. The aspect ratio of 1 had shown that the turbine also had better start-up as well as provided better torque and power output in comparison to the turbine with an aspect ratio of 1.5.
3. Larger turbines may be developed at a suitable size as well as with scalable modular solutions also being considered throughout the turbine development. This would result in small turbine diameters but larger wind farm densities to extract more of the offshore wind resource and effectively utilize the space of the ocean. The helical VAWT blade configuration can be built in modular sections allowing for ease of blade repair and maintenance in comparison to traditional HAWT systems.
4. The vertical axis design of the system proves suitable for offshore applications and with the ability to harness cross-flow wind resources, the turbine may reduce offshore costs resulting in

feasible power generation. The turbine also has the benefit of being modular by stacking the turbines on top of one another. By stacking the turbine, the system allows for a small turbine diameter as well as a small blade chord length. This allows for ease of manufacturing and deployment from onshore to offshore as well as offshore construction. The modular capabilities allow for ease of maintenance and reduction of wasted ocean spatial dispersion as VAWTs require less inter-row spacing of turbines.

5. The helical turbine, in comparison to other reference VAWT designs, show that the torque profile on the turbine rotor is smoother resulting in smoother power output from the turbine during operation. The choice of helical blade design with a 100 % blade wrap ensures that the blade profile is always within the flow, to reduce the torque ripple on the rotor which is usually experienced by other VAWT configurations.
6. The chosen design of turbine (Helical blade configuration) proves to be a favourable turbine design in comparison to similar turbines within the market. The results from a high level Annual Energy Production (AEP) indicate that the helical turbine has a higher capacity factor, lower inter-turbine wake losses and larger production per square kilometre in comparison to the commercially available HAWT and VAWT counterparts. This type of turbine has the ability to perform well under extreme weather conditions, normally occurring in offshore locations.
7. The system allows for the use of permanent magnet generators at the base of the turbine structures which means safer operations and maintenance regimes. This reduces the need for complex mechanical transmission systems such as gearboxes, reducing the points of critical failure of the system.

8.2 Future Work

The future work of this thesis study would lead toward back-end engineering design and investigation of suitable port facilities within South Africa. Suitable shipping vessels such as large barrages would be needed to transport the floating offshore platforms together with the turbine components for offshore assembly. The use of offshore subsea cables also needs to be investigated further concerning offshore hybridized electrical grids consisting of high voltage alternating current (HVAC) and high voltage direct current (HVDC) for the most optimum power transmission to onshore substations. The dynamic power generation requires to be modelled and integrated with grid integration studies to understand the influence of offshore transient power flow into the coastal electrical network. Many of the components of the entire system have the capabilities to be locally produced in the country resulting in significant economic value and decent job creation. This would be advantageous coupled with the onshore wind network of artisans and technicians allowing for further skills development in the offshore wind power market.

APPENDIX A

The following Appendix depicts the editing certificates from an accredited editor. The scope of the editing certificates includes language, layout and reference checks for the submitted journal article publications.

DR RICHARD STEELE
B.A., H.D.E., M. Tech. Hom
HOMEOPATH
Registration No. A07309 HM
Practice No. 0807524
Freelance academic editor
Associate member, Professional Editors' Guild of South Africa

[redacted]
Glenwood, Durban 4001
031-[redacted]/[redacted]
Fax 031-201-4989
Postal: P.O. Box 30043, Mayville 4058
Email: [redacted]

Quotation

Date: 24 February 2019

To: **Kumaresan Cunden**
For editing of journal article: **OFFSHORE WIND RESOURCE ASSESSMENT OFF THE SOUTH AFRICAN COASTLINE**
(IJMET)

Supervisor and co-author: PROF. FREDDIE INAMBAO
School of Engineering
Room 116A, Mech Eng Building
Howard college campus
University of KwaZulu-Natal
P/Bag x54001
Durban
4000

7 433 words at R0.23 per word, including references = R1 709
Formatting the article and reworking the references to suit journal Author Guidelines will be invoiced at R260 per hour.

I proof-read, language edit, reference edit, layout edit and meaning edit i.e. change wording to sharpen and/or clarify the meaning of sentences as appropriate. This is substantive editing, not just proof reading. My work includes the following:

- Ensuring that spelling, grammar, scientific notation, punctuation, line spacing and font is consistent and correct;
- Checking the List of References for consistency and style, and checking entries against online databases to check accuracy of spelling and reference detail;
- Ensuring that all references in the text appear in the List of References and vice versa;
- Ensuring that the article conforms to the Author Guidelines of journal being submitted to.

Thank you
Richard Steele
(*per email*)

DR RICHARD STEELE
BA, HDE, MTech(Hom)
HOMEOPATH
Registration No. A07309 HM
Practice No. 0807524
Freelance academic editor
Associate member: Professional Editors' Guild, South Africa

[redacted]
Glenwood, Durban 4001
031-201-6508/[redacted]
Postal: P.O. Box 30043, Mayville 4058
Email: [redacted]

EDITING CERTIFICATE

Re: **Kumaresan Cunden**
For editing journal article: **OFFSHORE VERTICAL AXIS WIND TURBINE SIMULATION**

I confirm that I have edited this article and the references for clarity, language and layout. I returned the document to the author with track changes so correct implementation of the changes and clarifications requested in the text and references is the responsibility of the author. I am a freelance editor specialising in proofreading and editing academic documents. My original tertiary degree which I obtained at the University of Cape Town was a B.A. with English as a major and I went on to complete an H.D.E. (P.G.) Sec. with English as my teaching subject. I obtained a distinction for my M.Tech. dissertation in the Department of Homoeopathy at Technikon Natal in 1999 (now the Durban University of Technology). I was a part-time lecturer in the Department of Homoeopathy at the Durban University of Technology for 13 years and supervised many Master's degree dissertations during that period.

Dr Richard Steele
09 January 2021
per email

DR RICHARD STEELE
BA HDE MTech(Hom)
HOMEOPATH
Registration No. A07309 HM
Practice No. 0807524
Freelance academic editor
Associate member: Professional Editors' Guild, South Africa

[redacted]
Glenwood, Durban 4001
031-201-6508/[redacted]
Postal: P.O. Box 30043, Mayville 4058
Email: [redacted]

EDITING CERTIFICATE

Re: **Kumaresan Cunden**
Journal article: **DESIGN, CONSTRUCTION AND TESTING OF A LOW-SPEED WIND TUNNEL**

I confirm that I have edited this article and the references for clarity, language and layout. I returned the document to the author with track changes so correct implementation of the changes and clarifications requested in the text and references is the responsibility of the author. I am a freelance editor specialising in proofreading and editing academic documents. My original tertiary degree which I obtained at the University of Cape Town was a B.A. with English as a major and I went on to complete an H.D.E. (P.G.) Sec. with English as my teaching subject. I obtained a distinction for my M.Tech. dissertation in the Department of Homoeopathy at Technikon Natal in 1999 (now the Durban University of Technology). I was a part-time lecturer in the Department of Homoeopathy at the Durban University of Technology for 13 years and supervised many master's degree dissertations during that period.

Dr Richard Steele
13 September 2021
per email

APPENDIX B

Appendix B contains the Journal acceptance letters for the published journal articles for the respective chapters of the thesis.

IAEME Publication

(Publishers of High Quality Peer Reviewed Refereed Scientific, Engineering & Technology, Medicine and Management International Journals)

www.iaeme.com

[redacted]

INTERNATIONAL JOURNAL OF MECHANICAL ENGINEERING & TECHNOLOGY (IJMET)

www.iaeme.com/ijmet/index.asp

Paper ID: IJMET_10_06_006

Date: 13-June-2019

Certificate of Publication

This is to certify that the research paper entitled "OFFSHORE WIND RESOURCE ASSESSMENT OFF THE SOUTH AFRICAN COASTLINE" authored by "Freddie L. Inambao and Kumaresan Cunden" had been reviewed by the Editorial Board and published in "International Journal of Mechanical Engineering & Technology (IJMET), Volume 10, Issue 06, June 2019, pp. 95-119; ISSN Print: 0976-6340 and ISSN Online: 0976-6359; Journal Impact Factor (2019): 10.6879 Calculated by GISI (www.jifactor.com); InfoBase Index IBI Factor for the year 2015–16 is 3.46; Thomson Reuters' Researcher ID: B-7384-2016".

Chief Editor

[redacted]

Plot: 03, Flat- S 1, Poomalai Santosh Pearls Apartment, Plot No. 10, Vaiko Salai 6th Street, Jai Shankar Nagar, Palavakkam, Chennai - 600 041, Tamilnadu, India.
E-mail: editor@iaeme.com

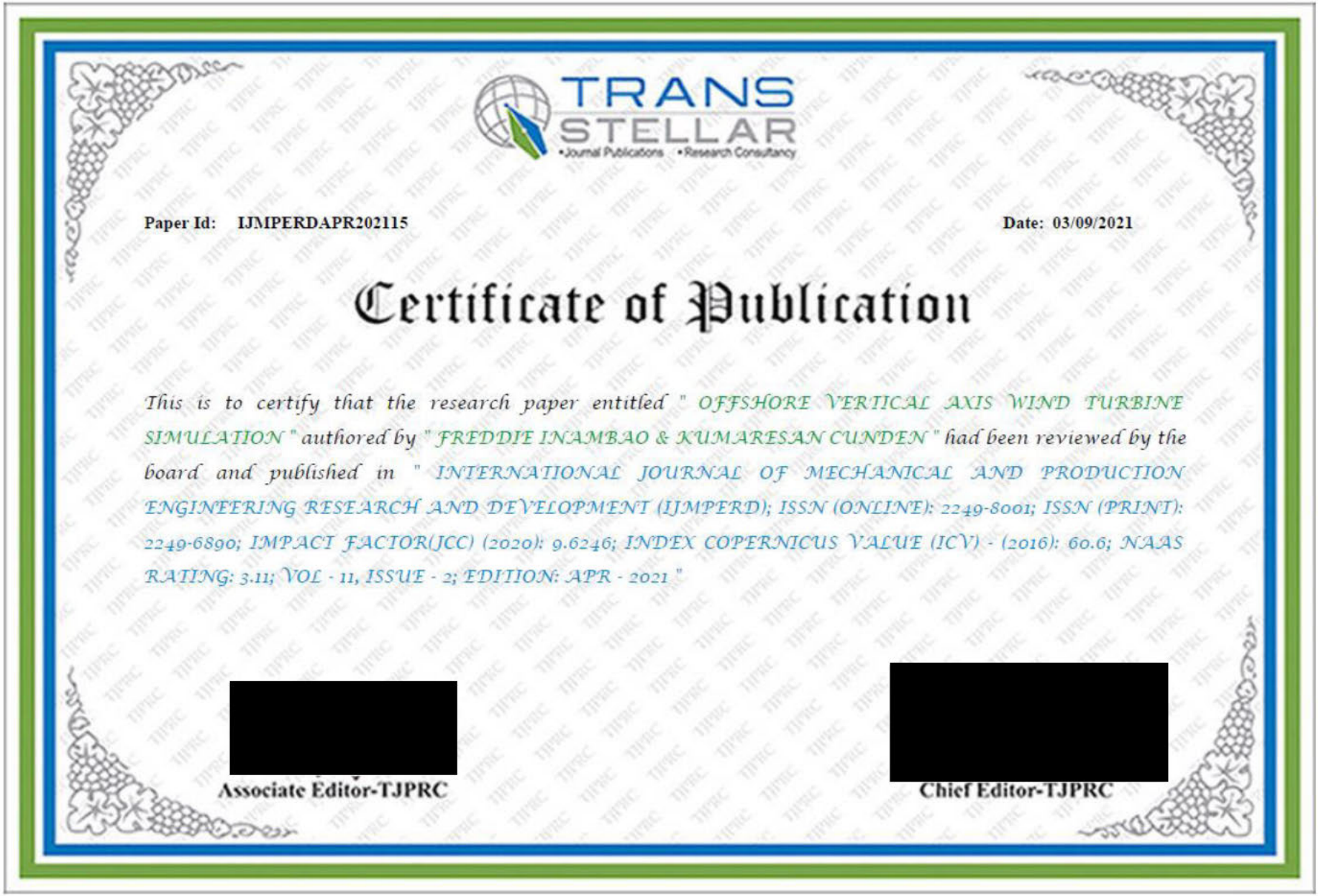
TRANS
STELLAR
•Journal Publications •Research Consultancy
Paper Id: IJMPERDAPR202115
Date: 03/09/2021
Certificate of Publication
This is to certify that the research paper entitled " OFFSHORE VERTICAL AXIS WIND TURBINE SIMULATION " authored by " FREDDIE INAMBAO & KUMARESAN CUNDEN " had been reviewed by the board and published in " INTERNATIONAL JOURNAL OF MECHANICAL AND PRODUCTION ENGINEERING RESEARCH AND DEVELOPMENT (IJMPERD); ISSN (ONLINE): 2249-8001; ISSN (PRINT): 2249-6890; IMPACT FACTOR(JCC) (2020): 9.6246; INDEX COPERNICUS VALUE (ICV) - (2016): 60.6; NAAS RATING: 3.11; VOL - 11, ISSUE - 2; EDITION: APR - 2021 "
[redacted]
Associate Editor-TJPRC
[redacted]
Chief Editor-TJPRC


TRANS
STELLAR
•Journal Publications •Research Consultancy
Paper Id: IJMPERDDEC202115
Date: 11/05/2021
Certificate of Publication
This is to certify that the research paper entitled " DESIGN, CONSTRUCTION AND TESTING OF A LOW-SPEED WIND TUNNEL " authored by " KUMARESAN CUNDEN & PROFESSOR FREDDIE L. INAMBAO " had been reviewed by the board and published in " INTERNATIONAL JOURNAL OF MECHANICAL AND PRODUCTION ENGINEERING RESEARCH AND DEVELOPMENT (IJMPERD); ISSN (ONLINE): 2249-8001; ISSN (PRINT): 2249-6890; IMPACT FACTOR(JCC) (2020): 9.6246; INDEX COPERNICUS VALUE (ICV) - (2016): 60.6; NAAS RATING: 3.11; VOL - 11, ISSUE - 6; EDITION: DEC-2021 "
[redacted]
Associate Editor-TJPRC
[redacted]
Chief Editor-TJPRC

TRANS STELLAR
• Journal Publications • Research Consultancy

Aug 03, 2023

To

Professor Freddie Inambao
University of KwaZulu-Natal
Private Bag X54001
Durban
4000
South Africa

Dear Professor. Freddie Inambao,

Subject: Primary Provisional Acceptance of research paper for publication in our Collabrative International Journal

Greetings.

It's our pleasure to inform you that, after the peer review of your paper, **Titled: "OFFSHORE WIND ENERGY REVIEW: THE POTENTIAL FOR SOUTH AFRICA"** authored by **"Kumaresan Cunden & Professor Freddie Inambao"** submitted to us for an evaluation by you on **Jul 26, 2023** has been provisionally accepted by the Review Board for publishing in "Scopus indexed journal".

Again, thank you for working with **TRANSSTELLAR**. We believe that our collaboration will help to accelerate the global knowledge creation and sharing one step further. **TRANSSTELLAR** looks forward to your final publication package. Please do not hesitate to contact us if you have any further questions.

Thanking you,
Yours sincerely,

[redacted]

Associate Editor
TJPRC Pvt Ltd.

TRANS STELLAR
• Journal Publications • Research Consultancy

Aug 03, 2023

To

Professor Freddie Inambao
University of KwaZulu-Natal
Private Bag X54001
Durban
4000
South Africa

Dear Professor. Freddie Inambao,

Subject: Primary Provisional Acceptance of research paper for publication in our Collabrative International Journal

Greetings.

It's our pleasure to inform you that, after the peer review of your paper, **Titled: "FABRICATION AND TESTING OF SMALL SCALE HELICAL WIND TURBINE"** authored by **"Kumaresan Cunden & Professor Freddie Inambao"** submitted to us for an evaluation by you on **Jul 26, 2023** has been provisionally accepted by the Review Board for publishing in **"Scopus indexed journal"**.

Again, thank you for working with **TRANSSTELLAR**. We believe that our collaboration will help to accelerate the global knowledge creation and sharing one step further. **TRANSSTELLAR** looks forward to your final publication package. Please do not hesitate to contact us if you have any further questions.

Thanking you,
Yours sincerely,

[redacted]

Associate Editor
TJPRC Pvt Ltd.

TRANS STELLAR
• Journal Publications • Research Consultancy

Aug 03, 2023

To

Professor Freddie Inambao
University of KwaZulu-Natal
Private Bag X54001
Durban
4000
South Africa

Dear Professor. Freddie Inambao,

Subject: Primary Provisional Acceptance of research paper for publication in our Collabrative International Journal

Greetings.

It's our pleasure to inform you that, after the peer review of your paper, **Titled:** "**COMPARISON OF HELICAL VAWT TO REFERENCE VAWT AND HAWT FOR OFFSHORE APPLICATIONS**" authored by "**Kumaresan Cunden & Professor Freddie Inambao**" submitted to us for an evaluation by you on **Jul 26, 2023** has been provisionally accepted by the Review Board for publishing in "Scopus indexed journal".

Again, thank you for working with **TRANSSTELLAR**. We believe that our collaboration will help to accelerate the global knowledge creation and sharing one step further. **TRANSSTELLAR** looks forward to your final publication package. Please do not hesitate to contact us if you have any further questions.

Thanking you,
Yours sincerely,

[redacted]

Associate Editor
TJPRC Pvt Ltd.